SEDE AMMINISTRATIVA: UNIVERSITÀ DEGLI STUDI DI PADOVA

DIPARTIMENTO DI GEOSCIENZE

SCUOLA DI DOTTORATO DI RICERCA IN: SCIENZE DELLA TERRA

CICLO: XXV

THERMOCHRONOLOGY OF THE POLISH AND UKRAINIAN CARPATHIANS

Direttore della Scuola: Ch.mo Prof. Massimiliano Zattin

Supervisore: Ch.mo Prof. Massimiliano Zattin

Co-supervisore: Ch.mo Prof. Stefano Mazzoli

Dottorando: Benedetta Andreucci

ABSTRACT

The Carpathian-Pannonian region's geodynamic evolution has been for the last decades object of debate for the scientific community. The aim of this study is to provide a further contribution to the understanding of the evolution of this territory. In fact, low temperature thermochronometry and paleotemperature studies allow to define thermal histories, which can be used, in turn, to infer the occurrence of thermal perturbations and of their extent, as well as the timing and spatial pattern of burial and exhumation. Several different processes such as B and A-type subduction, slab roll back, mantle uprise, gravitational collapse of the lithosphere have been proposed to have played a role in the evolution of this region. Reconstruction of thermal and of burial and exhumation history was then used as a tool to support or rule out some of the processes quoted above.

Three low temperature thermochronometers were used to date rocks belonging to the Polish and Ukrainian Carpathians, and the results were inverted to model time-temperature histories. Thermal histories were then integrated with observations on the structural and topographic setting of the region and with data regarding the thermal structure of the lithosphere and discussed to extrapolate constrains on burial and exhumation. Finally a compilation of the thermochronometry datasets referred to the study area, integrated with previously published geophysical data were used to discuss their consistency with the different geodynamic processes proposed for the Carpathian Pannonian region.

The results indicate that samples of the thrust belt were heated to variable temperatures, generally lower than 165°C and cooled to surface temperature between the Early and the Late Miocene. Since no regional heat flow transients affected the Carpathian thrust belt in Miocene time, its thermal history has to be entirely ascribed to burial and exhumation history.

Three sectors, characterized by different burial-exhumation histories and topographic, structural and geophysical features were identified in the study region. Burial depths become more homogeneous E-ward. Exhumation is interpreted to have occurred by erosion of the wedge during thrusting in the western sector (23-10 Ma), by erosion and tectonic denudation during post-thrusting extension in the central sector (10-6 Ma) , and by erosion of the wedge during post thrusting uplift in the eastern sector (12-6 Ma). These exhumation processes appear to be consistent with models for the evolution of the Carpathian-Pannonian region that do not comprise slab-related dynamics, such as that based on gravitational collapse. It also appears burial-exhumation history of the Ukrainian Carpathians reflects the regional dynamics of the Carpathian-Pannonian region, whereas that of the Polish Carpathians mainly depends on crustal processes.

RIASSUNTO

L'evoluzione geodinamica della regione Carpato-Pannonica è stata, negli ultimi anni, oggetto di dibattito all'interno della comunità scientifica. Scopo di questa tesi è contribuire alla comprensione dei processi che hanno portato alla formazione di tale territorio. L'analisi termo cronometrica di bassa temperatura si campioni di superficie, associata ad analisi che mirino alla ricostruzione delle paleotemperature permette di definire la storia termica dei campioni, che può essere, a sua volta, utilizzata per rilevare eventuali eventi termici del passato e per ricostruire l'evoluzione temporale ed il pattern spaziale di seppellimento ed esumazione nell'area di studio.

Diversi processi sono stati proposti come rilevanti nell'evoluzione della regione in esame, quali ad esempio subduzione ti tipo A e di tipo B, roll back e break-off di slab in subduzione, risalita astenosferica, collasso gravitazionale. La ricostruzione della storia termica e di seppellimento ed esumazione sono utilizzati, in questo studio, come vincolo che permetta di supportare od escludere alcuni dei processi elencati sopra.

Tre termocronometri di bassa temperatura sono stati utilizzati per datare rocce appartenenti ai Carpazi polacchi ed ucraini; i risultati sono poi stati invertiti per modellare per ciascun campione percorsi tempo-temperatura supportati dai dati. Le storie termiche così ottenute sono poi state integrate con osservazioni sulla assetto strutturale e topografico dell'area in esame e con dati riguardanti la struttura termica della litosfera, e discussi per estrapolare vincoli sulla storia di seppellimento ed esumazione. Infine una raccolta dei dati termocronometrici riferiti all'area di studio, provenienti dal presente studio e da letteratura precedente è stata utilizzata per discuterne la consistenza con i differenti scenari geodinamici proposti per l'evoluzione Neogenica della regione Carpato-Pannonica.

I risultati indicano che i campioni della thrust belt sono stati riscaldati fino a temperature variabili, benché generalmente inferiori ai 650°C, e successivamente raffreddati tra il Miocene Inferiore e il Miocene superiore. Poiché non è stata riscontrata la presenza, nella thrust belt, di evidenze relative a perturbazioni del campo termico durante il Miocene, ne deriva che la storia termica dei campioni in esame è interamente dipendente dalla loro storia di seppellimento ed esumazione.

L'area in esame è stata suddivisa, in fase di discussione, in tre settori caratterizzati da diverse storie di seppellimento ed esumazione e da un diverso assetto strutturale, topografico e dei parametri geofisici. Le profondità di seppellimento raggiunte appaiono progressivamente più omogenee spostandosi lungo strike dal settore occidentale a quello orinetale. L'esumazione della catena è avvenuta per erosione del prisma di accrezione durante il thrusting,nel settore occidentale (23-10Ma), per erosione e denudamento tettonico durante una fase estensionale post-thrusting nel settore centrale, e per erosione del wedge durante il sollevamento post-thrusting nel settore orientale. L'insieme di questi processi esumativi e della distribuzione spaziale del seppellimento lungo la catena sono maggiormente compatibili con modelli evolutivi per la regione Carpato-Pannonica che non comprendano dinamiche legate alla presenza di slab in subduzione, come ad esempio l'ipotesi basata sul collasso gravitativo della litosfera. Infine la storia di seppellimento-esumazione dei Carpazi ucraini è legata a dinamiche litosferiche, mentre quella dei Carpazi polacchi riflette dinamiche esclusivamente crostali.

TABLE OF CONTENTS

CHAPTER I.

INTRODUCTION

1.1. Overview

This study is aimed at reconstructing thermal and burial-exhumation history of the Polish and Ukrainian Carpathians, in order to provide constrains to the debated Neogene evolution of the Carpathian-Pannonian region. This is achieved through the application of low temperature thermochronometry, integrated with observations on the structural and topographic setting and with geophysical data published in previous studies.

In this chapter an introduction to the geology of the study region and to the analytical methodologies used is provided, the scientific questions are detailed and the main contents and the structure of the thesis are briefly outlined.

Figure 1.1 - position of the Carpathians in Europe (from the http://www.carpates.org website)

1.2. Geological setting

1.2.1. Introduction

The Carpathians are a 1500 Km long arc shaped mountain belt, representing the eastern prolongation of the Alps to which they are linked by the strike-slip Vienna Basin. To the south they are in continuity with the Dinarides, and in retro-wedge position they enclose the Pannonian Basin (Fig 1.1, Fig. 1.2 and Fig. 1.3).

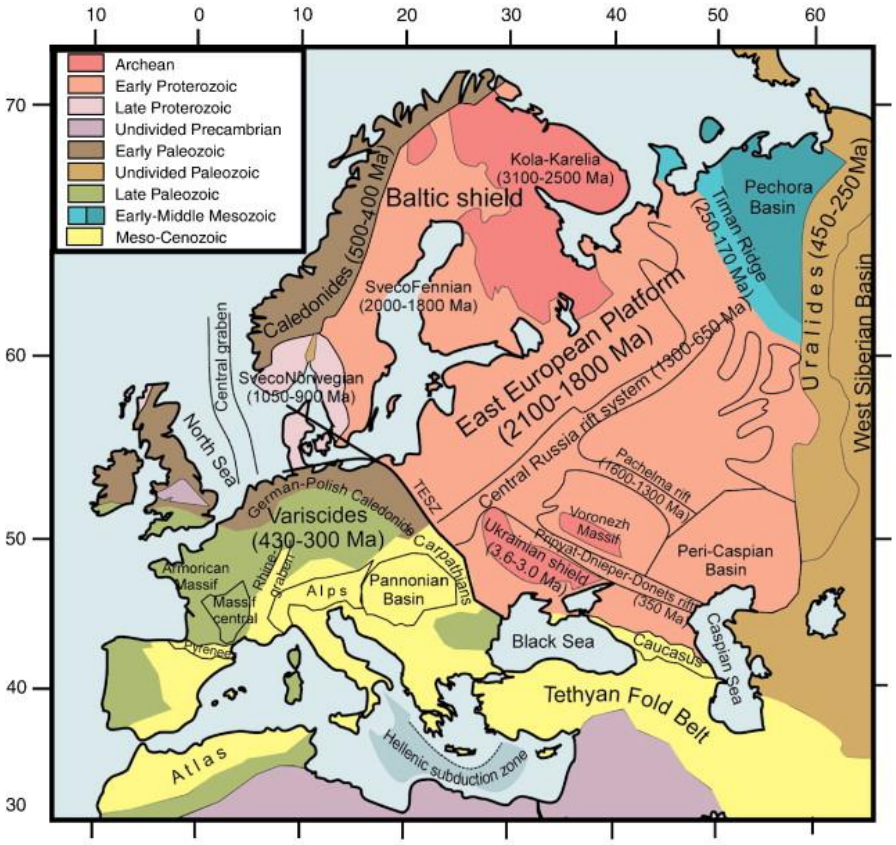

Figure 1.2- Tectonic sketch map of Europe (from Artemieva et al., 2006).)

The chain formed during the Alpine orogenesis by N to SE-ward collision between the ALCAPA (of African origin) and Tisza-Dacia (of European origin) microplates and the European plate (e.g. Jiricek, 1979; Nemcok et al., 1998; Sperner et al., 2002). As can be observed in Fig. 1.2 and Fig. 1.5, Eastern frontal thrust of the Carpathians overlaps with the Trans European Suture Zone (TESZ), that constitute a boundary between the thinner and more weak West European Platform and the thicker and stronger East European Craton (e.g. Phraoh, 1999; Tesauro et al., 2009).

A narrow zone of intensely deformed and sheared Mesozoic to Paleogene rocks, traditionally named “Pieniny Klippen Belt” (PKB, e.g. Birkenmajer, 2001), divides, in the northern and north-eastern Carpathians, the Mesozoic thrust belt, namely the Inner Carpathians (IC) from its accretionary wedge, the Outer Carpathians (OC; Fig. 1.3 and Fig. 1.5 e.g. Tasarova et al.,2009 and references therein).

The IC are made of Ercynian (and pre-Ercynian relics) basement and Meso-Cenozoic sedimentary cover; they underwent a first orogenetic phase between the Early and Late Jurassic due to the collision between the ALCAPA and Tisza-Dacia microplates (e.g. Faryad and Henjes-Kunst, 1997; Golonka et al., 2006). During the Middle-Late Cretaceous they underwent a second phase of deformation, due to the collision between the ALCAPA-Tisza-Dacia terranes and the European Platform (e.g. Golonka et al., 2006, Janak et al., 2001). The OC basin, built on thinned European continental crust, was filled with an Upper Jurassic to Miocene sedimentary succession that was subsequently deformed and accreted to the wedge between Paleocene and Quaternary (being still active in the Southern Carpathians e.g. Golonka et al., 2006; Linzer, 1996 and references

therein). In the Late Early to Late Miocene retro-wedge extension associated to escape tectonics took place, leading to the formation of the Pannonian Basin and shaping the Carpathian-Pannonian region to its present form (e.g. Huismans et al., 2001; Fodor et al., 2011; Kovac et al., 1990). Volcanism related to extension (e.g. Harangi and Lenkey., 2007) also occurred in association to retro-wedge dynamics.

The late Alpine evolution of the chain has been characterized by the progressive migration toward the E and SE of the collision and of all the associated features (e.g. Horváth, 1993; Jiricek, 1979; Sperner et al., 2002). This study focuses on the portion of the chain originated by the collision between the ALCAPA and the European Plates, and, in particular on the Polish and Ukrainian Outer Carpathians.

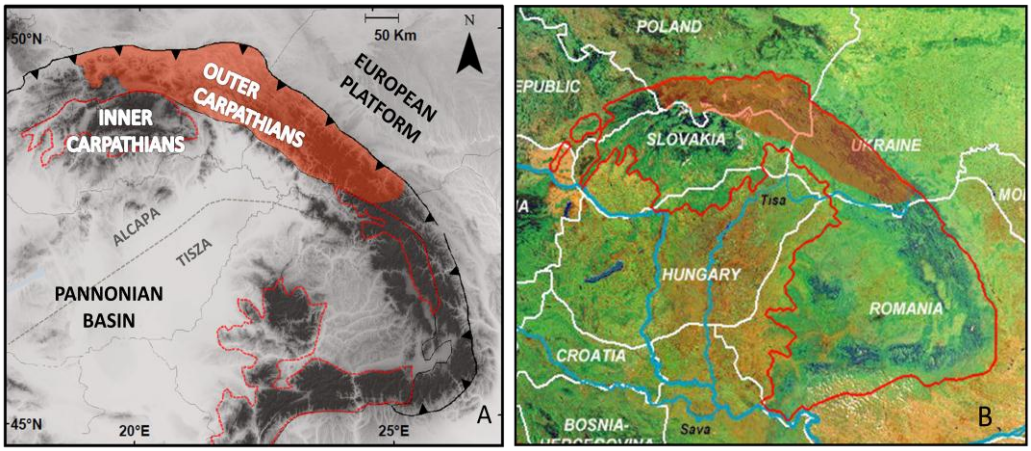

Figure 1.3 - (A) Simplified tectonic sketch of the Carpathians and (B) map of the Carpathians with elevation color code (from the http://www.carpates.org website)

1.2.2. The Polish and Ukrainian Carpathians

In the Polish and Ukrainian portion of the chain the alpine collision occurred between the Early Cretaceous (e.g. Nemeth and Putiš, 2002) and the Middle Miocene (Nemcok et al., 2006, Royden et al., 1992). The main stages of evolution of this portion of the chain are indicated in Fig. 1.4.

As the compressive front progressively turned from N to NE directed, the deformation involved first the westernmost region and it progressively moved eastward. Based on Nemcok et al., 2006 the thrusting terminated by 15.5 Ma in Western Poland, and by 11.5 Ma in Ukraine. In the Middle-Late Miocene, extension in retro-wedge position overlapped with compression at the accretionary front. The Pannonian basin formed as a retro-wedge basin in the IC domain (i.e. the upper plate) through a phase of major extension at 19-11.5 Ma, followed by a phase of minor extension and major subsidence between 11.5 and 5 Ma (Fodor et al., 2011).

In the meantime the innermost portion of the OC domain (i.e. the lower plate) experienced extension as well, as demonstrated by the formation of intramontane basins and occurrence of post-thrusting normal faults. These features are widespread along the Polish sector of the OC (Kovac et al., 1990, Jankowski et al., 2004; Mazzoli et al., 2010), whereas in Ukraine no major evidence of pervading post-thrusting extension can be observed.

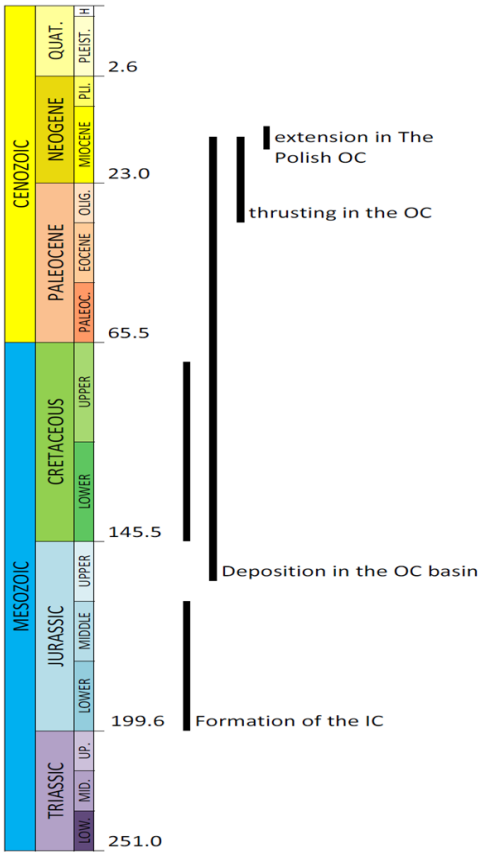

Figure 1.4- Schematic evolution chart of the study area

Some observations on the structure of the study area can be extrapolated from Fig.1.3 , Fig. 1.5 and Fig.1.6:

- In the westernmost sector (between 19° and ca. 21.5° E), to the South of the Flysch Belt, several IC units outcrop, covering an area which extends over 100 Km south of the PKB: The Tatricum, the Veaporicum, the Gemericum and some minor basement blocks and their respective sedimentary covers. South of the IC units the Neogene volcanic complexes bound the area covered by the pannonian sediments. In the Slovak and Polish IC, the Central Carpathian Paleogene basin represents the slightly deformed remnant of a forearc basin where sedimentation occurred between Eocene and Late Miocene. Finally normal faults reactivating and cutting thrusts (Jankowski et al., 2004; Mazzoli et al., 2010) and Neogene intramontane basins (e.g Orava basin) give to the OC in this sector complex structure and a topography characterized by heights and lows.
- In the central sector of the study area, between ca. 21.5° and 22.5° E, the IC units outcrop only along a narrow band immediately to the South of the PKB, as most of the IC domain is covered by the pannonian sediments. On the other hand the Neogene volcanics are the closer along the whole mountain belt to the lower plate (OC deposits). Furthermore the OC belt and its present foredeep reach in this area their maximum width. Finally, as it can be observed in Fig. 1.6 this is the area of the whole mountain belt characterized by the lowermost relief.

- The easternmost sector of the study area, comprised between ca. 22.5° and 25° E, represents the transition between a northern region where no IC unit and little PKB rocks outcrop and the OC sediments are overlain, to the SW, by either the pannonian sediments or the Neogene volcanics, and a southern region (at the boundary between Ukraine and Romania), where IC units outcrop to the SW of the OC, and Neogene volcanics are located further to the hinterland. The change of structural setting along this portion of the mountain belt is accompanied by the transition from a very low to an higher and higher relief (Fig. 1.6), by an higher imbrication of the thrust sheets and by a progressive narrowing of the OC band, whereas no evidence for post-thrusting extension is present. Finally it can be observed that a forearc basin likely to the Central Carpathian Basin is located in the southernmost portion of the study area.

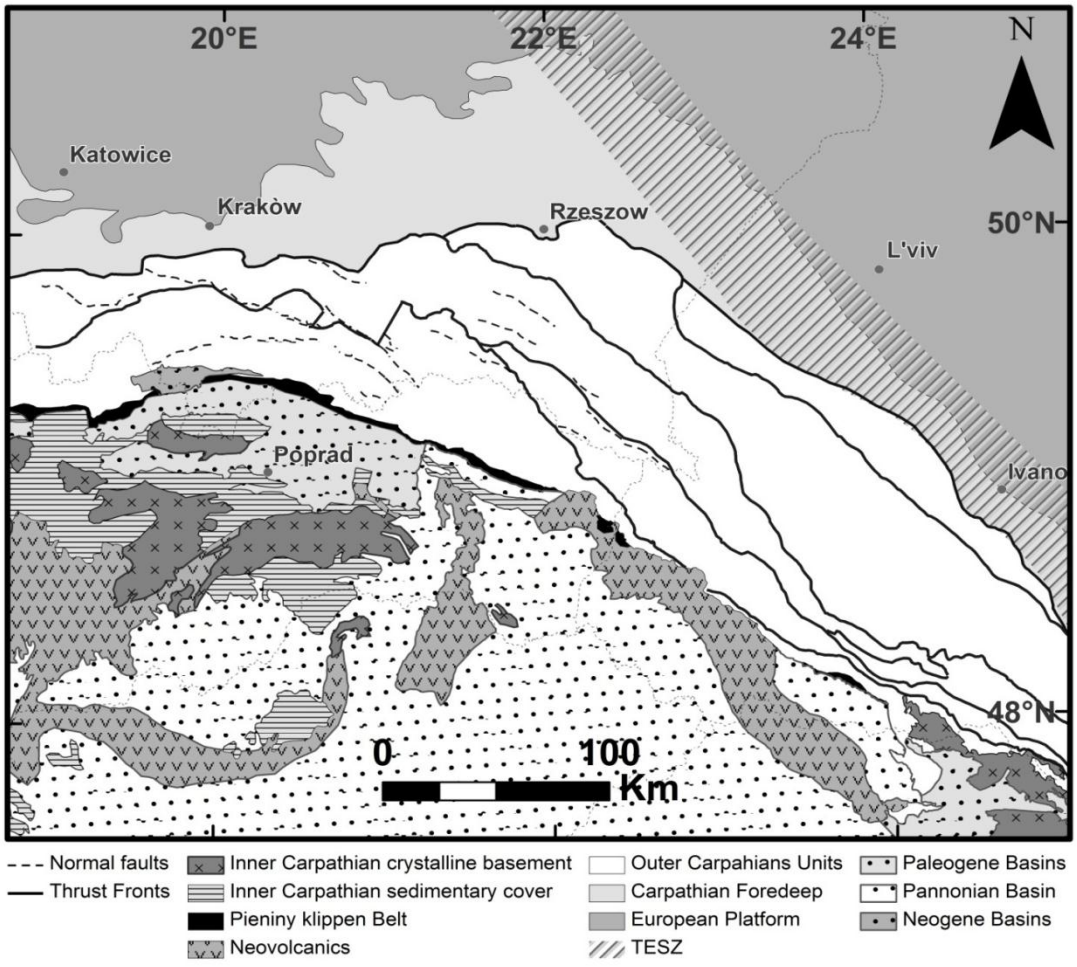

Figure 1.5- Tectonic sketch of the study area

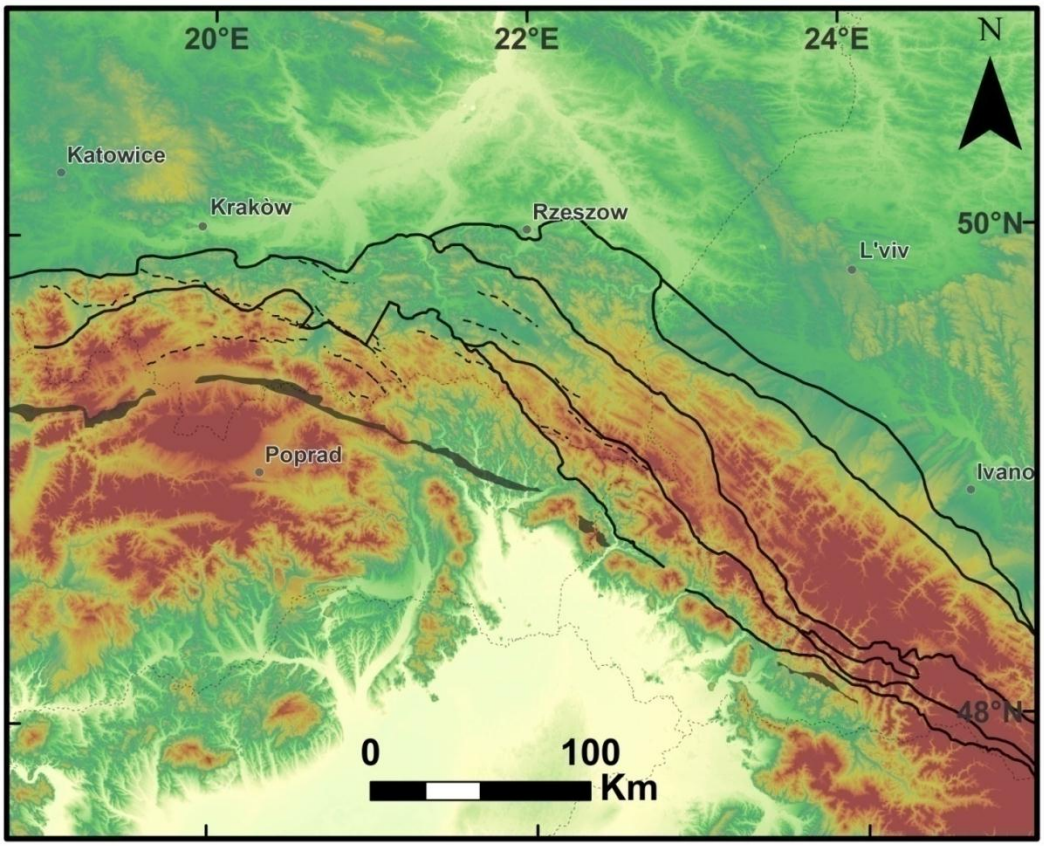

Figure 1.6. DEM of the study area

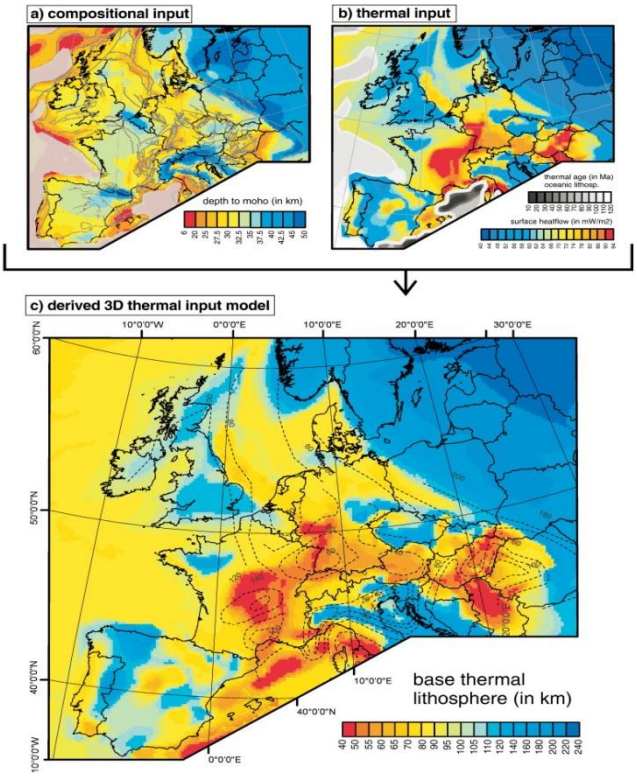

Figure 1.7- Steady state lithosphere thickness derived from surface heat flow and compositional input of the crust and mantle lithosphere (from Cloetingh at al., 2010). (a) Moho depth or crustal thickness (Dèzes and Ziegler, 2004); (b) surface heat flow and; (c) lithospheric thickness (Hardebol, 2010).

1.2.3. Stratigraphic overview of the Polish and Ukrainian Outer Carpathians

The OC, to which most of the samples analyzed in this thesis belong, are made up of a stack of thrust sheets characterized by different lithostratigraphy and tectonic structures. Sedimentary successions were uprooted from their substratum and accreted to the advancing prism between the Oligocene and the Middle-Late Miocene (in the Polish-Ukrainian region, Ślączka et al., 2006.). The sediments that constitute the thrust sheets were emplaced in the OC basin in the time span between the Late Jurassic and the Early Miocene (Ksiazkiewicz, 1962, 1977; Bieda et al., 1963; Mahel et al., 1968; Koszarski and Ślączka, 1976). The OC sedimentary successions testify an early stage of basin opening and progressive deepening between the Late Jurassic and the Kimmeridgian. Between the Tithonian and the Early Cretaceous the OC basin underwent rapid subsidence and deposition of calcareous flyschs, with main provenance from the European Platform occurred. In the Late Cretaceous the IC underwent a major stage of deformation and thrusting N-ward directed. The OC basin started then to be in a foredeep condition, and thick flysch sequences, with provenance mainly from the IC lasted until the Early Miocene. Between the Late Cretaceous and the Early Miocene the depocenters progressively shifted outward and E to SE ward, as described by Meulenkamp et al. (1996). Part of the several tectonic units (i.e. the principal thrust sheets) in which the OC prism is generally subdivided, that have been considered to represent single different sub-basins, can be generally traced along the whole Polish-Ukrainian OC, whereas others are present only in the Ukrainian Carpathians, as can be observed in Fig. 1.5. In Fig. 1.8 and Fig. 1.9, chronostratigraphic charts of respectively the Polish and the Ukrainian OC are reported.

1.2.4. Geodynamic evolution of the Carpathian-Pannonian area: an open question

The traditional and widely accepted interpretation of the Alpine evolution of the Carpathian-Pannonian region comprises subduction of oceanic lithosphere beneath the Alcapa and Tisza-Dacia microplates and subsequent opening of the Pannonian back-arc basin due to progressive slab retreat (e.g. Royden et al., 1992; Horváth et al., 1993). The main elements in favor of active subduction along the carpathian margin are the presence of a fast anomaly beneath the Southern Carpathians (in the Vrancea region) at depths of 60-300 Km (McKenzie, 1970, Fuchs et al., 1979, Wortel and Spakman, 2000; Sperner et al., 2001), the calc-alkaline volcanism that occurred at the boundary between the PB and the Carpathians and the deep (up to 240 Km, Dererova et al., 2006) lithospheric roots that are present beneath some tracts of the Carpathians. Huismans et al. (2001) propose a two stage evolution of extension in the PB: after a first stage of passive rifting induced by slab subduction and roll-back, an active rifting, induced by major astenosphere upwelling would have occurred. Lithospheric thinning higher than crustal thinning (Dererova et al., 2006; Bielik et al., 2004) and high heat flow (Pospisil et al. 2006) in the PB, and late-stage extension related volcanism (e.g Konecny et al., 2002) were interpreted as pieces of evidence for late stage mantle upwelling and active rifting. In this model the volcanic fields that border the PB are interpreted as subduction-related in the first stages and extension-

related in the late stages (Konecny et al., 2002). Horvath et al. (1996) and Sperner et al. (2001), based on the clockwise migration of tectonic activity and of volcanism and on the presence of what is interpreted as a slab remnant beneath the Southern Carpathians, suggest that a progressive slab break-off occurred, starting from the westernmost Carpathians and migrating E-ward and SE-ward.

In recent times several authors argued that the presence of slab subduction beneath the Carpathians is not adequately supported by observations, and several other possible explanations were proposed to justify the Neogene evolution of the Carpathian-Pannonian region.

Kovacs and Szabo (2008) show that even the early-stage volcanism along the PB margins does not necessarily require slab-subduction, being rather related to extension, and thus they propose that mantle flow coupled with eastward extrusion is more likely to have driven the regional evolution. Faccenna et al. (2003) show how astenospheric flows induced by subduction in the Mediterranean region can influence the dynamics of the single orogen, and they suggest therefore that astenospheric dynamics have a major role in the formation of the Carpathian-Pannonian region. Knapp et al. (2005) suggest that a process of lithosphere delamination could have occurred instead of oceanic subduction, being able to justify the high velocity body located beneath the Vrancea zone.

Gemmer and Houseman (2007) and Houseman and Gemmer (2007) demonstrated that gravitational instability of a previously thickened Pannonian lithosphere can induce, if triggered by a collapse of the overlying crust, lateral lithospheric “flow” and downwelling, being therefore able to lead to lithospheric thinning in the PB and lithospheric thickening and compression in the surrounding Carpathians.

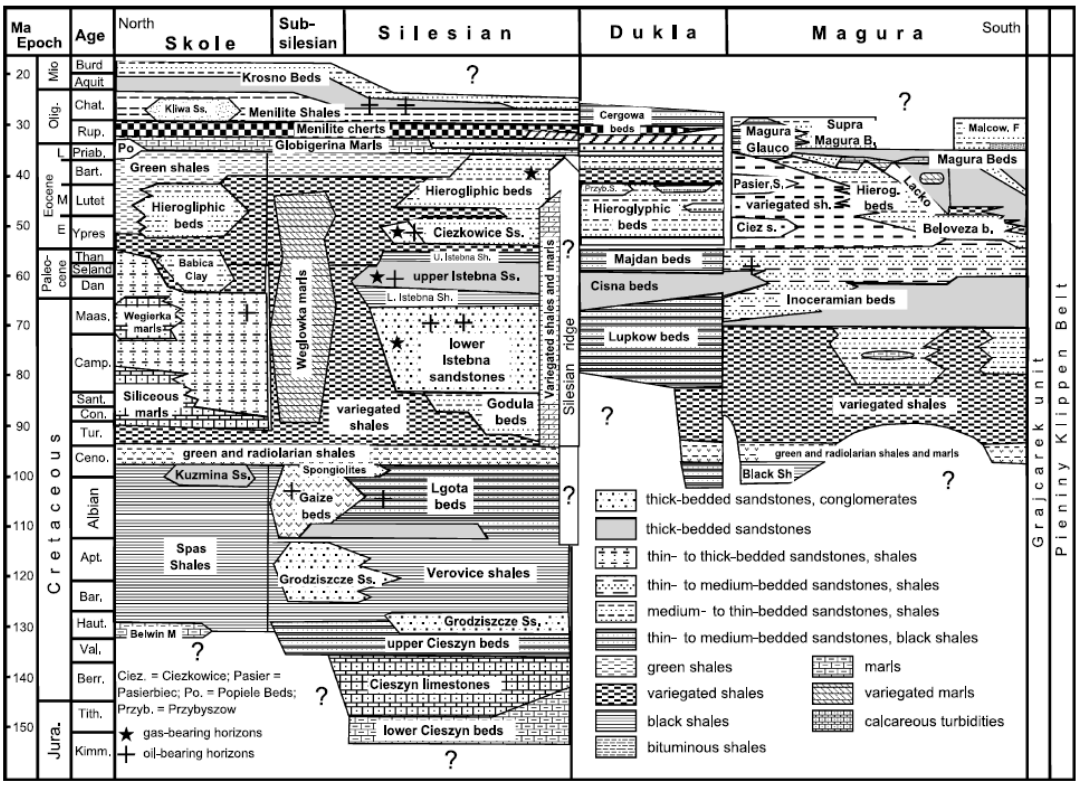

Figure 1.8- Chronostratigraphic chart of the Polish Outer Carpathians (from Golonka e Picha., 2006).

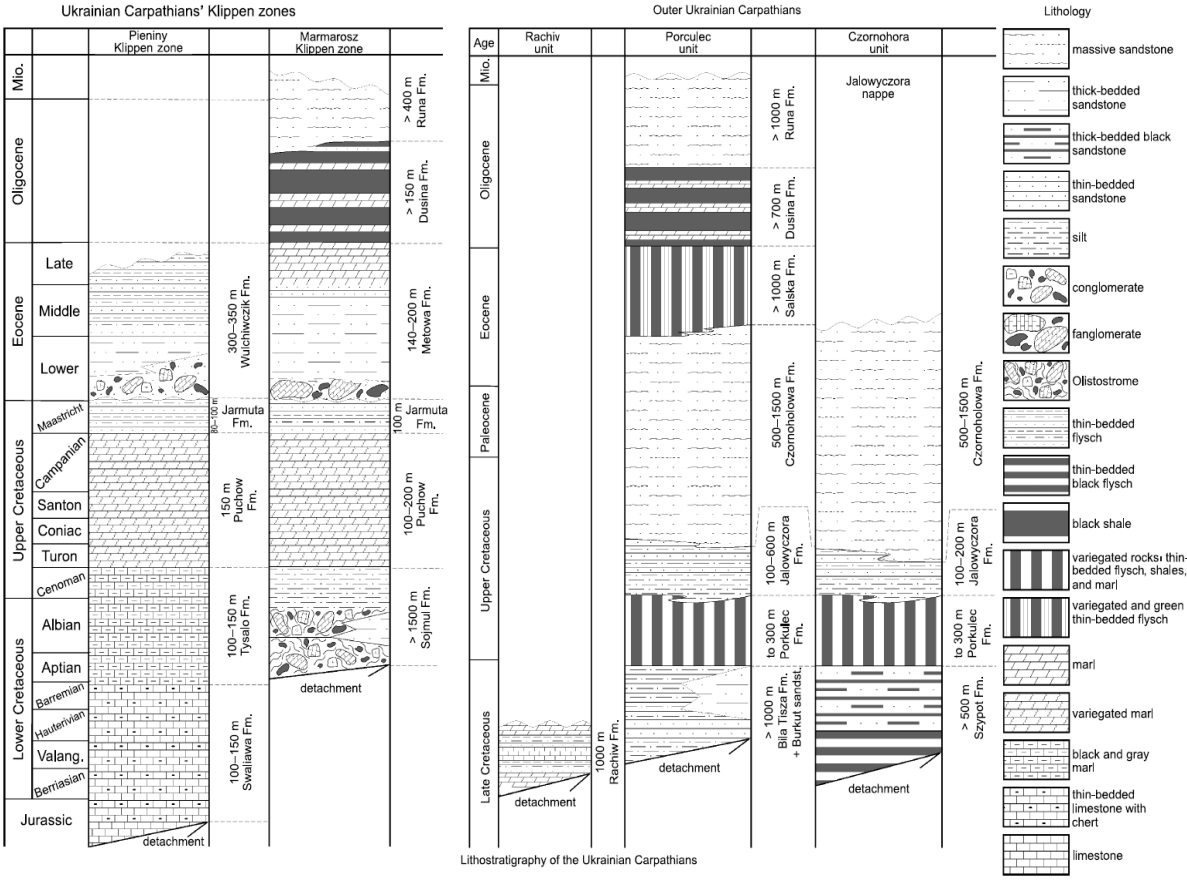

Figure 1.9- Chronostratigraphic chart of the Ukrainian Outer Carpathians (from Golonka e Picha., 2006).

1.3. Goals of the study

This study was aimed to reconstruct thermal and burial-exhumation history of the Polish and Ukrainian Carpathians in order to constrain the Neogene evolution of the Carpathian-Pannonian region. In particular the goals of this study can be summarized in the following points:

Heating and cooling of the thrust belt: were they due to thermal perturbations and/or to burial and exhumation? Did the positive thermal anomaly developed in the Pannonian Basin in the Middle Miocene play a role in heating the Polish and Ukrainian Carpathians?

Burial of the thrust belt: how thick was the eroded section? Was burial due to thickness of the sedimentary pile and/or to thrusts imbrication?

Exhumation of the thrust belt: when did it happen? Was it mainly erosional or tectonic? Was it driven by thrusting, post collisional uplift, extension…else?

Evolution of the Carpathian-Pannonian region: can thermochronology of the outer thrust belt tell us something to constrain it?

In addition, this work provided the opportunity to investigate two additional topics.

The dates of exhumation of the source rocks of the sediments forming the OC could be reconstructed and used for an estimate of the source terrains.

Finally the impact of apatite crystal defects like inclusions, abrasion, coating on reproducibility of apatite (U-Th)/He dates could be evaluated.

1.4. Introduction to methods

Thermochronometry is the discipline that, using different radioisotopic dating techniques, reconstructs the thermal history (thermochronology) of a rock or geologic terrain. Low temperature thermochronology of rocks is sensitive to their burial and exhumation histories in the uppermost portion of the crust (ca. 10-20 Km), and therefore is suitable for studying the recent evolution, in terms of vertical movements, of the mountain belts. Applying thermochronometry to the rocks of a thrust and fold belt allows to reconstruct, if the paleo-geothermal gradient and its evolution in time are sufficiently well known, their burial depth and the timing of their exhumation. In this study the zircon and apatite (U-Th)/He and the apatite Fission Tracks analysis were applied, in order retrace the thermal history of samples up to ca. 170°C and their burial-exhumation history along the uppermost 10-12 Km of the crust.

1.5. Thesis outline

Low Temperature Thermochronometry was applied in this work to address the questions listed above. Sampling, analysis and data discussion were first performed at a bigger scale, and finally the data were discussed at a regional scale.

In **Chapter 2** a synthesis of the background of thermochronometric methods used in this thesis is provided.

Chapter 3 and **Chapter 4** present the results of this thesis, together with a first interpretation. In particular in Chapter 3 the results referred to the Polish sector of the study area are displayed and discussed, whereas Chapter 4 focuses on the Ukrainian sector. The body of both chapters constitute a paper submitted to a scientific journal and additional information not included in the paper is provided in appendix to the chapters.

In **Chapter 5** a discussion of the two integrated datasets is provided and a compilation of the thermochronometric data referred to the portion of the Carpathian belt that formed by collision between the ALCAPA and the European plate is used to discuss the geodynamic implications of this work.

Chapter 6 summarizes the main conclusions of this thesis.

In **Appendix** the facilities and procedures used for sample preparation and analysis are described, and a brief dissertation on the evaluation of reliability of AHe dates of bad crystals is presented.

CHAPTER II.

METHODS

2.1. Introduction

In this chapter the fundamentals of the thermochronometrical methods used in this study are briefly presented. Thermochronometry as a discipline is relatively recent (the first FT papers date back to the 1960s: e.g. Fleischer and Price, 1964; Fleischer et al., 1965; Naeser 1967; Wagner 1968; 1969), and therefore it is subject to a rapid evolution of techniques and its potentialities and fields of application are still being investigated; furthermore many complications both theoretical and technical are still unsolved. Here, based on the plentiful literature available, the well consolidated and widely accepted principles and techniques of such discipline are presented, with the aim not to examine and discuss its details but to provide the reader with an adequate background to the comprehension of the main contents of the present study. The methods hereafter described, including sampling, analysis and interpretation, follow the same routine currently adopted in most of the centers where thermochronometry is performed.

Main references for this and the following paragraph are the synthetic works provided by Reiners, 2005, Reiners and Brandon., 2006.

Details on the analysis and interpretation of data and on complications arose during this work may be found in Chapters 3 and 4 and in Appendix I.

2.2. Principles of thermochronometry and basic glossary

The thermal sensitivity of radioactive systems depends on their tendency to turn from a closed to an open system condition with increasing temperatures. Thermochronometry plays on the sensitivity to a low temperature range (between ca. 30°C and 550°C) of some radioactive systems (**thermochronometers**) to understand thermal histories of rocks and minerals in that temperature range.

Three groups of thermochronometers are currently of common use: the (U-Th)/He and the Fission tracks systems, based on the production of respectively He and lattice defects (fission tracks) by decay of U and Th in U-Th bearing minerals (primarily apatite and zircon) and the $^{40}Ar/^{39}Ar$ systems based on the production of ^{40}Ar by the decay of ^{40}K in K bearing minerals (feldspar, micas, hornblende).

Thermal sensitivities of these thermochronometers can be quantitatively predicted, as the processes of removal of the daughter products of the radioactive decays (i.e. the opening of the system) can be well represented by thermally activated diffusion: this allows to use them to constrain thermal histories of minerals and of host rocks. In Fig: 2.1 the thermal sensitivities (represented by closure temperatures, see the text below for definition) of the most common thermochronometers are indicated.

Thermal history of a rock in such low temperature range results from the interaction between its movements relative to the earth's surface and the crustal thermal field and its variations in

space and time. As a consequence, in some settings and under proper assumptions thermochronometry can be eventually used to infer burial and exhumation history of rocks.
The low-temperature thermochronometers used in this study are the apatite and zircon (U-Th)/He systems (AHe and ZHe) and apatite fission track system (AFT).

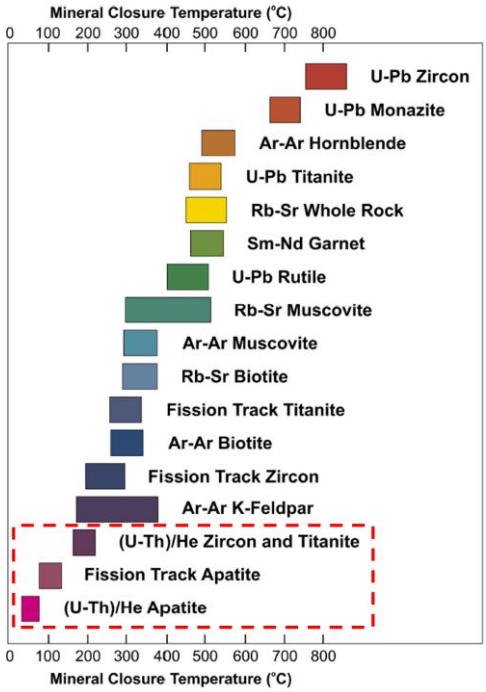

Figure 2.1- Nominal closure temperatures of various geochronometers and thermochronometers (from Gwilym, 2005). Systems are ordered by closure temperature on the Y-axis; the red dashed line indicates the thermochronometers used in this work.

In this work, and more in general in thermochronometry, some words of wide use are meant in a precise meaning, implying the need for a concise glossary.
The closure of a thermochronometer occurs through a range of decreasing temperatures for which the retention of products of the decay by the system progressively increase from 0% at the base (maximum temperature) to 100% at the top (minimum temperature): this temperature interval is defined **Partial Retention Zone** (**PRZ**). To give an estimate of thermal sensitivity of a thermochronometer the **closure temperature** ($\mathbf{T_c}$) concept is often used in place of the PRZ: this is defined as the temperature of a rock at its thermochronometric cooling age, assuming a steady monotonic cooling history. In Fig.2.2. a schematic representation of the PRZ and Tc concepts is presented. The word **reset** is used to refer to rocks that after having been hold for a certain time at low T were heated up to temperatures high enough to re-open the system, before the final cooling to surface temperature.
The word **exhumation** defines the movements of a rock with respect to the earth's surface (Reiners and Brandon, 2006). Exhumation can be either **tectonic** or **erosional** (or a combination of the two), as it always occur by **denudation**, understood as removal of rock or soil by tectonic (normal faulting or ductile thinning) and/or erosional processes (Reiners and Brandon 2006). **Rock uplift** and **surface uplift** are used to describe the vertical motion of a rock or of a portion

of the earth near or at the surface relative to a datum, such as sea level (England and Molnar, 1990; Reiners and Brandon; 2006). In Fig 2.3 the concepts of denudation and uplift are schematically illustrated.

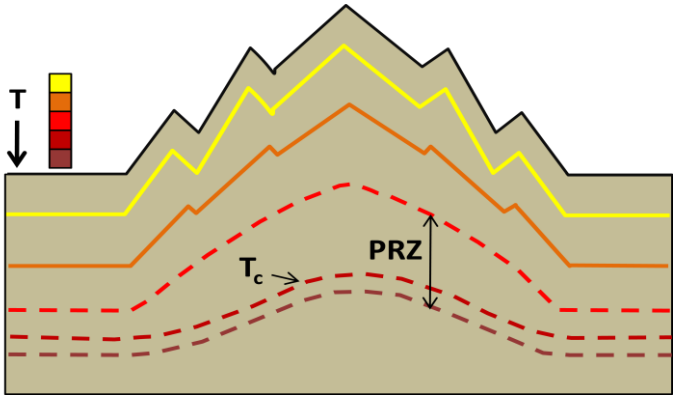

Figure 2.2- schematic representation of the PRZ and Tc concepts. After Vernon, 2008. Colored lines indicate isotherms; dashed lines indicate PRZ bounding isotherms and the Tc isotherm.

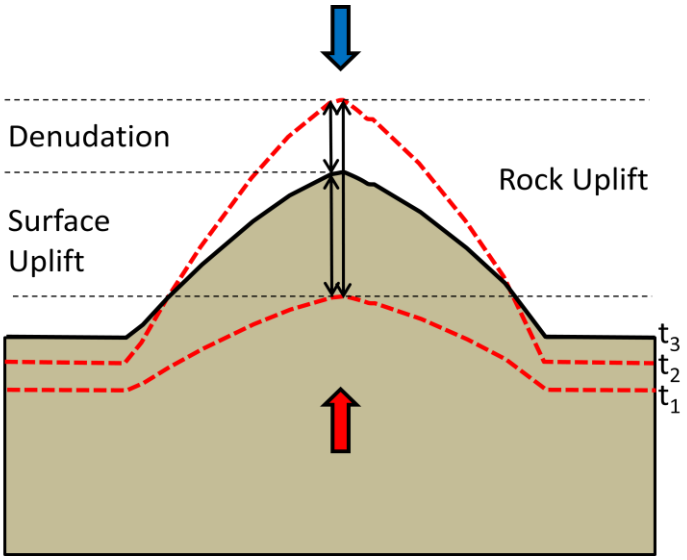

Figure 2.3- schematic representation of the denudation and uplift concepts. Dashed lines indicate paleo surface at times t_1 and t_2, whereas solid black line indicates the present day (t_3) surface. The red arrow indicates the rock uplifting forces (tectonics, buoyancy) and the blue arrow indicates the denudational processes (tectonics, erosion).

Sedimentary samples which has been hold at temperatures too low to open the thermochronometric system typically yield a wide range of ages, representing the cooling ages of their source rocks/terrains. **Detrital thermochronometry** is that branch of the low temperature thermochronometry which plays on this feature to constrain the cooling history of the source terrains of the sediments. A discrimination of the age populations present in the detrital sample is based on the distribution of the grain ages. In detrital thermochronometry the **Lag time** is the time elapsed from the closure of the thermochronometric system to its deposition. Lag time variations of sediments coming from the same orogen provide information on the evolution of the orogen itself: a growing orogen would generate a Lag time decrease in the sediments, whereas a decaying orogen would induce a Lag time increase.

2.3. Interpretation

2.3.1. From thermochronometric data to thermal history

In order to use thermochronometric dates to constrain thermal histories, laboratory stepwise heating experiments are commonly used to calibrate the relationship between decay product retention and temperature and time. The results are integrated with dates of boreholes samples, where present day thermal profile of the crust can be directly measured. Crustal sections exposed by normal faulting are also used to improve the understanding of the retention behavior of thermochronometers as a function of temperature and depth (Reiners and Brandon, 2006 and references therein). These studies give generally concordant results, suggesting that the relationship between daughter products retention and temperature is well understood.

The calibration of kinetic models for the retention of single thermochronometers allows one to define their PRZ and T_c for a given cooling rate. The thermochronometric age has a true temporal meaning by itself only in case of monotonic cooling, when it corresponds to the cooling through the closure temperature.

To reconstruct more complex thermal histories backward thermal modeling is used. Thermal modeling is based on kinetic models and allows to trace the envelope of the thermal histories that well fit the experimental data. The software used in this work for thermal modeling is HeFTy (Ketcham, 2005), which includes the available kinetic models for each thermochronometer. It allows both the inverse and the direct approaches, the second consisting of tracing a thermal history and obtaining thermochronometrical data based on the chosen kinetic models. The gauge of the match between the modeled thermal history and the experimental data is given by the Goodness Of Fit parameter (GOF), which indicates the probability of failing the null hypothesis that the model and data are different. In general a value of 0.05 or higher is considered not to fail the null hypothesis, and thus reflects an acceptable fit between model and data. A modeled thermal history is considered good when it has GOF>0.5 (Ketcham 2008).

2.3.2. From thermochronometric data to burial and exhumation history

Thermochronometric data are related to thermal history, which is in turn related, in most cases, to burial and exhumation history. There are, however several complications in the relationships between the three, since erosion rates influence both the crustal thermal field and the thermal sensitivities of the thermochronometers. In other words changes in erosion rates induce both an increase of the temperatures to which the thermochronometers are sensitive and a thermal advection of the isotherms, resulting in much younger thermochronometric ages. In Fig. 2.4. an example of such effect is shown (from Reiners and Brandon, 2006).

Thus, given a certain crustal thermal model, thermochronometric ages can be uniquely related to erosion rate only assuming it having been steady prior as well as after the closure of the

system. Shallow isotherms are able to recover more rapidly from transients, therefore the lower the T_c of the thermochronometer, the safer the assumption of steady state.

Under the assumption of a certain thermal field and of steady state erosion rate closure temperature and closure depth can be estimate, and the range of possible erosion rates can be defined. Changes in erosion rates with time can be estimate from measurements of multiple cooling ages from the same rock, taking care in considering transient thermal effects.

To this purpose vertical age transects are also of common use: the slope of age-elevation relationship constituting an estimate of erosion rate in the time interval of the cooling ages.

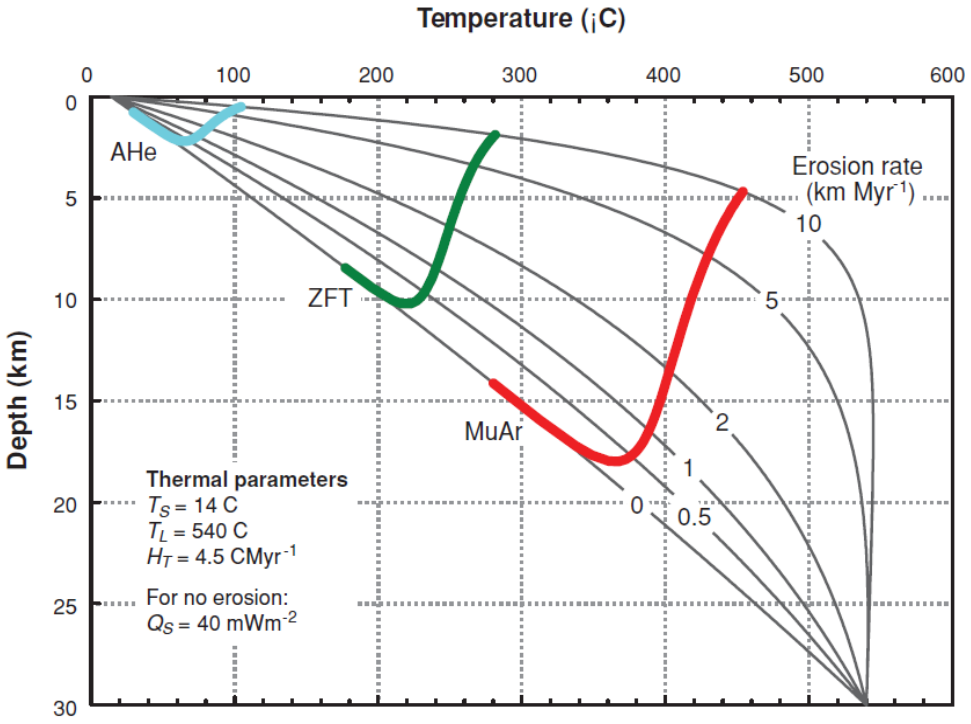

Figure 2.4. – Influence of erosion rate on the thermal profile and closure temperatures at steady state (Reiners and Brandon, 2006). The thermal profiles are steady-state solutions for a one-dimensional thermal field with a steady erosion rate. Temperature is held fixed at the top and bottom of a 30-km thick infinite layer. Erosion is represented by a steady velocity through the layer. The specific thermal parameters used for this model are based on the northern Apennines of Italy, which is a fairly typical convergent orogen. The color lines show the effective closure temperature for apatite He (AHe), zircon fission track (ZFT), and muscovite Ar (MuAr) as a function of increasing erosion rate.

2.4. Helium Thermochronometry

2.4.1. Introduction

(U-Th)/He dating is based on the α-decay of Uranium and Thorium. U-He radioisotopic system was discovered by Ernest Rutherford in the first decade of the 19th century. After a first flowering of He dating in the scientific community of that time, the method was gradually abandoned in the next few decades. By about 1940, when U-Pb dating became widely available, it also became evident that He dating provided, in most cases, largely underestimated formation ages, and He loss was recognized to be responsible for such underestimation (Reiners, 2001).

Only in 1987 Zeitler et al. first suggested that He ages could represent cooling rather than formation ages, opening the way to He thermochronometries.

In this section principles and applications of He thermochronometers are presented. The main references used, to which the reader is addressed for a deeper and wider study are the papers provided by Braun et al., 2006; Ehlers and Farley, 2003; Farley, 2000; Reiners and Brandon, 2006; Reiners, 2001; Reiners, 2004.

2.4.2. He ingrowth

(U-Th)/He thermochronometry is based on the production of He nuclei (α particles) by the U and Th decay series and, to a minor extent, by α- decay of ^{147}Sm. The equation for He ingrowth in time (t) is

$$1) \quad {}^{4}He = 8^{238}U(e^{\lambda_{238}t}-1) + 7^{235}U(e^{\lambda_{235}t}-1) + {}^{232}Th(e^{\lambda_{232}t}-1) + {}^{147}Sm(e^{\lambda_{147}t}-1)$$

where **He**, **U**, **Th** and **Sm** refer to present-day amounts, and **λ** is the decay constant ($\boldsymbol{\lambda}^{238}$ = 1.551 × 10^{-10} yr^{-1}; $\boldsymbol{\lambda}^{235}$ = 9.849 × 10^{-10} yr^{-1}; $\boldsymbol{\lambda}^{232}$ =4.948 × 10^{-11} yr^{-1}; $\boldsymbol{\lambda}^{147}$=0.654× 10^{-11} yr^{-1}). The coefficients preceding the U and Th abundances account for the multiple α particles emitted within each of the decay series.

This equation can be simplified, since the $^{238}U/^{235}U$ ratio has in the solar system a constant value of 137.88 (Steiger and Jäger, 1977).^{235}U can be then written as a function of ^{238}U and the ingrowth of helium with time can be written as a function of the elemental U, Th and He abundances or concentrations.

The He ingrowth equation assumes absence of ^{4}He, both initial and produced by sources extraneous to the crystal, and secular equilibrium among all daughters in the decay chain. In case of zircons these assumptions are valid in most cases, whereas, due to the lower U and Th content typically yielded by apatites, for such mineral phase the presence of external sources of He can be represented by U-Th rich inclusions (zircons, monazite) or coating (oxides and oxhydroxide). In this case a most careful selection of the grains to be analyzed is required.

2.4.3. Analytical procedures

Grain selection and packing are made under optical stereoscope. Intact, prismatic, unabraded and, inclusion free grains, are preferably selected for analysis. Selected grains are then digitally photographed and geometrically characterized by measuring each grain for its prism length (parallel to the c axis) and prism width in at least two different orientations (perpendicular to the c axis). Grains are than packed in Nb or Pt tubes or foils (Fig. 2.5.). A two-stage analytical procedure is commonly used to measure ^{4}He, U, Th and Sm. In the first stage the crystal is degassed by heating and ^{4}He is measured by gas-source mass spectrometry. In the second stage, after chemical dissolution of the crystal, U, Th and Sm contents are measured by inductively coupled plasma mass spectrometry.

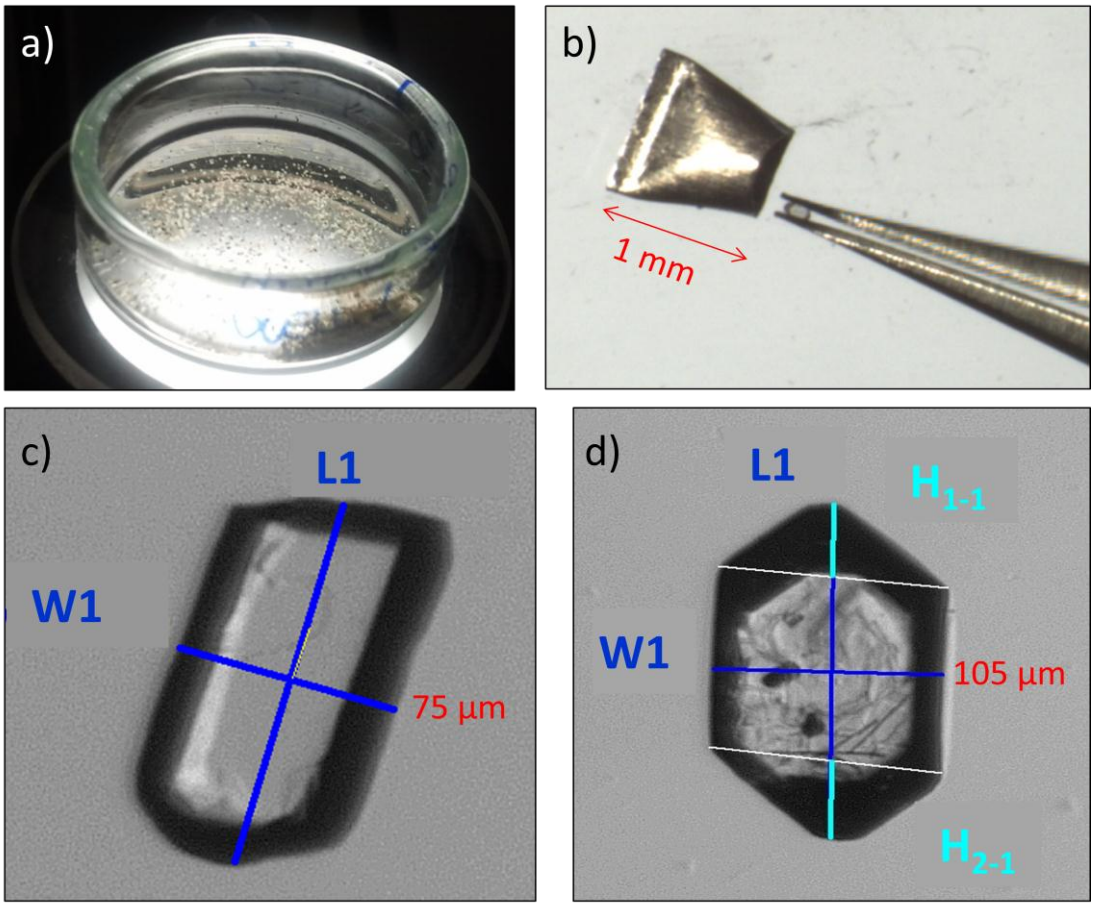

Figure 2.5. – Grain selection and picking: the grains are poured in a petri-dish for grain selection under optical microscope (a); the selected grains are photographed and measured, for apatite length (L) and width (W) are measured on two sides parallel to the c-axis (c) , for zircons the tips heights (H1, H2) are also measured (d). Grains are finally packed in Nb tubes (b).

2.4.4. α –ejection correction

The measurements described above account for the bulk He, U, Th and Sm contents, however the resulting dates require a correction for He loss occurred by ejection of α particles outside the crystal domain.

As a matter of facts, since the α particles emitted by U, Th and Sm travel a distance of ca. 20 µm, part of those emitted close to the crystal edges are ejected out of the crystal and injected in the surrounding phases (Fig. 2.6.). The loss of α particles leads to an underestimation of the age of the crystal. The magnitude of α-ejection is controlled by surface to volume ratio and by spatial distribution of the parent atoms relative to the crystal surface. Assuming an idealized geometry of the crystal and an homogeneous distribution of U, Th and Sm in the crystal, the fraction of He retained can be calculated as a function of the crystal size, as described by Farley (2002).

Therefore, to account for α-ejection it is a common practice to measure the physical dimensions of the crystal to be dated and to calculate an homogeneous α-ejection correction factor (HAC), to which the raw date has to be multiplied, to obtain the age corrected for ejection (Farley, 2002).

The assumption of homogeneous distribution of parent nuclides is in some cases unsatisfied due to the frequent occurrence of internal zonation: since zonation is a random feature, it affects age reproducibility between different crystals of the same sample: poor age reproducibility can be therefore caused by the application of α-ejection correction to zoned crystals (e.g. Ehlers and Farley, 2003).

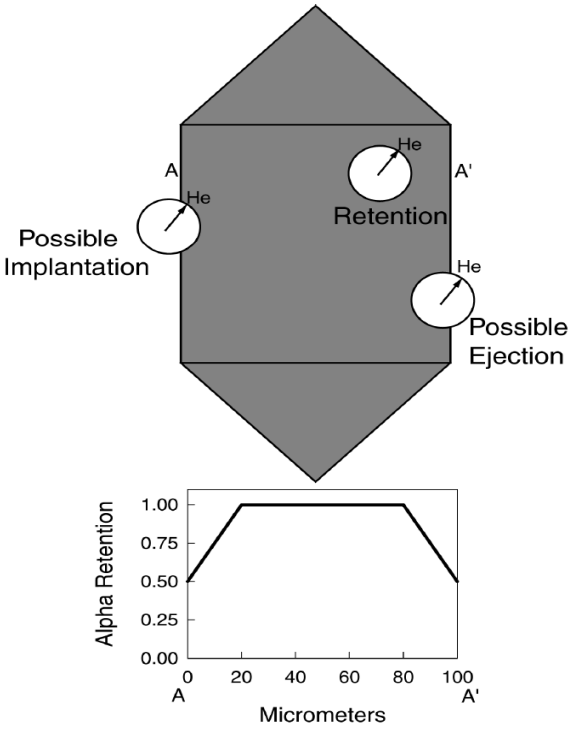

Fig. 2.6. – The effects of long α–stopping distances on He retention (from Farley, 2002) . The upper figure illustrates the three possibilities within a schematic crystal: α retention, possible α ejection, and possible α implantation. The center of the circle denotes the site of the parent U or Th nuclide, and the edge of the white circle labeled He indicates the locus of points where the α particle may come to rest; the arrow indicates one possible trajectory. The lower plot shows schematically how α retention changes from rim to core to rim along the path A-A'; exact equations defining the shape of this curve as a function of grain size were given by Farley et al. (1996).

2.4.5. Diffusion behavior

In order to use He dates to constrain thermal histories, an accurate knowledge of He diffusivity in the dated phases is required. Laboratory stepwise heating experiments have commonly been used to calibrate the relationship between diffusivity and temperature (e.g. Farley, 2000; Fechtig and Kalbitzer, 1966; Shuster et al., 2006), that is demonstrated to be well described by the Arrhenius relationship formulated as follows (Fechtig and Kalbitzer, 1966):

$$2) \quad \frac{D}{a^2} = \frac{D_0}{a^2} e^{\frac{-E_a}{RT}}$$

Where $\mathbf{D_0}$ is the frequency factor, that is diffusion at infinite temperature (m^2s^{-1}), $\mathbf{E_a}$ is the activation energy (J mol^{-1}), **T** is the temperature (K), **R** is the gas law constant (8.3145 J mol^{-1} K^{-1}) and **a** is the radius of the spherical diffusion domain (m; Fechtig and Kalbitzer 1966). The

diffusion domain size (a) corresponds, in most cases, to the crystal size (Farley, 2000; Reiners and Brandon, 2006), implying a dependence of T_c and PRZ on the grain size.

Kinetic models for He diffusion comprise the diffusion equation and the diffusion parameters (Ea, D0).

The currently accepted and most used model for He diffusion in apatite is that proposed by Farley (2000), based on the equation (2), nevertheless subsequent models have been proposed to account for radiation damages effect on He diffusivity. Shuster et al. (2006) demonstrated that, in fact, diffusivity generally decreases with increasing He content. This is interpreted to be due to the effects of He trapping by α-recoil lattice damages. Shuster et al. (2006) proposed then a kinetic model were diffusivity is a function of [He], and where the annealing of traps occurs with the same kinetics as He loss. Subsequent work by Shuster and Farley (2009) pointed out that trap annealing may correspond to fission track annealing. This implies that [He] is an inadequate proxy for traps as it diffuses out of the crystal earlier than trap annealing. Therefore Flowers et al.(2009) proposed a Radiation Damage Accumulation and Annealing Model (RDAAM) which uses the fission track annealing model of Ketcham (2007b) to characterize diffusivity-altering damage annealing.

As for He diffusion in Zircon the currently used diffusion model is that proposed by Reiners et al., 2004, also based on equation (2). An effect of radiation damages on He diffusion in zircons has also been demonstrated (e.g. Damon and Kulp; 1957), nevertheless a kinetic model accounting for such effect has not been formulated so far.

The diffusion parameters obtained by calibration of the diffusion equation through step heating experiments are used to estimate the PRZ and the T_c for He thermochronometers of given grain size and for given cooling rates.

PRZ for AHe varies between ca. 20°C and 60°C (Reiners and Brandon, 2006; Fig 2.7.), whereas closure temperatures are in the range 40°C-80°C (Fig. 2.8; Tab 2.1), for cooling rates of 10°C/Ma and diameter of the spherical domain of 60 µm, AHe T_c=67°C (Reiners and Brandon, 2006). As for ZHe the PRZ ranges between ca. 90°C (for hold time higher than 250 Ma) and 185°C (for minimum hold time; Fig 2.7); T_cs range between ca. 140°C and 200°C (Fig. 2.8; Tab. 2.1); e.g. for a 60 µm grain diameter and a cooling rate of 10°/Ma, T_c=183°C Tab 2.1.

Method (references)	E_a (kJ mol^{-1})	D_0 (cm^2 s^{-1})	a_s^* (μm)	Ω** (s^{-1})	$T_{c,10}$*** (C)
(U-Th)/He apatite (Farley 2000)	138	50	60	7.64×10^7	67
(U-Th)/He zircon (Reiners et al. 2004)	169	0.46	60	7.03×10^5	183
(U-Th)/He titanite (Reiners & Farley 1999)	187	60	150	1.47×10^7	200
FT apatite[1] (average composition[2]) (Ketcham et al. 1999)	147	—	—	2.05×10^6	116
FT Renfrew apatite[3] (low retentivity) (Ketcham et al. 1999)	138	—	—	5.08×10^5	104
FT Tioga apatite[3] (high retentivity) (Ketcham et al. 1999)	187	—	—	1.57×10^8	177
FT zircon[1] (natural, radiation damaged) (Brandon et al. 1998)	208	—	—	1.00×10^8	232
FT zircon (no radiation damaged) (Rahn et al. 2004, fanning model)	321	—	—	5.66×10^{13}	342
FT zircon (Tagami et al. 1998, fanning model)	324	—	—	1.64×10^{14}	338

*a_s is the effective spherical radius for the diffusion domain. Shown here are typical values.
**Ω for FT thermochronometers is measured directly from experimental heating experiments and is equal to $55 D_0 a_s^{-2}$ for He and Ar thermochronometers.
***$T_{c,10}$ is the effective closure temperature for 10°C Myr^{-1} cooling rate and the specified a_s value.
[1]Recommended values for most geologic applications.
[2]Average composition was taken from table 4 in Carlson et al. (1999). Equation 6 in Carlson et al. (1999) was used to estimate $r_{mr\,0} = 0.810$ for this composition. Closure parameters were then estimated using the HeFTy program (Ketcham 2005).
[3]Closure parameters were estimated from HeFTy and $r_{mr\,0} = 0.8464$ and 0.1398 for Renfrew and Tioga apatites, respectively, as reported in Ketcham et al. (1999).

Table 2.1- Closure parameters for He and FT thermochronometers (From Reiners and Brandon, 2006)

Method (references)	Retention level	E_a (kJ mol^{-1})	Ω[1] (s^{-1})
FT apatite[2] (average composition[3])	90%	127	2.67×10^5
(Ketcham et al. 1999)	10%	161	1.55×10^7
FT Renfrew apatite[4] (low retentivity)	90%	124	1.91×10^5
(Ketcham et al. 1999)	10%	150	4.39×10^6
FT Tioga apatite[4] (high retentivity)	90%	140	1.41×10^6
(Ketcham et al. 1999)	10%	232	3.38×10^{10}
FT Durango apatite	90%	160	1.02×10^{12}
(Laslett et al. 1987, Green 1988)	10%	195	2.07×10^{12}
FT zircon[2] (natural, radiation damaged)	90%	225	2.62×10^{11}
(Brandon et al. 1998)	10%	221	1.24×10^8
FT zircon (no radiation damage)	90%	272	5.66×10^{13}
(Rahn et al. 2004, fanning model)	10%	339	5.66×10^{13}
FT zircon	90%	231	1.09×10^{12}
(Tagami et al. 1998, fanning model)	10%	359	1.02×10^{15}

[1]Ω for FT thermochronometers is measured directly from experimental heating experiments.
[2]Recommended values for most geologic applications.
[3]Average composition was taken from **Table 4** in Carlson et al. (1999). Equation 6 in Carlson et al. (1999) was used to estimate $r_{mr\,0} = 0.810$ for this composition. PRZ parameters were then estimated using the HeFTy program (Ketcham 2005).
[4]PRZ parameters were estimated from HeFTy and $r_{mr\,0} = 0.8464$ and 0.1398 for Renfrew and Tioga apatites, respectively, as reported in Ketcham et al. (1999).

Table 2.2- Retentivity parameters for FT thermochronometers (from Reiners and Brandon, 2006)

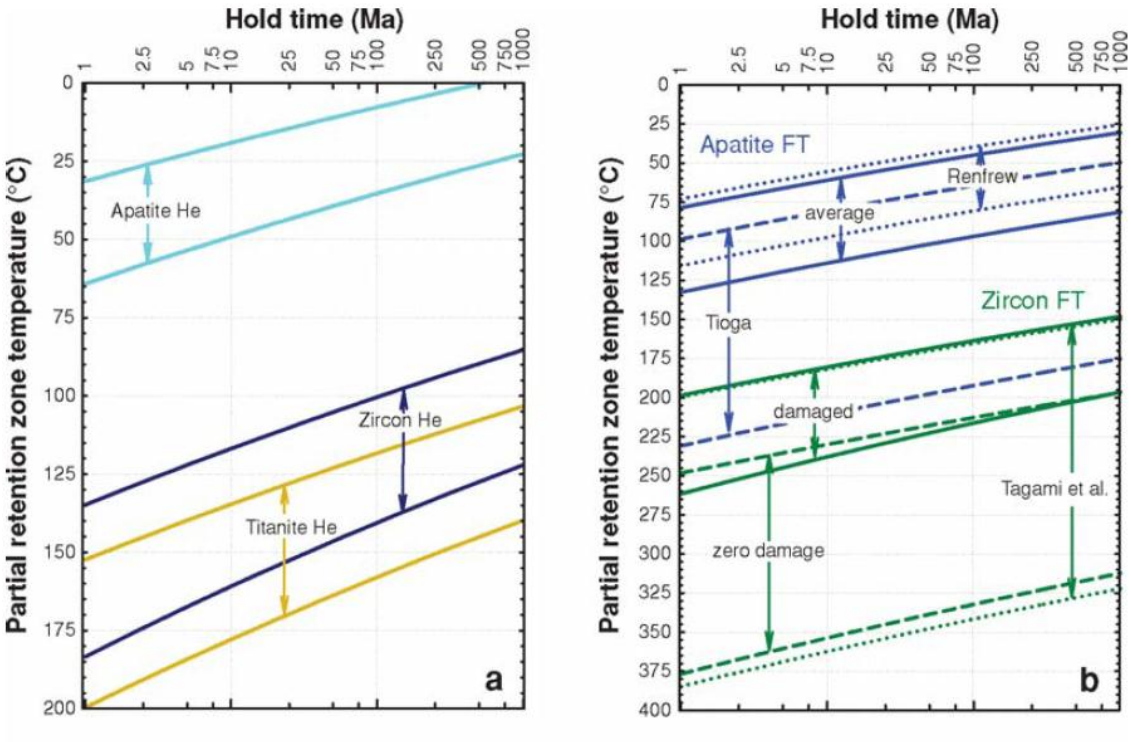

Figure 2.7. – Partial Retention Zones for He and FT thermochronometers as a function of hold time (from Reiners and Brandon, 2006). The upper and lower boundaries indicate respectively 90% and 10% retention; estimates were determined using the Closure program with parameters in Tab. 1 and 3 of Reiners and Brandon, 2006.

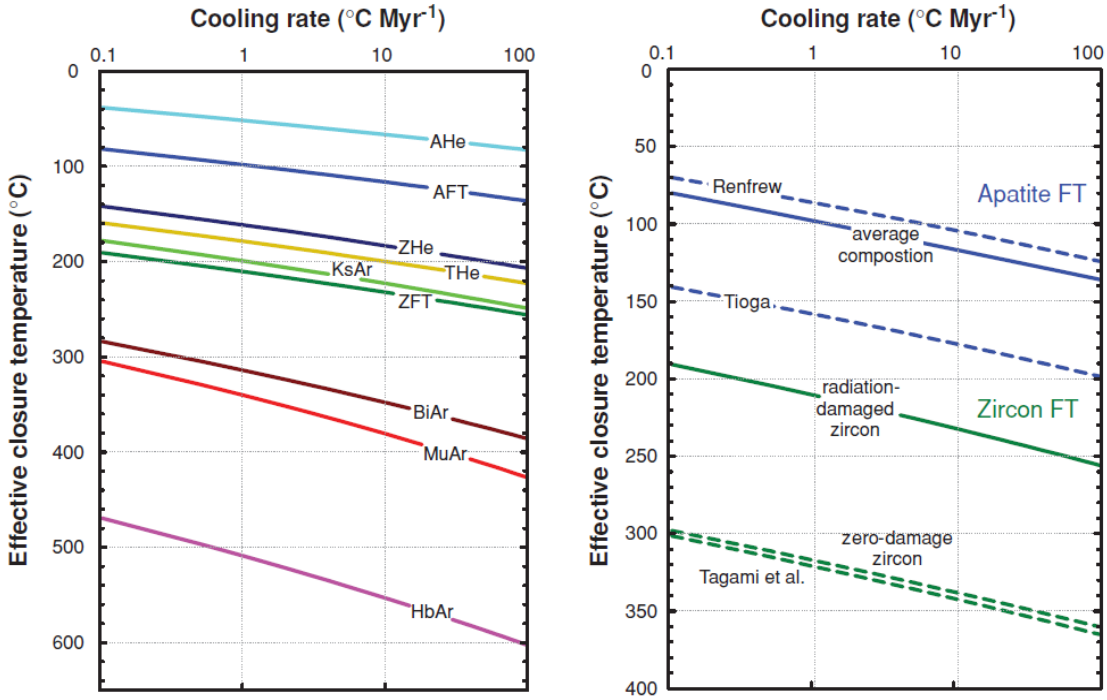

Figure 2.8. – Effective closure temperature (Tc) as a function of cooling rate for common He, FT, and Ar thermochronometers (from Reiners and Brandon, 2006). Estimates shown here are based on Equation 7 and parameters in Tables 1–2. Results were calculated using the CLOSURE program.

2.4.6. *The effect of slow cooling*

Actually the transition from retention to diffusion of radiogenic He can occur to be slow or incomplete. This is particularly true for samples which underwent slow cooling or prolonged stay in the PRZ. For such samples the thermochronometric ages have no meaning in terms of temperature, representing instead a more complex thermal history (Reiners 2001). In fact, the magnitude of the effect on age of subtle factors controlling He diffusion (like zonation, , crystal size, kinetic parameters) increases with decreasing cooling rates (Ehlers and Farley, 2003). Most of all, crystal size (of intact crystals) tends to correlate with age in case of slow cooling, since it affects both α-ejection and He diffusion kinetics. The correlation between crystal size and age may be then used to model thermal histories of samples that slowly cooled through the He PRZs.

2.4.7. *Data analysis and Interpretation*

In most studies 3 to 5 replicates of the same rock sample are analyzed. An example of the output spreadsheet is shown in Fig. 2.9, containing both the absolute content and the concentrations of the analyzed elements/isotopes, and both the raw and HAC corrected age values. The data are then processed to test their significance and their meaning.

Age reproducibility of crystals belonging to the same rock sample is first checked. In case of well reproducible samples the weighted mean of ages can be used for interpretation (as suggested by Fitzgerald et al., 2006) and the T_c concept can generally be applied, whereas in case of high dispersion single grain ages are preferably shown. As described in previous paragraphs many sources of age dispersion may be present.

sample	replicate	Th/U (atomic)	raw age (Ma)	±σ (Ma)	mass (μg)	mwar (um)	U (ppm)	Th (ppm)	Sm (ppm)	4He (nmol/g)	HAC	eU (ppm)	corrected age (Ma)	±σ (Ma)
PL 1	BA PL1_01	13.46	7.3	0.2	3.0	55.8	4.1	53.6	77.4	0.67	0.72	16.7	10.2	0.3
	BA PL1_05	0.74	7.3	0.1	2.0	40.0	54.4	39.5	136.4	2.53	0.66	63.6	11.1	0.2
	BA PL1_07	19.23	6.0	0.2	1.8	40.5	2.9	53.4	61.3	0.51	0.63	15.4	9.5	0.4
	BA PL1_09	22.44	4.1	0.2	1.4	42.3	5.4	117.1	337.2	0.73	0.64	32.9	6.3	0.4
	BA PL1_10	3.99	6.1	0.1	1.5	42.3	66.8	259.9	149.2	4.23	0.66	127.9	9.2	0.1
PL 5	BA PL5_01	0.42	9.5	0.2	0.9	34.0	87.9	36.3	341.2	4.99	0.59	96.4	16.1	0.3
	BA PL5_07	0.15	15.8	0.3	1.1	35.8	114.3	16.7	364.8	10.11	0.65	118.2	24.2	0.5
	BA_PL5_06	0.14	10.0	0.3	0.7	30.8	94.2	12.7	187.7	5.26	0.61	97.2	16.5	0.5
	BA_PL5_08	2.23	8.0	0.2	1.6	39.8	20.0	43.4	371.2	1.32	0.66	30.2	12.1	0.4

Figure 2.9. – He output data.

If age dispersion is only due to **differences in grain size** in crystals of a slowly cooled sample, then a correlation between grain age and radius will be observed. In this case age dispersion adds further information to the reconstruction of the thermal history of the sample.

In case age dispersion is due to **radiation damages** a correlation between grain age and eU should be observed. Also in this case dispersion do not preclude to use dates for reconstructing thermal histories, provided the RDAAM model of Flowes et al. (2009).

Age dispersion occurs in **partially reset samples** as well as in **unreset detrital samples**. Incomplete or null reset of detrital samples also implies that part or all of the LAG times are ≥0; in other words part or all of the depositional ages are younger than thermochronometric ages.

In case the sample is completely unreset ages actually indicate the cooling of the source rocks prior to erosion, transport and deposition. Thus ages from detrital unreset samples can be used for detrital thermochronology, which statistics usually require a larger number of data. On the other hand, partially reset ages cannot be used to infer information on the cooling of neither the detrital sample nor the source rocks.

In all the cases described above age dispersion can then be used to obtain information on the thermal history of the sample.

Nonetheless age dispersion can also be induced by crystal defects: in this case dispersion has no meaning in terms of thermal history, being due to the presence of biased ages.

- **zonation, inclusions and coating** may also tend to induce age dispersion, by leading to a violation of some of the the fundamental assumptions for He dating and HAC, such as uniform U-Th distribution in the crystal and absence of external He sources. In this case a correlation between age and U-Th contents (often expressed as effective uranium, eU= [U] + 0.235×[Th]) could be observed;
- Features like **abrasion and rounding** may also induce incorrect application of the HAC.
- Dispersion may be finally arising from **fractured and/or broken crystals** to which the model for diffusion kinetics and possibly the HAC are improperly applied.

2.5. Fission Track thermochronometry

2.5.1. Introduction

Fission track thermochronometry is based on the production of narrow lattice damages by the spontaneous fission of U. Such dating method has been widely used in the last 30+ years to constrain thermal histories in many geological settings. Early work by Naeser (1967) and Wagner (1968, 1969) first established the basic procedures that enabled FT dating to be routinely applied to geological problems. Fleischer et al. (1975) summarized the early studies of the broader discipline of nuclear track detection in solid state materials. More recent comprehensive overviews of fission track applications have been provided by Naeser and McCulloh (1989), Wagner and Van den Haute (1992), Gallagher et al. (1998), Van den Haute and De Corte (1998), Dumitru (2000) and Gleadow et al. (2002). The synthetic works of Tagami and O'Sullivan, 2005; Donelick et al., 2005; Reiners and Brandon., 2006; Braun et al., 2006, are used as main references for this paragraph, which presents an overview of the fission tracks (FT) dating method. Since in this PhD work apatite has been the only mineral phase dated by FT, this chapter deals in particular with the AFT dating method.

2.5.2. Formation of fission tracks

The FT analysis uses the radioactive system composed by ^{238}U and linear lattice damages (fission tracks) produced by its spontaneous fission in apatite and zircon (e.g. price and Walker, 1963; Fleischer et al., 1975). The assumption that fission tracks are generated only by decay of ^{238}U is

based on the low abundance/low decay constant of other isotopes decaying by spontaneous fission (Tab. 2.3.).

When an heavy unstable nucleus decays by spontaneous fission it splits into two nuclear fragments which are pushed away to each other by a combination of energy released by the nuclear fission and coulomb repulsion forces. The passage through the crystal lattice of the two positively charged nuclear fragments induces a change of electrostatic charge in the surrounding lattice region. Charge variation induces, in turn, widespread dislocation of atoms from their lattice positions, generating the high defect density which characterizes fission tracks (Fig. 2.10.; Ion explosion spike theory, Fleischer et al., 1965; 1975). Fresh FT have lengths of ca. 11 µm in zircon and ca. 16 µm in apatite (Reiners and Brandon, 2006).

The accumulation of fission tracks in time (***t***) is described by the decay equation properly modified to account for the fact that ^{238}U decays not only by spontaneous fission with a decay constant $\boldsymbol{\lambda_f}$ = 8.5 10^{-17} yr^{-1}) but also by α decay, with a much higher decay constant $\boldsymbol{\lambda_\alpha}$=1.5 10^{-10} yr^{-1} (Tagami and O'Sullivan, 2005):

3) $$N_s=\frac{\lambda_f}{\lambda_\alpha}\,^{238}N(e^{\lambda_\alpha t}-1)$$

$\mathbf{N_s}$ is the number of spontaneous fission tracks per unit volume; $^{238}\mathbf{N}$ is the number of ^{238}U atoms per unit volume.

	Relative Abundance (with respect to ^{238}U)	Half life (yr)	Half life for spontaneous fission (yr)
^{232}Th	4^{d}	1.40×10^{10}	1.0×10^{21}
^{234}U	5.44×10^{-5}	2.46×10^{5}	1.5×10^{16}
^{235}U	7.25×10^{-3}	7.04×10^{8}	1.0×10^{19}
^{238}U	1	4.47×10^{9}	8.2×10^{15}

Table 2.3- Relative abundances of U isotopes, total half life and half life due to spontaneous fission decay process.

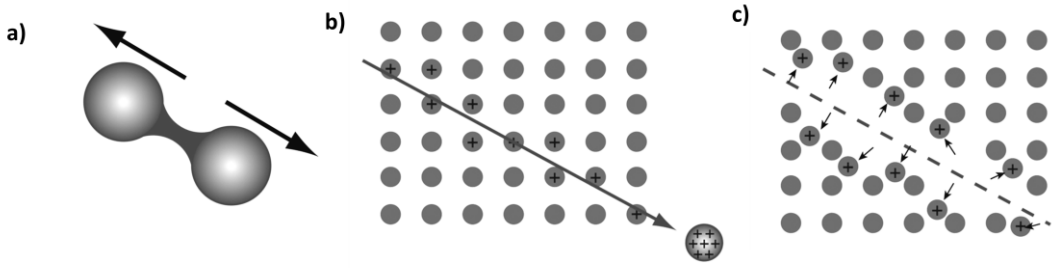

Figure 2.10. – The "Ion Explosion Spike" model for FT formation (from Fleischer et al., 1975). The Heavy nucleus splits in two nuclear fragments (a); the two positively charged fragments are pushed away from each other and along their track they tear off electrons from the atoms of the lattice (b); the positively charged atoms along the track dislocate from their lattice position due to repulsive electrostatic forces (c).

2.5.3. Analytical procedures and grain age calculation

To infer single crystal age the most commonly adopted technique is the External Detector Method (EDM), which main stages are schematically indicated in Fig. 2.11. The mineral grains to be dated are mounted in epoxy resin, polished and chemically etched. The tracks, and more in general the lattice defects, etch more rapidly than the intact crystalline lattice, and thus become visible for counting. After chemical etching the spontaneous tracks density of single mineral grain can be determined.

In order to determine the ^{238}U initial concentration, the EDM plays on the constant natural $^{235}U/^{238}U$ ratio ($7.252x10^{-3}$). A sheet of U-free mica is placed over the polished mount. Neutron irradiation in a nuclear reactor induces fission of ^{235}U. Nuclear fragments belonging to atoms placed close to the polished surfaces of the grains are injected in the mica sheet forming fission tracks in its lattice. Induced fission track density can be then measured on the mica surface after proper chemical etching. From ^{235}U the ^{238}U content is then calculated. The induced tracks are present also in the grain mount, but they are not revealed since the chemical etching of the minerals is done before the neutron irradiation. The mica monitor and the mount are assembled in the same slide and analyzed with an optical microscope implemented with a sliding table and a dedicated software. Before analyzing the sample three reference points in the mount and their correspondents in the mica are used to calibrate the system, so that the coordinates of the location on the external detector corresponding to the grains can be automatically calculated. The operator is then enabled to measure spontaneous and induced track density for the single mineral grains (Reiners and Brandon, 2006).

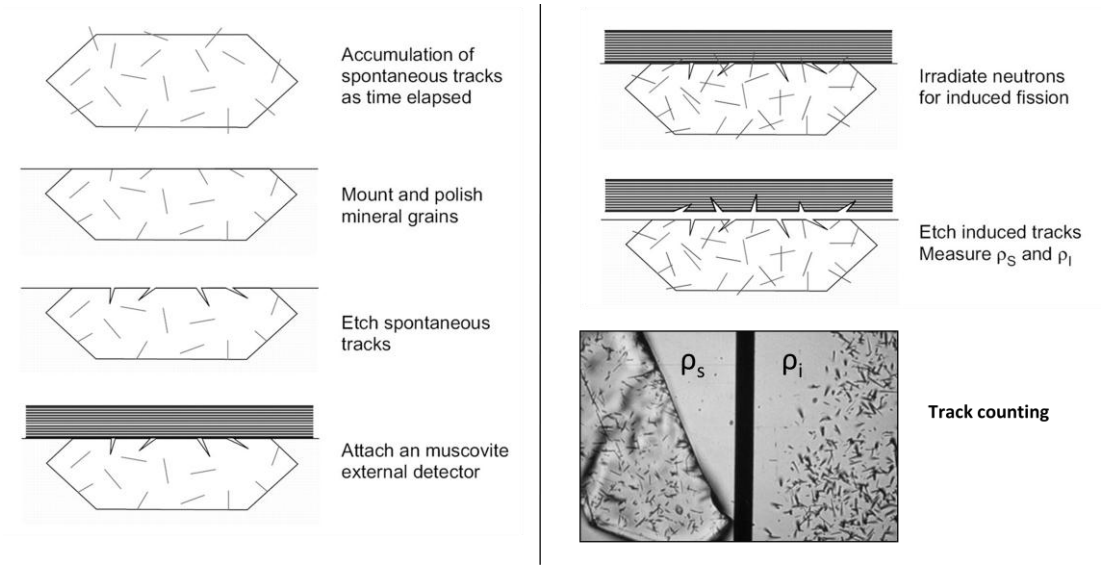

Figure 2.11. – schematic procedure for FT analysis with the EDM method (from Tagami and O'Sullivan, 2005). Source for the picture of spontaneous and induced tracks is the www.geotrack.com.au website.

The AFT age of a single apatite grain determined using the EDM method is given by:

$$4) \qquad t_i = \frac{1}{\lambda_d} ln\left(1 + \lambda_d \zeta \; g \; \rho_d \frac{\rho_{s,i}}{\rho_{i,i}}\right)$$

Where subscript **i** refers to grain i; $\mathbf{t_i}$ is fission track age of grain i; $\boldsymbol{\lambda_d}$ is the total decay constant of ^{238}U; **ζ** is the calibration factor based on EDM of fission track age standards, depending on the microscope and operator; **g** is the geometry factor for spontaneous fission track registration, $\boldsymbol{\rho_d}$ the induced fission track density for a uranium standard corresponding to the sample position during neutron irradiation, $\boldsymbol{\rho_{s,i}}$ is the spontaneous fission track density for grain i; $\boldsymbol{\rho_{i,i}}$ is the induced fission track density for the grain i (Donelick et al., 2005).

2.5.4. Retention and annealing of FT

As well as He diffusion, fission track annealing is a temperature dependent diffusional process, to which the Arrhenius law can be applied. However, in contrast to the He diffusion models, there is no accepted physical model of fission track annealing processes at the atomic level, since the process of fission track annealing is much more complicated than the diffusion of a single atomic species out of a mineral lattice, and still poorly known (Braun et al., 2006).

Fission tracks annealing models have thus been developed using a completely empirical approach, looking at what form of the annealing relationship best fit the data statistically (Braun et al., 2006).

Several kinetic models have been developed from different experiments: in the so-called fanning Arrhenius models, in a T^{-1}-ln(t) space, the annealing isopleths fan out from a single point (Laslett et al., 1987; Crowley et al., 1991; Ketcham et al., 1999); whereas in the curvilinear Arrhenius models (Ketcham et al., 1999; 2007) the annealing isopleths are slightly curved. The curvilinear Arrhenius models were obtained by imposing the model to fit both the experimental data and two benchmarks for annealing at geological timescales (Ketcham et al., 1999).

FT annealing behavior is independent on grain size, but it is demonstrated to vary with apatite chemistry, with retention increasing with increasing Cl/(F+Cl) ratio (Green et al., 1985), although other cations and anions substitutions also play a role (Carlson et al., 1999; Donelick et al., 1999; Ketcham et al., 1999; Barbarand et al., 2003). Moreover the annealing behavior also depends on the crystallographic orientation of the tracks with higher annealing rate for tracks orthogonal than tracks parallel to the C-axis of the crystal (Green et al., 1986; Donelick et al., 1999; Ketcham et al., 2007).

The D_{par}, i.e. the mean width of fission tracks etch pits, is a commonly used proxy for track retentivity of single crystals, first proposed by Ketcham et al.(1999). Other kinetic indicators alternative to D_{par} are Cl and OH contents (Ketcham et al., 1999; 2007b). The kinetic models proposed by Ketcham et al (1999; 2007) are, in fact, multi compositional models, accounting for the different kinetic behaviors of crystals belonging to the same rock (this typically occurs for sedimentary rocks). The single grain annealing equations in the multi compositional models differ to each other by a parameter r_{mr0}, defined by Ketcham et al (1999), which is calculated from the kinetic indicator (D_{par}, Cl, OH).

The effects of annealing can be quantified by measuring the lengths of horizontal confined tracks (Gleadow et al., 1986; Fig. 2.12.). This depends on the fact that tracks form continuously, and thus each track experiences a different portion of the integrated thermal history (Braun et al., 2006). Therefore the track lengths distribution, obtained by measuring a sufficient number

of horizontal confined tracks (preferably≥100) contains information on the thermal history experienced by the sample (Braun et al., 2006; Fig 2.13).

The AFT PRZ values are generally comprised between 30°C and 130°, but can be significantly different depending on cooling rate and apatite chemistry (Reiners and Brandon, 2006; Fig. 2.7). AFT Tcs generally vary between ca 80°C and 120°C, but still being largely affected by apatite composition. An apatite of "average" composition (Ketcham et al., 1999) has, for cooling rates of 10°C/Ma, Tc=116°C.

Figure 2.12. – Confined horizontal tracks: "Track in cleavage" (TINCLE) and "Track in track" (TINT)

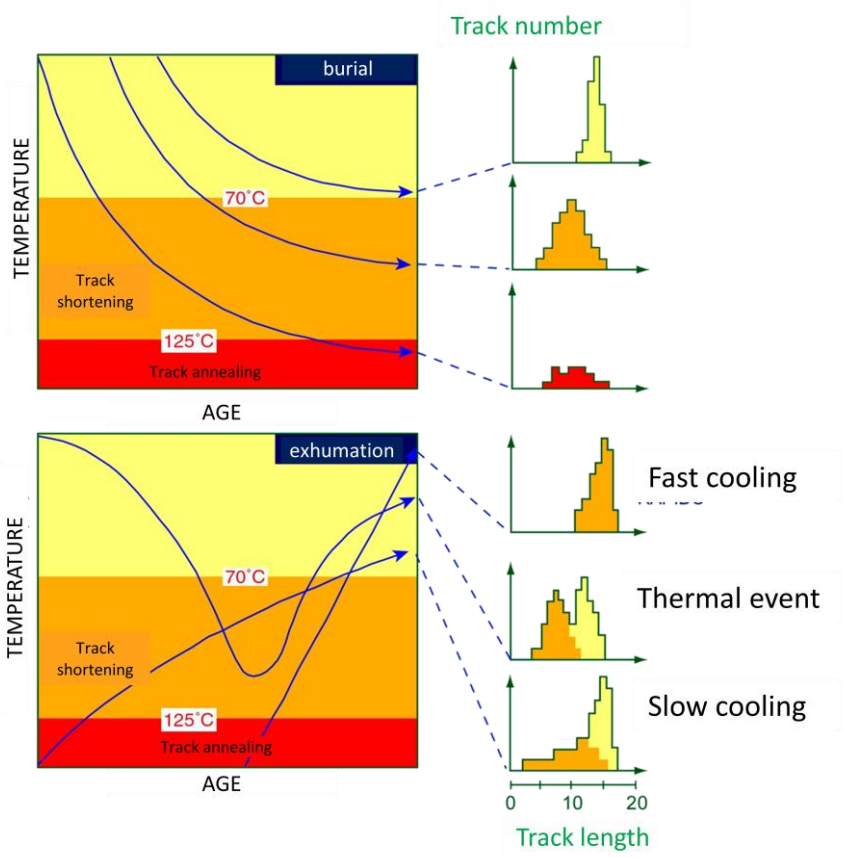

Figure 2.13. – relationship between track length distribution and thermal history

2.5.5. Data analysis and interpretation

Usually track densities are measured on 20 to 40 grains of the same sample, whereas 40 to 100 lengths are measured per sample. The measured parameters are the numbers of spontaneous and induced tracks, the area, the mean D_{par} of the grain for track density measurements, and the lengths, orientation with respect to C-axis and mean D_{par} for track lengths measurements.

Through dedicated softwares (e.g. Trackey, Dunkl, 2000) the density data are first processed to obtain single grain age data and respective statistical parameters to describe the whole population. The most common way to visualize AFT age data is with radial plots (Fig. 2.14.). The Y axis represents the standard error $((a_g-a_c)/\sigma)$ of the single grain age (a_g) with respect to the central age of the whole population (a_c) and the X axis represents the relative error ($1/\sigma$) decreasing toward the radial scale. Single grain ages are read on the intercept with the radial axis (plotted on a logarithmic scale) of the line drawn through the single grain point and the origin. The statistical parameter which best describes the age of an FT age population is the central age (Galbraith, 1988), which takes into account the lognormal nature of the ρ_s/ρ_i ratio (Vermeesch, 2008; eq. 4.).

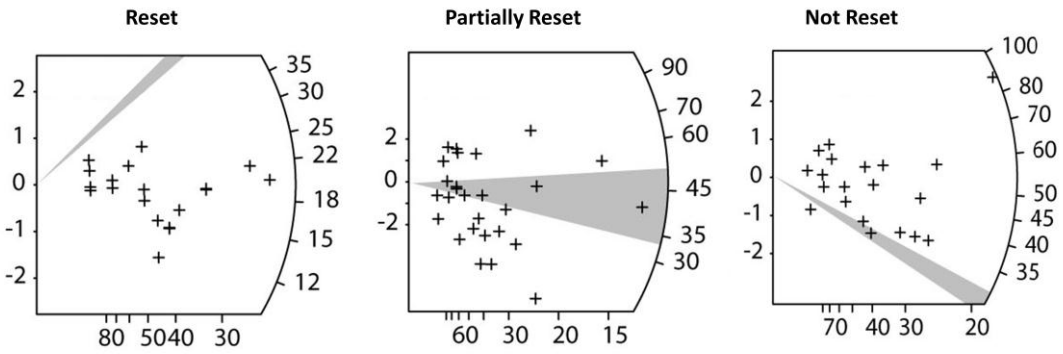

Figure 2.14. – Examples of Radial Plots referred to sedimentary rocks heated to different degree.

The χ-square statistical test (Galbraith, 1981) is used to define the probability that all the grains counted belong to a single population of ages. A probability ($P\chi^2$) of less than 5% is evidence of an asymmetric spread of single grain ages, and thus it indicates the presence of several age populations. An asymmetric spread in individual grain ages can result either from inheritance of detrital grains from mixed detrital source areas, or from differential annealing in grains of different compositions (Green et al. 1989).

A detrital sample is to be considered completely reset if all grain ages belong to the same population (high $P\chi^2$ value) and they are all younger than the depositional age. Partially reset samples are usually characterized by low $P\chi^2$ values (i.e. large dispersion) and have some grains younger and some older than the depositional age. Not reset samples are finally characterized by very low $P\chi^2$-square values and by thermochronometric ages all older than depositional ages.

To estimate the components in a mixed fission-track grain-age distribution (e.g. for non reset detrital samples), the binomial peak fitting algorithm of Galbraith and Green (1990) and Galbraith and Laslett (1993), implemented in the BINOMFIT software (by Brandon, 2002, 2007; summarized by Ehlers et al., 2005; Fig. 2.15) is used.

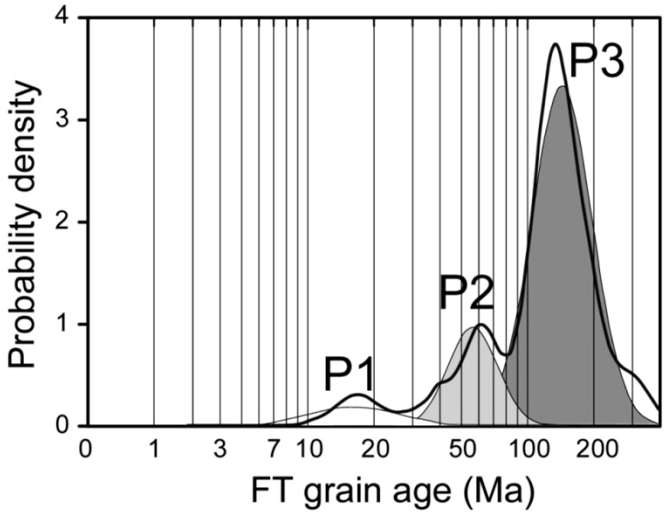

Figure 2.15. – Estimate of the components of a mixed grain age distribution made with the BINOMFIT program (Brandon, 2002; 2007). P1: 16.5±10.5 Ma (6.2% of the crystals); P2: 57.1±12.2 Ma (17.9% of the crystals); P3: 145.6 ±20.3 Ma (75.9% of the crystals).

CHAPTER III.

BURIAL AND EXHUMATION HISTORY OF THE POLISH OUTER CARPATHIANS INFERRED FROM LOW TEMPERATURE THERMOCHRONOLOGY

3.1. Chapter Overview

The present chapter is a journal paper submitted to Tectonophysiscs. AFT, AHe and ZHe data referred to the Polish Outer Carpathians are presented and discussed in order to infer burial depths as well as timing and driving processes of exhumation. A section is also dedicated to discuss the significance of detrital (not reset) ZHe ages in terms of exhumation of the source terrains and provenance analysis.

3.2. Paper

B. Andreucci* (1), A. Castelluccio (1), M. Zattin (1), S. Mazzoli (2), R. Szaniawski (3), and L. Jankowski (4)

(1) Department of Geosciences, University of Padua, Italy;
(2) Department of Earth Sciences, University of Naples “Federico II”, Italy;
(3) Institute of Geophysics, Polish Academy of Science, Warsaw, Poland;
(4) Polish Geological Institute-Carpathian Branch, Cracow, Poland;

3.2.1. Abstract

New apatite and zircon (U-Th-(Sm))/He and apatite fission track data, integrated with previously published apatite fission track data, are used to infer the thermal history of the Outer Polish Carpathian accretionary wedge, where thrusting ceased between 15.5 and 11.5 Ma and overlapped with extension during its final stages. The results of this study allowed us to constrain cooling ages of the source terrains of the sediments and to reconstruct the burial and exhumation history of the accretionary wedge.

Exhumation of source rocks through the ZHe PRZ occurred both in response to the Variscan (Late Devonian to Triassic) and Alpine (Late Jurassic to Early Paleocene) orogenesis, suggesting sedimentary provenance both from the southern margin and basement heights within the Outer Carpathian basin.

Burial temperatures generally decrease toward the foredeep. The uppermost structural units of the wedge underwent burial temperatures comprised between 70° and 160°C, corresponding to depths of 3.6-8.6 Km, whereas the outer thrust sheets were buried at temperatures lower than 70°C and depths lower than 3.6 Km.

Exhumation of the accretionary wedge through the AFT PAZ and AHe PRZ occurred between the Early and the Late Miocene, progressively migrating toward the east. We suggest that both

erosional exhumation of the wedge induced by thrusting and coupled erosional and tectonic exhumation induced by extensional tectonics occurred. In particular, exhumation related to extension appears to have played a major role in the eastern sector, whereas in the central and western sectors erosion of the wedge during accretion was the dominant process.

3.2.2. Introduction

The target of this study is the Polish sector of the Outer Carpathians, a thin skinned thrust and fold belt, where thrusting is interpreted to have ceased at about 15.5 to 11.5 Ma (Nemcok et al., 2006). The mountain chain is characterized by a complex topography (Fig.3.1) and a general low relief associated with a complex structural setting also involving normal faults reactivating pre-existing thrusts (Fig.3. 2, Jankowski et al., 2004; Mazzoli et al., 2010).

A general decrease in relief from the western to the eastern portion of the studied area may be observed in Fig.3.1. In particular, the western and central sectors are characterized by alternation of heights and lows and by increasing relief towards the inner part of the chain. The Eastern sector is rather characterized by a generally low relief, decreasing from the center towards both the inner and the outer portions of the chain.

In Fig. 3.2 it can be observed that along the study area the relative position of the tectonic elements also changes, and that normal faults reactivate or dissect pre-existing thrust faults (Jankowski et al., 2004; Mazzoli et al., 2010), also locally controlling Neogene intramontane basins (Orawa-Nowy Targ and Nowy Sacz basins).

Variations in relief, topography and relative position of the structural elements all suggest that different scenarios of burial and exhumation can be expected throughout the study area, pointing to a complex interplay between the two processes –thrusting and extension- suitable to drive exhumation.

According to this setting, thermochronological (Anczkiewicz and Swierczewska, 2008; Mazzoli et al., 2010; Zattin et al., 2011), paleotemperature (Swierczewska, 2005; Syrek, 2009) and paleo fluid pressure (Hurai et al., 2006) studies indicate a complex spatial pattern of burial temperatures and cooling ages.

Given this context, reconstructing the thermal history of rocks cropping out along the chain and identifying the extent, rate and spatial pattern of burial and exhumation processes is essential to constrain the contribution of the different processes to the development and evolution of the Polish Outer Carpathians. To this purpose new (U-Th-(Sm))/He dating was performed respectively on 39 apatite and 18 zircon samples and fission track analysis was performed on 4 apatite samples, in order to integrate the already published AFT dataset (Mazzoli et al., 2010; Zattin et al., 2011). The analysis of these datasets is carried out in this paper to reconstruct t-T paths, that, in turn, are used to constrain burial and exhumation history of the wedge.

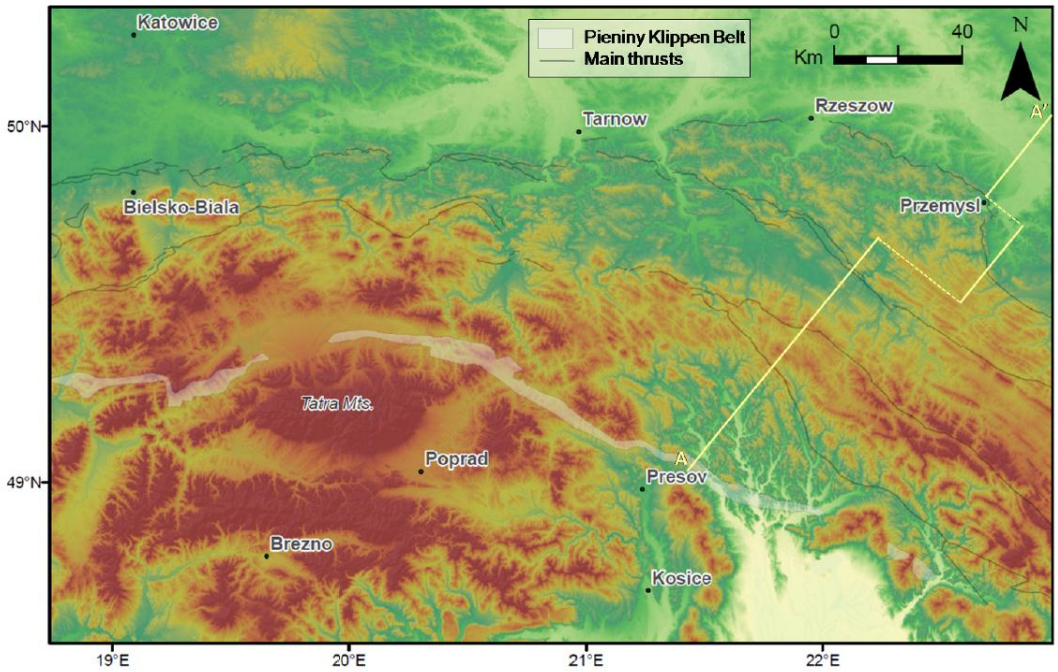

Figure 3.1 – Dem of the study area with main thrusts and Pieniny Klippen Belt (PKB). Location of the A-A' profile, reported in Fig.3.3, is indicated.

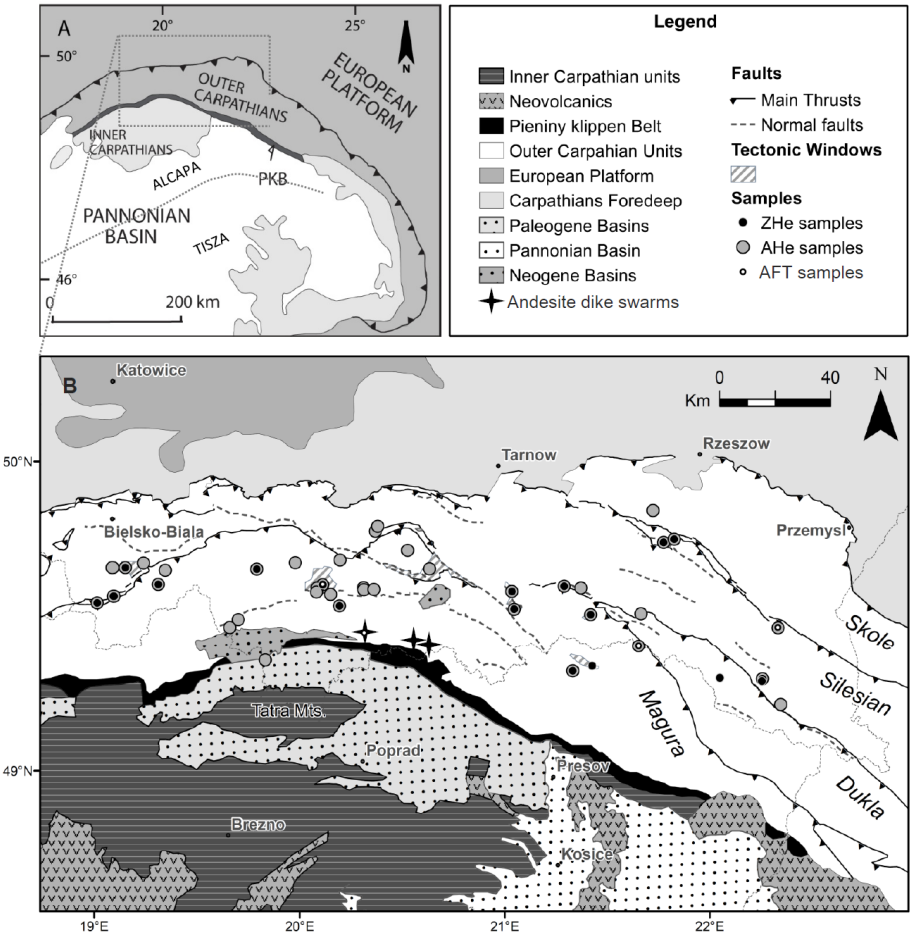

Fig. 3.2 – a) tectonic sketch map of the Carpathians showing subdivision of Inner and Outer Carpathians, separated by the Pieniny Klippen Belt (PKB). b) tectonic sketch map of the study area with AHe, ZHe and AFT sample location. Legend is referred to Fig 3.2.b.

3.2.3. Geological setting

The Carpathians, extending for over 1300 Km across Central and Eastern Europe, formed during the Tertiary by a NE- and E-ward migration of an accretionary wedge in front of the Alcapa and Tisza Dacia microplates (e.g. Jiricek, 1979; Nemcok et al., 1998; Sperner et al., 2002). Two noteworthy characteristics of the Cenozoic evolution of the chain are: (i) the progressive rotation of the main compression axis, from *ca.* N-S to *ca.* NW-SE, accompanied by a south-eastward migration of the tectonic activity (e.g. Horváth, 1993; Jiricek, 1979; Sperner et al., 2002); (ii) the occurrence, starting from the late Early-Middle Miocene, of retro-wedge extension, leading to the formation of the Pannonian and several minor intramontane basins (e.g.Kovac et al., 1990), and of extension-related volcanic complexes (e.g. Konecny et al., 2002; Pécskay et al., 2006; Seghedi et al.,2004).

Based on rock lithology and age of individual tectonic units, the Carpathians are traditionally divided into two domains (e.g. Tasarova et al., 2009 and reference therein): the Inner Carpathians (IC) and the Outer Carpathians (OC). They are separated by the so called "Pieniny Klippen Belt" (PKB), a narrow zone of strongly deformed and sheared Mesozoic to Paleogene rocks, traditionally interpreted as an oceanic suture (Birkenmajer, 2001).

The IC, constituting a prolongation of the Eastern Alps, are made of Variscan basement and younger sedimentary cover and were deformed between the Late Jurassic and the Late Cretaceous.

The OC formed during the Tertiary as an accretionary wedge, composed of Upper Jurassic to Lower Miocene flysch sediments, thrust over Neogene strata of the Carpathian foredeep (Oszczypko et al 1998). As deformation progressively migrated along strike toward the SE, thrusting and accretion of the OC were diachronous, having ceased between the Middle Miocene in the Western Carpathians and the Pleistocene in the Southern Carpathians (Matenco and Bertotti, 2000; Nemcok et al., 2006).

This study focuses on the Outer Polish Carpathians, where thrusting is interpreted to have ceased between 15.5 and 11.5 Ma, according to most recent studies (Nemcok et al, 2006), or between 15 and 13 Ma, according to Sperner et al.(2002, and reference therein). South of the frontal thrust sheets (traditionally grouped in the Skole Unit), the Magura Unit constitutes the structurally uppermost tectonic element of the Polish OC wedge. It forms a roof sequence overriding a series of thrust sheets - traditionally grouped in the Dukla and Silesian Units – that are also exposed in a series of tectonic windows. Recent studies highlight the presence of normal faults, roughly parallel to the strike of the thrust belt, dissecting and/or reactivating pre-existing thrusts along this whole portion of the chain (Jankowski et al., 2004; Mazzoli et al., 2010). An example can also be observed in Fig. 3.3, reporting the balanced section of the A-A' profile (indicated in Fig.3.1) Post thrusting extension is likely due to gravitational collapse of the orogenic wedge (Zattin et al., 2011).

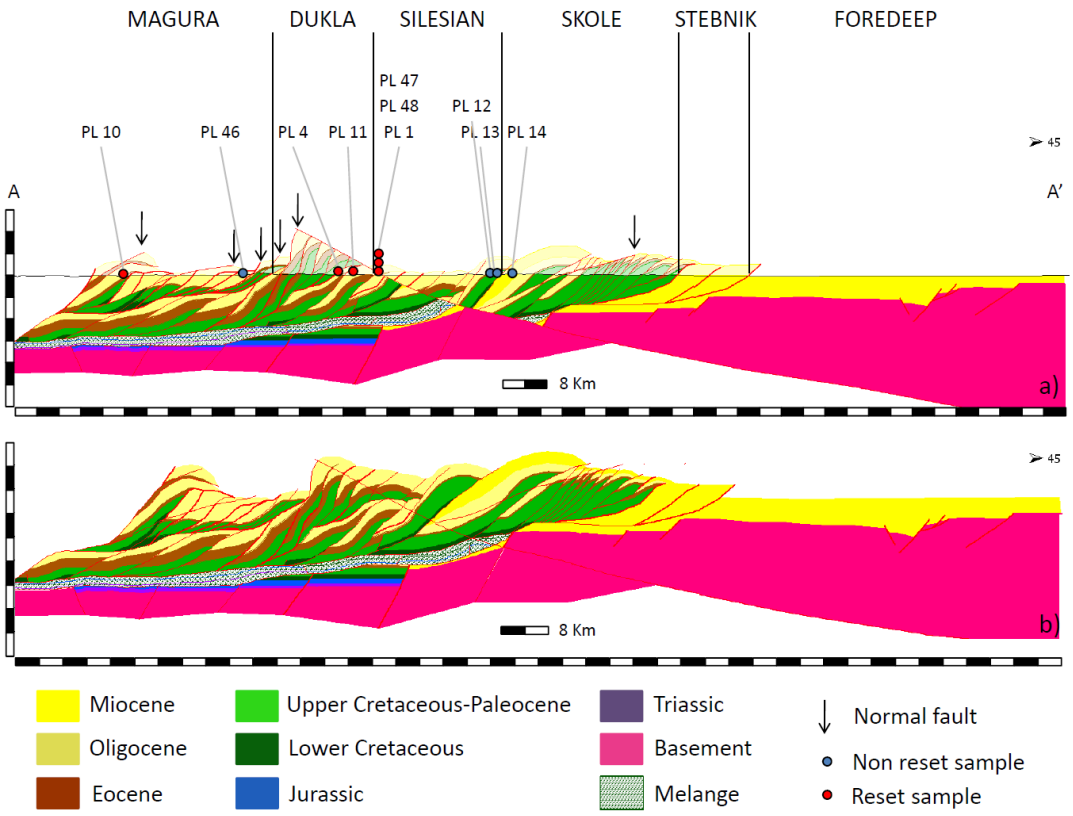

Fig. 3.3 – Geological cross-section (located in Fig. 3.1) through the Polish Carpathians (after Gagala et al., 2012, modified based on Jankowski et al., 2004 and our own field observations). Sampling sites (red and blue dots) are projected normal to the section trace. (a) Cross-section showing the thickness of eroded strata. (b) Restoration of normal faults carried out using the software 2D Move (by Midland Valley Exploration). The simple shear algorithm has been applied to accommodate the displacement along listric normal faults (the shear angle applied is of 90°).

3.2.4. Thermochronometry

Previous paleothermal studies

A complex paleo-thermal pattern is inferred from previous studies based on paleo temperature and paleo pressure indicators and low temperature thermochronometers.

Based on X-ray diffraction studies of Illite/smectite in shales, Swierczewska (2005) provides maximum paleotemperatures for the Magura nappe ranging between 75°C and possibly 165°C. The spatial distribution of maximum paleotemperatures is complex, with maxima in correspondence of the tectonic windows and minima in correspondence of the Neogene intramontane basins.

Hurai et al. (2006) calculate, from densities and trapping pressures of buoyant fluid inclusions, a thickness of the overburden, comprised between 5 and 11 Km and a burial temperatures of 155-195°C in the innermost Polish OC.

Vitrinite data from Syrek (2009), referred to the Magura Nappe, indicate a complex areal distribution of paleotemperatures. These are characterized by maxima and minima matching with those presented by Swierczewska (2005) but generally by lower temperatures (0.4< Ro% <0.76).

Three published sets of AFT data (Anczkiewicz and Swierczewska, 2008; Mazzoli et al.,2010; Zattin et al., 2011) document a highly variable annealing degree of fission tracks, although clearly decreasing towards the outer portions of the chain. This implies differential burial depths, generally increasing toward the inner part of the wedge.

Cooling ages obtained from AFT datasets range between the Early Oligocene and the Late Miocene. Post thrusting (<11 Ma) ages are concentrated in the eastern sector and appear to be related with extensional tectonics. Mazzoli et al. (2010) and Zattin et al. (2011) suggest that post-thrusting cooling was mainly controlled by tectonic exhumation in the eastern Polish OC, whereas older (Oligocene-Early Miocene) exhumation in the western sector was dominantly triggered by erosion.

Samples and methods

Samples for apatite and zircon (U-Th-Sm)/He (AHe and ZHe) and apatite fission track (AFT) analysis were collected from siliciclastic sandstones along the whole study area (Fig. 3.2). Care was taken in collecting samples across the main tectonic boundaries and in correspondence of sites where structural measurements were taken (see Mazzoli et al., 2010 and Zattin et al., 2011). A total of 48 sites were sampled; 40 of the 48 samples were selected for AHe analysis, and 18 of the 48 were selected for ZHe analysis. An overview of sample properties is presented in Tab 3.11 Apatite and Zircon separates were obtained through magnetic and heavy liquid separation following the conventional procedures described in Donelick et al. (2005).

(U–Th-(Sm))/He dating was carried out at the He dating laboratory of the University of Arizona in Tucson. Handpicked apatite and zircon grains were photographed and measured for alpha-ejection correction following methods described respectively in Reiners and Brandon (2006) and Hourigan et al.(2005). Single crystals were loaded into 0.8 mm Nb tubes, and degassed under vacuum by heating with a Nd-YAG laser. The concentration of ^{4}He was determined by ^{3}He isotope dilution and measurement of the $^{4}He/^{3}He$ ratio through a quadrupole mass spectrometer. U, Th and Sm concentrations were obtained by isotope dilution using an inductively coupled plasma mass spectrometer. Alpha-ejection correction was applied to derive a corrected (U–Th-(Sm))/He ages.

AFT dating and confined tracks measurement were performed at the department of Geosciences of the University of Padua. CN5 glass was used to monitor neutron fluence during irradiation at the Oregon State University Triga Reactor, Corvallis, USA. The calculation of central ages (Galbraith and Laslett, 1993) was performed through the TRACKEY software (4.2 version; Dunkl, 2000). The Chi-square (χ^2) test was used to assess the homogeneity of age populations: a population is considered homogeneous for $P(\chi^2)$ higher than 5%. Through the use of the BINOMFIT software (summarized by Ehlers et al., 2005) minimum ages were calculated for partially reset samples belonging to both new and previously published datasets. In order to achieve a kinetic parameter and to identify different kinetic populations, Dpar of single crystal and length was measured.

Sample	Coordinates		Elevation (m)	Sedimentary unit	Lithology	Depositional age
PL1	49°18.629'	22°16.055'	615	Krosno beds	Sandstone	Late Oligocene
PL4	49°18.927'	22°3.883'	504	Menilite beds	Sandstone	Late Oligocene
PL5	49°33.869'	21°4.988'	523	Magura sandstones	Sandstone	Eocene
PL6	49°35.957'	21°1.009'	373	Menilite beds, Ropa window	Sandstone	Late Oligocene
PL7	49°38.831'	21°10.073'	289	Magdalena sandstones	Sandstone	Early Oligocene
PL8	49°31.618'	21°25.652'	420	Menilite	Sandstone	Early Oligocene
PL10	49°20.559'	21°20.233'	356	Magura sandstones	Sandstone	Eocene-Oligocene
PL11	49°31.711'	21°40.066'	459	Cergowa sandstones	Sandstone	Oligocene
PL12	49°45.546'	21°47.065'	373	Istebna sandstones	Sandstone	Late Cretaceous- Early Paleocene
PL13	49°46.138'	21°50.812'	315	Istebna sandstones	Sandstone	Late Cretaceous- Early Paleocene
PL14	49,51.741	21°44.518'	231	Krosno Beds	Sandstone	Miocene
PL15	49°40.898'	19°11.817'	364	Cieszynites sill		
PL16	49°39.880'	19°6.399'	468	Cieszyn Beds	Sandstone	Late Jurassic -Early Cretaceous
PL18	49°39.803'	19° 2.706'	626	Godula sandstones	Sandstone	Middle-Late Cretaceous
PL19	49°32.905'	18°58.535'	825	Krosno Beds	Sandstone	Oligocene
PL20	49°34.258'	19°3.300'	495	Krosno beds	Sandstone	Oligocene
PL21	49°39.578'	19°18.396'	414	Muczna sandstones	Sandstone	Late Cretaceous
PL22	49°36.774'	19°16.387'	530	Cieszyn Beds	Sandstone	Late Jurassic -Early Cretaceous
PL23	49°40.126'	19°45.784'	504	Magura sandstones	Sandstone	Middle-Late Eocene
PL24	49°41.523'	19°57.288'	434	Magura sandstones	Sandstone	Middle-Late Eocene
PL25	49°37.265'	20° 5.005'	492	Krosno Beds	Sandstone	Late Oligocene-Early Miocene
PL26	49°35.043'	20° 7.925'	699	Magura sandstones	Sandstone	Middle Eocene - Early Oligocene
PL27	49°42.110'	20°10.646'	692	Magura sandstones	Sandstone	Middle Eocene - Early Oligocene
PL28	49°33.194'	20°10.646'	1058	Magura sandstones	Sandstone	Middle Eocene - Early Oligocene
PL29	49°30.226'	19°40.477'	639	Magura sandstones	Sandstone	Middle Eocene-Oligocene
PL30	49°28.652'	19°37.994'	621	Miocene	Sandstone	Miocene
PL31	49°27.095'	20°18.996'	667	Andesites Mount Wzar	Andesite	Serravallian-Tortonian
PL32	49°36.078'	20°17.773'	608	Magura sandstones	Sandstone	Midlle Eocene-Early Oligocene
PL33	49°36.420'	20°17.829'	521	Menilite Beds	Sandstone	Oligocene
PL34	49°36.482'	20°20.888'	602	Magura sandstones	Sandstone	Midlle Eocene-Early Oligocene
PL35	49°40.533'	20°37.452'	427	Krosno Beds	Sandstone	Late Oligocene
PL36	49°44.118'	20°30.878'	478	Magura sandstones	Sandstone	Middle Eocene-Oligocene
PL37	49°47.803'	20°21.176'	357		Sandstone	Cretaceous
PL38	49°48.742'	20°21.848'	316	Cergowa sandstones	Sandstone	Early Oligocene
PL39	49°160.37'	23°24.712	402	Foredeep	Sandstone	Eocene
PL40	49°22.344'	19°48.712'	757	Podhale deposits	Sandstone	Late Eocene
PL41	49°36.62'	20°3.837'	520	Krosno beds	Sandstone	Late Oligocene-Early Miocene
PL42	49°35.839'	20°3.722'	562	Magura sandstones	Sandstone	Middle Eocene - Early Oligocene
PL43	49°37.208'	21°17.808'	428	Menilite shales	Sandstone	Oligocene
PL44	49°36.822'	21°22.799'	378	Magura sandstones	Sandstone	Late Oligocene
PL46	49°25.377'	21°39.819'	513	Magura sandstones	Sandstone	Late Oligocene
PL47	49°28.061'	22°21.471'	376	Krosno beds	Sandstone	Late Oligocene
PL48	49°13.683'	22°21.871'	542	Krosno beds	Sandstone	Late Oligocene

Table 3.1 – Overview sample properties

AHe results

Several apatite crystals (between one and five) were dated for each sample. Due to the generally bad quality of apatites belonging to sedimentary rocks, it was possible to fulfill the standard requirements for AHe analysis (intact, clear, prismatic crystals; e.g. Ehlers and Farley, 2003) only in few cases. Most of the picked crystals were inclusions-bearing and oxide-oxhydroxide coated and, in some cases, rounded and/or abraded. Since the observed inclusions were generally small (less than a few percent of the length, height and width of the host crystal), based on Vermeesch et al. (2007), it can be confidently assumed that they generally induced no significant

effect on ages. On the other hand, the potentially rich in U and Th coatings might have significantly influenced the results. As a matter of fact, both accuracy and precision could have been affected by either alpha-implantation (in case most of the coat was lost before analysis) and Th and U excess (in case most of the coat was analyzed with the grain).

A first check of data quality was made identifying exceptionally high or low values of U, Th, and He concentration and relative errors: straightforward outliers and crystals with pronounced anomalous values were rejected (see Tab 3.2 for details); the accepted crystals are presented in Tab 3.2.

Despite the crystals' quality and the frequent occurrence of suspiciously high Th concentrations (up to ten times higher than the common natural value), age reproducibility of replicates is generally acceptable (Fig 3.4.a). The standard deviation for each sample is comprised within the 20% of the mean sample age ($q_{3/4}(\sigma/\mu)=0.2$) in most cases (Fig.3.4.b).

A further check of data quality was made by testing the correlation between age and some of the measured parameters. Low [Th] and Th/U lead to older ages (Fig.3.5). This, coupled with the frequent occurrence of anomalously high Th concentrations, suggests that the presence of Th-rich coatings might have had an impact on ages. In particular, underestimated ages could derive from excess Th, whereas low Th contents could have led, by α-implantation, to overestimated ages.

Hence, besides an effect on data reproducibility, yet acceptable, a systematic effect of bad data quality, and particularly of the presence of Th-rich coating, cannot be ruled out. Nonetheless, it appears that the potential systematic effect does not invalidate the analyses, since AFT and AHe reset ages generally match well (Fig.3.6 and 3.7). Anyway, in order to use the safest approach, single grain corrected ages rather than mean ages are used in the interpretation and discussion of the results.

A total of 26 completely reset samples (their single grain ages being well reproducible and always younger than stratigraphic age), 10 partially reset (lower reproducibility and single grain ages partly younger and partly older than stratigraphic age) and 3 non reset samples (low reproducibility and single grain ages always older than stratigraphic age) can be identified. In Fig.3.6, AHe single grain ages are indicated for both reset and non reset samples.

Corrected ages of fully reset grains range between 6.2 and 24.19 Ma. Relatively young ages (*ca.*10 Ma) occur mainly in the eastern sector (Fig.3.7). It is noteworthy that, for some samples belonging to the eastern sector, an AFT-AHe age-inversion occurs (samples PL 1 and PL 6 showing AFT ages of *ca*. 7 Ma and AHe ages of *ca.* 10 Ma). We suggest that this is due to an overestimation of AHe ages induced by alpha implantation or other factors of AHe age variability.

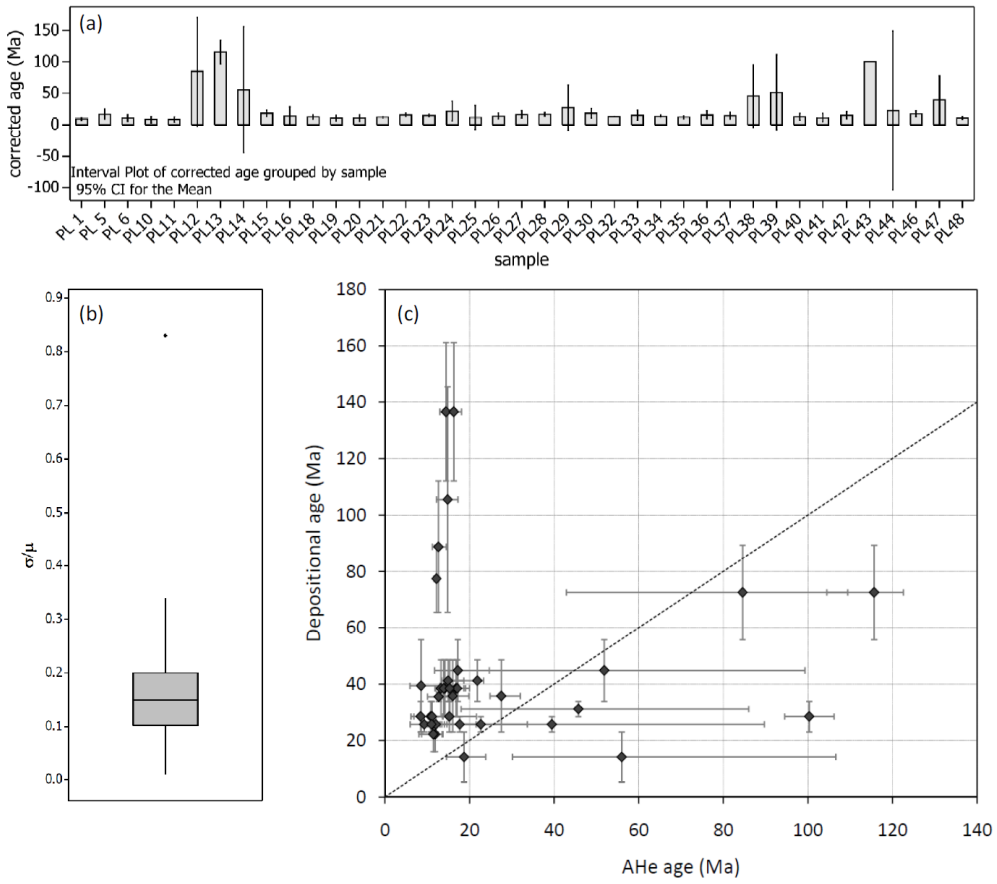

Figure 3.4 – a) interval plot of AHe ages (grey bars) with 95% confidence interval for the mean (black bars); b) boxplot of sample σ/μ; c) AHe mean ages plotted against depositional ages. Error bars indicate the range of AHe ages for the single sample (maximum age + positive error/ minimum age + negative error)

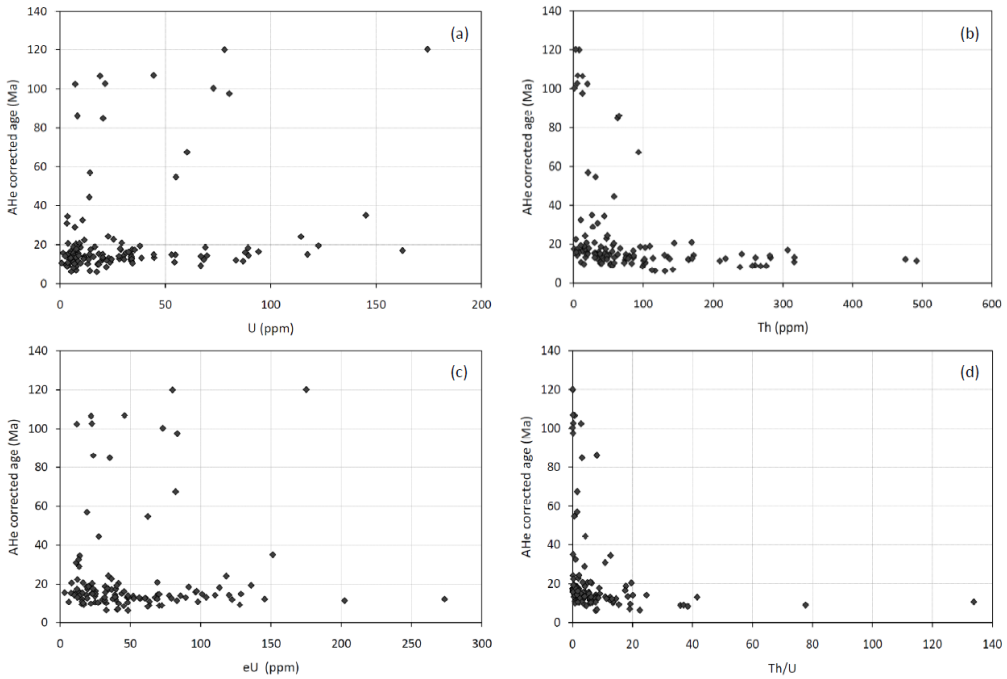

Figure 3.5 – AHe ages plotted against concentration of U (a), Th (b) and effective uranium (c; eU=[U] + 0.235×[Th]) and Th/U ratio (d).

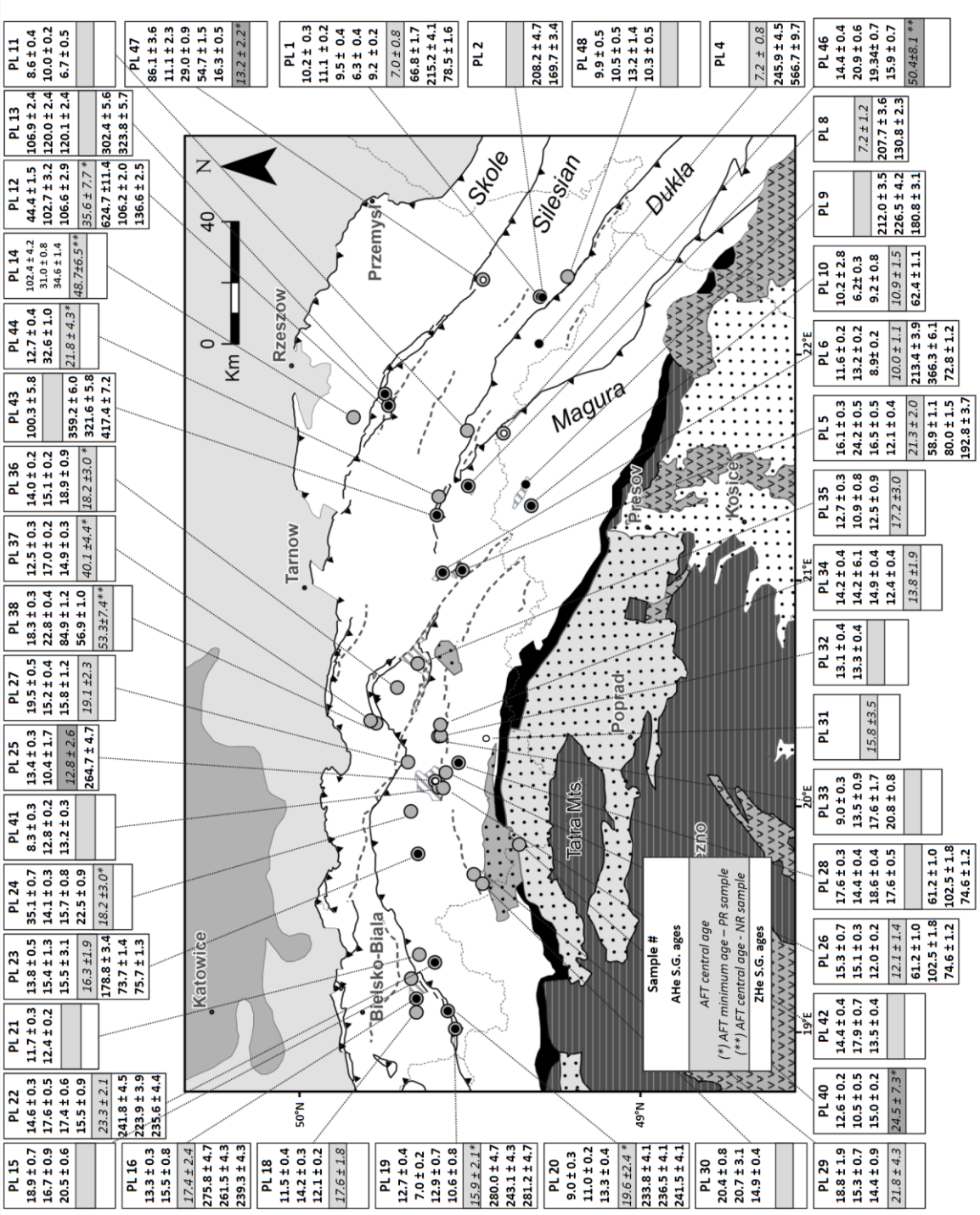

Fig. 3.6 – AHe, AFT and ZHe data with sample position. AFT ages from this study are indicated by the dark grey fields. Minimum AFT ages for partially reset samples are calculated after Zattin et al. (2011), using the Binomfit software (Brandon, 1992).

AFT results

The four analyzed samples yielded a general low spontaneous fission track density and thus only 11 to 20 crystals per sample were used for fission track counting and 20 to 40 lengths were measured per sample, except for sample 25, where no confined track was found. Dpar of samples PL 25, PL 46 and PL 47 are generally comprised within the 1-1.7 interval, sample PL 31 yield Dpar comprised between 1.5 and 2.5. In all the analyzed samples only one kinetic population was identified.

Results are displayed in Table 3.3, and reported in Fig. 3.6 and Fig. 3.7. In Fig.3.8 radial plots of the analyzed samples indicate that only sample PL 25 was completely reset after deposition, yielding a central age of 12.8 ± 2.6 Ma; samples PL 46 and PL 47 were partially reset, yielding minimum ages of respectively 13.2 ± 2.2 Ma and 16.3±1.4 Ma. Sample PL 31 belongs to the andesitic dyke swarms exposed along the so called "Pieniny Andesite Line": central age of 15.8± 3.5 overlaps with both K/Ar dates ranging between 13.5 and 11 Ma (Birkenmajer and Pécskay, 2000) and other AFT dates of 20.4 ± 3.9 and 22.6 ± 5.1 (Tokarski et al., 2006 and reference therein).

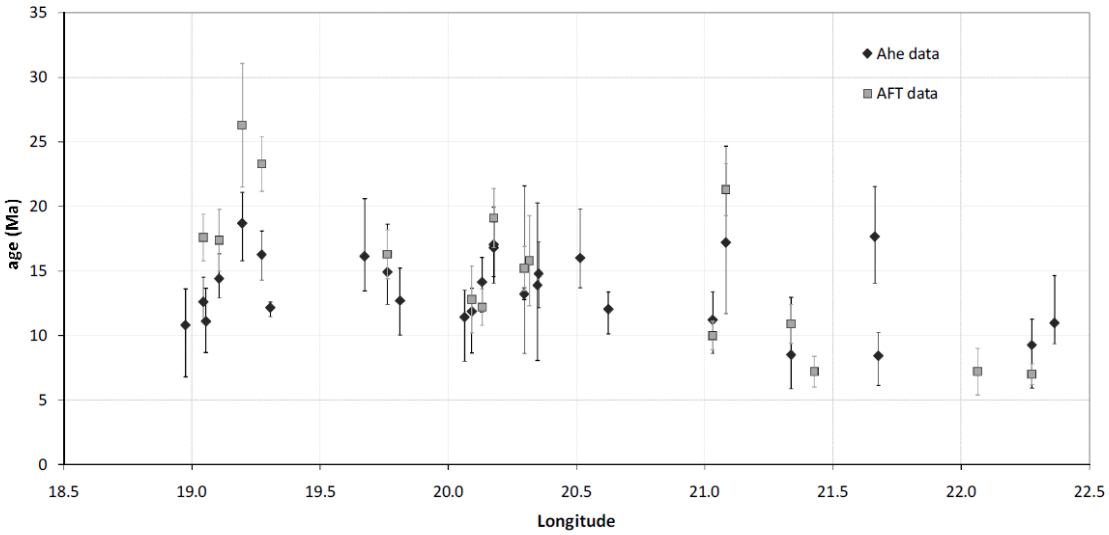

Figure 3.7 – AFT and AHe data with 1σ error plotted along the X coordinate.

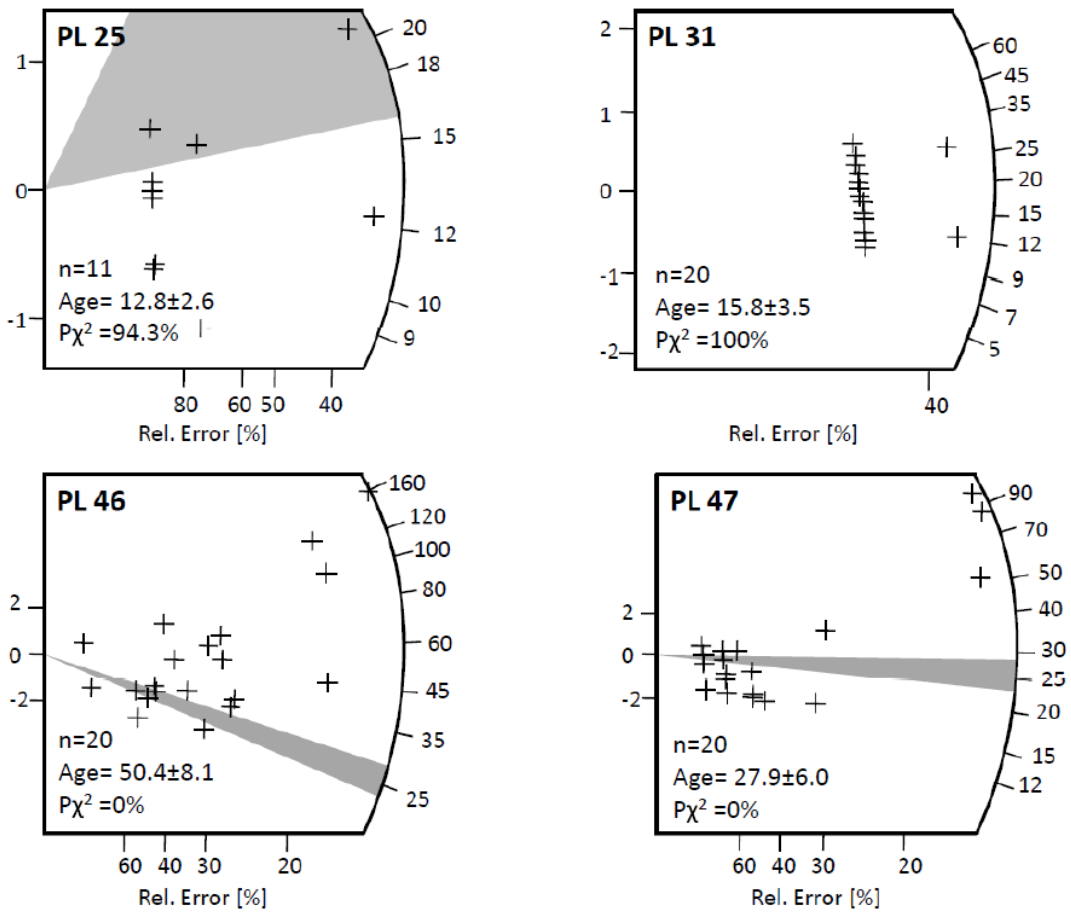

Figure 3 8 – Radial plots for AFT samples with depositional ages (grey areas).

ZHe results

Between 1 and 3 crystals were dated for each sample; the analyzed grains were of good quality and the measured parameters show no significant anomalies. The results are shown in Table 3.4. However the pronounced negative correlation between age and eU shown in Fig. 3.9 indicates that part of the ZHe age variability does not depend on the actual thermal history of the crystal, being affected by anomalies like U-Th zonation or presence of U-Th rich inclusions or coatings. Nonetheless the dates are all undoubtedly older than stratigraphic ages (Fig. 3.10), meaning that the samples never reached the total reset of the ZHe system (about 200°C; Reiners and Brandon, 2006; Reiners et al., 2004) after deposition. ZHe ages, despite the imprecision and inaccuracy expected on the basis of age-eU correlation, constitute an estimate of cooling ages through temperatures in the range of 200°-160°C (ZHe PRZ, Reiners et al, 2004). The main peak ages are Triassic and Late Cretaceous-Paleocene, with minor peaks between Late Devonian and Middle Permian, in the Early Jurassic and Early-Middle Cretaceous (Fig.3.11).

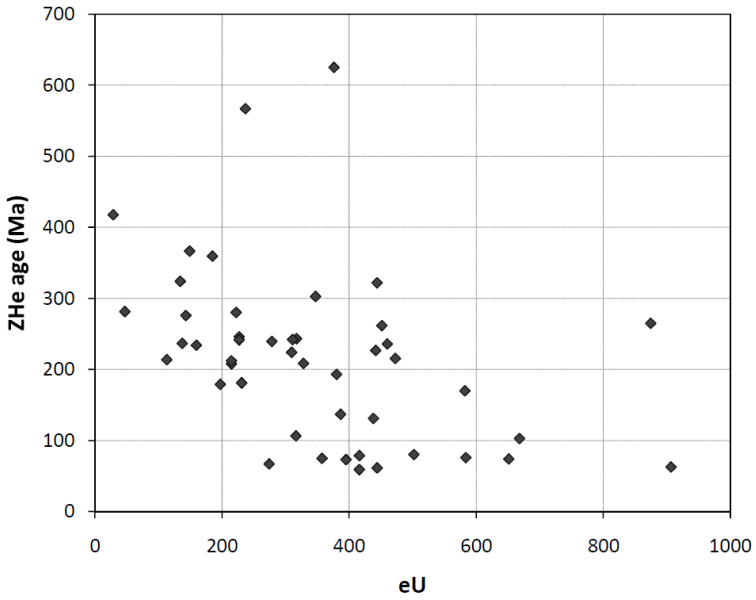

Figure 3.9 – ZHe single grain ages plotted against effective Uranium concentration (eU=[U] + 0.235×[Th]).

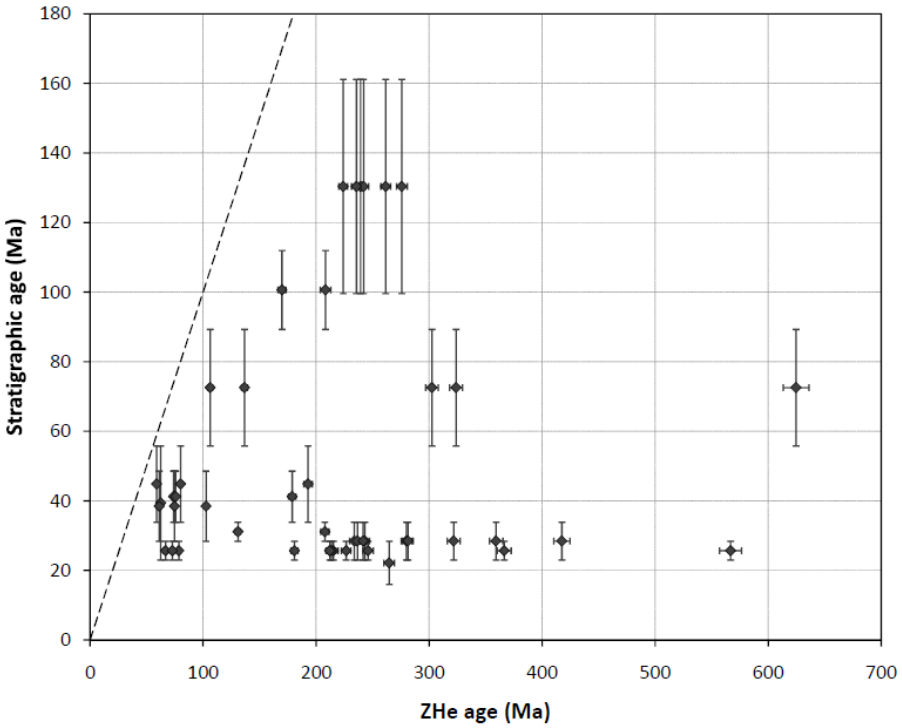

Figure 3.10 – ZHe single grain ages plotted against depositional ages.

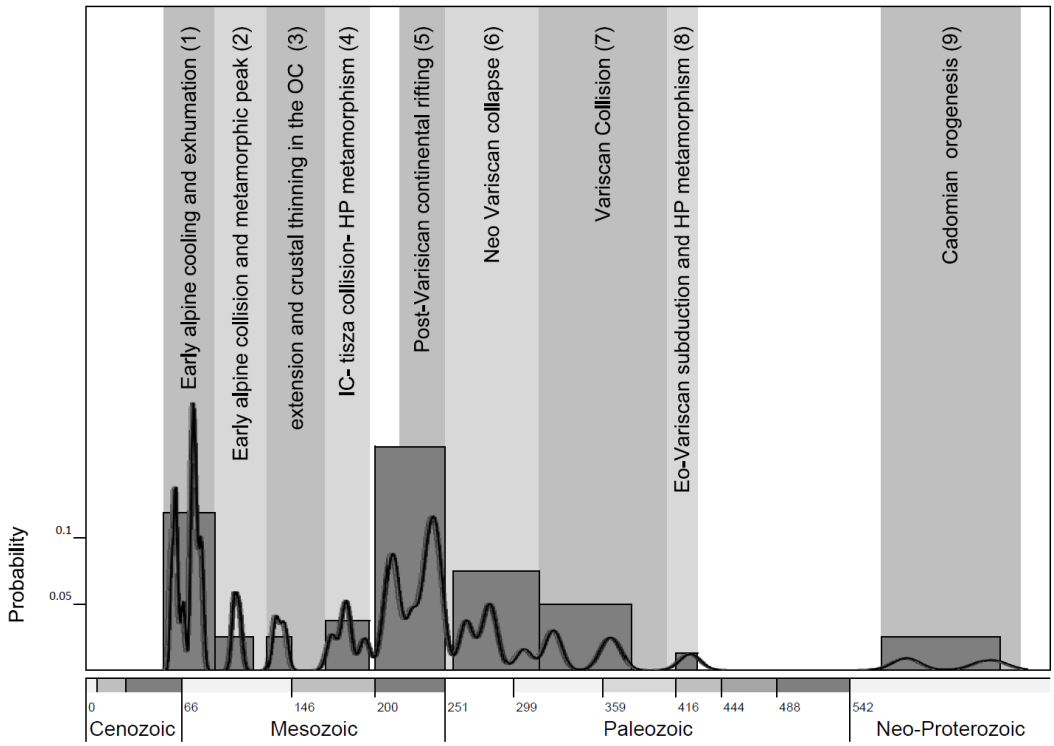

Figure 3.11 – Histogram and probability density plot of ZHe associated to principal geodynamic events documented in the Northern Carpathian region (Alcapa block, OC basin and European foreland). Bin width was arbitrarily set on the basis of duration of single geodynamic phase. Principal events indicated in figure are: (9) Cadomian orogenesis (age data from Budzyń et al., 2006; 2008; Michalik et al., 2006; Poprawa et al.,2004; 2005, Putiš et al., 2008); (8) Eo-Variscan stage (duration based on Kohut, 2002, age data from Plašienka et al., 1997); (7) Variscan collision and associated tectonics, magmatism and metamorphism (duration based on Kohut, 2002; age data from Budzyń et al., 2006; Dallmeyer et al., 1996; 2005; Janak et al., 1999; Maluski et al., 1993; Poller et al., 2000); (6) Neo-Variscan stage, gravitational collapse and associated magmatism and metamorphism (duration based on Kohut, 2002; age data from Broska and Huer, 2001; Finger et al., 2003; Hraško et al., 2002); (5) Post-Variscan (or pre-Alpine) extension and continental rifting (age data from Budzyn et al., 2006; Ondrejka and Huer, 2001; Poprawa et al., 2006); (4) IC Carpathians-Tisza collision and HP metamorphism (age data from Faryad and Henjeskunst, 1997); (3) Extension and crustal thinning in the OC (age data: e.g. Kusiak et al., 2004; Poprawa et al.,2002; 2005); (2) Early Alpine collision and metamorphic peak (age data: e.g. Dallmeyer et al., 2005; Janak et al., 2001); (1) Early Alpine cooling and exhumation (age data: e.g. Dallmeyer et al., 2005; Danisik et al., 2011; Janak et al., 2001; Plasienka et al., 2007).

Thermal Modeling

To integrate the AHe, ZHe and AFT data, testing plausible thermal histories, backward thermal modeling was performed on 10 samples, using the software HeFTy (Ketcham, 2005). AFT age and length, AHe and ZHe (where present) data were used for modeling; only one AHe and one ZHe replicates were used for each sample.

Modeling was based on the fission-track annealing model of Ketcham et al. (2007), the diffusion kinetics of the Durango apatite after Farley (2000) and zircon after Reiners et al. (2004). A homogeneous distribution of U and Th in apatites and zircons was assumed. Constrains used were temperature comprised between 0 and 20°C during depositional age interval and post-depositional maximum burial temperature lower than *ca*. 160-200°C where ZHe data were present. A surface temperature of 20°C was assumed.

The results of thermal modeling are reported in Fig. 3.12 and the best fitting paths are summarized in Fig. 3.13. Two slightly different groups of t-T paths can be identified in Fig.3.13. Several samples (PL 5, 18, 20, 22) require a prolonged (ca. 50 to 15 Ma) stay in the PAZ, followed by a relatively rapid cooling (average cooling rate of ca. 8°C/Ma) down to temperatures lower than 45°C, terminated by 15-10 Ma. A second group of samples require heating up to temperatures higher than 110-120°C and rapid cooling (average cooling rate of ca. 20°C/Ma) down to temperatures lower than 45°C between 15 and 5 Ma. In both cases, after the main cooling stage, a stage characterized by a considerably lower cooling rate (*ca*.1°C Ma to 4°C/Ma) occurred.

The obtained thermal paths, can be summarized in the following five stages: (i) pre-depositional cooling of the source rocks through temperatures of 210-130°C (between Devonian and Paleocene); (ii) deposition in the Outer Carpathian basins, (between Late Jurassic and Early Miocene); (iii) heating to temperatures higher than the AHe total annealing temperature (70°C) and lower than the ZHe PRZ (160°C), followed, in some cases, by several Ma stay in the AFT PAZ; (iv) rapid cooling (mean cooling rates comprised between 8 and 20°C/Ma) down to temperatures lower than 45°C (between Early and Late Miocene); and (v) slower cooling (average rates lower than ca. 1.3°C/Ma) down to surface temperature.

Figure 3.12 – Thermal modeling for samples belonging to the western sector (a) PL 22, PL 20, PL 18, to the central sector (b) PL 26, PL 27, PL 34 and to the eastern sector (c) PL 5, PL 6, PL 1, PL 10. Acceptable paths envelope (not ruled out by the data, with goodness of fit, GOF>0.05), Good paths envelope (supported by the data; GOF>0.5) and best fitting path are indicated (respectively with light and dark grey areas and black solid line. The light grey bars indicate the end of thrusting based on Nemcok et al.(2006). Modeling was performed using the HeFTy software (Ketcham et al., 2007). Temperature comprised between 0 and 20°C during the period corresponding to stratigraphic age was the only constrain applied a priori.

a)

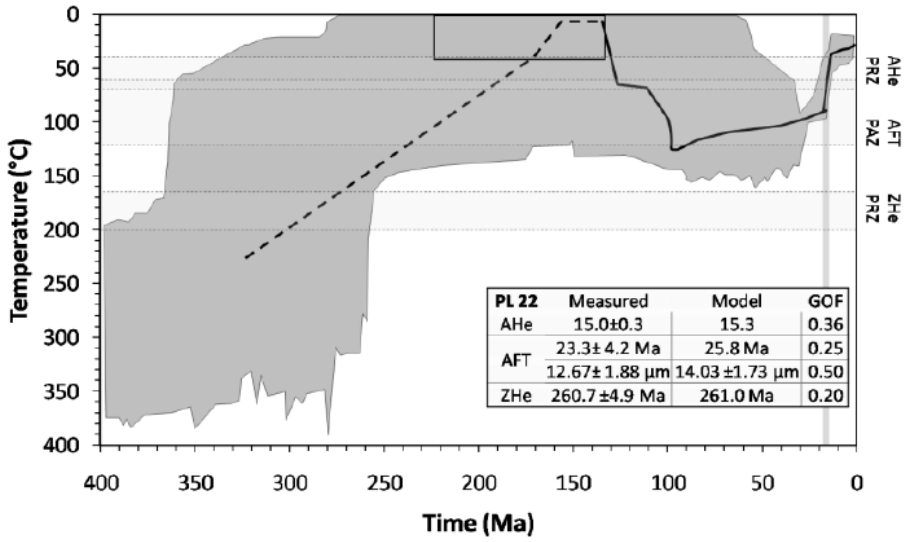
Temperature (°C)
Time (Ma)
AHe PRZ
AFT PAZ
ZHe PRZ
PL 22 | Measured | Model | GOF
AHe | 15.0±0.3 | 15.3 | 0.36
AFT | 23.3± 4.2 Ma | 25.8 Ma | 0.25
AFT | 12.67± 1.88 µm | 14.03 ±1.73 µm | 0.50
ZHe | 260.7 ±4.9 Ma | 261.0 Ma | 0.20

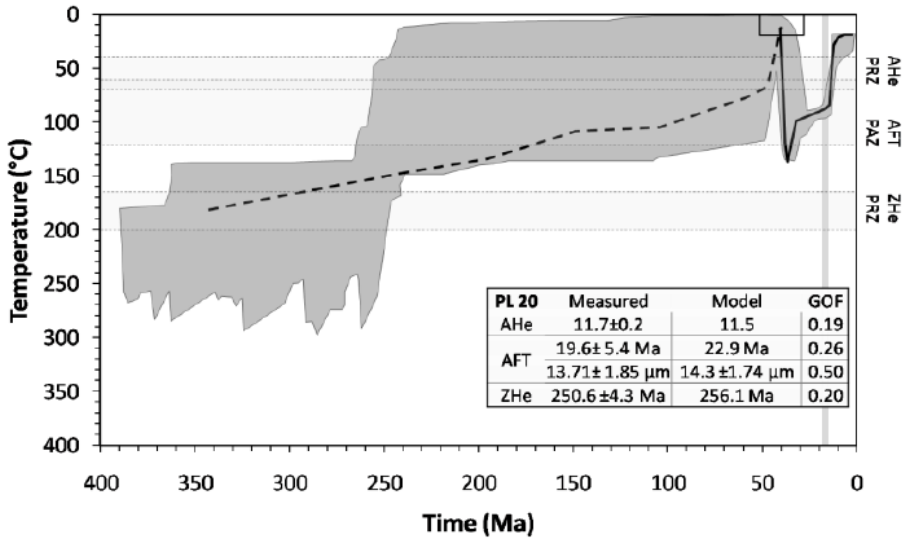
Temperature (°C)
Time (Ma)
AHe PRZ
AFT PAZ
ZHe PRZ
PL 20 | Measured | Model | GOF
AHe | 11.7±0.2 | 11.5 | 0.19
AFT | 19.6± 5.4 Ma | 22.9 Ma | 0.26
AFT | 13.71± 1.85 µm | 14.3 ±1.74 µm | 0.50
ZHe | 250.6 ±4.3 Ma | 256.1 Ma | 0.20

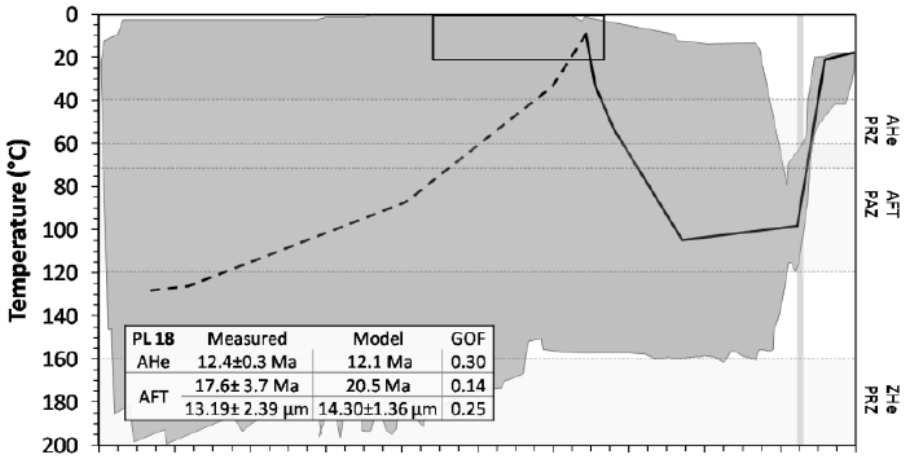
Temperature (°C)
AHe PRZ
AFT PAZ
ZHe PRZ
PL 18 | Measured | Model | GOF
AHe | 12.4±0.3 Ma | 12.1 Ma | 0.30
AFT | 17.6± 3.7 Ma | 20.5 Ma | 0.14
AFT | 13.19± 2.39 µm | 14.30±1.36 µm | 0.25

b)

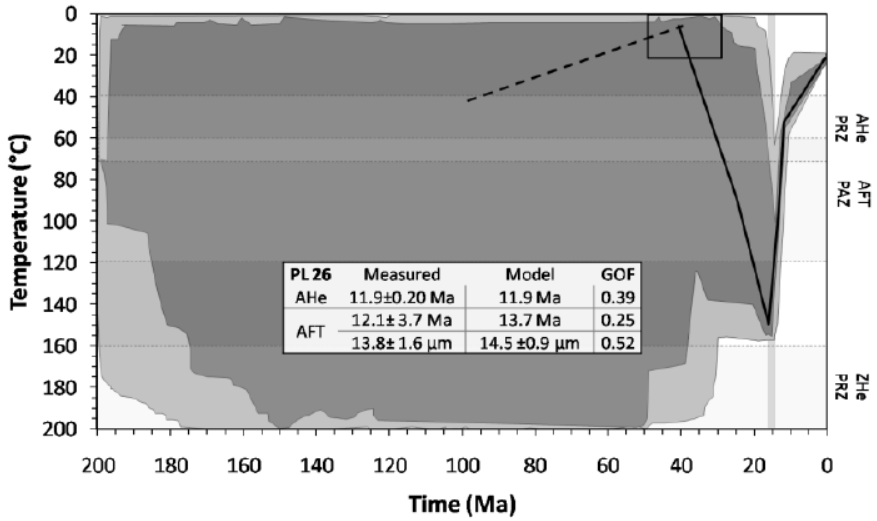
Temperature (°C)
Time (Ma)
AHe PRZ
AFT PAZ
ZHe PRZ
PL 26 | Measured | Model | GOF
AHe | 11.9±0.20 Ma | 11.9 Ma | 0.39
AFT | 12.1± 3.7 Ma | 13.7 Ma | 0.25
13.8± 1.6 µm | 14.5 ±0.9 µm | 0.52

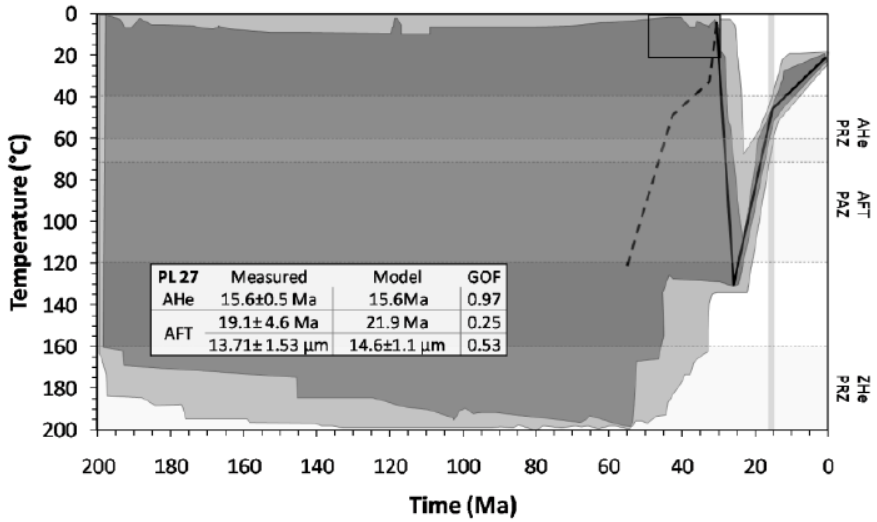
Temperature (°C)
Time (Ma)
AHe PRZ
AFT PAZ
ZHe PRZ
PL 27 | Measured | Model | GOF
AHe | 15.6±0.5 Ma | 15.6Ma | 0.97
AFT | 19.1± 4.6 Ma | 21.9 Ma | 0.25
13.71± 1.53 µm | 14.6±1.1 µm | 0.53

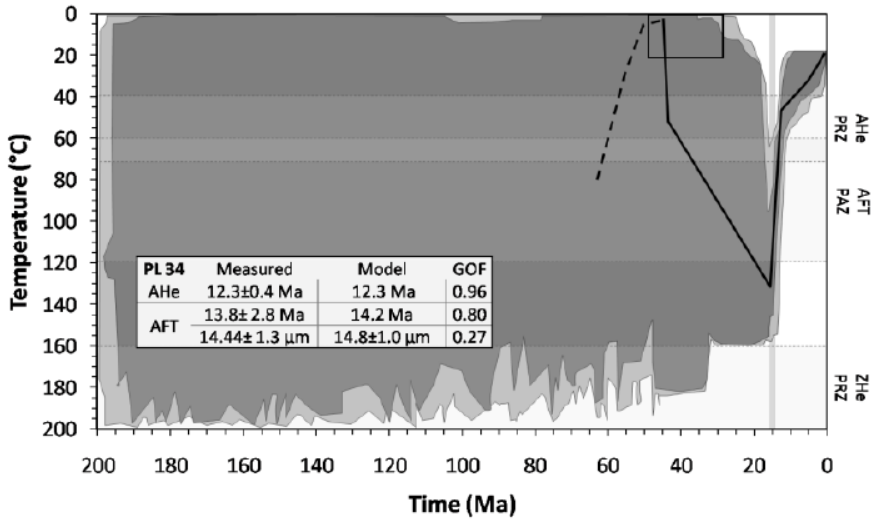
Temperature (°C)
Time (Ma)
AHe PRZ
AFT PAZ
ZHe PRZ
PL 34 | Measured | Model | GOF
AHe | 12.3±0.4 Ma | 12.3 Ma | 0.96
AFT | 13.8± 2.8 Ma | 14.2 Ma | 0.80
14.44± 1.3 µm | 14.8±1.0 µm | 0.27

c)

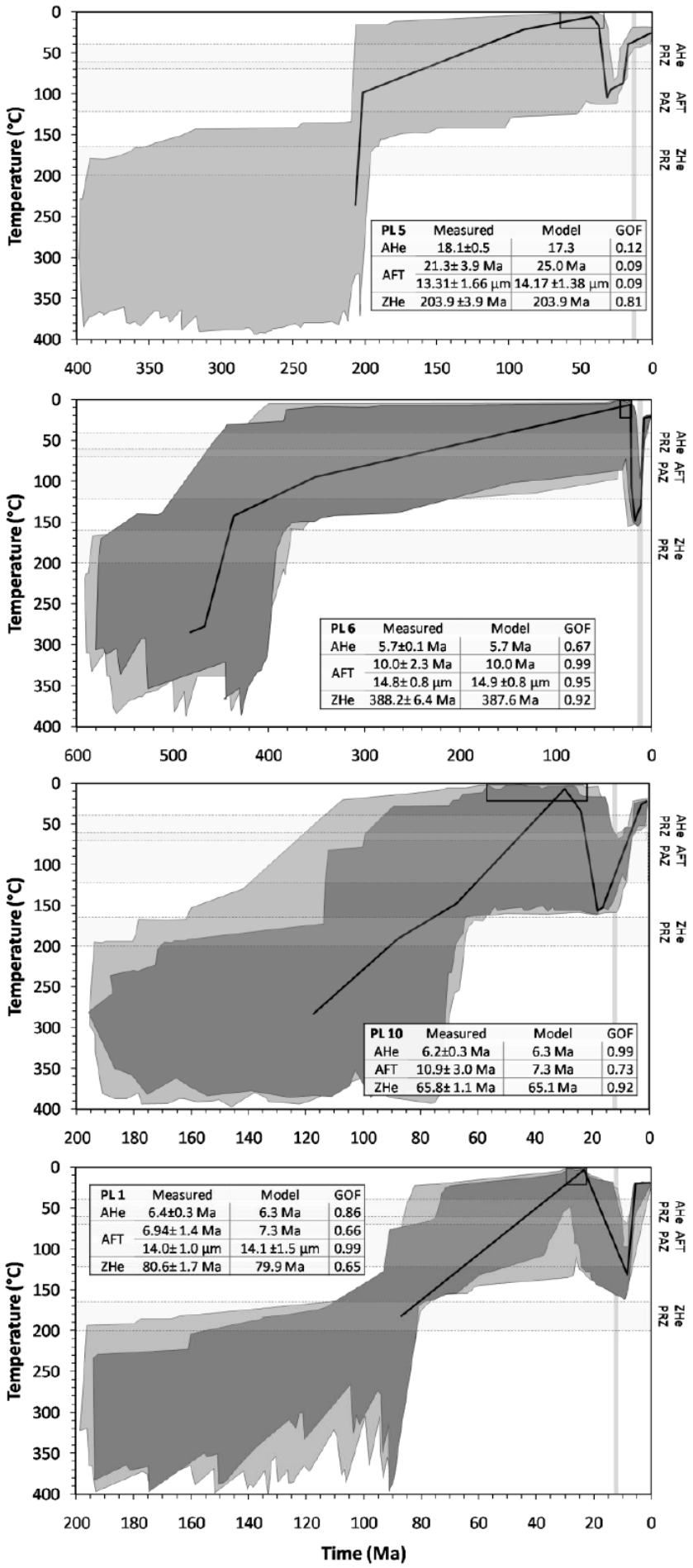
Temperature (°C)
Time (Ma)
AHe PRZ
AFT PAZ
ZHe PRZ
PL 5 | Measured | Model | GOF
AHe | 18.1±0.5 | 17.3 | 0.12
AFT | 21.3± 3.9 Ma | 25.0 Ma | 0.09
AFT | 13.31± 1.66 µm | 14.17 ±1.38 µm | 0.09
ZHe | 203.9 ±3.9 Ma | 203.9 Ma | 0.81
PL 6 | Measured | Model | GOF
AHe | 5.7±0.1 Ma | 5.7 Ma | 0.67
AFT | 10.0± 2.3 Ma | 10.0 Ma | 0.99
AFT | 14.8± 0.8 µm | 14.9 ±0.8 µm | 0.95
ZHe | 388.2± 6.4 Ma | 387.6 Ma | 0.92
PL 10 | Measured | Model | GOF
AHe | 6.2±0.3 Ma | 6.3 Ma | 0.99
AFT | 10.9± 3.0 Ma | 7.3 Ma | 0.73
ZHe | 65.8± 1.1 Ma | 65.1 Ma | 0.92
PL 1 | Measured | Model | GOF
AHe | 6.4±0.3 Ma | 6.3 Ma | 0.86
AFT | 6.94± 1.4 Ma | 7.3 Ma | 0.66
AFT | 14.0± 1.0 µm | 14.1 ±1.5 µm | 0.99
ZHe | 80.6± 1.7 Ma | 79.9 Ma | 0.65

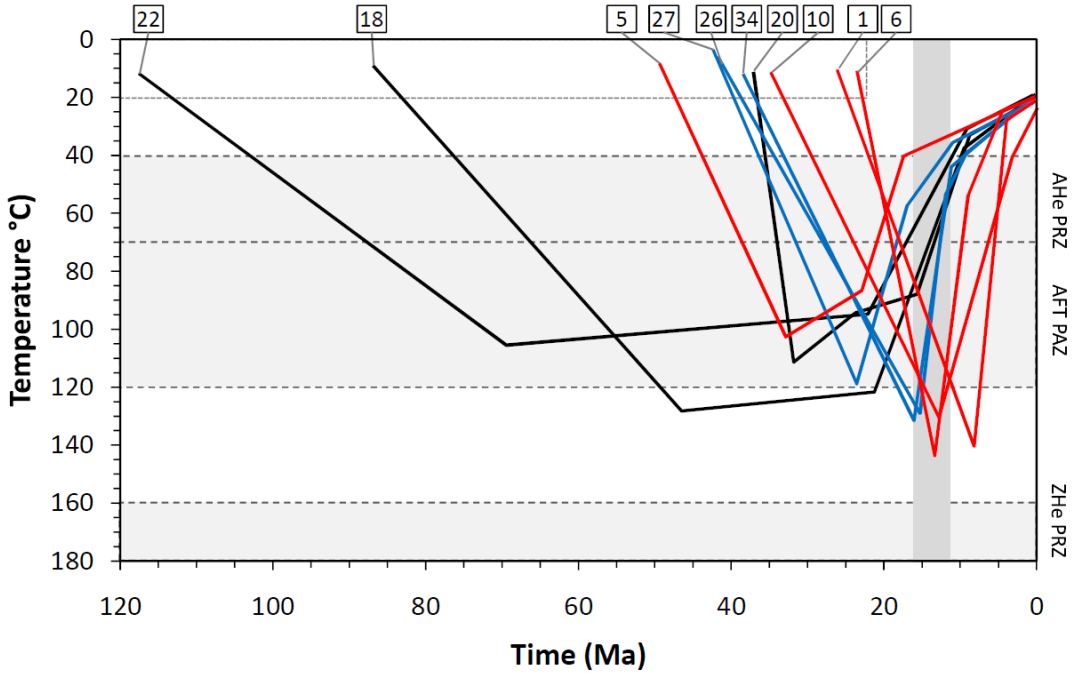

Figure 3.13 – Mean thermal histories provided by thermal modeling. The box defined by dashed line indicates depositional age, the grey field indicates the end of thrusting (Nemcok et al.,2006). Paths indicated by black line are referred to the western sector (Fig.3.11.a), paths indicated by blue lines are referred to the central sector (Fig.3.11.b) and paths indicated by red lines are referred to the eastern sector (Fig.3.11.c).

3.2.5. Discussion and interpretation

Assumptions on paleo- thermal structure

To extrapolate information on burial and exhumation from thermal histories, assumptions on the thermal field and its evolution in time are required. Present day heat flow in the studied area ranges between 40 and – locally – 80 mW/m^2 (Pospisil et al., 2006). Considering thermal conductivities of rocks forming the accretionary prism as comprised between 1.7 and 3.5 W/(m·°C), a present day geothermal gradient between 23-47°C/Km (low conductivity) and 13-23°C/Km (high conductivity) can be assessed (the highest values of 23° and 47°C/Km being confined to local heat flow maxima; Pospisil et al., 2006). Nonetheless, paleo-geothermal gradients may significantly differ from present ones. In particular it cannot be neglected that, due to extension in the Pannonian Basin, isotherm uplift below the Pannonian Basin, volcanism and subsurface magmatism in the Inner Carpathians (and less importantly in the innermost Outer Carpathians) occurred, having possibly induced an increase in geothermal gradient in the region. In this regard, it is worth of note that the paleo-thermal structure of the Polish Outer Carpathians is rather complex, being characterized by marked changes in the degree of AFT reset (e.g. sample PL 36 yielded partially reset and sample PL 35 completely reset AFT, Fig. 3.6). In particular relative minima of burial temperatures are recorded from Neogene basins (Orava-Nowy Targ, this study; Nowy Sacz, Swierczewska, 2005), whereas relative maxima occur in tectonic windows (this study; Swierczewska, 2005; Syrek, 2009). This indicates that no significant thermal overprint occurred after accretion (15-11.5 Ma), since in that case a much simpler thermal structure would be expected along the chain, with maximum degree of reset close to

the source of heating (i.e. the Pannonian Basin and the Neogene volcanic complexes), progressively decreasing with distance from it. Positive thermal perturbations extended to the whole study area during sedimentation and accretion can also be ruled out: as a matter of fact, some samples belonging to the lower stratigraphic levels show no or little degree of reset. A low geothermal gradient is thus required to justify low temperatures suffered by samples buried beneath a several Km thick sedimentary succession. Two examples are reported in Tab. 3.5, where stratigraphic position, highest temperature possibly reached, minimum thickness estimate for the overlying sedimentary pile and consequent maximum geothermal gradient are indicated. On the other hand, a localized thermal perturbation is expected close to andesites emplaced in the innermost Outer Polish Carpathians (Fig. 3.2), although the wide range of ages obtained for cooling of such rocks (ca.11-22 Ma: Birkenmajer and Pécskay, 2000; Tokarski et al., 2006 and reference therein) does not allow to better circumscribe the age of local perturbation. Localized thermal effects of Neogne volcanics is excluded on the basis of their distance from the Outer Carpathian Units (minimum of 30 Km). A constant geothermal gradient is therefore assumed throughout the study area, with values close to the lower estimates of present day gradients (13-23 °C/Km). A mean value of 18 °C/Km (the same assumed by Swierczewska, 2005 and matching with the minimum values inferred by Hurai et al, 2006) is used to estimate paleo-depths and exhumation rates from thermal paths.

Cooling of source rocks

Cooling below the ZHe PRZ of the source rocks of the sediments constituting the Magura Nappe can be described on the basis of the ZHe dataset. Several ZHe age clusters were identified (Fig. 3.11), the most numerous being referred to the Triassic (15 samples, 207.7-245.9 Ma) and the Late Cretaceous-Paleocene (10 samples; 62.4-80 Ma). The principal metamorphic and/or magmatic events recognized in the Inner Carpathian basement (e.g. Dallmeyer et al., 1996; Janak et al., 2001; Plasienka et al., 2007;) were compared with age clusters, as shown in Fig. 3.10. Permian, Devonian-Carboniferous and Early Devonian age clusters are referred to a Variscan basement unaffected by the Alpine Orogenesis. Triassic ages are likely related to unroofing (Németh et al., 2011 and reference therein) and magmatic intrusions (Uher et al.,2002) during late- to post-Variscan (and/or pre-Alpine, Uher et al., 2002) extensional stages. The Late Jurassic, Early to Middle Cretaceous and Late Cretaceous to Paleocene age clusters are related to early Alpine collision and subsequent exhumation. Provenance of the sediments of Alpine ZHe age is most likely from the Inner Carpathian basement, whereas Variscan ages could derive from the southern margin as well as from basement heights within the basin.

Heating and burial of the accretionary wedge

The present dataset allows one constraining paleotemperature patterns for the accretionary wedge. In samples belonging to the innermost thrust sheets (Magura, Dukla and innermost Silesian Units), the AHe system underwent a complete reset, the AFT system underwent partial to total reset, and the ZHe system was not reset. New data agree therefore with previously

published AFT and illite-smectite data indicating that the innermost trust sheets reached temperatures in the range of the AFT PAZ or, in some cases, slightly higher. On the other hand, the occurrence of non-reset AHe samples in the outer thrust sheets constrains, for this area, paleo-temperatures lower than 40 °C. However, it has to be specified that the data referred to the outermost portions of the chain (outermost Silesian and Skole Units) belong strictly to the eastern sector. All the inferred paleo-temperatures are 10° to 30°C lower than those obtained by Hurai et al. (2006), and in good agreement with paleo-temperature patterns presented by Swierczewska (2005) and Syrek (2009).

Given that no regional thermal anomaly occurred during sedimentation, heating of rocks entirely depends on burial. As pointed out by Mazzoli et al. (2010), significant heating (> 70-100 °C) is recorded by the uppermost strata of the stratigraphic successions (e.g. samples PL 1, PL 35, PL 25, see Fig. 3.6 and Table 1, 2 and 3), whereas samples occupying lower positions in the stratigraphic successions were heated to a lesser extent (see Tab 3.5). The lack of correlation between stratigraphic age and degree of reset indicates that sedimentary burial was responsible for heating only to a minor extent. It follows that a major role in heating was played by tectonic loading. This is also confirmed by the higher degree of reset of samples gathered inside tectonic windows (i.e. from footwall rocks) with respect to those collected outside them (i.e. in the hanging wall block; samples PL 35- PL 36; PL 6- PL5; Fig 3.5, 3.11, 3.12). Assuming a surface temperature of 5 °C, estimated burial depths for the innermost thrust sheets range between 3.6 and 8.6 Km, whereas the outer thrust sheets were buried at depths lower than 3.6 Km.

sample	structural position	depositional age	maximum paleo-temperature	minimum thickness of overburden	maximum paleo-geothermal gradient
PL 12	Silesian unit	Late Cretaceous- early Paleocene	> 70°C	3.2 Km	>20°C/Km
PL 13	Silesian unit	Late Cretaceous- early Paleocene	> 70°C	3.2 Km	>20°C/Km

Minimum thickness of the sedimentary overburden is inferred from the balanced section presented in Fig.3.

Table 3.5 – Examples of samples characterized by low reset despite the deep position in the sedimentary succession

Cooling and exhumation of the accretionary wedge

Cooling paths of rocks belonging to the wedge can be described on the basis of coupled ages and AFT lengths data and supported by thermal models. As already pointed out, heating and subsequent cooling mainly depend on tectonic burial and exhumation, implying the nearly correspondence between cooling and exhumation paths. The eastward younging trend described by Zattin et al. (2010), well compatible with the progressive eastward migration of the tectonic activity, is supported by new data presented in this study (Fig. 3.7 and 3.13). Thermal paths indicate that rocks of the wedge, either being buried up to temperatures higher than 120° or not, and either or not having undergone several Ma permanence in the AFT PAZ, were rapidly exhumed (at a rate of 0.4-1.1 mm/yr) through the AFT PAZ and AHe PRZ by 15-5 Ma, the subsequent stage of exhumation being characterized by a significantly lower rate (less than 0.2-0.05 mm/yr). Besides this, it can be observed that several samples, mostly belonging to the western sector, underwent a relatively long stay in the PAZ. Some of them also require a first stage of cooling down to temperatures still comprised within the PAZ preceding the main, rapid

cooling stage (which for such samples occurred at rates of *ca.* 0.8 °C/Ma, corresponding to exhumation rates of 0.4 mm/yr). Thermal paths of other samples, belonging to the central and eastern sectors, require a shorter stay in the PAZ, immediately followed by rapid cooling at rates comprised between *ca.* 11 and 20 °C/Ma (corresponding to exhumation rates of 1.1-0.6 mm/yr).
Considering the whole dataset, we can group as 'slowly cooled samples' those that yield dispersed AHe ages – coupled, in some instances, with partially reset AFT data (Fig.3.6) – whereas we term 'rapidly cooled samples' those yielding less dispersed AHe ages coupled with completely reset AFT. It can be speculated that 'slowly cooled samples' were exhumed by erosion of the wedge induced by thrusting, whereas 'rapidly cooled samples' were exhumed by a combination of erosion and tectonic unroofing induced by extension. Both processes – erosional exhumation induced by thrusting and erosional plus tectonic exhumation related with extension – are likely to have occurred throughout the whole study area. Nevertheless, tectonic exhumation related with extension appears to be more confined to circumscribed areas in the western and central sectors, whereas it is more widespread in the eastern sector. A straightforward relationship between exhumation and extensional tectonics in the eastern sector, can be inferred from Fig.3.3. As a matter of fact, the completely reset samples belonging to the Magura (PL 10), Dukla (PL 4 and PL 11) and Silesian (PL 1, PL 47 and PL 48) units are located at the footwalls of extensional faults, whereas non reset and partially reset samples are located at the hangingwalls (PL 46, Magura Unit; PL 12 and 13, Silesian Unit; PL 14, Skole Unit). This picture is consistent with eastward changes in topography, characterized by decreasing relief and a transition from an alternation of heights and lows to a generally low and apparently 'collapsed' topography (area comprised between *ca.*21° and *ca.*22.5° of longitude, Fig. 3.1)

3.2.6. Conclusions

This work allowed us reconstructing the thermal evolution and constraining burial and exhumation history of the Outer Polish Carpathians.
Three main conclusions may be drawn regarding cooling of the source rocks, and burial and exhumation history of the wedge:
Provenance of source terrains are from rocks that cooled below the ZHe PRZ during three main stages: a pre-Variscan stage, a Variscan stage and an Alpine stage. The two principal age clusters are referred to the Triassic and Late Cretaceous-Paleocene, and can be related to Post-Variscan extension and Early Alpine collision, respectively. Alpine ages likely come from the southern margin of the Outer Carpathian sedimentary basin, whereas Variscan and pre-Variscan ages are compatible with provenances from both the southern margin and basement heights within the basin.
Heating of the wedge was mainly due to tectonic and, less importantly, to sedimentary burial, the spatial pattern of reset degree being mainly dependent on wedge geometry. The innermost thrust sheets reached burial temperatures higher than the AHe total reset temperature and lower than the ZHe PRZ minimum temperature. Assuming a constant and homogeneous paleo-geothermal gradient of 18°C/Km, burial of the innermost units of the Outer Polish Carpathians

was comprised between 3.6 and 8.6 Km, whereas burial of the outermost thrust sheets was lower than 3.6 Km.

Cooling of the wedge, assumed to result essentially from exhumation, represents the most controversial aspect to be assessed, due to the complex interplay among different processes. As a matter of fact, thrusting was progressively overlapped by extension during the Late Miocene, thereby providing two processes suitable to induce exhumation. Thermal models indicate that cooling occurred mainly between the Early and the Late Miocene, by a first stage of relatively rapid exhumation (at rates of 0.4-1.1 mm/yr) terminated by 15-5 Ma, followed by a stage of slow exhumation (at rates of 0.2-0.05 mm/yr). The first stage of rapid exhumation is likely related to tectonic exhumation or to erosional exhumation enhanced by uplift associated with thrusting or normal faulting, whereas the last stage of exhumation reflects post-orogenic erosion. Two slightly different paths of cooling, and consequently of exhumation, are inferred based on thermal models. The first is characterized by lower cooling and exhumation rates, generally lower burial temperatures and long (i.e. several Ma) permanence in the PAZ. The second path involves higher burial temperatures and faster cooling rates. We suggest that slower exhumation was driven by erosion of the wedge during accretion, whereas faster exhumation consisted of coupled erosional and tectonic unroofing associated with extensional tectonics. Tectonic exhumation appears to have been dominant in the eastern sector, where also topographic and geologic features suggest a more widespread occurrence of extension.

3.2.8 Data Tables

Table 3.2 – Apatite (U-Th-Sm)/He analytical data

sample	replicate	Th/U (atomic)	raw age (Ma)	±σ (Ma)	mass (µg)	mwar (um)	U (ppm)	Th (ppm)	Sm (ppm)	4He (nmol/g)	HAC	eU (ppm)	corrected age (Ma)	±σ (Ma)
PL 1	BA PL1_01	13.46	7.3	0.2	3.0	55.8	4.1	53.6	77.4	0.67	0.72	16.7	10.2	0.3
	BA PL1_05	0.74	7.3	0.1	2.0	40.0	54.4	39.5	136.4	2.53	0.66	63.6	11.1	0.2
	BA PL1_07	19.23	6.0	0.2	1.8	40.5	2.9	53.4	61.3	0.51	0.63	15.4	9.5	0.4
	BA PL1_09	22.44	4.1	0.2	1.4	42.3	5.4	117.1	337.2	0.73	0.64	32.9	6.3	0.4
	BA PL1_10	3.99	6.1	0.1	1.5	42.3	66.8	259.9	149.2	4.23	0.66	127.9	9.2	0.1
PL 5	BA PL5_01	0.42	9.5	0.2	0.9	34.0	87.9	36.3	341.2	4.99	0.59	96.4	16.1	0.3
	BA PL5_07	0.15	15.8	0.3	1.1	35.8	114.3	16.7	364.8	10.11	0.65	118.2	24.2	0.5
	BA_PL5_06	0.14	10.0	0.3	0.7	30.8	94.2	12.7	187.7	5.26	0.61	97.2	16.5	0.5
	BA_PL5_08	2.23	8.0	0.2	1.6	39.8	20.0	43.4	371.2	1.32	0.66	30.2	12.1	0.4
PL 6	BA PL6_02	5.81	7.1	0.1	1.4	36.5	86.9	491.9	289.2	7.80	0.61	202.5	11.6	0.2
	BA PL6_04	12.53	8.0	0.1	1.6	33.3	23.1	282.0	465.4	3.93	0.61	89.4	13.2	0.2
	BA_PL6_05	35.99	5.7	0.1	2.1	41.8	7.6	267.8	143.5	2.18	0.64	70.6	8.8	0.2
PL 10	BA_PL10_01	6.52	6.0	1.6	0.7	34.8	13.2	83.6	75.4	1.06	0.58	32.8	10.2	2.8
	BA_PL10_02	7.73	4.2	0.2	2.2	46.5	17.4	131.4	348.8	1.12	0.69	48.3	6.2	0.3
	BA_PL10_03	15.43	6.3	0.5	2.3	45.8	3.7	56.1	307.0	0.59	0.68	16.9	9.2	0.8
PL 11	BA_PL11_01	4.62	5.8	0.3	1.7	42.8	22.0	99.2	350.0	1.43	0.67	45.3	8.6	0.4
	BA_PL11_03	5.82	7.5	0.2	3.7	60.0	17.9	101.5	163.3	1.70	0.75	41.8	10.0	0.2
	BA_PL11_04	8.14	4.4	0.3	1.5	42.3	14.2	112.7	195.1	0.97	0.66	40.7	6.7	0.5
PL 12	BA_PL12_01	4.29	29.7	1.0	1.5	44.5	13.9	58.2	332.9	4.51	0.67	27.6	44.4	1.5
	BA_PL12_04	0.26	59.5	1.9	0.9	31.3	21.4	5.4	320.7	7.44	0.58	22.7	102.6	3.2
	BA_PL12_06	0.70	65.9	1.8	1.2	36.5	19.0	13.0	427.3	8.07	0.62	22.1	106.6	2.8
PL 13	BA_PL13_01	0.14	68.3	1.5	1.5	37.0	44.5	6.1	316.9	17.14	0.64	45.9	106.9	2.4
	BA_PL13_04	0.11	83.5	1.6	1.3	44.3	78.1	8.2	178.4	36.38	0.70	80.0	119.9	2.4
	BA_PL13_05	0.02	76.0	1.5	0.8	37.5	174.4	3.1	263.6	72.36	0.63	175.1	120.1	2.4
PL 14	BA_PL14_01	2.85	63.1	2.6	0.9	35.8	7.2	20.0	275.2	4.20	0.62	11.9	102.4	4.2
	BA_PL14_02	10.86	23.2	0.6	3.8	69.0	3.3	34.7	161.7	1.47	0.75	11.4	30.9	0.8
	BA_PL14_03	12.70	24.4	1.0	2.6	50.3	3.6	44.3	160.5	1.88	0.71	14.0	34.6	1.4
PL 15	BA_PL15_03	17.79	11.4	0.4	1.6	32.5	6.3	109.6	217.8	2.00	0.60	32.1	18.9	0.7
	BA_PL15_05	17.54	10.2	0.5	1.6	34.0	5.0	85.8	188.9	1.41	0.61	25.2	16.7	0.9
	BA_PL15_06	19.58	12.4	0.4	1.6	35.5	7.6	144.7	216.8	2.82	0.60	41.6	20.5	0.6
PL 16	BA_PL16_06	1.77	9.1	0.2	2.3	45.3	34.0	58.6	557.7	2.37	0.68	47.8	13.3	0.3
	BA_PL16_07	4.19	10.5	0.5	1.8	44.0	7.4	30.1	74.6	0.83	0.68	14.5	15.5	0.8
PL 18	BA_PL18_04	6.31	8.0	0.2	1.9	52.0	34.0	209.0	660.9	3.65	0.69	83.1	11.5	0.4
	BA_PL18_05	24.67	10.0	0.2	2.7	51.0	11.7	281.0	497.5	4.27	0.71	77.7	14.2	0.3
	BA_PL18_06	2.03	8.8	0.2	3.0	50.0	83.5	165.5	291.7	5.82	0.73	122.4	12.1	0.2
PL 19	BA_PL19_01	7.91	7.7	0.2	1.4	32.8	28.2	217.4	289.5	3.33	0.61	79.3	12.7	0.4
	BA_PL19_03	19.08	4.8	0.1	1.9	52.8	7.7	142.7	97.9	1.08	0.69	41.2	7.0	0.2
	BA_PL19_04	3.45	8.6	0.5	1.5	40.3	34.0	114.3	445.2	2.87	0.67	60.8	12.9	0.7
	BA_PL19_05	133.83	7.1	0.6	2.5	50.5	0.8	103.2	41.3	0.97	0.67	25.0	10.6	0.8
PL 20	BA_PL20_01	37.03	5.1	0.2	1.0	36.5	7.6	275.9	175.6	2.02	0.57	72.5	9.0	0.3
	BA_PL20_02	13.62	6.8	0.1	1.3	36.3	23.8	316.1	407.6	3.65	0.62	98.1	11.0	0.2
	BA_PL20_04	10.93	8.7	0.2	1.7	40.5	29.7	316.3	364.5	4.94	0.65	104.0	13.3	0.4
PL 21	BA_PL21_03	12.41	7.4	0.2	1.7	43.5	8.3	100.6	177.3	1.30	0.63	31.9	11.7	0.3
	BA_PL21_01	14.51	7.1	0.1	1.0	34.8	33.6	476.1	184.8	5.58	0.57	145.5	12.4	0.2
PL 22	BA_PL22_01	1.26	10.7	0.2	2.9	49.5	30.3	37.2	103.7	2.26	0.74	39.0	14.6	0.3
	BA_PL22_02	0.02	10.2	0.3	0.7	37.3	34.2	0.7	150.5	1.90	0.58	34.4	17.6	0.5
	BA_PL22_04	0.16	11.8	0.4	1.2	40.0	35.4	5.4	198.8	2.35	0.68	36.7	17.4	0.6
	BA_PL22_06	5.34	9.7	0.5	1.6	33.8	6.1	32.0	63.0	0.72	0.62	13.7	15.5	0.9

sample	replicate	Th/U (atomic)	raw age (Ma)	±σ (Ma)	mass (µg)	mwar (um)	U (ppm)	Th (ppm)	Sm (ppm)	4He (nmol/g)	HAC	eU (ppm)	corrected age (Ma)	±σ (Ma)
PL 23	BA_PL23_01	2.44	9.6	0.3	2.3	43.0	15.9	37.8	200.9	1.30	0.69	24.8	13.8	0.5
	BA_PL23_02	4.39	10.7	0.9	1.9	44.3	4.8	20.6	288.7	0.58	0.69	9.7	15.4	1.3
	BA_PL23_03	1.05	11.3	2.3	3.6	53.8	6.3	6.5	89.8	0.48	0.73	7.8	15.5	3.1
PL 24	BA_PL24_01	0.19	25.3	0.5	2.4	47.8	145.1	26.5	304.1	20.72	0.72	151.4	35.1	0.7
	BA_PL24_03	1.23	8.7	0.2	1.3	35.5	66.9	80.2	273.1	4.05	0.62	85.7	14.1	0.3
	BA_PL24_04	3.62	10.8	0.5	2.0	44.8	8.7	30.7	111.7	0.93	0.69	15.9	15.7	0.8
	BA_PL24_07	0.30	15.8	0.6	2.2	44.3	11.5	3.3	126.5	1.06	0.70	12.3	22.5	0.9
PL 25	BA_PL25_01	0.40	9.5	0.2	2.4	46.3	44.7	17.2	331.0	2.53	0.71	48.7	13.4	0.3
	BA_PL25_02	2.19	5.9	1.0	0.6	31.0	18.1	38.6	236.9	0.87	0.56	27.2	10.4	1.7
PL 26	BA_PL26_01	0.98	10.0	0.5	1.6	40.5	18.4	17.7	493.0	1.25	0.65	22.6	15.3	0.7
	BA_PL26_04	0.42	11.2	0.2	3.0	53.3	117.4	48.0	324.1	7.77	0.74	128.7	15.1	0.3
	BA_PL26_05	3.45	8.5	0.2	3.1	51.5	22.1	74.2	115.2	1.82	0.70	39.5	12.0	0.2
PL 27	BA_PL27_01	0.47	12.4	0.3	1.2	35.0	122.6	56.7	133.1	9.13	0.64	136.0	19.5	0.5
	BA_PL27_03	1.04	10.1	0.3	2.5	39.0	20.3	20.6	210.7	1.39	0.67	25.1	15.2	0.4
	BA_PL27_07	5.43	11.3	0.9	3.9	54.8	1.5	7.7	19.0	0.20	0.72	3.3	15.8	1.2
PL 28	BA_PL28_01	1.49	13.6	0.3	5.1	63.8	14.5	21.1	232.1	1.46	0.78	19.5	17.6	0.3
	BA_PL28_02	2.54	9.0	0.2	1.0	36.8	69.7	172.7	171.0	5.40	0.63	110.3	14.4	0.4
	BA_PL28_03	1.42	11.9	0.2	1.4	40.5	69.0	95.8	410.6	5.93	0.64	91.5	18.6	0.4
	BA_PL28_04	1.64	11.7	0.3	1.5	41.0	28.8	46.2	219.1	2.54	0.67	39.7	17.6	0.5
PL 29	BA_PL29_01	4.15	11.9	1.2	1.5	41.0	9.7	39.4	276.2	1.24	0.63	19.0	18.8	1.9
	BA_PL29_02	1.35	10.5	0.5	1.7	45.3	33.5	44.2	174.6	2.51	0.69	43.9	15.3	0.7
	BA_PL29_03	7.76	9.6	0.6	1.3	43.5	6.8	51.2	323.6	1.00	0.67	18.8	14.4	0.9
PL 30	BA_PL30_01	6.40	12.9	0.5	1.6	41.3	9.3	57.9	325.5	1.63	0.63	22.9	20.4	0.8
	BA_PL30_02	5.00	14.2	2.1	1.9	43.0	3.8	18.6	175.2	0.65	0.69	8.2	20.7	3.1
	BA_PL30_03	9.11	11.4	0.3	6.5	61.0	3.5	31.3	202.5	0.69	0.77	10.9	14.9	0.4
PL 32	BA_PL32_03	41.56	8.4	0.2	1.4	40.5	6.4	260.4	139.2	3.10	0.64	67.6	13.1	0.4
	BA_PL32_04	7.64	8.6	0.3	1.9	44.0	11.5	85.9	522.7	1.52	0.65	31.7	13.3	0.4
	BA_PL33_01	77.71	5.8	0.2	1.3	40.0	3.4	255.8	328.0	2.00	0.64	63.5	9.0	0.3
PL 33	BA_PL33_02	18.43	8.3	0.6	1.5	34.8	7.6	135.7	207.4	1.79	0.62	39.4	13.5	0.9
	BA_PL33_03	2.14	10.4	1.0	0.6	31.8	8.1	16.8	76.6	0.68	0.59	12.1	17.6	1.7
	BA_PL33_05	3.38	14.2	0.6	1.8	44.5	9.2	30.3	213.6	1.27	0.68	16.3	20.8	0.8
PL 34	BA_PL34_01	3.17	9.2	0.3	1.4	39.0	28.0	86.5	240.2	2.43	0.65	48.3	14.2	0.4
	BA_PL34_03	20.12	8.3	3.6	0.7	34.3	2.4	47.9	331.0	0.64	0.59	13.7	14.2	6.1
	BA_PL34_04	1.19	10.6	0.3	2.5	47.5	54.8	63.5	277.8	4.01	0.71	69.7	14.9	0.4
	BA_PL34_05	11.32	9.1	0.3	5.5	56.3	4.3	48.0	224.5	0.79	0.73	15.6	12.4	0.4
PL 35	BA_PL35_01	3.13	8.9	0.2	2.8	51.8	11.2	34.3	131.2	0.94	0.70	19.3	12.7	0.3
	BA_PL35_02	3.00	7.7	0.5	1.9	47.0	3.7	10.8	22.2	0.26	0.71	6.2	10.9	0.8
	BA_PL35_03	7.68	8.3	0.6	1.5	44.5	13.6	101.9	214.2	1.70	0.67	37.6	12.5	0.9
PL 36	BA_PL36_02	2.34	10.2	0.2	2.8	50.0	33.8	77.3	165.1	2.88	0.73	52.0	14.0	0.2
	BA_PL36_03	2.77	11.5	0.2	4.3	60.8	14.1	38.2	250.2	1.46	0.76	23.1	15.1	0.2
	BA_PL36_05	0.95	12.1	0.6	1.3	41.3	16.6	15.4	138.9	1.33	0.64	20.2	18.9	0.9
PL 37	BA_PL37_01	5.57	7.6	0.2	0.7	35.8	30.4	164.9	280.6	2.87	0.61	69.1	12.5	0.3
	BA_PL37_02	1.94	11.0	0.1	1.7	40.3	162.5	306.6	305.6	14.02	0.65	234.6	17.0	0.2
	BA_PL37_04	1.46	9.9	0.2	1.4	41.5	52.9	75.2	172.9	3.80	0.67	70.6	14.9	0.3
PL 38	BA_PL38_01	1.18	13.2	0.2	2.7	48.0	89.2	103.1	249.2	8.10	0.72	113.4	18.3	0.3
	BA_PL38_04	1.91	14.5	0.3	1.1	38.3	25.4	47.5	355.2	2.91	0.64	36.6	22.8	0.4
	BA_PL38_05	3.17	59.6	0.8	3.0	51.0	20.5	63.3	496.1	11.64	0.70	35.4	84.9	1.2
	BA_PL38_06	1.51	40.6	0.7	1.8	48.5	14.2	21.0	519.5	4.36	0.71	19.2	56.9	1.0

sample	replicate	Th/U (atomic)	raw age (Ma)	±σ (Ma)	mass (µg)	mwar (um)	U (ppm)	Th (ppm)	Sm (ppm)	4He (nmol/g)	HAC	eU (ppm)	corrected age (Ma)	±σ (Ma)
PL 39	BA_PL39_01	2.19	14.5	0.5	0.8	32.8	22.9	48.7	466.9	2.73	0.59	34.3	24.3	0.9
	BA_PL39_02	1.59	42.8	0.6	1.5	37.8	60.3	93.3	493.3	19.21	0.64	82.2	67.4	0.9
	BA_PL39_03	0.17	69.1	1.2	2.8	48.0	80.3	13.0	199.3	31.31	0.71	83.4	97.6	1.7
	BA_PL39_04	0.79	11.3	0.3	0.9	37.3	28.5	22.0	337.5	2.07	0.63	33.6	17.9	0.5
PL 40	BA_PL40_01	5.80	8.0	0.1	1.6	40.0	24.5	138.3	320.0	2.48	0.63	57.0	12.6	0.2
	BA_PL40_02	7.68	6.5	0.3	0.8	37.8	9.7	72.9	461.6	0.97	0.62	26.9	10.5	0.5
	BA_PL40_03	5.55	9.0	0.1	1.2	35.8	44.5	240.7	439.1	4.95	0.60	101.1	15.0	0.2
	BA_PL41_01	38.42	4.4	0.1	0.7	33.8	6.4	238.1	137.2	1.50	0.53	62.3	8.3	0.3
PL 41	BA_PL41_02	8.62	8.9	0.1	2.2	48.0	20.3	170.7	223.0	2.93	0.69	60.4	12.8	0.2
	BA_PL41_03	1.99	7.9	0.2	1.0	37.0	38.7	75.0	192.2	2.41	0.60	56.3	13.2	0.3
PL 42	BA_PL42_01	0.60	10.4	0.3	3.6	50.5	9.0	5.3	234.7	0.59	0.72	10.2	14.4	0.4
	BA_PL42_02	8.87	11.4	0.5	1.2	40.5	7.7	67.0	193.9	1.47	0.64	23.5	17.9	0.7
	BA_PL42_04	4.02	10.0	0.3	2.7	55.0	20.4	79.9	228.7	2.13	0.74	39.1	13.5	0.4
PL 43	BA_PL43_01	0.02	58.1	3.4	0.5	31.3	72.8	1.2	127.8	23.03	0.58	73.1	100.3	5.8
PL 44	BA_PL44_03	2.37	8.3	0.2	1.5	38.5	34.0	78.5	183.2	2.37	0.66	52.4	12.7	0.4
	BA_PL44_04	1.00	22.1	0.7	2.1	44.5	10.7	10.4	102.2	1.58	0.68	13.2	32.6	1.0
PL 46	BA_PL46_01	1.50	9.1	0.3	1.4	33.8	89.5	130.8	310.4	5.94	0.63	120.2	14.4	0.4
	BA_PL46_02	5.96	12.7	0.4	0.7	34.5	29.3	170.0	416.4	4.79	0.60	69.2	20.9	0.6
	BA_PL46_03	0.28	12.4	0.4	1.0	36.8	37.9	10.4	337.7	2.73	0.64	40.4	19.4	0.7
	BA_PL46_04	0.13	10.1	0.4	0.8	34.0	31.3	3.9	195.2	1.76	0.63	32.2	15.9	0.7
PL 47	BA_PL47_01	8.11	49.8	2.1	0.7	34.3	8.3	65.4	1028.1	6.73	0.58	23.6	86.1	3.6
	BA_PL47_03	6.18	6.5	1.3	0.9	33.5	6.4	38.8	77.5	0.56	0.59	15.6	11.1	2.2
	BA_PL47_04	4.02	20.3	0.6	2.3	47.5	7.1	27.7	59.8	1.50	0.70	13.6	29.0	0.9
	BA_PL47_05	0.59	33.7	0.9	0.9	33.8	55.0	31.8	217.7	11.42	0.62	62.5	54.7	1.5
	BA_PL47_06	1.75	9.9	0.3	0.9	33.5	32.5	55.6	267.5	2.46	0.61	45.6	16.3	0.5
PL 48	BA_PL48_01	0.84	6.6	0.3	1.5	39.3	18.4	15.1	192.9	0.79	0.67	21.9	9.9	0.5
	BA_PL48_02	1.74	6.4	0.3	0.9	33.8	34.4	58.4	359.8	1.69	0.61	48.1	10.5	0.5
	BA_PL48_03	6.10	8.1	0.9	0.9	37.0	5.1	30.5	33.1	0.54	0.61	12.3	13.2	1.4
	BA_PL48_04	6.05	6.8	0.3	1.6	42.8	6.9	40.6	253.6	0.62	0.66	16.4	10.3	0.5

12 crystals were excluded from this compilation and not taken in account in the discussion. Criteria for discarding a crystal were: a) outlier age value accompanied by marked imperfections observed in the grain (bad shape, inclusions); b) outlier age value accompanied by extremely high or low analytical values; c) outlier age value with no apparent meaning (e.g. non reset age in crystal belonging to a sample with completely reset AFT age).

Sample	No. of crystals	Spontaneous		Induced		$P(\chi)^2$ (%)	Dosimeter		Age ± SE (Ma)	Mean confined track lenght ± SE (μm)	SD (μm)	No. of tracks measured	Mean Dpar ± SD (μm)	Minimum age ± SE (Ma)
		r_s	N_s	r_i	N_i		r_d	N_d						
PL 25*	11	1.52	28	23.47	433	94.3	11.50	5405	12.8±2.6	n.d.	n.d.	n.d.	n.d.	12.8±2.6
PL 31	20	0.39	22	5.01	286	100.0	11.19	5318	15.8±3.5	n.d.	n.d.	n.d.	2.03±0.39	15.8±3.5
PL 46	20	10.24	376	35.60	1308	0.0	10.94	5201	50.4±8.1	10.26±0.37	2.43	44	1.617±0.38	36.3±6.3
PL 47	20	5.70	239	29.20	1224	0.0	10.88	5172	27.9±6.0	11.56±0.22	1.70	59	1.31±0.37	13.2±2.2

Central ages calculated using dosimeter glass CN5 and z-CN5=366.76±2.9, z*-CN5=345.53±18.45 (* indicates the sample analyzed with z*; z and z* correspond to different operators) and the sofwtare TrackKey vers. 4.2 (Dunkl, 2002). r_s: spontaneous track densities (x 105 cm-2) measured in internal mineral surfaces; N_s: total number of spontaneous tracks; r_i and r_d: induced and dosimeter track densities (x 106 cm-2) on external mica detectors (g=0.5); N_i and N_d: total numbers of tracks; $P(\chi^2)$: probability of obtaining χ^2-value for n degrees of freedom (where n=number of crystals-1); a probability >5% is indicative of an homogenous population. Minimum age is the peak age of the youngest age population obtained for partially reset samples using the BINOMFIT software (Brandon 1992). Sample preparation: Apatite grains were separated using heavy liquids and magnetic separation techniques. Mounts of apatite in epoxy were polished and then etched with 5M HNO3 at 20°C for 20 s to reveal spontaneous fission tracks. Samples were then irradiated with a CN5 dosimeter in the reactor at the Radiation Center of Oregon State Univ. with a nominal neutron fluence of 9x1015 n cm^{-2}. After irradiation induced fission tracks in the low-U muscovite detector were revealed by etching with 40% HF at 20°C for 45 min. Samples were analyzed with a Zeiss Axioskop microscope equipped with a digitizing tablet and drawing tube and controlled by the program FTStage 3.11 (Dumitru, 1993). FT ages were calculated using the external-detector and the zeta-calibration methods with IUGS age standards and a value of 0.5 for geometry correction factor. χ^2 test was used to detect whether the data sets contained any extra-Poissonian error.

Table 3 – Apatite Fission Track analytical data

sample	replicate	Th/U (atomic)	raw age (Ma)	±σ (Ma)	mass (µg)	half width (µm)	U (ppm)	Th (ppm)	eU (ppm)	4He (nmol/g)	HAC	corrected age (Ma)	±σ (Ma)
PL 1	BA_PL1_02zr	0.5	47.9	1.2	2.6	35.5	247.8	111.4	274.0	71.03	0.72	66.8	1.7
	BA_PL1_01zr	0.2	159.1	3.1	2.4	39.8	455.9	70.9	472.6	410.81	0.74	215.2	4.1
	BA_PL1_03zr	0.7	56.9	1.2	2.6	40.0	359.7	240.2	416.1	128.31	0.73	78.5	1.6
PL2	BA_PL2_02zr	0.3	151.3	3.4	2.8	37.3	307.0	90.0	328.2	271.12	0.73	208.2	4.7
	BA_PL2_03zr	0.2	136.6	2.7	9.6	50.3	559.0	98.3	582.1	433.77	0.80	169.7	3.4
PL 4	BA_PL4_01zr	0.3	181.2	3.3	2.4	39.3	211.1	67.6	227.0	225.23	0.74	245.9	4.5
	BA_PL4_02zr	0.7	398.5	6.8	2.2	34.3	203.7	140.8	236.8	526.60	0.70	566.7	9.7
PL 5	BA_PL5_01zr	0.3	41.6	0.8	2.6	32.8	390.3	109.3	416.0	93.65	0.71	58.9	1.1
	BA_PL5_02zr	0.4	59.1	1.1	3.3	38.8	460.2	177.2	501.9	160.62	0.74	80.0	1.5
	BA_PL5_03zr	0.2	139.8	2.7	2.7	36.8	366.6	58.2	380.3	290.01	0.72	192.8	3.7
PL 6	BA_PL6_01zr	0.4	170.1	3.1	6.7	56.8	104.4	37.2	113.1	105.25	0.80	213.4	3.9
	BA_PL6_02zr	0.9	271.1	4.5	3.8	38.3	123.4	109.0	149.0	222.91	0.74	366.3	6.1
	BA_PL6_04zr	0.8	53.7	0.9	3.3	38.8	334.4	258.4	395.1	114.85	0.74	72.8	1.2
PL 8	BA_PL8_01zr	0.6	162.4	2.8	6.5	45.8	190.3	104.8	215.0	190.83	0.78	207.7	3.6
	BA_PL8_02zr	0.2	90.0	1.6	1.9	31.0	415.4	97.1	438.2	214.19	0.69	130.8	2.3
PL 9	BA_PL9_01zr	0.7	156.0	2.6	3.0	43.0	183.4	132.7	214.6	182.98	0.74	212.0	3.5
	BA_PL9_02zr	0.1	166.8	3.1	3.3	37.3	430.4	49.0	441.9	403.07	0.74	226.5	4.2
	BA_PL9_03zr	0.4	135.1	2.3	5.2	36.5	210.3	87.4	230.8	170.12	0.75	180.8	3.1
PL 10	BA_PL10_03zr	0.1	46.5	0.8	3.6	39.3	889.3	72.8	906.4	228.19	0.75	62.4	1.1
PL 12	BA_PL12_01zr	0.5	478.6	8.7	5.0	44.8	338.3	161.0	376.2	1012.92	0.77	624.7	11.4
	BA_PL12_02zr	0.2	77.1	1.5	3.1	35.3	302.5	58.5	316.2	132.30	0.73	106.2	2.0
		0.2	101.9	1.9	5.4	36.0	369.7	71.3	386.5	214.05	0.75	136.6	2.5
PL 13	BA_PL13_01zr	0.3	233.4	4.3	4.8	46.5	325.3	92.8	347.1	445.77	0.77	302.4	5.6
	BA_PL13_02zr	0.5	259.2	4.6	7.3	57.3	119.3	63.1	134.1	191.67	0.80	323.8	5.7
PL 16	BA_PL16_01zr	0.9	209.8	3.6	4.6	44.0	118.5	103.5	142.8	164.50	0.76	275.8	4.7
	BA_PL16_02zr	0.8	184.5	3.0	2.3	34.3	385.0	283.0	451.5	456.24	0.71	261.5	4.3
	BA_PL16_04zr	0.2	186.6	3.3	3.7	49.8	263.8	62.4	278.5	284.79	0.78	239.3	4.3
PL 19	BA_PL19_01zr	0.7	226.6	3.8	9.4	54.5	192.0	128.7	222.2	276.90	0.81	280.0	4.7
	BA_PL19_02zr	0.3	187.0	3.3	5.6	43.0	297.8	82.9	317.3	325.22	0.77	243.1	4.3
	BA_PL19_03zr	0.7	215.4	3.6	4.5	45.5	40.5	27.8	47.0	55.64	0.77	281.2	4.7
PL 20	BA_PL20_01zr	0.5	170.1	3.0	3.4	35.0	142.4	72.8	159.6	148.52	0.73	233.8	4.1
	BA_PL20_02zr	0.3	179.0	3.1	5.0	39.0	128.0	39.6	137.3	134.58	0.76	236.5	4.1
	BA_PL20_03zr	0.3	175.8	3.0	3.0	38.5	211.7	64.9	226.9	218.43	0.73	241.5	4.1
PL 22	BA_PL22_01zr	0.2	186.1	3.5	6.9	40.0	296.9	59.2	310.8	316.91	0.77	241.8	4.5
	BA_PL22_02zr	0.4	160.5	2.8	3.4	32.8	284.9	104.9	309.6	271.68	0.72	223.9	3.9
	BA_PL22_03z	0.2	180.5	3.3	4.8	43.3	442.3	75.0	459.9	454.53	0.77	235.6	4.4
PL 23	BA_PL23_01z	0.3	128.8	2.4	2.9	34.3	184.2	55.2	197.1	138.34	0.72	178.8	3.4
	BA_PL23_02z	0.1	54.3	1.0	3.8	36.5	637.0	60.8	651.3	191.45	0.74	73.7	1.4
	BA_PL23_03zr	0.2	51.5	0.9	1.6	32.5	552.8	131.3	583.6	162.62	0.68	75.7	1.3
PL 25	BA_PL25_01zr	0.4	182.5	3.2	2.0	31.3	809.4	276.5	874.4	873.83	0.69	264.7	4.7
PL 28	BA_PL28_01zr	0.5	42.7	0.7	2.1	32.8	397.9	196.6	444.1	102.53	0.70	61.2	1.0
	BA_PL28_02zr	0.2	71.5	1.3	2.1	32.8	639.9	119.3	668.0	259.02	0.70	102.5	1.8
	BA_PL28_03zr	0.9	55.3	0.9	3.9	38.0	295.8	261.1	357.2	106.96	0.74	74.6	1.2
PL 43	BA_PL43_01zr	0.8	257.1	4.3	2.1	36.0	156.1	122.7	185.0	262.06	0.72	359.2	6.0
	BA_PL43_02zr	0.1	233.0	4.2	2.9	35.3	433.5	44.5	444.0	569.33	0.72	321.6	5.8
	BA_PL43_03zr	0.6	340.2	5.9	6.7	60.3	25.2	15.5	28.8	54.44	0.81	417.4	7.2

Table3. 4 – Zircon (U-Th)/He analytical data

CHAPTER IV.

THERMOCHRONOLOGY OF THE UKRAINIAN CARPATHIANS

4.1. Chapter Overview

This chapter is a journal paper in preparation. It presents AFT, AHe, ZHe and vitrinite data collected along three transects in the Ukrainian Carpathians. In this work the temporal and spatial relationships between the Pannonian Basin and thermochronology and burial-exhumation history of the Ukrainian Carpathians were investigated. Reconstructing these relationships allowed to go back to the processes responsible for thermal and burial-exhumation history, and to add constrains to the geodynamic evolution of the Carpathian-Pannonian region.

4.2. Paper

B. Andreucci (1), M. Zattin (1), S. Corrado (2), S. Mazzoli (3), A. Castelluccio (1), R. Szaniawski (4), and L. Jankowski (5)

(1) Department of Geosciences, University of Padua, Italy;
(2) Department of Earth Sciences, University of Roma Tre, Italy;
(3) Department of Earth Sciences, University of Naples “Federico II”, Italy;
(4) Institute of Geophysics, Polish Academy of Science, Warsaw, Poland;
(5) Polish Geological Institute-Carpathian Branch, Cracow, Poland;

4.2.1. Abstract

The Carpathian-Pannonian region is constituted by a wide extensional basin (the Pannonian Basin) surrounded by the arc shaped Carpathian mountain Belt. The Pannonian Basin formed in the Miocene by extension in retro-wedge position, while at the Carpathian front compression and thrusting were still active. The Ukrainian region represents a key area to the understanding of the relationship between the Pannonian Basin and the Carpathian mountain belt, thanks to its simple structural setting and to the progressive transition that can be clearly observed between the two regions.

In this study the effect of opening of the Pannonian Basin on thermal and burial-exhumation history of the Ukrainian Carpathians is investigated. Low temperature thermochronometry and vitrinite reflectance analysis have been applied to the Ukrainian Carpathians in order to constrain their paleo-thermal structure and to reconstruct their thermal and burial-exhumation history. The results show that burial and heating of the wedge reached their maximum in the central units (up to 170°C and 6 km), decreasing both toward the innermost and the outermost thrust sheets. Cooling and Exhumation occurred between ca. 12 and 5 Ma, through a first rapid stage (exhumation rates over 1 mm/yr) followed by a slower stage from ca. 5 Ma to present. We suggest that exhumation of the wedge occurred after the end of thrusting by erosion enhanced

by isostatic uplift, the lower extent of burial and exhumation of the innermost units being ascribed to crustal thinning occurred during the opening of the Pannonian Basin.

4.2.2. Introduction

The Carpathians are an arc-shaped fold and thrust belt that extends in Central-Eastern Europe for over 1300 Km. They formed during the Tertiary by continental collision between the Adriatic microplate and the European continent (e.g. Jiricek, 1979; Nemcok et al., 1998; Sperner et al., 2002, Royden et al., 1982; Horva´ th et al., 2006). During the final stages of thrusting, between ca. 19 and 11 Ma (Fodor, 2011), the region located in retro-wedge position underwent a prolonged stage of lithospheric thinning and extension (e.g. Csontos et al., 1992; Kovac et al., 1990) accompanied by heating and extension-related volcanism along its margins (e.g. Konecny et al., 2002; Pécskay et al., 2006; Seghedi et al.,2004). The wide depression formed during this stage, i.e. the Pannonian Basin, is characterized at present by an high heat flow (up to 110 mW/m2, Pospisil et al., 2006, Lenkey, 1999) and thinned lithosphere (Horvath, 1993; Dererova et al., 2006), as opposed to the thrust and fold belt which is characterized by an higher relief, a low heat flow (30-70 mW/m2, Pospisil et al., 2006) and a thickened lithosphere (Horvath, 1993; Dererova et al., 2006). The contrast of relief, lithospheric thickness and heat flow between the Pannonian Basin and the Carpathians is particularly evident in the Ukrainian region (Fig. 4.1, Fig. 4.2), where a progressive transition between the features characterizing the two settings can be observed in a band wide less than 50 km (Fig. 4.1, Fig. 4.2).

The Ukrainian Carpathians (UC) represent therefore a potential key region to the understanding of the relationship existing between the Pannonian Basin and the carpathian fold and thrust belt.

In this work we applied low-temperature thermochronometry and vitrinite reflectance analysis to samples belonging to the UC, to constrain the evolution in time of the thermal conditions of the wedge, and its burial-exhumation history. The results were then discussed considering their relationship with the Pannonian Basin and its associated features in order to investigate how positive thermal perturbation, extension and subsidence, occurred in the Pannonian Basin, affected the UC during their cooling, uplift and exhumation.

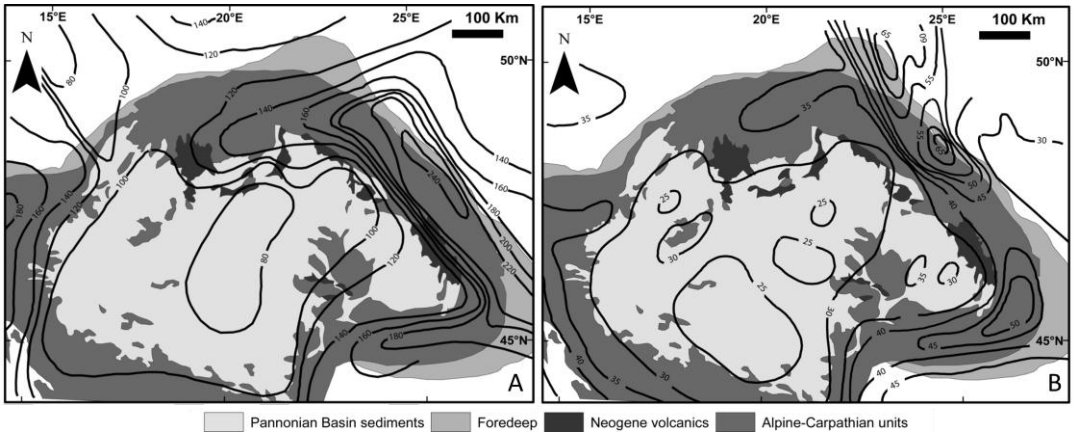

Fig. 4.1 – (A) Lithospheric (from Dererova et al., 2006) and (B) crustal thickness (from Bielik et al., 2004) of the Carpathian-Pannonian region.

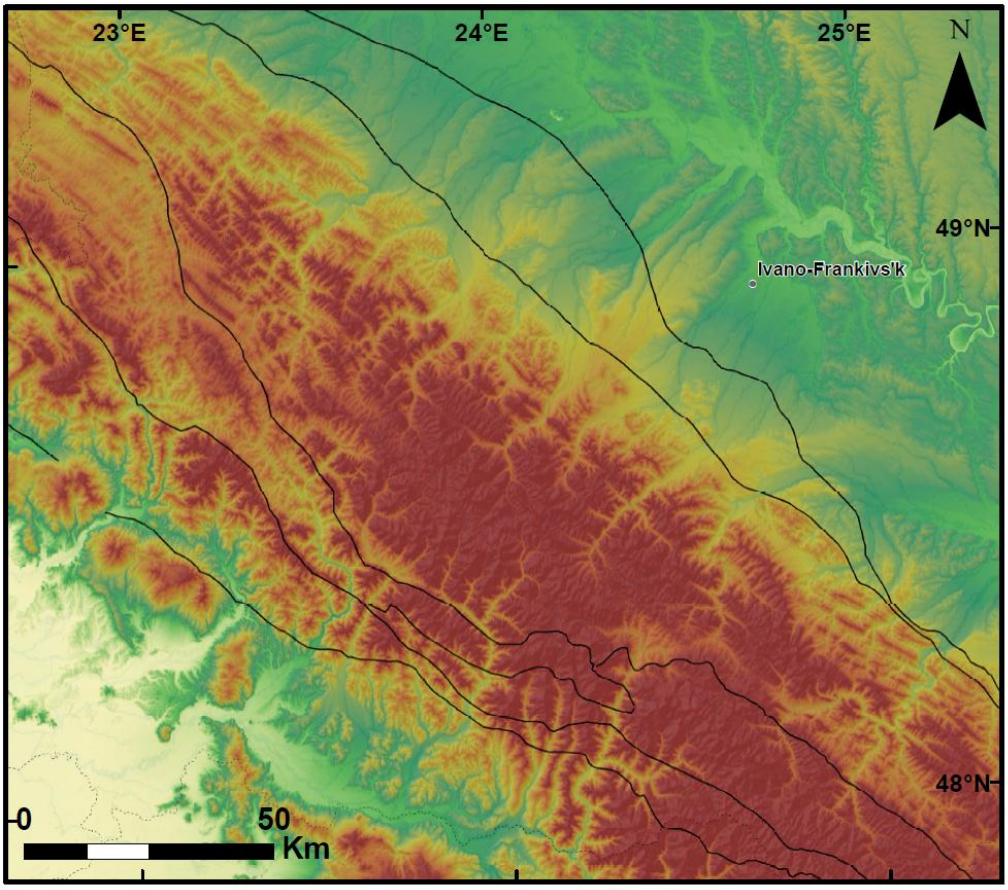

Figure 4.2- DEM of the study region

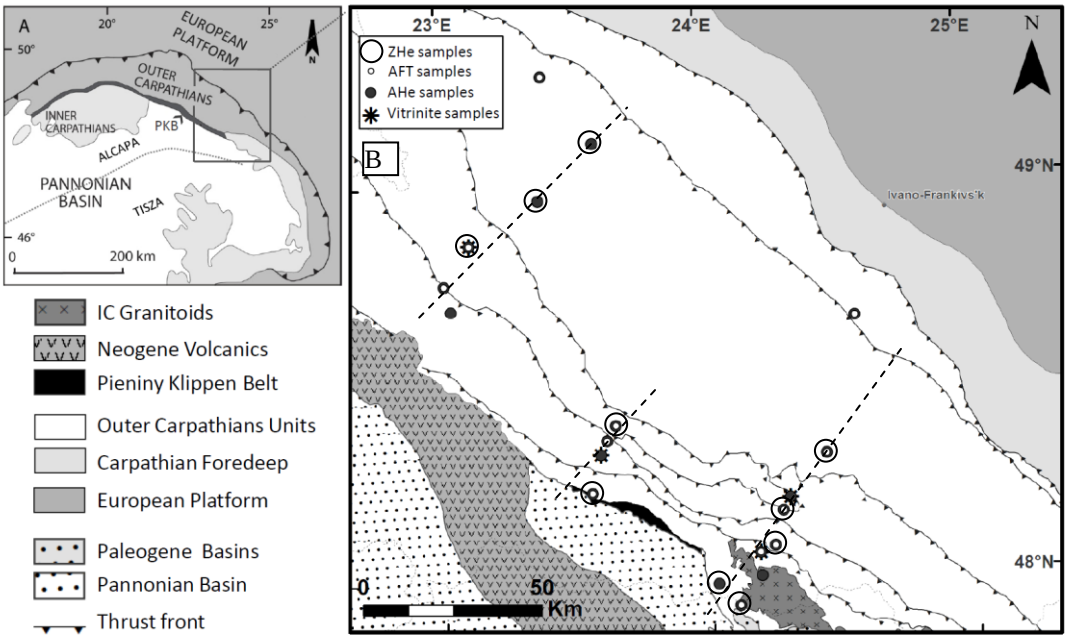

Fig. 4.3 – A- tectonic sketch map of the Carpathians. B- tectonic sketch map of the study area with AHe, ZHe and AFT sample location along the three sections a), b), c). Legend is referred to B.

4.2.3. Geological setting

The Carpathians are part of the Alpine orogenic system, and formed between Upper Cretaceous and Neogene by the collision between the Alcapa and Tisza-Dacia microplates and the European Platform (Fig. 4.3, e.g. Jiricek, 1979; Nemcok et al., 1998; Sperner et al., 2002).

Based on rock lithology and age of individual tectonic units, the Carpathians can be divided into two domains (e.g. Tasarova et al., 2009 and reference therein): the Inner Carpathians (IC) and the Outer Carpathians (OC). In the Northern and Eastern Carpathians, the contact between these domains is represented by the "Pieniny Klippen Belt" (PKB, Fig. 4.3), a narrow band of strongly deformed and sheared Mesozoic to Paleogene rocks, traditionally interpreted as an oceanic suture (Birkenmajer, 2001). The IC are a prolongation of the Eastern Alps, they are made of Variscan basement and its sedimentary cover and were deformed between the Late Jurassic and the Late Cretaceous.

The OC formed during the Tertiary as an accretionary wedge, composed of Upper Jurassic to Lower Miocene flysch sediments, thrust over Neogene strata of the Carpathian foredeep (Oszczypko et al 1998).

The evolution of the Carpathians was characterized by a progressive migration of compression E to SE ward, accompanied by rotation of the compression axis from N-S to WNW-ESE (e.g. Horváth, 1993; Jiricek, 1979; Sperner et al., 2002). Nonetheless along the whole Ukrainian region thrusting is interpreted to have ceased by 11.5 Ma (Nemcok et al., 2006), with no major shift of the depocenters along strike. In Fig. 4.3 it can be observed that the front of the chain overlaps, in this region, to the Trans European Suture Zone (TESZ), that constitutes the boundary between the thick crust and lithosphere of the East European Platform, i.e. the European Craton, and the thinner West European Platform, made by younger terranes (e.g. Pharaoh, 1999).

During the Early-Middle Miocene time, while compression was still active at the front, the Pannonian Basin formed (e.g. Kovac et al., 1990, Fodor 2000) and extension related volcanism occurred in retro wedge position (e.g. Konency et al., 2002; Pécskay et al., 2006; Seghedi et al.,2004). The proper extensional phase of the Pannonian Basin occurred between 19 and 11.5 Ma (e.g. Fodor, 2011; Horvath and Cloething, 1996), whereas between 11.5 and 5 Ma the basin underwent minor extension and major subsidence (Fodor, 2011). In the Transcarpathian Basin (i.e. the portion of the Pannonian Basin in the study area, Fig.4.3) the main stage of extension occurred between 17.5 and 14 Ma (Huismans et al., 2011).

4.2.4. Methods

Low temperature thermochronometry coupled, in some cases, with vitrinite reflectance analysis was applied to 18 samples collected along three transects of the study area (Tab. 4.1, Fig. 4.3). 15 samples are from siliciclastic sandstones of the flysch belt, samples PL 58 and PL 59 are from the IC basement and sample PL 60 is from the basement cover. Samples for vitrinite analysis were collected from siltstones of the accretionary wedge.

He analysis was performed at the Radiogenic Helium Dating Laboratory of the University of Arizona (Tucson), following the procedures described in Reiners et al. (2004). Handpicked apatites and zircons were measured for alpha-ejection correction following methods described in Reiners et al. (2007). Single crystals were loaded into 0.8 mm Nb tubes, and degassed under vacuum by heating with a Nd-YAG laser. The concentration of 4He was determined by 3He isotope dilution and measurement of the 4He/3He ratio through a quadrupole mass spectrometer. U, Th and Sm (only for apatite) concentrations were obtained by isotope dilution using an inductively coupled plasma mass spectrometer.
Intact, euhedral, inclusions and coating free grains are recommended for obtaining good analytical data (e.g. Ehlers and Farley, 2003); nonetheless in apatites from sedimentary rocks (and, to a lesser extent, zircons) such criteria are rarely met (Fig. 4.4). Based on Vermeesch et al.(2007), no significant impact on AHe dating is expected from inclusions. Therefore grains with good shape (euhedral or subhedral, intact) were preferably chosen for analysis. Anyway grains with big inclusions were discarded and, when possible, inclusions free grains were selected. As for oxide-oxhydroxide coating, in some cases alteration was pervasive to the whole rock sample and it was impossible to select uncoated crystals. In such cases the alteration grunge surrounding the crystals was mechanically removed after picking, so that the packed grains were as much as possible coating-free. For those grains a He implantation effect can be expected (Murray et al, 2011; Orme and Reiners, 2010; Reiners, 2010). Correlation of single grain ages with eU, [U], [Th], [Sm], Th/U and grain size was tested to find possible age biases and to interpret age dispersion.

AFT analysis was performed at the FT laboratory of the University of Padua. CN5 glass was used to monitor neutron fluence during irradiation at the Oregon State University Triga Reactor, Corvallis, USA. The calculation of central ages (Galbraith and Laslett, 1993) was performed through the TRACKEY software (4.2 version; Dunkl, 2000). The Chi-square ($\chi 2$) test was used to assess the homogeneity of age populations: a population is considered homogeneous for $P(\chi 2)$ higher than 5%. Through the use of the BINOMFIT software (summarized by Elhers et al., 2005) minimum ages were calculated for partially reset samples. Dpar of single crystal was measured and used as kinetic parameter. Where possible track densities were measured on over 20 grains per sample, whereas , due to the low U content, no track length measurement could be performed.

A suite of four samples for vitrinite reflectance analysis was collected; two samples belong to the innermost units (PL 68 and PL 61) and two to the central units (
Vitrinite reflectance analyses were performed at the Academic Laboratory of Basin Analysis (ALBA) of the University Roma Tre (Rome). Whole-rock samples were mounted on epoxy resin and polished according to standard procedures (Bustin 1990). Random reflectance (Ro%) was measured under oil immersion, with a Zeiss Axioplan microscope, in reflected monochromatic non-polarized light equipped MPS200 photometric system. An average 20 measurements were

performed on vitrinite fragments for each sample (only slightly fractured and/or altered). Mean reflectance and standard deviation values were calculated for all measurements. Paleotemperatures were obtained according to Barker and Pawlewicz(1994) as samples were not collected in stratigraphic continuity to allow a proper modelling.

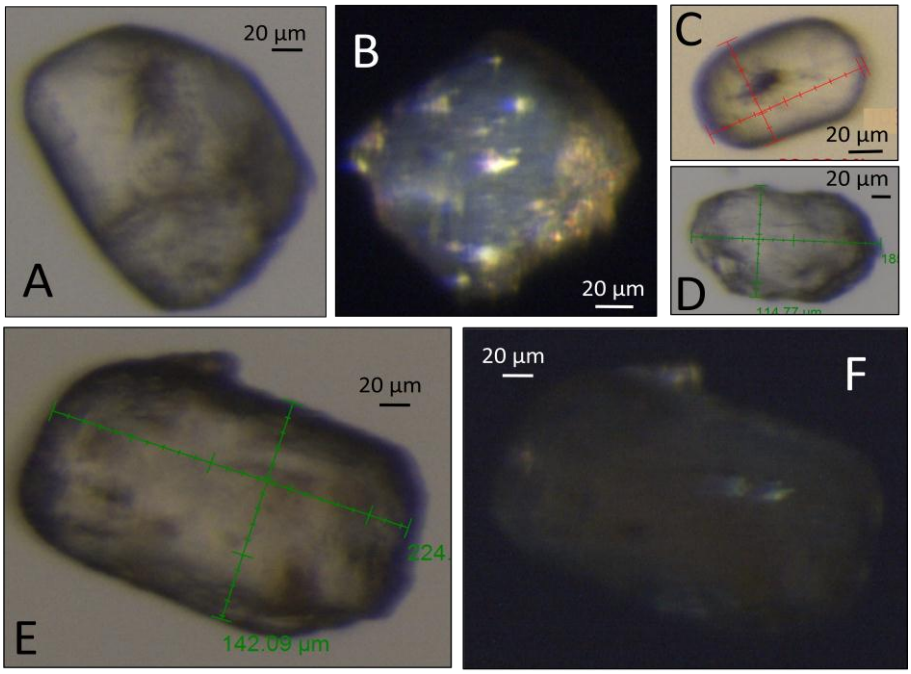

Figure 4.4 – Examples of bad crystal features: coating (A, B, E, F), inclusions (C) , abrasion (D). A- sample PL60_3; B- PL61, not packed; C- PL56_3; D-PL54_1; E and F - PL68_2

4.2.5. Results

A total of 18 samples were dated by AHe, 13 by AFT and 10 by ZHe methods. Vitrinite reflectance analysis was performed on 4 samples. A summary of the results is presented in Tab. 4.1 and Fig.4.5.

Sample	Latitude	Longitude	elevation (m)	depositional age	AHe w.m.age ± 1σ (Ma)	AFT central age ± 1σ (Ma)	ZHe mean age ± 1σ (Ma)	Vitrinite R_0%
PL 39	23.40600	49.27800	402	Eocene	32.06 ± 0.39	73 ± 9.1		
PL 50	23.59728	49.10535	394	Late Eocene - Oligocene	92.53 ± 1.18		160.39 ± 143.89	
PL 52	23.01528	48.75490	375	Late Cretaceous	5.60 ± 0.11	6.20 ± ± 0.7	50.45 ± 27.04	
PL 53	23.03987	48.69062	334	Eocene	8.75 ± 0.12			
PL 54	23.11432	48.85612	754	Oligocene	6.94 ± 0.10	7.10 ± ± 1.2		1.48 ± 0.09
PL 55	23.38268	48.96420	577	Oligocene	8.19 ± 0.15		252.14 ± 156.42	
PL 56	24.57653	48.65198	408	Early - Middle Miocene	12.94 ± 0.23	25.10 ± ± 5.8		
PL 58	24.18608	48.00190	442		10.51 ± 0.14			
PL 59	24.10122	47.92877	358		8.57 ± 0.14	8.60 ± ± 1.4	41.11 ± 9.41	
PL60	24.02183	47.98445	312	Eocene	6.10 ± 0.12		±	
PL 61	24.18275	48.06155	582	Early Cretaceous	8.40 ± 0.214	11.60 ± ± 1.7		0.69 ± 0.04
PL 62	24.24030	48.07738	471	Early Cretaceous	10.77 ± 0.17	10.10 ± ± 1.3	111.58 ± 14.62	
PL 63	24.27502	48.16510	551	Early Cretaceous	9.08 ± 0.10	9.80 ± ± 1.4	±	
PL 64	24.30370	48.19787	577	Late Cretaceous - Paleocene	7.72 ± 0.09			1.51 ± 0.10
PL 65	24.44802	48.30572	877	Oligocene	7.25 ± 0.09	10.10 ± ± 1.2	177.37 ± 37.72	
PL 67	23.55803	48.22262	206	Eocene	6.61 ± 0.13	71.00 ± ± 10.1	94.81 ± 27.97	
PL 68	23.59305	48.31918	423	Late Cretaceous - Early Paleocene	8.51 ± 0.10			0.72 ± 0.07
PL 69	23.61838	48.35420	459	Early Cretaceous	5.72 ± 0.09	8.7 ± ± 0.9		
PL 70	23.65317	48.39232	530	Eocene	6.97 ± 0.09	9.70 ± ± 1.5	75.17 ± 23.01	

Table 4.1- overview of sample properties and synthesis of the results.

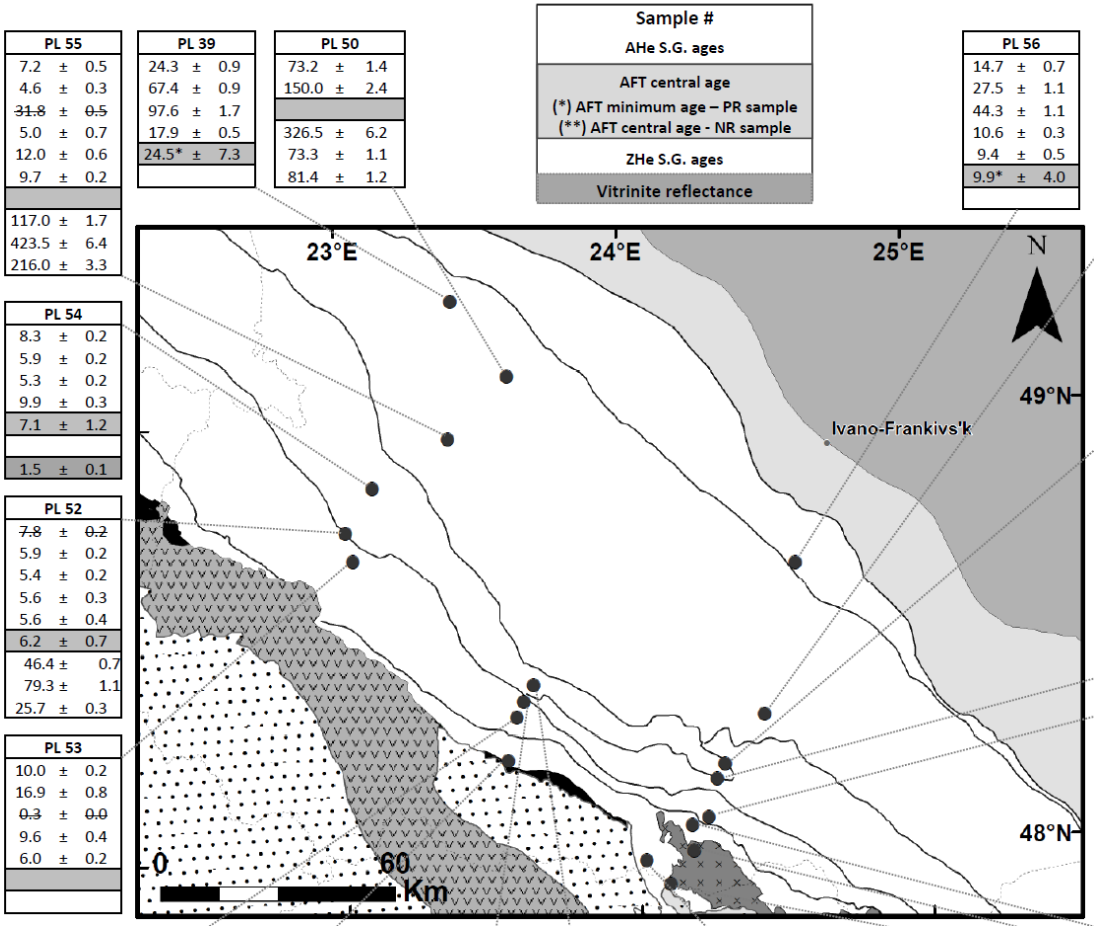

Figure 4.4- AHe, AFT, ZHe and vitrinite data with sample position. Minimum AFT ages for partially reset samples are calculated using the Binomfit software (Brandon, 1992).

AHe data

Three to five replicates were dated for each sample; the results are reported in Tab. 4.2.

As described in the previous section, in most cases the dated grains were far from the ideal, being often rounded, abraded, coated and inclusion bearing. Data dispersion, occurrence of anomalous values in the measured and calculated parameters, correlation between ages and such parameters are used as proxies to evaluate the impact of crystal defects on dates.

As can be observed in Fig. 4.6 most of the analyzed grains yield fairly reproducible ages. Outliers were tested for each sample using the program Outlier (Dunkl 2002) which uses the Grubbs (Grubbs, 1950, 1969), the Dixon (Dixon, 1953) and the Gauss-g (Szalma, 1984) tests. Given the low number of data (3-5) per sample the results of these tests give only a rough estimation of outliers, and grains can be confidently discarded only in presence of other independent evidence of age biases. Four outliers were detected within the dataset, the three tests giving consistent results (Tab. 4.2).

Analytical data are in general acceptable, although critically low He and U concentrations (less than 1 mole/g and less than 10 ppm) occur in several grains, leading in some cases to high percent-error (Tab. 4.2); critically high Th concentration and high Th/U are also frequent in the analyzed grains. Anomalous values are underlined in Tab. 4.2.

Correlations between ages and crystal size, eU and other parameters ([Th], [U], [Sm], Th/U) were tested for each sample. As reported in the data repository, significant correlations were found only in few cases, implying that age dispersion is, in most cases controlled by the interplay of several factors. A negative correlation between age and Th/U and/or [Th] is observed in samples PL 59 and PL 63, suggesting a possible dependence of ages on oxide coating (e.g. Murray e al., 2011; Reiners et al., 2010; Orme and Reiners 2010). A positive correlation between grain ages and eU and/or [U] can be observed in samples PL 62 and PL 64, which we interpret as an effect of radiation damages. Grain ages of samples 59 and 68 positively correlate with grain radius: this can be simply explained by the effect of slow cooling in absence of other controlling factors (e.g. external sources of He, trapping effect of radiation damages etc.).

Grains were discarded only in case of occurrence of at least two proxies for bias, e.g. outlier ages or anomalous values of the measured parameters occurring in crystals with noticeably bad features. Four grains were excluded from data discussion, and reported in Tab. 4.2 as crossed fields; further details can be found in caption of Tab. 2.

Since the sample ages are generally well reproducible (Fig. 4.6), error-weighted mean sample age are also reported in tab 4.3 and used for discussion.

As indicated in Fig. 4.7, 15 of the 18 analyzed samples are completely reset, yielding AHe ages which are both well reproducible and far younger than depositional ages. Two samples appear partially reset (high age dispersion, occurrence of grain ages close or older than the depositional ages), and one is not reset (very high dispersion, all the grain ages older than the depositional ages). The weighted mean ages of the reset samples are comprised between 5.6 and 10.7 Ma.

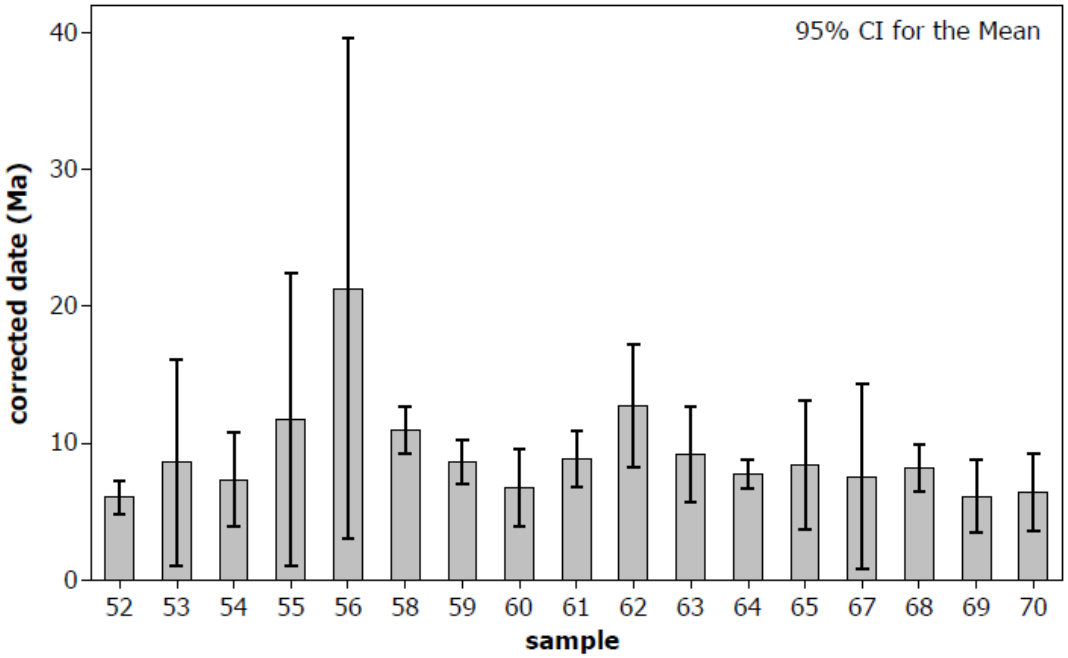

Figure 4. 6- Interval plot of the corrected ages grouped per sample.

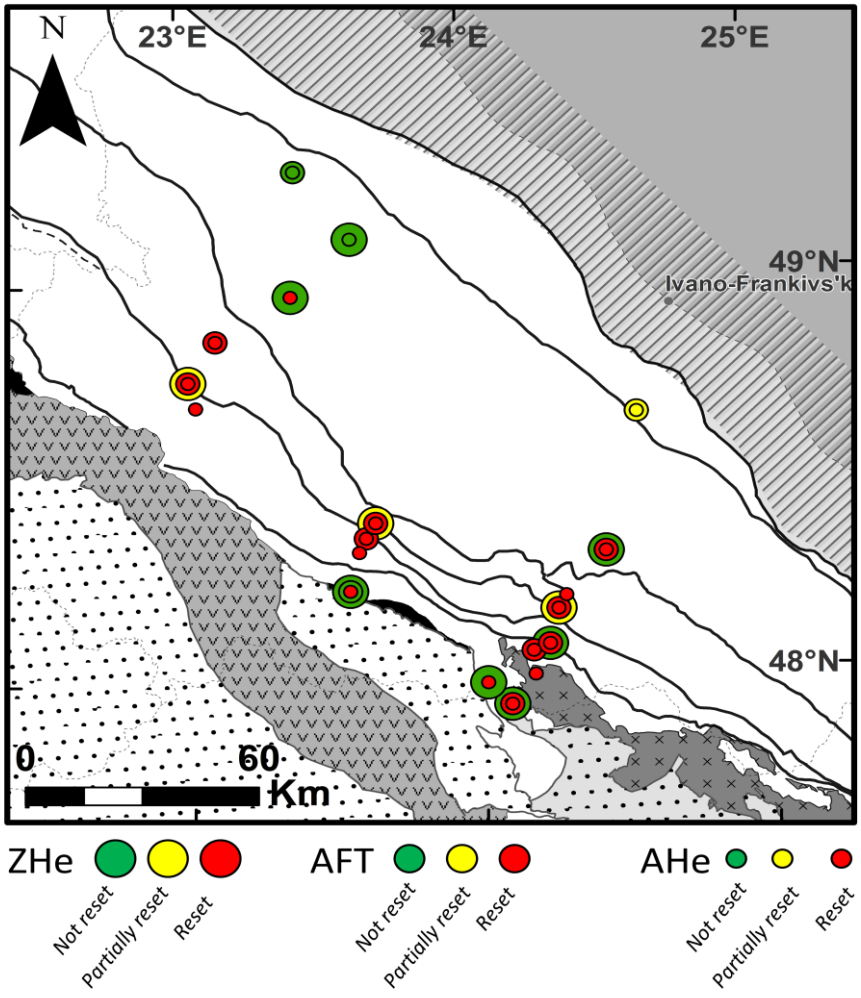

Figure 4.7 – degree of reset of AHe, AFT and ZHe samples

AFT data

The results of AFT dating are presented in Tab. 4.4 and in the radial plots in Fig. 4.8. Due to the generally low spontaneous track density of the analyzed grains, track counting was performed on 14 to 22 grains per sample, whereas in none of the 13 samples track length measurement could be performed. The average Dpar (diameter of etch figures parallel to the crystallographic c-axis, Ketcham et al.,1999) of the samples ranges between 1.5 and 2.1. Two different kinetic populations were identified in sample PL 67, the more retentive population being the one with the higher mean Dpar.

Three of the 13 analyzed samples are unreset to partially reset (Fig.4. 8). The central ages of the totally reset samples are comprised between 6.2 and 11.6 Ma, whereas the minimum ages of the partially rest samples are respectively 9.9 Ma for sample PL 56 and 35.2 Ma for sample PL 67.

Sample	No. of crystals	Spontaneous		Induced		$P(\chi)^2$ (%)	Dosimeter		Age ± SE (Ma)	Mean confined track lenght ± SE (µm)	SD (µm)	No. of tracks measured	Mean Dpar ± SD (µm)	Minimum age ± SE (Ma)
		r_s	N_s	r_i	N_i		r_d	N_d						
PL 39	11	1.22	252	40	766	0.2	12.4	5903	73 ± 9.1	n.d.	n.d.	n.d.	1.58 ± 0.27	
PL 52	20	0.85	75	34.06	3018	71.1	13.60	6465	6.2 ± 0.7	n.d.	n.d.	n.d.	1.73 ± 0.74	
PL 54*	21	0.68	41	22.77	1363	95.2	13.81	6053	7.1 ± 1.2	n.d.	n.d.	n.d.	1.45 ± 0.14	
PL 56*	21	3.17	238	21.04	1579	0.0	11.10	5743	25.1 ± 5.8	n.d.	n.d.	n.d.	1.60 ± 0.22	9.9 ± 7.1
PL 59	14	0.92	38	26.66	1104	53.2	13.70	6514	8.6 ± 1.4	n.d.	n.d.	n.d.	1.82 ± 0.20	
PL 61	15	1.13	52	23.25	1074	79.0	13.07	6113	11.6 ± 1.7	n.d.	n.d.	n.d.	1.55 ± 0.21	
PL 62	19	0.86	63	19.31	1413	50.3	12.39	5891	10.1 ± 1.3	n.d.	n.d.	n.d.	1.55 ± 0.21	-
PL 63	15	0.92	50	23.65	1281	51.2	13.65	6490	9.8 ± 1.4	n.d.	n.d.	n.d.	1.57 ± 0.27	-
PL 65	22	0.76	79	16.96	1759	65.7	12.30	5850	10.1 ± 1.2	n.d.	n.d.	n.d.	2.06 ± 0.32	-
PL 67	20	4.65	372	15.83	1414	0.0	12.81	6092	71.0 ± 10.1	n.d.	n.d.	n.d.	2.10 ± 0.41	35.2 ± 7.1
PL 69	20	1.55	94	44.78	2715	18.3	13.76	6539	8.7 ± 0.9	n.d.	n.d.	n.d.	1.71 ± 0.24	-
PL 70	20	0.99	47	1111.00	23.394	25.3	12.64	6012	9.7 ± 1.5	n.d.	n.d.	n.d.	1.81 ± 0.25	-

Central ages calculated using dosimeter glass CN5 and z-CN5=366.76±2.9, z*-CN5=345.53±18.45 (* indicates the sample analyzed with z*) and the sofwtare TrackKey vers. 4.2 (Dunkl, 2002). r_s: spontaneous track densities (x 105 cm-2) measured in internal mineral surfaces; N_s: total number of spontaneous tracks; r_i and r_d: induced and dosimeter track densities (x 106 cm-2) on external mica detectors (g=0.5); N_i and N_d: total numbers of tracks; $P(\chi^2)$: probability of obtaining χ^2-value for n degrees of freedom (where n=number of crystals-1); a probability >5% is indicative of an homogenous population. Minimum age is the peak age of the youngest age population obtained for partially reset samples using the BINOMFIT software (Brandon 1992). Sample preparation: Apatite grains were separated using heavy liquids and magnetic separation techniques. Mounts of apatite in epoxy were polished and then etched with 5M HNO3 at 20°C for 20 s to reveal spontaneous fission tracks. Samples were then irradiated with a CN5 dosimeter in the reactor at the Radiation Center of Oregon State Univ. with a nominal neutron fluence of 9x1015 n cm^{-2}. After irradiation induced fission tracks in the low-U muscovite detector were revealed by etching with 40% HF at 20°C for 45 min. Samples were analyzed with a Zeiss Axioskop microscope equipped with a digitizing tablet and drawing tube and controlled by the program FTStage 3.11 (Dumitru, 1993). FT ages were calculated using the external-detector and the zeta-calibration methods with IUGS age standards and a value of 0.5 for geometry correction factor. χ^2 test was used to detect whether the data sets contained any extra-Poissonian error.

Table 4.3 – AFT analytical data

Figure 4. 8 - Radial plots for AFT samples with depositional ages (grey areas). Samples are grouped based on the profiles indicated in Fig. 4.3.

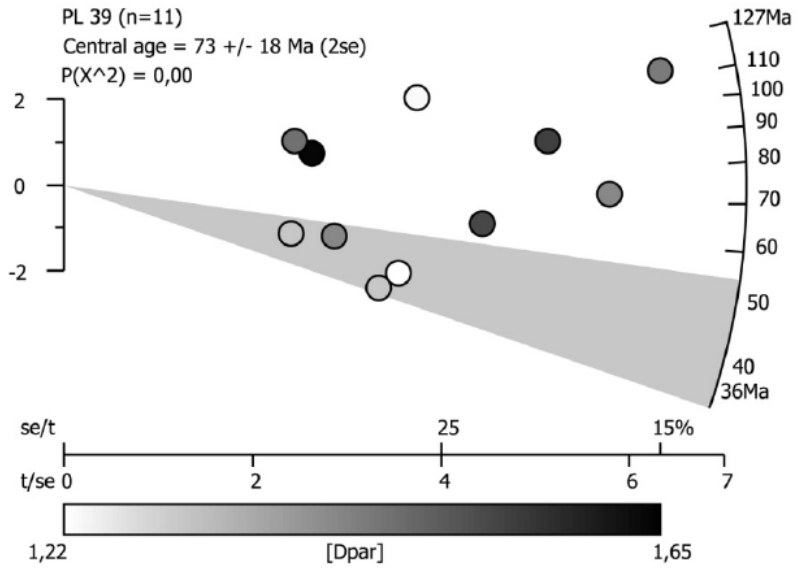
PL 39 (n=11)
Central age = 73 +/- 18 Ma (2se)
P(X^2) = 0,00
127Ma
110
100
90
80
70
60
50
40
36Ma
2
0
-2
se/t
25
15%
t/se 0
2
4
6
7
1,22
[Dpar]
1,65

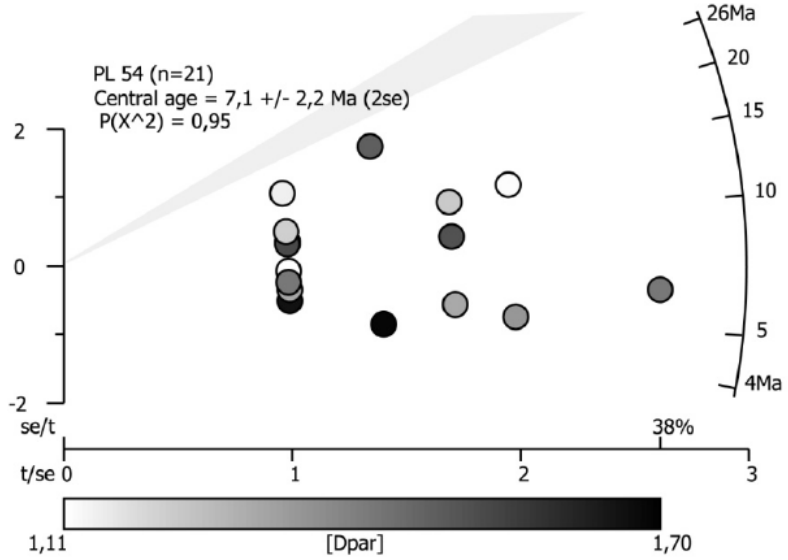
PL 54 (n=21)
Central age = 7,1 +/- 2,2 Ma (2se)
P(X^2) = 0,95
26Ma
20
15
10
5
4Ma
2
0
-2
se/t
38%
t/se 0
1
2
3
1,11
[Dpar]
1,70

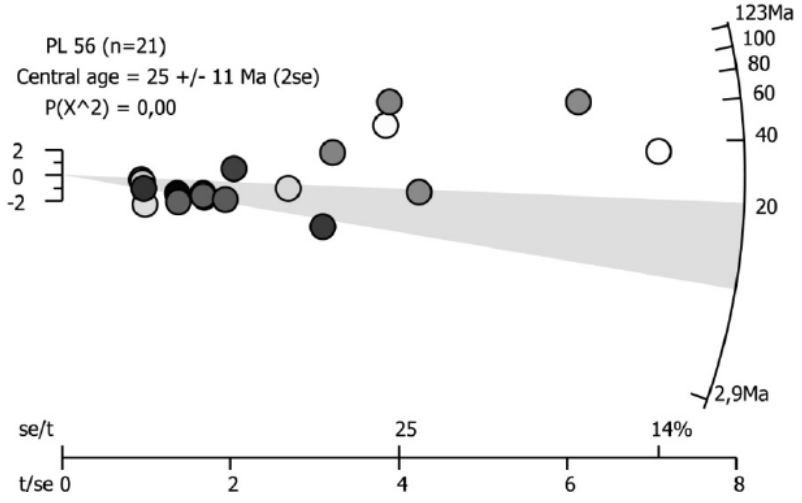
PL 56 (n=21)
Central age = 25 +/- 11 Ma (2se)
P(X^2) = 0,00
123Ma
100
80
60
40
20
2,9Ma
2
0
-2
se/t
25
14%
t/se 0
2
4
6
8

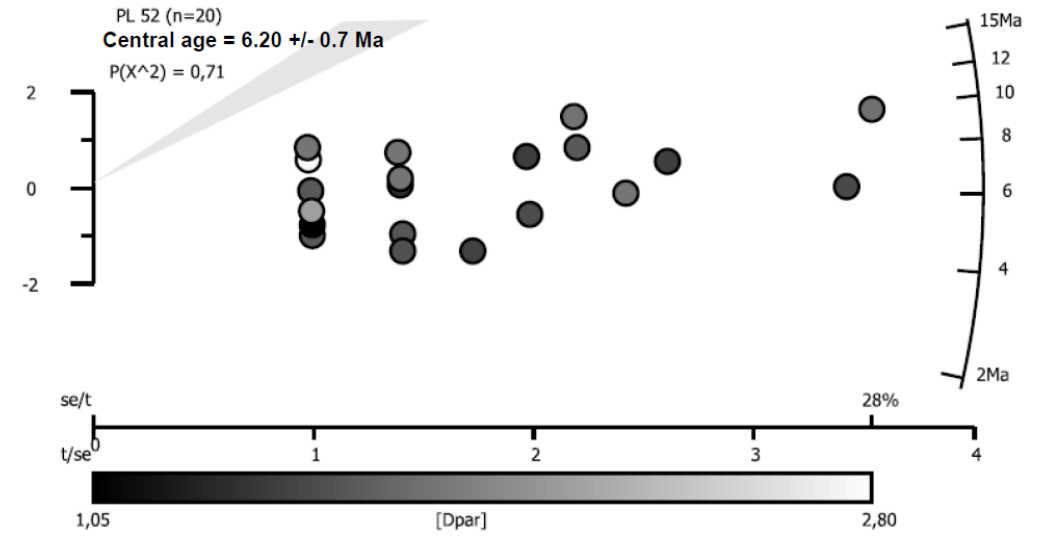
PL 52 (n=20)
Central age = 6.20 +/- 0.7 Ma
P(X^2) = 0,71
2
0
-2
15Ma
12
10
8
6
4
2Ma
se/t
28%
t/se 0
1
2
3
4
1,05
[Dpar]
2,80

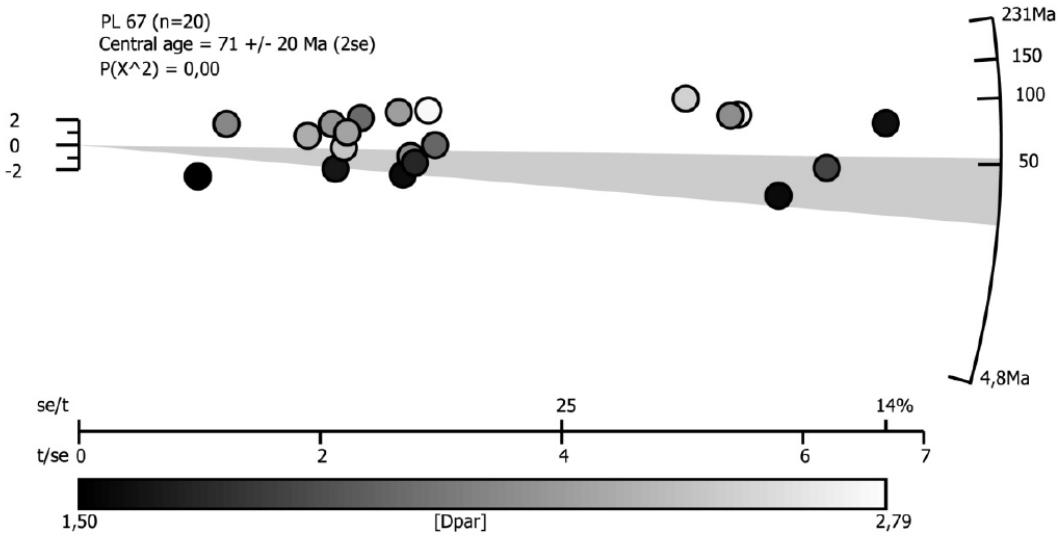
PL 67 (n=20)
Central age = 71 +/- 20 Ma (2se)
P(X^2) = 0,00
2
0
-2
231Ma
150
100
50
4,8Ma
se/t
25
14%
t/se 0
2
4
6
7
1,50
[Dpar]
2,79

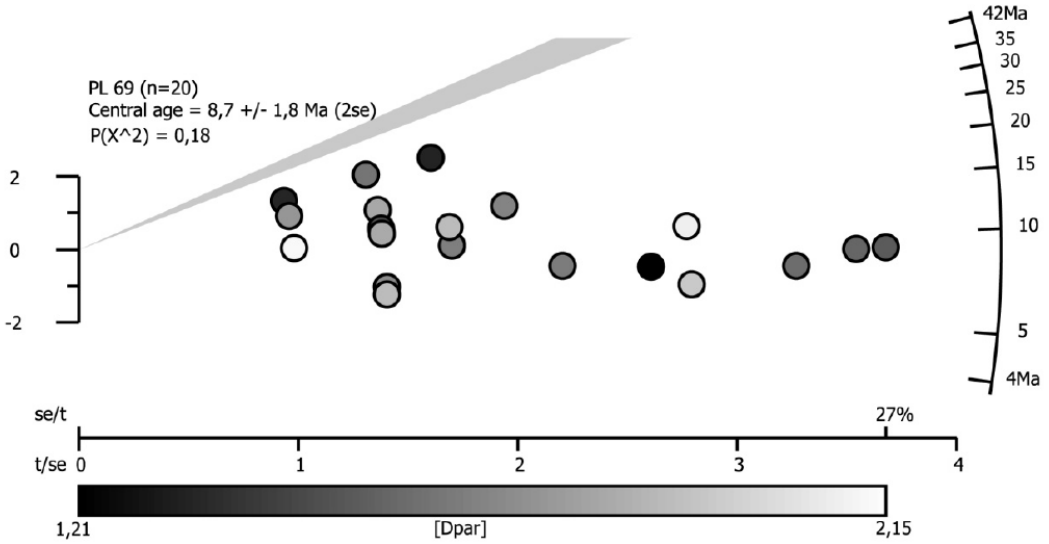
PL 69 (n=20)
Central age = 8,7 +/- 1,8 Ma (2se)
P(X^2) = 0,18
2
0
-2
42Ma
35
30
25
20
15
10
5
4Ma
se/t
27%
t/se 0
1
2
3
4
1,21
[Dpar]
2,15

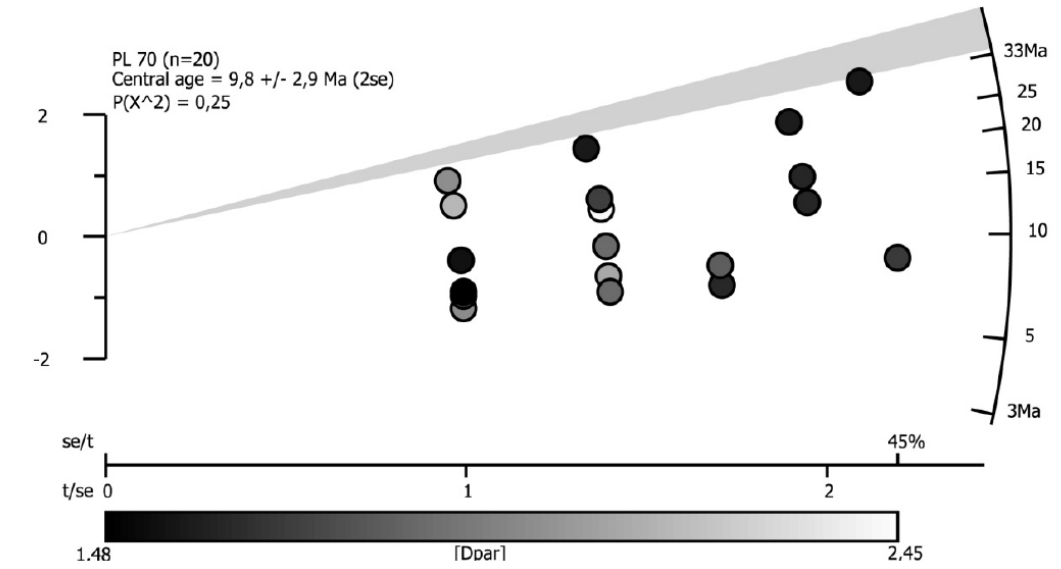
PL 70 (n=20)
Central age = 9,8 +/- 2,9 Ma (2se)
P(X^2) = 0,25
2
0
-2
33Ma
25
20
15
10
5
3Ma
se/t
45%
t/se 0
1
2
1.48
[Dpar]
2,45

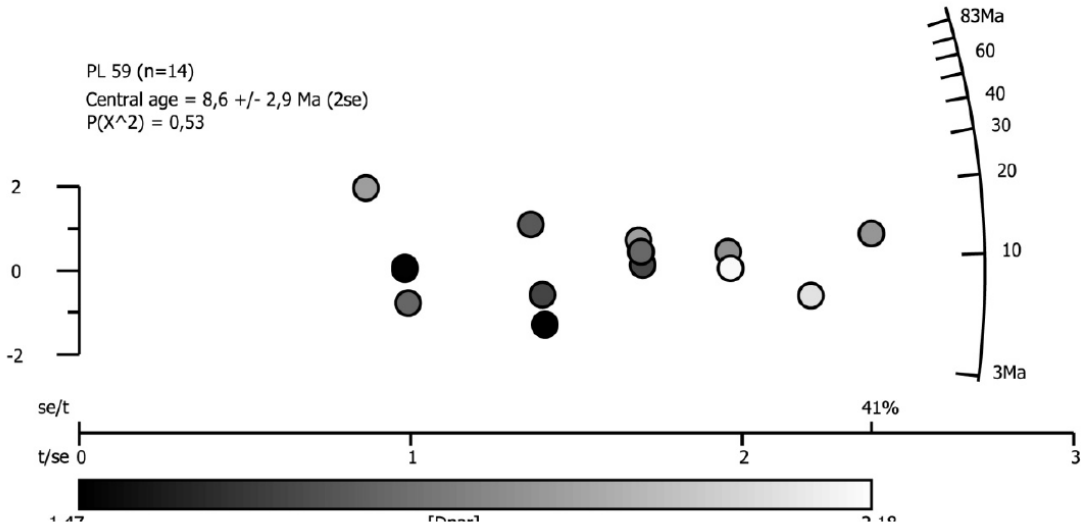
PL 59 (n=14)
Central age = 8,6 +/- 2,9 Ma (2se)
P(X^2) = 0,53
2
0
-2
83Ma
60
40
30
20
10
3Ma
se/t
41%
t/se 0
1
2
3

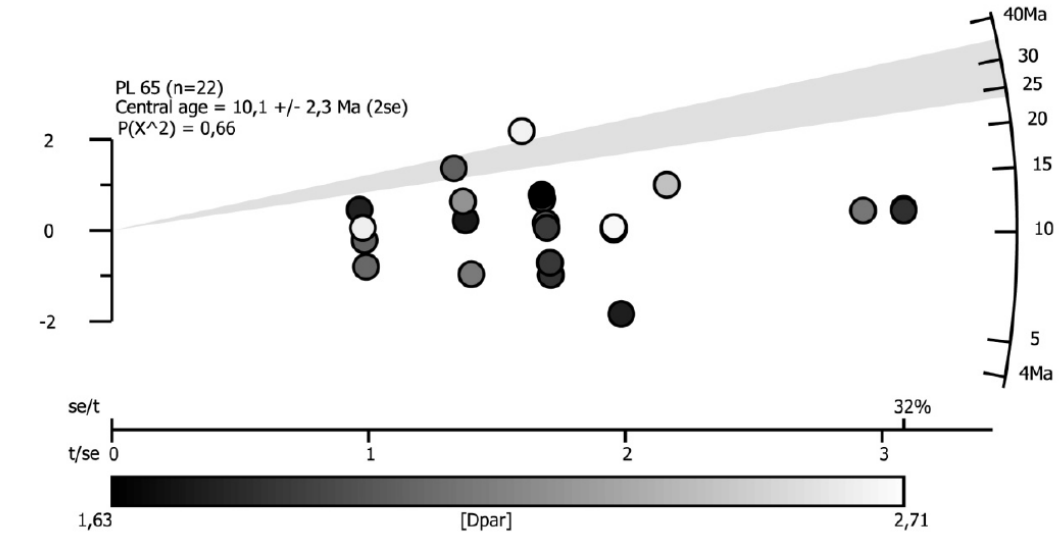
PL 65 (n=22)
Central age = 10,1 +/- 2,3 Ma (2se)
P(X^2) = 0,66
2
0
-2
40Ma
30
25
20
15
10
5
4Ma
se/t
32%
t/se 0
1
2
3
1,63
[Dpar]
2,71

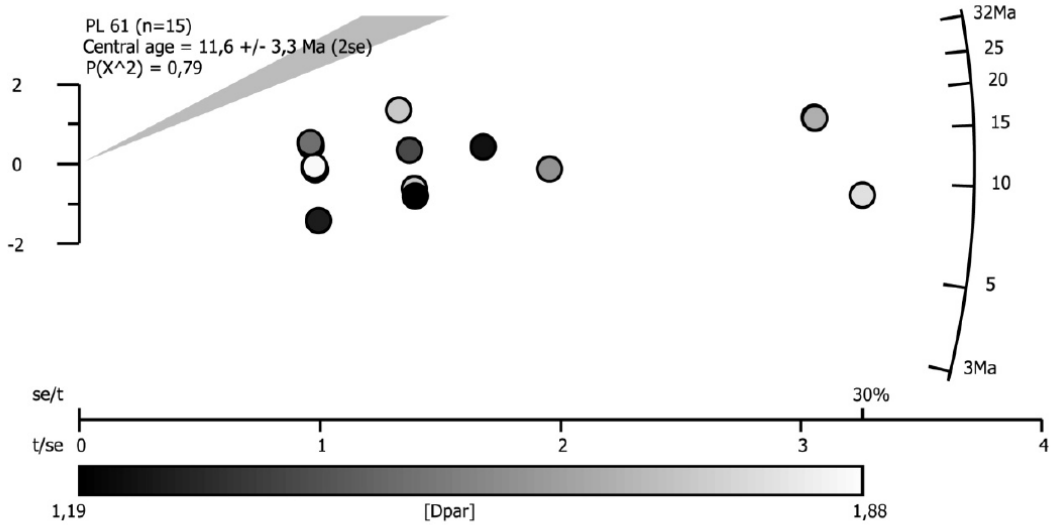
PL 61 (n=15)
Central age = 11,6 +/- 3,3 Ma (2se)
P(X^2) = 0,79
2
0
-2
32Ma
25
20
15
10
5
3Ma
se/t
30%
t/se 0
1
2
3
4
1,19
[Dpar]
1,88

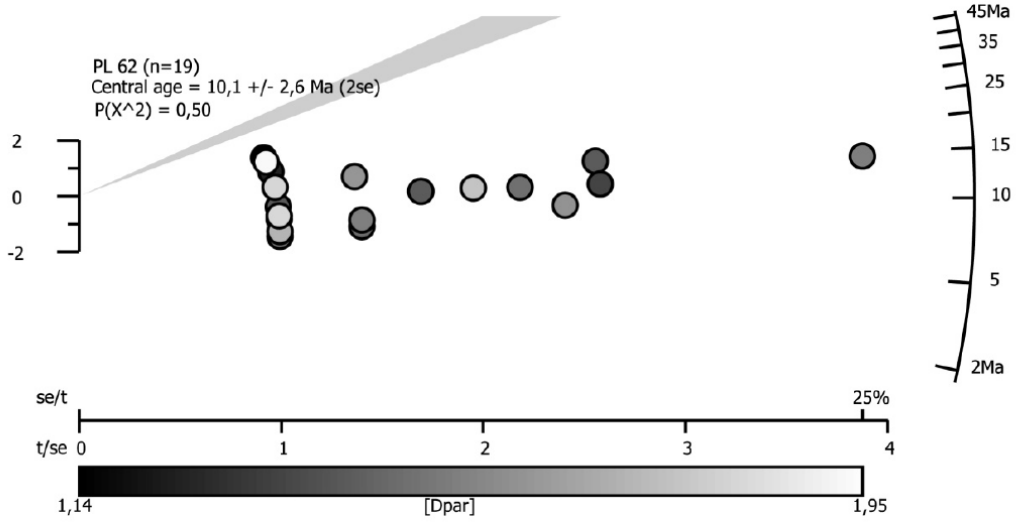
PL 62 (n=19)
Central age = 10,1 +/- 2,6 Ma (2se)
P(X^2) = 0,50
2
0
-2
45Ma
35
25
15
10
5
2Ma
se/t
25%
t/se 0
1
2
3
4
1,14
[Dpar]
1,95

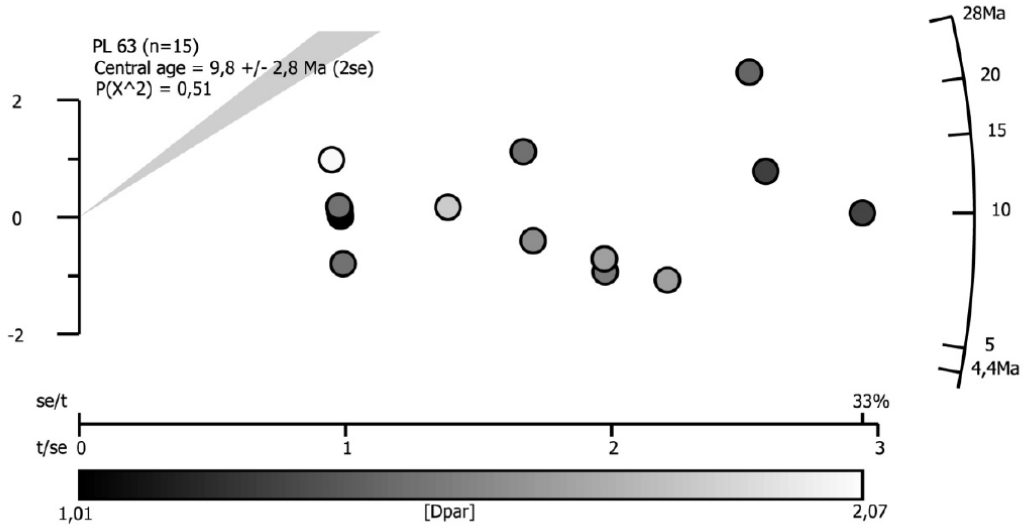
PL 63 (n=15)
Central age = 9,8 +/- 2,8 Ma (2se)
P(X^2) = 0,51
2
0
-2
28Ma
20
15
10
5
4,4Ma
se/t
33%
t/se 0
1
2
3
1,01
[Dpar]
2,07

ZHe data

Three grains of good quality were selected and analyzed for each sample, the results are presented in Tab. 4.5. The analytical values show no significant anomaly. All the analyzed grains yield ZHe age older than the stratigraphic age, indicating that none of the analyzed samples was completely reset. Therefore the ZHe single grain ages represent an indication of cooling age of the source rocks through the ZHe PRZ. The probability density plot (Fig. 4.9) of the ZHe ages shows the main peaks at X and Y Ma.

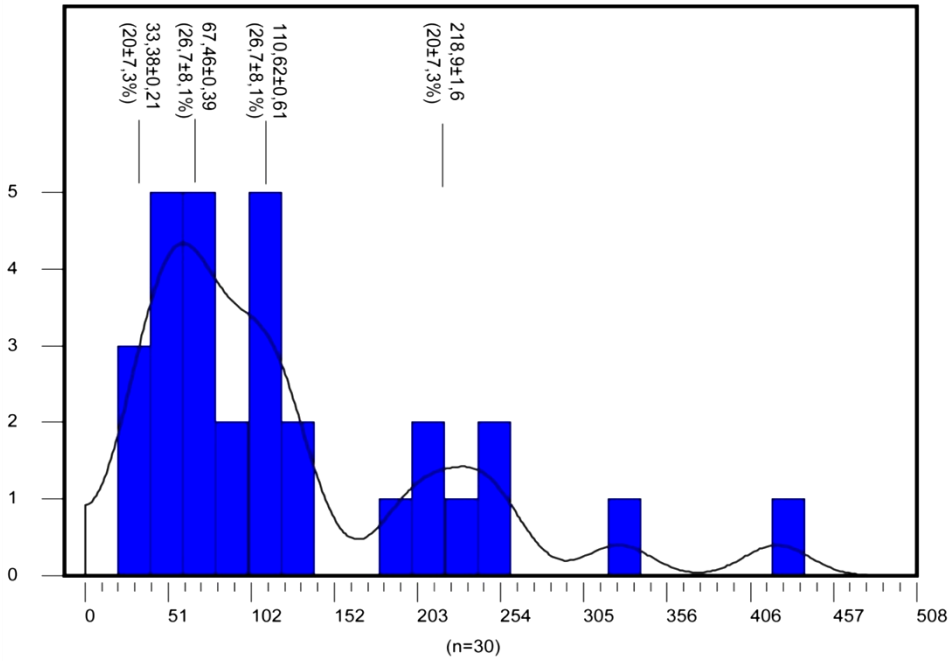

Fig. 4.9_ Histogram and Kernel density distribution of the ZHe dataset. The histogram and Kernel density distribution were realized using the software DensityPlotter (Vermeesch, 2012) using for the histogram a bin width of 20 and for the Kernel density distribution a ban-width of 20. Ages and percentages of the main peaks are also indicated.

Vitrinite reflectance data

Four samples were analyzed. The analyses were carried out at the Roma Tre University following the standard procedures described in (Bustin 1990). Calculation of the maximum paleotemperatures was based on Barker and Pawlewicz (1994). The results are presented in Tab. 4.6 and Fig. 4.10.

Sample	%Ro	±σ %Ro	n_ tot	n_ ok	histogram quality	EQ temp Ro B. e P 1994
PL-54	1.475	0,087	36	16	good	166.827257
PL-61	0.691	0,035	36	9	not good	105.676173
PL-64	1.51	0,102	43	21	good	168.71852
PL-68	0.719	0,0747	21	19	good	108.879522

Table 4.6 – Vitrinite analytical data

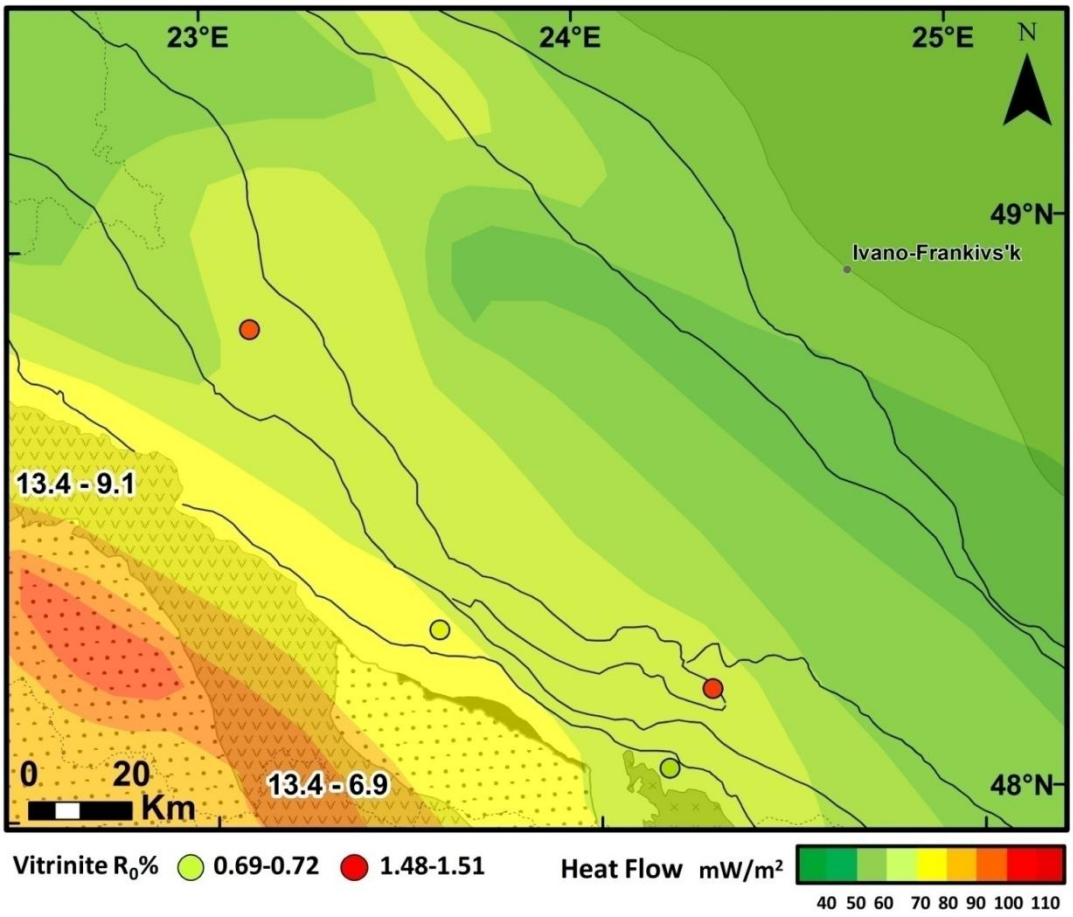

Figure 4.10 – Present day heat flow (from Pospisil et al., 2006) in the Ukrainian Carpathians and vitrinite data. The timing of volcanic activity is also indicated (from Huismans et al., 2001, and reference therein)

4.2.6. Discussion

Paleo-thermal field

To interpret the thermochronometric data in terms of thermal history, the assumption of a crustal thermal field is required. The present day heat flow of the Ukrainian Outer Carpathians (Fig. 4.10, Pospisil et al., 2006) is comprised between 30 and 80 mW/m2, progressively increasing toward the Pannonian Basin, which positive thermal anomaly was induced by Miocene extension and astenospheric uprise. Miocene calc-alkaline volcanism also occurred along the inner side of the Carpathian arc but, as described by Lenkey et al. (2002), calculations of the thermal evolution of volcanic intrusions show that the elevated temperature and heat flow around an intrusion dissipates in a few million years (e.g. Fowler and Nisbet, 1982; Horv'ath et al., 1986). Furthermore, since no anomalously high radioactive isotope concentration (Surányi et al., 2002) is present in the volcanic rocks, no contribution to the high heat flow is expected from radiogenic heat production (Lenkey et al. 2002). Therefore the high heat flow has to be ascribed not to the volcanic fields themselves, but rather to lithospheric extension which led to extension and volcanism in the Pannonian Basin. We expect the positive thermal anomaly to have developed at about the same time of major astenosphere uprise in the PB (Fig. 4.10), i.e.

between ca.14 and 11 Ma (Huismans et al., 2001), with a decreasing extent toward the foredeep.

Kotarba and Koltun (2006) show that in the outermost thrust sheets no major heat flow transients occurred since the Oligocene. This confirms that even in the past no heat flow increase was registered in the outermost thrust sheets, being confined to the innermost portion of the accretionary wedge.

Some observations can be made to understand the development and extent of such thermal anomaly in the Ukrainian OC. In Fig. 4.10 It can be observed that samples located closer to the Pannonian Basin (PL 61, PL 68) underwent a lower maximum paleotemperature than samples located farther (PL 64, PL 54). This can also be observed in sample PL 67 (Fig.4.5 and 4.7), which is located very close to the Pannonian Basin and underwent only a partial reset of the AFT system, as opposed to the other AFT samples, located to the NE, that are completely reset. This suggests that heating of rocks in the UC was mainly due to burial and therefore perturbation of the thermal field only had a minor effect.

A constrain to the maximum paleo-geothermal gradient reached in the Ukrainian OC at the time of extension and mantle uprise in the Pannonian Basin can be inferred from the stratigraphic position and vitrinite reflectance value referred to the sample PL 68. Based on Slaczka et al. (2006) the sample is located in the Porkulec tectonic Unit, where sedimentary succession reaches a thickness of more than 6 Km. The depositional age of the sample is Upper Cretaceous-Lower Paleocene (Jankowski et al., 2007), implying a minimum sedimentary burial of 2.7 Km (based on Slaczka et al. 2006). Vitrinite reflectance analysis indicates that sample PL 68 was heated up to 108.9°C: considering the sedimentary burial underwent by the sample, the geothermal gradient must have been then no higher than 37°C/Km (if a surface temperature of 10°C is assumed). The sample PL 68 is one of the closer to the area with high heat flow (Fig. 4.10) and therefore we accept the geothermal gradient of ca. 37°C/Km as a maximum value for the whole study area.

As a consequence, considering the high present day heat flow values, we have to assume a sufficiently high average thermal conductivity to justify a geothermal gradient no higher than ca. 37°C/Km. A further constrain on thermal conductivity is given by the present day geothermal gradient of 20-24°C/Km measured in wells in the outermost thrust sheets (Kotarba and Koltun, 2006). Dererova et al. (2006) uses values of thermal conductivity comprised between 2 and 2.5 W/m °C. Based on the two constrains described above we can restrict such range and we assume a value of 2.2 W/m °C. In Tab. 4.7 our estimate for the present day geothermal gradient are presented: for each heat flow interval (Fig. 4.10) an average value is indicated. We estimate post-extensional gradients comprised between ca. 36.4°C/km in the innermost and ca. of 18.2°C/km in the outermost thrust sheets, with local heat flow minima reaching minimum values of 15°C/Km. Vityk et al. (1996, and references therein) propose a similar trend, with estimates of gradients slightly higher (up to 3-5 degrees) than those proposed in this work.

Our paleo-geothermal gradient estimate leads us to another consideration. It could be expected that after 11 Ma a progressive thermal relaxation occurred, leading to a decrease of the heat flow from higher to present day values. But, in fact, the present day values are as high as the

maximum allowed geothermal gradients. This implies that the thermal anomaly developed in the Middle Miocene in this region has had approximately the same extent as today.

To summarize we assume that (a) the innermost units of the UC were interested by an increase of the geothermal gradient between ca. 14 and 11 Ma which has then remained constant until present (b) such effect is decreasing with distance from the Pannonian Basin and (c) in the study area the geothermal gradient has been comprised, since ca. 14-11 Ma, between 13.6 and 37°C/Km and, finally, (d) the increased geothermal gradient had only a minor effect in heating the rocks of the UC, which thermal history was determined mainly by burial and exhumation history.

	Heat Flow (mW/m^2)	Geothermal Gradient (°C/Km)
k=2.0 W/m °C	80	40.0
	70	35.0
	60	30.0
	50	25.0
	40	20.0
	30	15.0

	Heat Flow (mW/m^2)	Geothermal Gradient (°C/Km)	Average Gradient (°C/Km)	
k=2.2 W/m °C	80	36.4	34.1	
	70	31.8		29.6
	60	27.3	25.0	
	50	22.7		20.4
	40	18.2	15.9	
	30	15.0		

	Heat Flow (mW/m^2)	Geothermal Gradient (°C/Km)
k=2.5 W/m °C	80	32.0
	70	28.0
	60	24.0
	50	20.0
	40	16.0
	30	12.0

Table 4.7 – Geothermal gradient estimate from the present day heat flow assuming constant thermal conductivity (k).

Thermal history

The degree of reset of the samples (Fig. 4.7) and the vitrinite reflectance data (Fig. 4.10) indicate that the UC were heated to over ca. 120°C in the central portions and that heating degree decreases towards both the Pannonian Basin and the foredeep. In particular samples close to the Pannonian Basin underwent temperatures of ca. 110°C, whereas samples belonging to the outermost units of the accretionary prism were heated at temperatures lower than ca. 60°C.

Simplified cooling histories can be obtained using the concept of closure temperature (Tc; e.g. Reiners and Brandon, 2006). Cooling histories obtained by plotting in the t-T space the closure temperatures against their average cooling ages have not to be considered as precise predictions, but they may be used to give a first indication of the expected cooling paths.

As described in previous section, samples were heated and cooled mainly by burial and exhumation. Since no evidence for normal faulting with consistent displacement can be observed in the field (e.g. Jankowski et al., 2006), we expect cooling rates compatible with erosional exhumation rates in similar geodynamic contexts (maximum values lower than 1.5 mm/yr, e.g. N-Apennines, Thomson et al., 2010; S-Apennines, Schiattarella et al., 2005). Based on the estimated geothermal gradients (Tab. 4.7) we consider therefore that reasonable values for cooling rates are comprised between 10 and 60°C/Myr. Closure temperatures were then estimated assuming an average cooling rate of 35°C/Myr and, in the case of AHe, using the average grain radius for each sample (details can be found in caption of Tab. 4.8 and Fig. 4.11). Closure temperatures were then calculated using the Closure software (Brandon et al., 1998). Cooling paths are reported in three distinct plots, corresponding to the three sampled transects (Fig. 4.11).In Fig. 4.11 It can be observed that all the cooling paths are characterized by a first

stage of rapid to extremely rapid cooling, occurred between ca. 12 and 5 Ma, followed by a stage of slower cooling to surface temperature. Another observation that can be made is that the onset of rapid cooling occurred later in the NW. Cooling rates for the single tracts of the thermal histories were calculated and are reported in Tab. 4.8 Two sets of cooling rates can be identified for the stage of rapid cooling: four samples yield a cooling rate of 15-20°C/Myr, whereas five samples yield extremely rapid cooling rates (ca. instantaneous).

We suggest that, at least in three cases, the extremely rapid cooling is actually a biased result induced by imprecision and inaccuracy of AHe ages. AHe dates of samples PL 59 and PL 63 are negatively correlated with the Th/U ratio, and PL 59 also with [Th] and grain size. Sample PL 54 also displays an apparent negative correlation of AHe dates with [Th] and Th/U. These correlations can be interpreted as an effect of Th rich coating (Murray et al., 2012; Orme and Reiners, 2010, Reiners, 2010) and consequent He implantation. This interpretation is also supported by the abundance of coated grains in these samples (Fig. 4.4). Since most of the coating material was removed before analysis, we assume that ages are generally overestimated. Overestimation due to He implantation decreases with increasing grain size and Th/U ratio and, therefore more rich in Th and bigger grains, yielding younger ages, are considered more reliable. Using the youngest AHe age for each grain instead of the weighted average of dates we obtained more reasonable cooling rates, comprised within 10 and 30°C/Myr.

Samples PL 52 and PL 62 yield reproducible AHe ages (Tab 4.3., Fig. 4.5): reproducibility of dates, particularly in case of apatite grains far from the ideal, can be safely used as a proxy for rapid cooling (e.g. Ehlers and Farley, 2003). Therefore in this case we cannot rule out that the samples cooled very rapidly through the AFT and AHe closure temperatures. Nonetheless, as previously described, based on the paleo-geothermal gradients indicated in Tab. 4.7, we imposed to all thermal histories a maximum cooling rate of 60°C/Myr.

Thermal modeling was also performed on 13 samples using the HeFTy software (Ketcham et al, 1997), in order to more robustly test the thermal histories indicated in Fig.4.11.

Due to AHe age dispersion we used, for some samples, a merit value for acceptable fits lower than the default value of 0.05 (see caption of Fig. 4.12 for details). In some cases this was not sufficient to obtain acceptable paths, and therefore we used for modeling only 2-3 of the AHe dates, the criteria used to select the crystals for modeling are described in caption of Fig. 4.12. In most cases we did not impose maximum values for cooling rates, but as described above we applied the threshold of 60°C/Myr to the rapidly cooled samples.

Thermal models are presented in Fig. 4.12: they generally support the t-T paths presented in Fig. 4.11, being characterized by a first stage of fast cooling (average cooling rates are comprised between 15 and 30°C/Myr) through the temperature interval of ca 120-40°C, followed by a stage of slower cooling (average rates of 3-6°C/Myr). Modeled t-T paths also confirm that cooling occurred progressively later toward the NW (Fig. 4.12).

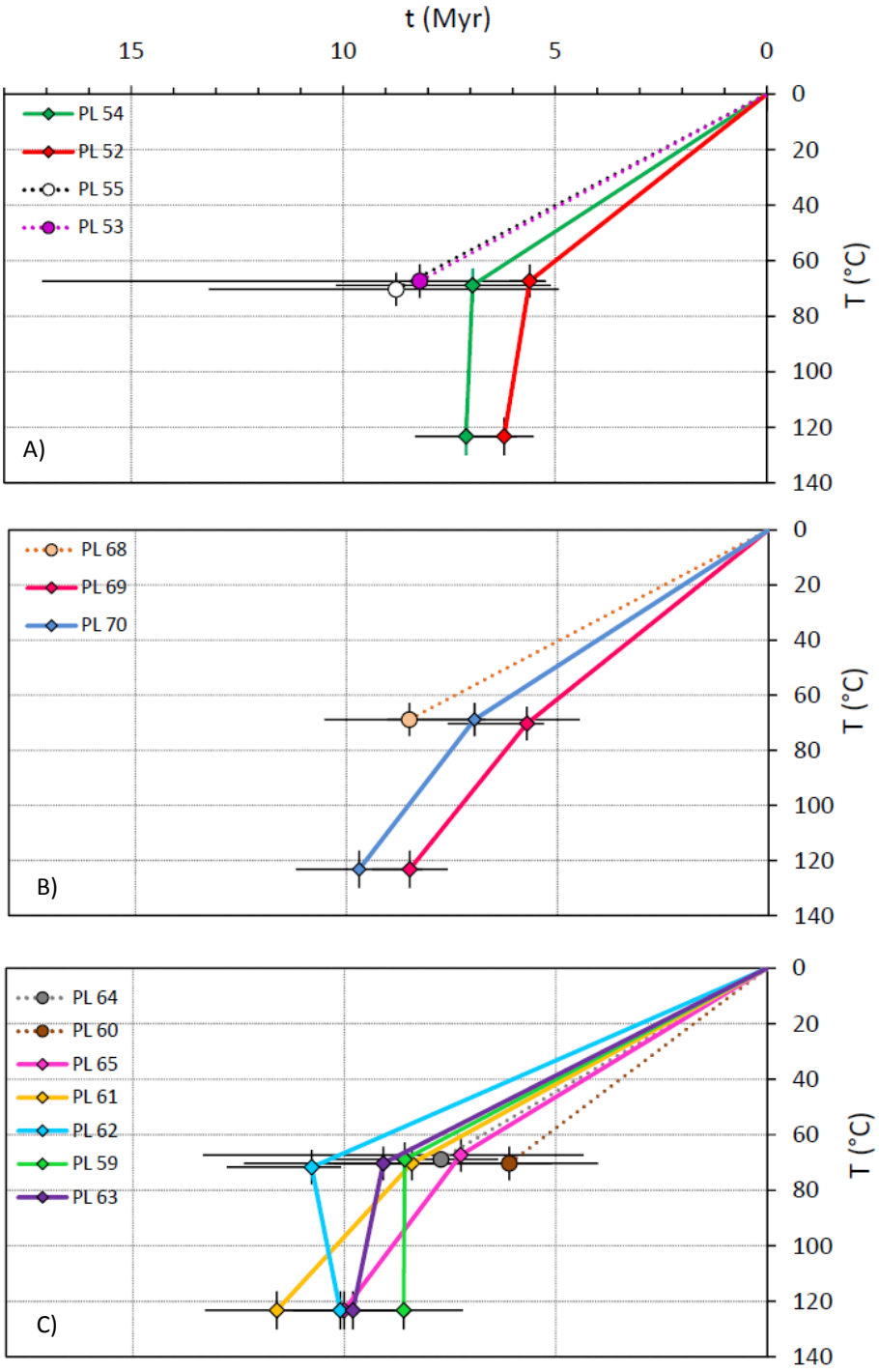

Figure 4.11 – Thermal paths obtained by plotting the Tc against sample weighted average or central ages, with relative uncertainties. Closure temperatures were calculated using the Closure software (Brandon et al., 1998), assuming a cooling rate range of 10-60°C/Ma. Thermal paths were grouped by single transect (A, B, C).

sample	cooling rate (°C/Myr)	± (°C/Myr)	AFT Tc (°C)	± (°C)	AHe Tc (°C)	± (°C)	AFT age (Ma)	± (Ma)	AHe w.m.a. (Ma)	w.m.a. error (Ma)	negative dispersion (Ma)	positive dispersion (Ma)	Δage AFT-AHe (Myr)	ΔTc AFT-AHe (°C)	cooling rate between AFT and AHe Tc (°C/Myr)	time averaged cooling rate between AHe Tc and surface temperature (°C/Myr)
PL 52	35	25	123.25	6.85	67.3	6	6.2	0.7	5.60	0.11	0.39	0.48	0.60	55.95	92.75	10.24
PL 54	35	25	123.25	6.85	68.85	6.05	7.1	1.2	6.94	0.10	1.84	3.23	0.16	54.4	instantaneous	8.47
PL 50	35	25	123.25	6.85	64.9	5.3			88.13		20.71	59.83				0.62
PL 53	35	25	123.25	6.85	70.3	6.1			8.75		2.94	8.91				6.89
PL 55	35	25	123.25	6.85	67.30	6.00			8.19		3.84	4.42				7.00
PL 56	35	25	123.25	6.85	67.3	6	25.1	5.8	12.94	0.23	4.04	32.51				4.43
PL 58	35	25	123.25	6.85	71.7	6.2			10.51	0.14	1.80	3.07				5.87
PL 59	35	25	123.25	6.85	68.85	6.05	8.6	1.4	8.57	0.14	2.22	1.71	0.03	54.4	instantaneous	6.86
PL 61	35	25	123.25	6.85	70.3	6.1	11.6	1.7	8.40	0.214	0.74	1.84	3.20	52.95	16.57	7.18
PL 62	35	25	123.25	6.85	71.7	6.2	10.1	1.3	10.77	0.17	0.68	2.01	0.00	51.55	instantaneous	5.73
PL 63	35	25	123.25	6.85	70.3	6.1	9.8	1.4	9.08	0.10	3.98	3.30	0.72	52.95	73.68	6.64
PL 65	35	25	123.25	6.85	67.3	6	10.01	1.2	7.25	0.09	2.90	6.10	2.76	55.95	20.27	7.90
PL 60	35	25	123.25	6.85	70.30	6.10			6.10		2.10	4.65				9.89
PL 64	35	25	123.25	6.85	68.85	6.05			7.72		1.38	1.07				7.62
PL 67	35	25	123.25	6.85	70.3	6.1	71	10.1	6.61	0.13	3.88	10.88				9.12
PL 69	35	25	123.25	6.85	70.3	6.1	8.5	0.9	5.72	0.09	0.41	1.88	2.78	52.95	19.07	10.54
PL 70	35	25	123.25	6.85	68.85	6.05	9.7	1.5	6.97	0.09	2.49	2.07	2.73	54.4	19.90	8.45
PL 68	35	25	123.25	6.85	68.85	6.05			8.51		1.80	2.02				6.92

Table 4.8 – Closure temperatures for the AFT and AHe systems and cooling rates between the AFT and AHe Tc and between the AHe Tc and the surface temperature. Tc were estimated using the Closure software, assuming a cooling rate range of 10-60°C/Ma and, using the average grain size of each sample for AHe. Cooling rates between the AFT and AHe Tc were calculated from the average Tcs and respectively the AFT central age and AHe weighted mean age. Cooling rates between are time averaged cooling rates, and, therefore; a surface temperature of 10°C is assumed.

Burial and exhumation history

As described in previous sections, heating and cooling were mainly determined by burial and exhumation. Based on burial temperatures, constrained by thermochronometrical data and estimated geothermal gradients, ranges of possible burial depths were estimated for each sample and are presented in Tab. 4.9. Burial depths reach the maximum values of ca. 6 Km in the central portion of the accretionary wedge (sample PL 65), and they decrease both toward the foredeep and the Pannonian Basin. Samples closer to the Pannonian Basin underwent maximum burial depths of 2.6-4 Km, whereas samples of the outermost thrust sheets were buried at depths lower than 2-3 Km.

Exhumation rates for the fast cooling stage were estimated both from cooling rates obtained from the t-T paths in Fig. 4.11 and from the modeled thermal histories. In most cases the two estimates well match, and point to average exhumation rates of 0.7-1 mm/yr. In the few cases of mismatch between the two estimates, the one based on thermal modeling has to be considered the most reliable.

We stress that exhumation rates (referred to the first, faster stage) indicated in Tab. 4.9, are average rates, and that based on ranges of possible cooling rates, consistently higher (up to 1.4 mm/yr) or lower (down to 0.3 mm/yr) exhumation rates cannot be ruled out.

Maximum burial values allowed for each sample are reported in Fig. 4.13.

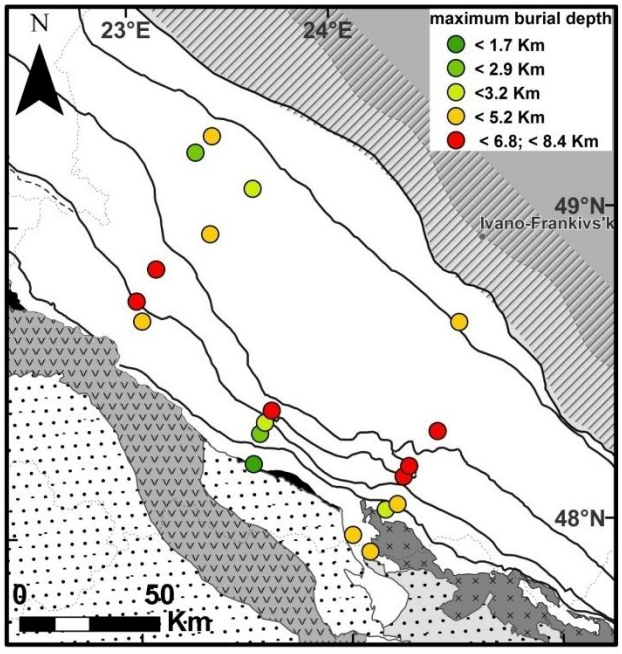

Figure 4.13 – maximum burial depth reached by the samples. Burial depths estimates are presented in Tab. .9.

sample	geothermal gradient	±	ZHe reset	AFT reset	AHe reset	a) average minimum burial depth calculated from Tc: cooling rate (°C/Myr)	AFT Tc (°C)	± (°C)	AHe Tc (°C)	± (°C)	burial depth min (mm/yr)	exhumation rate	b) average minimum burial depth calculated from thermal modeling: cooling rate (°C/Myr)	burial depth	exhumation rate	c) Burial depth ranges estimated from PRZs and vitrinite reflectance: ZHe PRZ 90%-10%		AFT PAZ 90%-10%		AHe PRZ 90%-10%		T max from R0%	burial depth max (m)	burial depth min (m)	burial depth range (m)
PL 39	20.4	2.3	-	0	0	35.0	123.3	6.9	67.3	6.0	-	-	-	-	-	174.5	± 22.5	82.0	± 29	52.3	± 20.9		1.6		<1.6
PL 50	25	2.3	0	-	0				64.9	5.3						174.5	± 22.5	82.0	± 29	52.3	± 20.9		3.2		<3.2
PL 52	29.6	2.3	1	2	2	60*	123.3	6.9	67.3	6.0	2.6	1.4	30.0	3.0	0.9	174.5	± 22.5	82.0	± 29	52.3	± 20.9		6.8	4.5	4.5-6.8
PL 53	29.6	2.3	-	-	2				70.3	6.1										52.3	± 20.9		4.8		<4.8
PL 54	29.6	2.3	-	2	2	60*	123.3	6.9	68.9	6.1	2.6	1.4	30.0	3.0	0.9			82.0	± 29	52.3	± 20.9	166.8	5.7		ca. 5.7
PL 55	29.6	2.3	0	-	2				67.3	6.0						174.5	± 22.5			52.3	± 20.9		5.2		<5.2
PL 56	15.9	2.3	0	1	1		123.3	6.9	67.3	6.0						174.5	± 22.5	82.0	± 29	52.3	± 20.9		4.6		<4.6
PL 58	29.6	2.3	-	-	2				71.7	6.2										52.3	± 20.9		-		
PL 59	29.6	2.3				60*	123.3	6.9	68.9	6.1	2.6	1.4	30.0	3.0	0.9	174.5	± 22.5	82.0	± 29	52.3	± 20.9		5.2		2.6-5.2
PL 60	29.6	2.3	0	-	2				70.3	6.1						174.5	± 22.5			52.3	± 20.9		5.2		<5.2
PL 61	29.6	2.3	-	2	2	16.6	123.3	6.9	70.3	6.1	3.3	0.5	30.0	3.0	0.9			82.0	± 29	52.3	± 20.9	105.7	3.2	3.2	ca. 3.2
PL 62	29.6	2.3	0	2	2	60*	123.3	6.9	71.7	6.2	2.6	1.4	25.0	3.2	0.7	174.5	± 22.5	82.0	± 29	52.3	± 20.9		5.2		2.6-5.2
PL 63	29.6	2.3	1	2	2	60*	123.3	6.9	70.3	6.1	2.6	1.4	30.0	3.0	0.9	174.5	± 22.5	82.0	± 29	52.3	± 20.9		6.8	4.5	4.5-6.8
PL 64	29.6	2.3	-	-	2				68.9	6.1						174.5	± 22.5	82.0	± 29	52.3	± 20.9	168.7	5.4		ca.5.4
PL 65	25	2.3	0	2	2	20.3	123.3	6.9	67.3	6.0	3.9	0.8	30.0	3.0	0.9	174.5	± 22.5	82.0	± 29	52.3	± 20.9		6.3		3.9-6.3
PL 67	34.1	2.3	0	0	2		123.3	6.9	70.3	6.1						174.5	± 22.5	82.0	± 29	52.3	± 20.9		1.4		ca.1.4
PL 68	34.1	2.3	-	-	2				68.9	6.1										52.3	± 20.9	108.9	2.9	2.9	2.9
PL 69	29.6	2.3	-	-	2	19.0	123.3	6.9	70.3	6.1	3.1	0.6	30.0	3.0	0.9					52.3	± 20.9	-	-		3.1
PL 70	29.6	2.3	1	2	2	19.9	122.2	6.9	68.9	6.1	3.2	0.6	25.0	3.2	0.7	174.5	±22.5	82.0	± 29	52.3	± 20.9		6.8	4.5	4.5-6.8

a) average burial depths and exhumation rates estimated with the Age2.dot software using average geothermal gradient, average cooling rate for each sample and averga Tc (from tab.7). b) average burial depths and exhumation rates estimated with the Age2.dot software using average geothermal gradient, average cooling rate for each sample obtained from thermal models. c) estimate made for 10-20 Ma hold time using the Closure software

Table 4.9 – Estimate of burial depths and exhumation rates. Burial depths were estimated a) from the Tc values presented in Tab. 4.8, using the Age2.dot software (Brandon et al., 1998), assuming present day cooling rates of 3-6°C/Ma (from Fig. 4.8 and 4.10) and cooling rates through the AFT Tc from Tab. 4.8; geothermal gradients assume a k=2.2 W/m°C (Tab. 4.7). b) burial depths and exhumation rates were estimated using the Age2.dot software (Brandon et al., 1998) from the average cooling rates obtained for the fast cooling stage in the thermal models. c) Burial depths maximum values were estimated from PRZ of the AFT, AHe and ZHe systems and from present day geothermal gradients, assuming a surface temperature of 10°C.

Interpretation

In the light of the results presented in this work and of the abundant literature available (e.g. Huismans et al., 2001; Dererova et al., 2006, Sperner et al., 2002), we discuss in this section the relationship between the features of the Pannonian Basin and the UC in order to infer constrains on the geodynamic evolution of this region.

The burial depth pattern along the chain (Fig. 4.13), coupled with the uniform cooling ages (except the NW-ward younging trend, that will be discusses later on) indicates that the UC exhumed by a first rapid stage of enhanced erosion during post-thrusting isostatic uplift, followed by a second stage of slower erosion. Toward the foredeep the extent of exhumation decreases, indicating that crustal thickening mainly occurred as a response to thrusting, and that the lower extent of exhumation depends on the lower thickness of the prism in the most distal portions . As for the portion of the wedge close to the Pannonian Basin, we suggest that crustal thinning occurred during the opening of the PB, was responsible to a lower isostatic uplift in the post-thrusting stage.

The progressively lower extent of denudation toward the PB is the principal effect that the opening of the basin had on the UC, since the increased geothermal gradient, as described in section 5.1, had only a minor effect.

The trend of younging exhumation toward the NW appears related to the decrease of the relief (Fig. 4.2). In Fig. 4.14 It can be observed that, even though very dispersed, a positive trend of AHe and AFT ages with elevation is present at a regional scale. At the single profile scale no trend of AHe ages with elevation can be observed, whereas AFT ages positively correlate with elevation. This indicates that, at a regional scale, during exhumation both the AFT and AHe closure isotherms were relatively flat with respect to the relief. At a local scale the AHe closure isotherm was influenced by topography, as opposed to AFT closure isotherm that remained undisturbed. The trend of north-westward younging exhumation ages depends therefore on the decreasing relief coupled with relatively flat isotherms during exhumation. This is consistent with exhumation occurred by erosion of the accretionary wedge during isostatic uplift where the decreasing relief toward the NW is a consequence of a lower initial thickness of the accretionary prism, having induced a lower uplift.

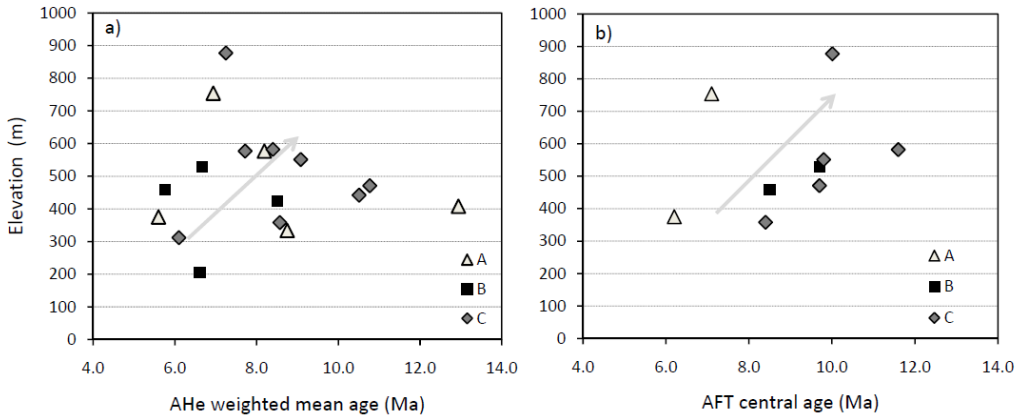

Figure 4.14 – Age-Elevation relationship for AHe and AFT dates. Samples are grouped by transect (Fig. 4.3)

In Fig. 4.15 a synthesis of the main steps in the evolution of the PB and of the UC are indicated. Two main features are worth noting. First, we point to the fact that at ca. 12-11 Ma several major events occurred in the Carpathian Pannonian region. At this time the major extensional phase in the PB terminated and the post-rift subsidence stage started (Huismans et al., 2001; Fodor, 2011). At the same time compression in the UC ceased and major tectonic activity, from that time on, was focused on the Romanian Carpathians. Furthermore at 12-11 Ma the main stage of uplift and exhumation of the UC started. The concurrence of these events points out that the main extensional stage in the PB was tightly related to compression in the UC. Furthermore the end of compression in the UC and extension in the PB were also related to the cessation of gravitational tear below the UC and to their subsequent uplift. These events can be well explained either by the slab roll-back and break-off theory (e.g. Horvath et al., 2006; Sperner et al., 2002) or by the gravitational collapse theory (e.g. Houseman and Gemmer, 2007). In both cases extension in the PB coeval to compression and gravitational tear below the UC can be satisfyingly explained. In the first model, slab roll back would induce astenosphere upwelling in the PB and concurrently compression in the UC. Subsequent slab break-off would induce the end of extension in the PB and isostatic rebound of the UC.
The gravitational collapse model comprises a first phase of extension of thickened crust in the PB region, triggering lithosphere thinning below the PB and lithosphere thickening below the UC. The lithospheric flow from below the PB to the Carpathians would give reason for extension and mantle upwelling in the PB and thrusting in the UC. We propose S-ward migration of the lithospheric flow, occurred at ca. 12-11 Ma as demonstrated by the shift of tectonic activity, caused the end of active lithospheric flow from below the PB to the UC and consequent cessation of tear and uplift of the UC.

The second noteworthy piece of information that is indicated in Fig. 4.15 is that the only feature that did not undergo a major change at 12-11 Ma is the lithospheric thickness (Fig.0). As a matter of fact our data indicate that thermal anomaly induced by extension lasted until present day with about the same extent as that of its rise. Therefore it appears that, even though lithosphere below the PB did not undergo further thinning and extension after 11-12 Ma, still no reduction of the astenospheric plume occurred. We suggest that the deep lithospheric root that remained below the UK (e.g. Dererova et al., 2009), associated to compression and lithospheric downwelling in the Romanian Carpathians, that has been active till present day (e.g. Sperner et al., 2002, Nemcok et al., 2006), have been responsible for the preservation of thinned lithosphere in the PB.

Even though our data, integrated with previously published geophysical data, do not allow to rule out any of the geodynamic models proposed for the Carpathian-Pannonian region, we find that a SE-ward progressive detachment of an oceanic slab should be testified by evidence for sunk slabs at progressively shallower depths toward the SE, as described by Ren et al. (2012). Since no clear evidence for sunk slabs below the Carpathians can be found in the upper 400 Km

(Ren et al., 2012) we support gravitational collapse as the most likely process driving the Miocene evolution of the Carpathian-Pannonian region.

Finally we point to the role that the TESZ had in the formation of the Carpathian-Pannonian region. We observe that in correspondence of this major lithospheric boundary the Carpathians reach their maximum lithospheric and crustal thickness (Fig. 4.1 and Fig. 4.3). The thicker lithosphere of the East European Platform likely constituted an obstacle to frontal accretion and outward migration of collision along the Ukrainian and Romanian Carpathians leading to crustal and lithospheric over-thickening. Furthermore we observe that, between 11 and 9 Ma, tectonic activity rapidly migrated SE ward along this lineament (e.g. Nemcok et al., 2006). Based on the model of gravitational instability of the lithosphere we propose that the TESZ impeded the downwelling lithosphere to further migrate outward, inducing a lateral shift of downwelling and, consequently, of major compression.

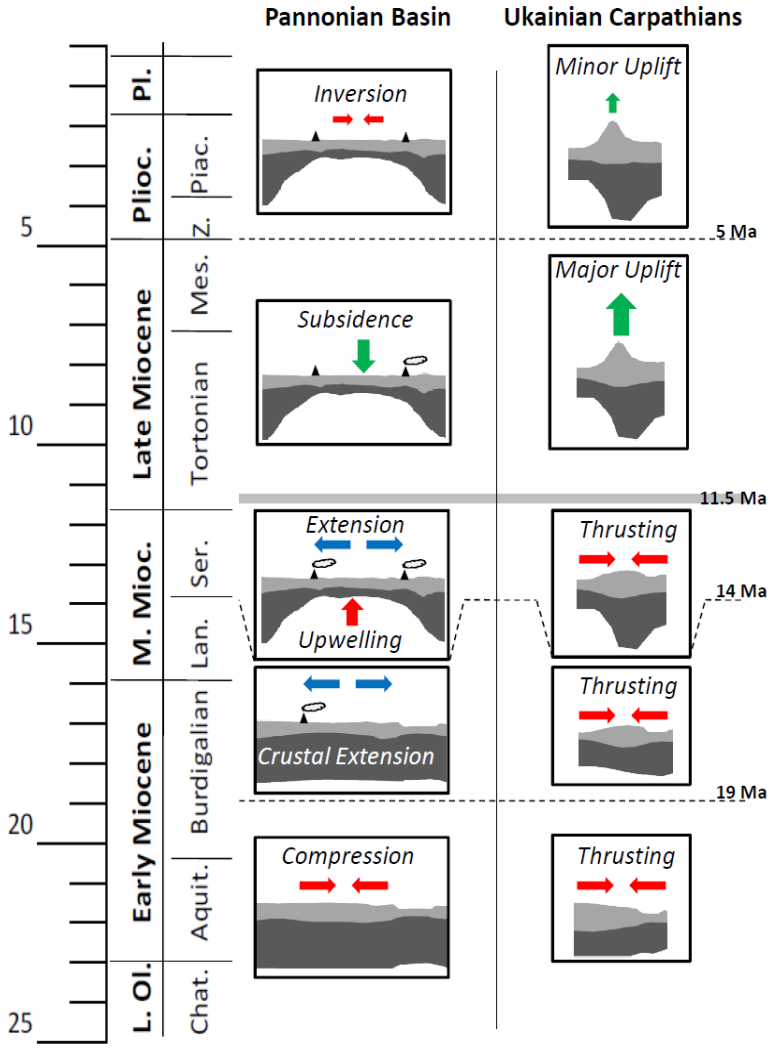

Figure 4.15 – Synthesis of the main steps in the Neogene evolution of the Pannonian Basin (from Huismans et al., 2001 and Fodor et al., 2011) and of the Ukrainian Carpathians (from Nemcok et al., 2006 and from this work)

4.2.7. Conclusions

The application of low temperature thermochronometry and vitrinite reflectance analysis allowed us to constrain the paleo-thermal structure of the UC, as well as to define their thermal and burial-exhumation history.

We propose that an increase of geothermal gradient occurred between 14.5 and 11 Ma, during extension in the Pannonian Basin. Our data indicate that gradients remained then constant until present day.

Heating of the wedge follows the regional elevation trend, reaching the maximum values of ca. 170°C in the central thrust sheets, whereas the outermost and innermost thrust sheets were respectively heated to less than 60°C and less than ca. 120°C. As heating entirely depends on burial, the trend of burial mimics the one described above. Burial varies from 2.6-4 Km in the innermost portions of the chain, to 6 Km in the central thrust sheets, and less than 2-3 Km in the outermost thrust sheets and in the foredeep.

Cooling occurred in two main phases, the first, between ca. 12 and ca. 5 Ma, characterized by high average cooling rates (15-30°C/Myr), and the second, from ca 5 Ma to present, characterized by moderate average cooling rates (3-6°C/Myr).

Timing of exhumation corresponds to timing of cooling, and exhumation rates in the central thrust sheets (up to more than 1 mm/yr in the rapid stage) are higher than in the more internal thrust sheets (ca.0.7-1 mm/yr in the rapid stage). We interpret that exhumation occurred by erosion of the wedge during isostatic uplift after the cessation of thrusting. The region where denudation reached its maximum extent would then correspond to the more thickened portion of the wedge. Denudation had a lower extent close to the Pannonian basin due to crustal thinning occurred during the opening of the PB. Exhumation ages are progressively younger toward the NW, this trend is related with the progressive decrease of the relief. Such progressive decrease of the relief toward the NW is due to a lower uplift depending on lower thickness of the accretionary prism.

Finally the data presented in this paper allowed us to formulate some considerations on the evolution of the Carpathian-Pannonian region.

The influence of the PB on the thermal history of the UC is restricted to the innermost units.

At 12-11 Ma a major change in the dynamics of the region occurred. In this stage the PB passed from a regime of major extension to major subsidence and minor extension; collision in the UC terminated and the major uplift stage started; the focus of tectonic activity migrated southward. These events can be ascribed both to slab break off and termination of lithosphere downwelling below the UC.

Lithosphere thickness below the UC did not significantly change from Middle Miocene to present day. We suggest that active compression in the Romanian Carpathians and thickened lithosphere beneath the UC contributed to preserve such thinned lithosphere.

The over-thickened lithosphere and crust of the UC can be ascribed to the presence of the TESZ, that acted as an obstacle to the migration of collision and frontal accretion further to the foreland, rather inducing higher imbrication of the thrust sheets and lateral shift of the collision.

4.3. Appendix to chapter IV

4.3.7. Data Tables

sample	replicate	Th/U	raw date (Ma)	1s ± date (Ma)	1s ± date %	Ft 238U	Ft 235U	Ft 232Th	Ft 147Sm	Rs (µm)	corr date (Ma)	1s ± date (Ma)	1s ± date %	ppm eU	ppm U	d ppm U	ppm Th	d ppm Th	ppm Sm	d ppm Sm	nmol 4He/g	d nmol 4He/g
Pl 39	BA_Pl39_01	2.188	14.26	0.46	3.26			0.5941		32.8	**24.00**	**0.78**	3.26	34.32	22.86		48.75		466.92		2.69	
	BA_Pl39_02	1.587	41.45	1.07	2.57			0.6353		37.8	**65.24**	**1.68**	2.57	82.21	60.29		93.28		493.28		18.59	
	BA_Pl39_03	0.166	67.07	1.76	2.63			0.7078		48.0	**94.76**	**2.49**	2.63	83.37	80.32		12.96		199.33		30.39	
	BA_Pl39_04	0.791	10.89	0.48	4.41			0.6272		37.3	**17.36**	**0.77**	4.41	33.63	28.47		21.96		337.51		2.00	
Pl 50	12B757_BA_Pl50_1_Ap	0.301	45.51	0.85	1.86	0.6238	0.5754	0.5754	0.6986	36.46	**73.18**	**1.37**	1.87	55.63	52.04	0.75	15.27	0.24	302.38	4.40	13.490	0.175
	12B998_BA_Pl50_Ap2	0.854	93.39	1.45	1.55	0.6281	0.5802	0.5802	0.7035	36.94	**150.00**	**2.35**	1.57	61.30	51.27	0.75	42.67	0.63	238.25	3.46	30.644	0.286
Pl 52	~~12B758_BA_Pl52_1_Ap~~	~~1.738~~	~~5.67~~	~~0.12~~	~~2.20~~	~~0.7399~~	~~0.7045~~	~~0.7045~~	~~0.8287~~	~~54.90~~	~~7.77~~	~~0.17~~	~~2.21~~	~~81.03~~	~~57.95~~	~~0.83~~	~~98.19~~	~~1.40~~	~~175.80~~	~~2.52~~	~~2.447~~	~~0.047~~
	12B759_BA_Pl52_3_Ap	3.232	3.71	0.12	3.36	0.6517	0.6061	0.6061	0.7298	39.78	**5.88**	**0.20**	3.36	81.45	46.80	0.66	147.43	2.13	85.87	1.26	1.617	0.052
	12B760_BA_Pl52_4_Ap	85.337	3.61	0.12	3.26	0.7074	0.6681	0.6681	0.7923	48.28	**5.39**	**0.18**	3.26	37.00	1.80	0.04	149.79	2.13	58.87	0.87	0.727	0.022
	12B761_BA_Pl52_5_Ap	0.896	3.59	0.17	4.73	0.6530	0.6076	0.6076	0.7313	39.95	**5.57**	**0.26**	4.74	29.89	24.80	0.35	21.65	0.31	300.81	4.50	0.576	0.026
	12B999_BA_Pl52_Ap7	4.199	3.18	0.23	7.09	0.5921	0.5406	0.5406	0.6631	33.23	**5.61**	**0.40**	7.09	27.37	13.95	0.20	57.11	0.82	109.17	1.78	0.468	0.033
Pl 53	12C001_BA_Pl53_Ap1	1.720	7.99	0.13	1.59	0.8048	0.7775	0.7775	0.9014	74.67	**10.01**	**0.16**	1.59	46.51	33.36	0.48	55.94	0.80	283.61	4.04	1.989	0.023
	12C002_BA_Pl53_Ap2	2.938	11.27	0.50	4.47	0.6832	0.6411	0.6411	0.7652	44.22	**16.90**	**0.76**	4.47	35.88	21.44	0.31	61.42	0.92	248.85	3.56	2.176	0.095
	~~12C003_BA_Pl53_Ap3~~	~~2.131~~	~~0.20~~	~~0.03~~	~~16.30~~	~~0.7190~~	~~0.6810~~	~~0.6810~~	~~0.8052~~	~~50.46~~	~~0.28~~	~~0.05~~	~~16.30~~	~~37.89~~	~~25.46~~	~~0.36~~	~~52.88~~	~~0.76~~	~~132.17~~	~~1.92~~	~~0.040~~	~~0.007~~
	12C004_BA_Pl53_Ap4	2.079	6.47	0.26	4.08	0.6861	0.6443	0.6443	0.7684	44.67	**9.63**	**0.39**	4.09	49.47	33.51	0.48	67.92	0.97	125.57	1.87	1.710	0.067
	12C005_BA_Pl53_Ap5	40.648	3.93	0.13	3.30	0.6905	0.6493	0.6493	0.7734	45.38	**6.00**	**0.20**	3.30	26.63	2.58	0.04	102.31	1.46	232.73	3.38	0.573	0.018
Pl 54	12B762_BA_Pl54_1_Ap	7.638	5.95	0.13	2.25	0.7419	0.7067	0.7067	0.8310	55.36	**8.27**	**0.19**	2.25	48.12	17.50	0.25	130.28	1.88	128.77	1.85	1.545	0.031
	12B763_BA_Pl54_2_Ap	62.977	3.86	0.13	3.32	0.6896	0.6483	0.6483	0.7724	45.24	**5.92**	**0.20**	3.32	71.56	4.64	0.09	284.78	4.10	213.60	3.13	1.506	0.046
	12B764_BA_Pl54_3_Ap	34.558	3.67	0.12	3.29	0.7272	0.6902	0.6902	0.8145	52.13	**5.28**	**0.17**	3.29	49.40	5.54	0.08	186.64	2.67	105.89	1.52	0.985	0.030
	12C006_BA_Pl54_Ap4	5.626	6.61	0.17	2.64	0.6899	0.6486	0.6486	0.7727	45.29	**9.91**	**0.26**	2.64	31.48	13.75	0.19	75.44	1.08	301.04	4.33	1.130	0.028
Pl 55	12B765_BA_Pl55_1_Ap	0.505	4.55	0.28	6.24	0.6362	0.5891	0.5891	0.7125	37.87	**7.22**	**0.45**	6.24	39.67	35.56	0.51	17.49	0.25	105.19	1.58	0.957	0.058
	12B766_BA_Pl55_2_Ap	1.301	3.15	0.21	6.51	0.6886	0.6472	0.6472	0.7713	45.08	**4.65**	**0.30**	6.51	11.86	9.14	0.13	11.59	0.17	48.02	0.71	0.200	0.013
	~~12B767_BA_Pl55_3_Ap~~	~~1.740~~	~~20.67~~	~~0.31~~	~~1.51~~	~~0.6626~~	~~0.6182~~	~~0.6182~~	~~0.7421~~	~~41.22~~	~~31.79~~	~~0.48~~	~~1.51~~	~~60.23~~	~~43.07~~	~~0.62~~	~~73.04~~	~~1.07~~	~~218.60~~	~~3.26~~	~~6.654~~	~~0.069~~
	12B768_BA_Pl55_4_Ap	2.013	3.11	0.43	13.90	0.6327	0.5852	0.5852	0.7086	37.46	**5.04**	**0.70**	13.90	12.63	8.65	0.13	16.96	0.24	55.05	0.93	0.210	0.029
	12B769_BA_Pl55_5_Ap	0.373	7.94	0.38	4.85	0.6625	0.6181	0.6181	0.7420	41.21	**12.03**	**0.58**	4.85	26.11	24.05	0.37	8.75	0.14	368.33	5.33	1.113	0.052
	12B770_BA_Pl55_6_Ap	0.783	5.62	0.11	2.04	0.5868	0.5348	0.5348	0.6572	32.74	**9.72**	**0.20**	2.05	272.39	230.95	3.28	176.36	2.51	178.11	2.58	8.112	0.134
Pl 56	12B771_BA_Pl56_1_Ap	1.634	9.38	0.44	4.74	0.6492	0.6034	0.6034	0.7271	39.46	**14.70**	**0.70**	4.74	20.00	14.55	0.22	23.18	0.35	288.81	4.18	1.015	0.047
	12B772_BA_Pl56_2_Ap	9.307	17.57	0.70	3.96	0.6687	0.6250	0.6250	0.7489	42.07	**27.45**	**1.09**	3.96	14.54	4.64	0.09	42.11	0.60	144.36	2.12	1.393	0.053
	12B773_BA_Pl56_3_Ap	1.004	26.54	0.67	2.54	0.6066	0.5565	0.5565	0.6794	34.64	**44.33**	**1.13**	2.55	37.06	30.13	0.43	29.50	0.42	565.65	8.15	5.317	0.120
	12B774_BA_Pl56_4_Ap	2.087	5.91	0.17	2.85	0.5767	0.5237	0.5237	0.6459	31.82	**10.57**	**0.30**	2.85	57.26	38.74	0.55	78.80	1.13	272.93	3.99	1.812	0.048
	12B775_BA_Pl56_5_Ap	15.626	5.87	0.31	5.28	0.6589	0.6142	0.6142	0.7380	40.73	**9.40**	**0.50**	5.27	19.36	4.23	0.07	64.41	0.92	133.11	2.03	0.620	0.032
Pl 58	12B776_BA_Pl58_1_Ap	2.923	7.79	0.13	1.71	0.7287	0.6919	0.6919	0.8162	52.44	**10.90**	**0.19**	1.72	27.24	16.31	0.23	46.48	0.66	301.35	4.40	1.148	0.016
	12B777_BA_Pl58_2_Ap	3.428	6.94	0.21	3.02	0.7838	0.7538	0.7538	0.8779	66.98	**8.98**	**0.27**	3.02	13.93	7.80	0.11	26.08	0.38	271.02	3.88	0.529	0.015
	12B778_BA_Pl58_3_Ap	2.864	10.03	0.51	5.06	0.7862	0.7565	0.7565	0.8806	67.78	**12.93**	**0.65**	5.06	22.34	13.49	0.19	37.66	0.54	316.56	4.55	1.217	0.060
	12B779_BA_Pl58_4_Ap	2.573	8.95	0.37	4.19	0.8020	0.7743	0.7743	0.8982	73.54	**11.27**	**0.47**	4.19	18.52	11.65	0.17	29.23	0.42	329.29	4.71	0.903	0.037
	12B780_BA_Pl58_5_Ap	2.940	7.19	0.49	6.78	0.6760	0.6331	0.6331	0.7571	43.13	**10.90**	**0.74**	6.78	13.27	7.93	0.11	22.73	0.33	143.99	2.06	0.516	0.035
Pl 59	12B781_BA_Pl59_1_Ap	0.491	6.63	0.16	2.35	0.6649	0.6208	0.6208	0.7447	41.54	**10.04**	**0.24**	2.35	26.32	23.66	0.34	11.32	0.17	118.58	1.72	0.928	0.018
	12B782_BA_Pl59_2_Ap	3.033	5.63	0.39	6.95	0.6302	0.5824	0.5824	0.7058	37.18	**9.21**	**0.64**	6.95	16.86	9.95	0.15	29.41	0.42	113.62	1.66	0.511	0.035
	12B783_BA_Pl59_3_Ap	10.899	4.66	0.17	3.75	0.7313	0.6948	0.6948	0.8191	53.00	**6.60**	**0.25**	3.75	18.88	5.40	0.08	57.36	0.84	48.73	0.73	0.476	0.017
	12B784_BA_Pl59_4_Ap	5.245	5.72	0.32	5.59	0.7134	0.6748	0.6748	0.7991	49.40	**8.27**	**0.46**	5.59	16.13	7.33	0.11	37.46	0.54	17.20	0.34	0.496	0.027
	12B785_BA_Pl59_5_Ap	0.802	6.24	0.21	3.40	0.6905	0.6493	0.6493	0.7734	45.38	**9.12**	**0.31**	3.40	36.97	31.23	0.45	24.41	0.35	163.74	2.37	1.227	0.039

Table 4.2 - - AHe analytical data

sample	replicate	Th/U	raw date (Ma)	1s ± date (Ma)	1s ± date %	Ft 238U	Ft 235U	Ft 232Th	Ft 147Sm	Rs (µm)	corr date (Ma)	1s ± date (Ma)	1s ± date %	ppm eU	ppm U	d ppm U	ppm Th	d ppm Th	ppm Sm	d ppm Sm	nmol 4He/g	d nmol 4He/g
PL 60	12B786_BA_PL60_1_Ap	4.836	4.22	0.29	6.78	0.7030	0.6632	0.6632	0.7873	47.49	**6.18**	**0.42**	6.78	14.90	7.07	0.11	33.32	0.48	39.59	0.58	0.338	0.023
	12B787_BA_PL60_2_Ap	4.264	7.88	0.29	3.63	0.7727	0.7412	0.7412	0.8654	63.48	**10.37**	**0.38**	3.63	10.95	5.54	0.08	23.02	0.33	202.40	2.93	0.472	0.017
	12B788_BA_PL60_3_Ap	3.368	4.21	0.11	2.69	0.7649	0.7325	0.7325	0.8567	61.23	**5.61**	**0.15**	2.69	18.16	10.25	0.15	33.66	0.48	65.98	0.94	0.411	0.010
	12B789_BA_PL60_4_Ap	6.931	4.38	0.21	4.87	0.6356	0.5884	0.5884	0.7119	37.80	**7.22**	**0.35**	4.87	39.43	15.24	0.22	102.95	1.48	418.55	5.99	0.941	0.045
	12B790_BA_PL60_5_Ap	8.644	2.93	0.21	7.24	0.7066	0.6672	0.6672	0.7914	48.14	**4.31**	**0.31**	7.24	13.36	4.48	0.07	37.76	0.54	37.13	0.54	0.212	0.015
PL 61	12B791_BA_ PL61_1_Ap	13.865	5.96	0.47	7.83	0.6592	0.6145	0.6145	0.7383	40.77	**9.50**	**0.74**	7.83	12.35	2.96	0.05	39.96	0.58	183.03	2.70	0.404	0.031
	12C007_BA_PL61_Ap2	42.949	5.94	0.20	3.37	0.7761	0.7451	0.7451	0.8692	64.51	**7.93**	**0.27**	3.37	12.87	1.19	0.02	49.71	0.71	21.10	0.32	0.415	0.013
	12C008_BA_PL61_Ap3	8.919	5.73	0.25	4.44	0.6548	0.6097	0.6097	0.7334	40.19	**9.17**	**0.41**	4.44	25.21	8.29	0.12	72.03	1.05	211.32	3.05	0.786	0.034
PL 62	12B792_BA_PL62_1_Ap	5.640	7.59	0.38	5.06	0.7238	0.6864	0.6864	0.8107	51.43	**10.75**	**0.54**	5.06	11.68	5.09	0.07	28.01	0.40	317.29	4.61	0.491	0.024
	12B793_BA_PL62_2_Ap	2.411	7.81	0.37	4.77	0.6560	0.6109	0.6109	0.7347	40.34	**12.20**	**0.58**	4.78	15.43	9.94	0.15	23.36	0.35	70.70	1.08	0.646	0.030
	~~12B794_BA_PL62_3_Ap~~	~~0.374~~	~~14.16~~	~~0.36~~	~~2.51~~	~~0.7439~~	~~0.7089~~	~~0.7089~~	~~0.8331~~	~~55.82~~	~~**19.10**~~	~~**0.48**~~	~~2.52~~	~~76.42~~	~~70.38~~	~~1.00~~	~~25.69~~	~~0.37~~	~~267.97~~	~~3.84~~	~~5.741~~	~~0.124~~
	12B795_BA_PL62_4_Ap	1.335	8.26	0.24	2.88	0.7412	0.7058	0.7058	0.8301	55.19	**11.27**	**0.33**	2.88	11.07	8.48	0.12	11.03	0.16	24.98	0.41	0.487	0.013
	12B796_BA_PL62_5_Ap	4.161	7.94	0.17	2.20	0.7830	0.7529	0.7529	0.8770	66.72	**10.32**	**0.23**	2.20	12.39	6.34	0.09	25.73	0.37	181.70	2.65	0.536	0.011
PL 63	12B797_BA_PL63_1_Ap	2.377	6.55	0.39	5.93	0.6655	0.6215	0.6215	0.7454	41.63	**10.06**	**0.60**	5.94	28.94	18.74	0.28	43.41	0.63	328.37	4.79	1.024	0.060
	12B798_BA_PL63_2_Ap	13.598	3.03	0.13	4.16	0.6065	0.5564	0.5564	0.6793	34.63	**5.32**	**0.22**	4.16	36.08	8.77	0.13	116.23	1.65	73.81	1.12	0.591	0.024
	12B844_BA_PL63_3_Ap	1.190	7.94	0.15	1.90	0.6629	0.6187	0.6187	0.7425	41.27	**12.15**	**0.23**	1.91	99.97	78.56	1.14	91.10	1.31	303.55	4.46	4.223	0.064
	12B845_BA_PL63_4_Ap	4.602	5.03	0.14	2.88	0.7201	0.6822	0.6822	0.8065	50.67	**7.18**	**0.21**	2.88	27.75	13.51	0.19	60.61	0.86	77.60	1.13	0.750	0.020
	12B846_BA_PL63_5_Ap	0.885	8.94	0.14	1.61	0.8143	0.7882	0.7882	0.9120	78.70	**11.03**	**0.18**	1.61	38.67	32.15	0.46	27.73	0.40	255.62	3.74	1.845	0.020
PL 64	12C009_BA_PL64_Ap1	4.612	5.47	0.08	1.37	0.7373	0.7016	0.7016	0.8258	54.32	**7.61**	**0.10**	1.37	50.62	24.62	0.35	110.67	1.59	311.05	4.46	1.495	0.014
	12C010_BA_PL64_Ap2	6.639	5.60	0.14	2.47	0.7154	0.6770	0.6770	0.8012	49.76	**8.08**	**0.20**	2.47	80.65	31.99	0.49	207.03	2.95	309.85	4.52	2.436	0.055
	12C011_BA_PL64_Ap3	0.665	5.65	0.26	4.55	0.6777	0.6350	0.6350	0.7590	43.39	**8.41**	**0.38**	4.55	77.11	66.92	0.96	43.38	0.63	214.11	3.10	2.313	0.101
	12C012_BA_PL64_Ap4	11.336	4.33	0.33	7.53	0.6631	0.6188	0.6188	0.7427	41.29	**6.86**	**0.52**	7.53	15.19	4.22	0.06	46.67	0.69	44.01	0.66	0.356	0.027
PL 65	12B847_BA_PL65_1_Ap	5.631	7.10	0.14	1.91	0.6229	0.5744	0.5744	0.6977	36.36	**11.91**	**0.23**	1.91	42.07	18.37	0.27	100.85	1.46	362.92	5.32	1.620	0.026
	12B848_BA_PL65_2_Ap	9.781	3.99	0.10	2.53	0.6512	0.6057	0.6057	0.7294	39.72	**6.44**	**0.16**	2.53	67.68	20.89	0.30	199.14	2.83	203.05	2.91	1.460	0.034
	12B849_BA_PL65_3_Ap	13.987	2.48	0.08	3.13	0.5915	0.5399	0.5399	0.6625	33.17	**4.49**	**0.14**	3.12	95.49	22.72	0.33	309.69	4.43	742.25	10.76	1.291	0.038
	12B850_BA_PL65_4_Ap	9.290	8.16	0.16	1.99	0.6542	0.6090	0.6090	0.7327	40.11	**13.09**	**0.26**	1.99	81.70	26.12	0.38	236.52	3.40	326.78	4.76	3.610	0.061
	12851_BA_PL65_5_Ap	9.506	3.92	0.29	7.38	0.6622	0.6178	0.6178	0.7417	41.17	**6.21**	**0.46**	7.37	20.78	6.54	0.10	60.60	0.87	82.85	1.28	0.441	0.032
PL 67	12852_BA_PL67_1_Ap	1.923	11.79	0.32	2.68	0.7031	0.6632	0.6632	0.7874	47.50	**17.04**	**0.46**	2.69	45.77	31.77	0.45	59.56	0.85	537.78	7.84	2.913	0.072
	12853_BA_PL67_2_Ap	52.914	3.54	0.20	5.69	0.7402	0.7048	0.7048	0.8291	54.97	**4.99**	**0.28**	5.69	9.87	0.75	0.02	38.80	0.56	117.83	1.73	0.192	0.011
	12854_BA_PL67_3_Ap	6.791	4.84	0.18	3.77	0.7430	0.7079	0.7079	0.8321	55.61	**6.69**	**0.25**	3.77	7.84	3.07	0.04	20.30	0.30	62.17	0.92	0.206	0.007
	12855_BA_PL67_4_Ap	28.384	2.24	0.35	15.77	0.7212	0.6835	0.6835	0.8078	50.90	**3.25**	**0.51**	15.77	10.40	1.39	0.03	38.34	0.55	152.84	2.23	0.129	0.020
	12856_BA_PL67_5_Ap	2.777	3.68	0.13	3.62	0.6505	0.6048	0.6048	0.7285	39.62	**5.82**	**0.21**	3.63	59.88	36.60	0.54	99.07	1.47	159.15	2.29	1.179	0.041
PL 68	12B857_BA_PL68_1_Ap	0.850	4.85	0.25	5.05	0.6395	0.5927	0.5927	0.7162	38.27	**7.68**	**0.39**	5.06	99.41	83.21	1.18	68.94	0.99	107.88	1.78	2.557	0.126
	12B858_BA_PL68_2_Ap	1.606	8.18	0.14	1.75	0.7974	0.7690	0.7690	0.8931	71.76	**10.34**	**0.18**	1.76	36.37	26.59	0.38	41.63	0.61	276.62	3.96	1.595	0.022
	12B859_BA_PL68_3_Ap	3.374	5.99	0.14	2.26	0.7091	0.6700	0.6700	0.7942	48.59	**8.65**	**0.20**	2.26	30.28	17.08	0.24	56.16	0.80	226.03	3.24	0.978	0.020
	12B860_BA_PL68_4_Ap	2.614	4.85	0.15	3.02	0.6933	0.6524	0.6524	0.7765	45.84	**7.15**	**0.22**	3.02	75.23	47.06	0.67	119.88	1.71	155.18	2.28	1.949	0.055
	12B861_BA_PL68_5_Ap	1.388	4.81	0.17	3.59	0.7009	0.6609	0.6609	0.7851	47.13	**6.96**	**0.25**	3.59	39.07	29.65	0.43	40.11	0.58	247.95	3.59	1.006	0.034
PL 69	12B862_BA_PL69_1_Ap	4.297	5.20	0.18	3.51	0.7263	0.6892	0.6892	0.8134	51.93	**7.34**	**0.26**	3.51	22.49	11.33	0.17	47.47	0.70	103.40	1.50	0.629	0.021
	12B863_BA_PL69_2_Ap	39.343	3.56	0.08	2.21	0.6925	0.6515	0.6515	0.7756	45.70	**5.43**	**0.12**	2.21	44.84	4.48	0.06	171.76	2.46	158.05	2.35	0.871	0.016
	12B864_BA_PL69_3_Ap	0.573	4.08	0.13	3.18	0.7340	0.6978	0.6978	0.8221	53.57	**5.59**	**0.18**	3.18	39.07	34.54	0.49	19.28	0.28	94.37	1.39	0.845	0.025
PL 70	12B865_BA_PL70_1_Ap	8.576	6.25	0.10	1.61	0.7274	0.6905	0.6905	0.8147	52.18	**8.89**	**0.14**	1.61	62.84	21.20	0.31	177.19	2.54	275.92	3.95	2.126	0.026
	12B866_BA_PL70_2_Ap	45.597	3.03	0.16	5.40	0.6789	0.6364	0.6364	0.7604	43.57	**4.73**	**0.26**	5.40	34.76	3.04	0.04	134.97	1.95	70.13	1.06	0.573	0.030
	12B867_BA_PL70_3_Ap	8.494	3.63	0.11	2.93	0.6600	0.6154	0.6154	0.7392	40.87	**5.75**	**0.17**	2.93	46.41	15.76	0.23	130.44	1.86	212.81	3.14	0.911	0.025
	12B869_BA_PL70_5_Ap	12.185	3.96	0.11	2.86	0.6536	0.6083	0.6083	0.7321	40.03	**6.39**	**0.182**	2.86	88.36	23.31	0.33	276.81	4.00	208.86	3.04	1.894	0.050

sample	corr date (Ma)	1s ± date (Ma)	1s ± date %	w.m.a. (Ma)	w.m.a. error (Ma)	min age (Ma)	max age (Ma)	negative dispersion (Ma)	positive dispersion (Ma)	morph comments	comment
PL 39	**24.00**	**0.78**	3.26	**32.06**	**0.39**	16.59	97.25	15.46	65.20	inclusions	
	65.24	**1.68**	2.57							inclusions, slightly broken, abraded	
	94.76	**2.49**	2.63							rounded, abraded, inclusions	
	17.36	**0.77**	4.41							rounded, 1 biotite inclusion?	
PL 50	**73.18**	**1.37**	1.87	**92.53**	**1.18**	71.82	152.36	20.71	59.83	abraded, small oval inclusion, rounded	
	150.00	**2.35**	1.57							abraded, coated, inlcusions, rounded	
PL 52	~~**7.77**~~	~~**0.17**~~	~~2.21~~	**5.60**	**0.11**	5.21	6.07	0.39	0.48	~~slightly abraded, several small inclusions, very slightly broken~~	~~outlier*~~
	5.88	**0.20**	3.36							small mat inclusion. Slightly brokem	
	5.39	**0.18**	3.26							abraded. Several mat inclusions	high Th/U and Th; very low U
	5.57	**0.26**	4.74							small mat inclusion	
	5.61	**0.40**	7.09							slightly abraded, coated, small inclusions	
PL 53	**10.01**	**0.16**	1.59	**8.75**	**0.12**	5.80	17.66	2.94	8.91	abraded, inclusions, broken	
	16.90	**0.76**	4.47							slightly abraded, small inclusions	
	~~**0.28**~~	~~**0.05**~~	~~16.30~~							~~very abraded, coated, several big inclusions, partly broken. Very bad grain~~	
	9.63	**0.39**	4.09							abraded, very small mat inclusions, broken, pretty good grain	
	6.00	**0.20**	3.30							coated with reddish dots, inclusions, rounded	very low U; very high Th
PL 54	**8.27**	**0.19**	2.25	**6.94**	**0.10**	0.54	10.17	6.41	3.23	very abraded, big inclusions, rounded, maybe broken, very bad sample	high Th/U
	5.92	**0.20**	3.32							abraded, very slightly coated, big mat inclusions, maybe broken, very bad crystal	very high Th/U
	5.28	**0.17**	3.29							very abraded, slightly coated with small black dots on the surface, small inclusions, rounded, partly broken. Very bad crystal	very high Th/U
	9.91	**0.26**	2.64							slightly abraded, coated, inclusions	high Th/U
PL 55	**7.22**	**0.45**	6.24	**8.19**	**0.15**	4.34	12.61	3.84	4.42	inclusions and broken	
	4.65	**0.30**	6.51							very slightly abraded. Broken	
	~~**31.79**~~	~~**0.48**~~	~~1.51~~							~~abraded. 1 pretty big inclusion (1/5 of the length of crystal). Partialy rounded.~~	~~outlier*~~
	5.04	**0.70**	13.90							v. small inclusion. Maybe broken in the pack	high error; low He
	12.03	**0.58**	4.85							v. sm inclusions. Slightly broken	
	9.72	**0.20**	2.05							2 spots of coating, several lg incl. rounded	
PL 56	**14.70**	**0.70**	4.74	**12.94**	**0.23**	8.90	45.45	4.04	32.51	coated, inclusions, rounded	
	27.45	**1.09**	3.96							abraded, inclusions, broken, picture of rough edges sketched on ft data sheet	low U
	44.33	**1.13**	2.55							1 big red inclusion, other smaller ones, rounded	
	10.57	**0.30**	2.85							abraded, many small inclusions, rounded	
	9.40	**0.50**	5.27							slightly abraded, many small mat (black-red) inclusions.	low U
PL 58	**10.90**	**0.19**	1.72	**10.51**	**0.14**	8.71	13.58	1.80	3.07	very abraded, back spots on the surface, pretty big inclusions, both opague and transparent. Maybe broken along the c-axis. Very bad shape	
	8.98	**0.27**	3.02							very abraded, coated with black dots, inclusions, partly broken, very bad crystal	
	12.93	**0.65**	5.06							abraded, coated, big inclusions, "good shape, thin fragment, but still very abraded and with inclusions"	
	11.27	**0.47**	4.19							abraded, coated (black dots), inclusions, broken	
	10.90	**0.74**	6.78							abraded, coated, inlcusions, could be broken. Very bad crystal	
PL 59	**10.04**	**0.24**	2.35	**8.57**	**0.14**	6.36	10.28	2.22	1.71	inclusions, broken	
	9.21	**0.64**	6.95							slightly abraded, slightly coated, inclusions, slightly broken	
	6.60	**0.25**	3.75							slightly abraded, black spots coating, many inclusions, rounded. "bad crystal, maybe broken in the pack?"	
	8.27	**0.46**	5.59							abraded, inclusions 15um, transparent plus other small ones, rounded.	
	9.12	**0.31**	3.40							abraded, slightly coated, small inclusions, broken	
PL 60	**6.18**	**0.42**	6.78	**6.10**	**0.12**	4.00	10.75	2.10	4.65	very small inclusions	
	10.37	**0.38**	3.63							smal inclusions, not perfect	
	5.61	**0.15**	2.69							very little abrasion, possibly black/red very small spotted coating, inlusions, many mat and small, little rounded.	
	7.22	**0.35**	4.87							big black inclusions, maybe very small pieces missing	
	4.31	**0.31**	7.24							slightly abraded, very few small inclusions	
PL 61	**9.50**	**0.74**	7.83	**8.40**	**0.214**	7.67	10.25	0.74	1.84	coated	low U
	7.93	**0.27**	3.37							v. abraded, many big inclusions, might be broken, very very bad crystal	very low U; very high Th
	9.17	**0.41**	4.44							slightly abraded, small black inclusions	
PL 62	**10.75**	**0.54**	5.06	**10.77**	**0.17**	10.09	12.78	0.68	2.01	abraded, mat and transparent pretty big inclusions, rounded	
	12.20	**0.58**	4.78							inclusions, rounded, partly broken	
	~~**19.10**~~	~~**0.48**~~	~~2.52~~							~~inclusions. "could not measure l1 and l2. I measured it along the based and considered L1 = L2.~~	~~outlier*~~
	11.27	**0.33**	2.88							ver small mat inclusions, slightly rounded	
	10.32	**0.23**	2.20							small inclusions. Might not have used a 11.5 mag on size 2	

sample	corr date (Ma)	1s ± date (Ma)	1s ± date %	w.m.a. (Ma)	w.m.a. error (Ma)	min age (Ma)	max age (Ma)	negative dispersion (Ma)	positive dispersion (Ma)	morph comments	comment
PL 63	**10.06**	**0.60**	5.94	**9.08**	**0.10**	5.10	12.38	3.98	3.30	small inclusions	
	5.32	**0.22**	4.16							Slighlty abraded, small inclusions, slightly rounded	
	12.15	**0.23**	1.91							Big, possibly zircous inlcusions.	
	7.18	**0.21**	2.88							abraded, inclusions, broken, morph index unclear. Could be 1.5 or 1	
	11.03	**0.18**	1.61							abraded, inclusions, rounded, broken	
PL 64	**7.61**	**0.10**	1.37	**7.72**	**0.09**	6.35	8.80	1.38	1.07	very abraded, many big inclusions, broken. Very bad grain	
	8.08	**0.20**	2.47							very abraded, inclusions, slightly rounded, bad crystal	
	8.41	**0.38**	4.55							slighlty abraded, inclusions, rounded, broken slighlty	
	6.86	**0.52**	7.53							small black inclusions, slighlty abraded	
PL 65	**11.91**	**0.23**	1.91	**7.25**	**0.09**	4.35	13.35	2.90	6.10	Abraded, pretty big inclusions, broken	
	6.44	**0.16**	2.53							slighlty abraded, inclusions	
	4.49	**0.14**	3.12							abraded, inclusions, fractured	
	13.09	**0.26**	1.99							many small black inclusions. Broken/fractured	
	6.21	**0.46**	7.37							slighlty abraded, small black inclusions	
PL 67	**17.04**	**0.46**	2.69	**6.61**	**0.13**	2.73	17.50	3.88	10.88	inlcusions	outlier*
	4.99	**0.28**	5.69							slighlty abraded, inclusions	low U
	6.69	**0.25**	3.77							many mat inclusions	
	3.25	**0.51**	15.77							slighlty abraded, inlcuions "see picture"	low U
	5.82	**0.21**	3.63							very few very small inclusions	
PL 68	**7.68**	**0.39**	5.06	**8.51**	**0.10**	6.71	10.53	1.80	2.02	very slighlty abraded, small inclusions	
	10.34	**0.18**	1.76							abraded, red oxide coating, inclusions, slightly rounded, slighlty broken, "pretty bad grain"	
	8.65	**0.20**	2.26							slighlty abraded, many small inclusions, slightly broken	
	7.15	**0.22**	3.02							abraded, coated, inclusions, slightly broken	
	6.96	**0.25**	3.59							abraded, red coating, inlcuions, slightly broken	
PL 69	**7.34**	**0.26**	3.51	**5.72**	**0.09**	5.31	7.60	0.41	1.88	very abraded, inclusions, probably broken "too abraded to tell, very bad crystal"	
	5.43	**0.12**	2.21							abraded, incluions, slighlty brokem. "Could not measure L1(2) but it can be inferred from the side 1" very bad crystal	low U
	5.59	**0.18**	3.18							abraded, very few inclusions, slighlty broken	
PL 70	**8.89**	**0.14**	1.61	**6.97**	**0.09**	4.48	9.03	2.49	2.07	very abraded, slight part of the coating is included, could not remove it, inclusions, slighlty rounded, not broken byt very badly abraded, can't be sure. Very bad	
	4.73	**0.26**	5.40							abraded, small inclusions	low U
	5.75	**0.17**	2.93							abraded, red coat part included in the pack, small mat inclusions, rounded	
	6.39	**0.182**	2.86							coated, inclusions, broken. Very bad crystal	

Table 4.3 – AHe weighted mean age (w.m.a.) and commentrs on grains and data quality.

A)

sample	replicate	pmol He	1s ± pmol He	% 1s ± He	U (ng)	1s ± ng U (ng)	% 1s ± ng U	ng Th (ng)	1s ± ng Th (ng)	% 1s ± ng Th	Th/U (atomic)	raw date (Ma)	1s ± date (Ma)	1s ± date %	Ft 238U	Ft 235U	Ft 232Th	Ft 147Sm	Rs (µm)	corr date (Ma)	1s ± date (Ma)
PL 50	12C147_BA_PL50_Zr1	1.078805	0.013835	1.282476	0.773139	0.011192	1.447608	0.258709	0.003735	1.443777	0.343284	240.63	4.53	1.881274	0.735	0.697716	0.697716	0.915437	45.14	326.48	6.20
	12C148_BA_PL50_Zr2	0.259735	0.001550	0.596596	0.892386	0.012923	1.448101	0.156906	0.002291	1.459800	0.180378	52.82	0.79	1.504592	0.722	0.682437	0.682437	0.910816	42.72	73.28	1.11
	12C149_BA_PL50_Zr3	0.428315	0.002775	0.647990	1.211047	0.017629	1.455647	0.283798	0.004077	1.436620	0.240407	63.27	0.96	1.517483	0.778	0.745792	0.745792	0.92972	54.60	81.42	1.24
PL 52	12C150_BA_PL52_Zr1	0.268116	0.001895	0.706799	1.297531	0.019164	1.476939	0.522865	0.007471	1.428877	0.413400	35.67	0.54	1.515438	0.772	0.738559	0.738559	0.927595	52.95	46.38	0.71
	12C151_BA_PL52_Zr2	0.927432	0.004664	0.502874	2.486744	0.036004	1.447842	0.876125	0.012503	1.427048	0.361438	64.95	0.92	1.422673	0.821	0.79405	0.79405	0.943678	68.49	79.29	1.13
	12C152_BA_PL52_Zr3	0.080022	0.000239	0.298273	0.673074	0.009779	1.452813	0.585963	0.008331	1.421774	0.893113	18.62	0.23	1.247900	0.732	0.693968	0.693968	0.914307	44.52	25.67	0.32
PL 55	12C153_BA_PL55_Zr1	1.418269	0.003231	0.227802	3.000818	0.043861	1.461619	0.247026	0.003557	1.440001	0.084450	87.43	1.26	1.445513	0.747	0.710638	0.710638	0.919314	47.37	116.97	1.70
	12C154_BA_PL55_Zr2	1.714939	0.010752	0.626942	0.916526	0.013259	1.446691	0.365152	0.005191	1.421464	0.408722	316.29	4.71	1.488375	0.744	0.707712	0.707712	0.918438	46.85	423.47	6.38
	12C155_BA_PL55_Zr3	0.965598	0.006215	0.643638	1.080022	0.015637	1.447861	0.346547	0.004981	1.437347	0.329177	155.69	2.33	1.497387	0.721	0.681442	0.681442	0.910513	42.57	215.97	3.26
PL 59	12C156_BA_PL59_Zr1	0.165290	0.001032	0.624218	0.949510	0.013758	1.448943	0.196485	0.002807	1.428423	0.212290	31.42	0.47	1.505296	0.742	0.705778	0.705778	0.917859	46.51	42.40	0.64
	12C157_BA_PL59_Zr2	0.237621	0.000996	0.418957	1.662791	0.024413	1.468180	0.969649	0.013825	1.425727	0.598241	23.74	0.32	1.352138	0.767	0.733148	0.733148	0.926001	51.78	31.13	0.42
	12C158_BA_PL59_Zr3	0.179152	0.000816	0.455707	0.869178	0.012654	1.455876	0.154388	0.002239	1.450020	0.182223	37.44	0.55	1.458734	0.753	0.717326	0.717326	0.921309	48.61	49.81	0.73
PL 60	12C159_BA_PL60_Zr1	0.766325	0.003237	0.422374	1.674476	0.024384	1.456199	0.191592	0.002782	1.452211	0.117381	84.04	1.24	1.473615	0.767	0.732973	0.732973	0.925949	51.74	109.58	1.62
	12C160_BA_PL60_Zr2	0.435523	0.001534	0.352311	0.875515	0.012761	1.457561	0.082681	0.001205	1.457372	0.096882	91.73	1.34	1.463397	0.721	0.681702	0.681702	0.910592	42.61	127.10	1.87
	12C161_BA_PL60_Zr3	0.275752	0.000814	0.295350	0.684187	0.009872	1.442948	0.359754	0.005125	1.424605	0.539424	67.56	0.89	1.315243	0.693	0.650186	0.650186	0.900929	38.31	98.05	1.30
PL 62	12C162_BA_PL62_Zr1	1.922178	0.020892	1.086916	2.081873	0.030179	1.449617	0.523663	0.007474	1.427325	0.258046	163.22	2.87	1.758190	0.790	0.759606	0.759606	0.933753	58.01	206.38	3.65
	12C163_BA_PL62_Zr2	0.783976	0.008550	1.090601	0.918938	0.013562	1.475867	0.491970	0.007061	1.435185	0.549226	141.92	2.44	1.716210	0.745	0.708379	0.708379	0.918638	46.97	191.00	3.30
	12C164_BA_PL62_Zr3	0.447565	0.004864	1.086839	0.813559	0.011806	1.451206	0.140024	0.002062	1.472673	0.176569	99.55	1.76	1.769440	0.739	0.701536	0.701536	0.916586	45.78	134.73	2.39
PL 63	12C165_BA_PL63_Zr1	0.522415	0.005884	1.126302	1.153211	0.016712	1.449148	0.177068	0.002543	1.436204	0.157518	82.44	1.48	1.794831	0.730	0.691644	0.691644	0.913605	44.15	112.96	2.04
	12C166_BA_PL63_Zr2	0.027013	0.000349	1.293678	0.107359	0.001585	1.476440	0.041197	0.000600	1.455939	0.393666	43.59	0.81	1.869405	0.699	0.657421	0.657421	0.903163	39.23	62.61	1.18
	12C167_BA_PL63_Zr3	0.716836	0.007765	1.083263	1.494778	0.021773	1.456634	0.526965	0.007526	1.428245	0.361663	83.40	1.44	1.727359	0.767	0.733845	0.733845	0.926206	51.93	108.88	1.89
PL 65	12C168_BA_PL65_Zr1	1.385110	0.014716	1.062427	3.016227	0.043691	1.448539	1.654203	0.023542	1.423135	0.562631	76.56	1.28	1.668677	0.761	0.726794	0.726794	0.924122	50.46	100.97	1.69
	12C169_BA_PL65_Zr2	0.490740	0.005577	1.136513	1.887832	0.027556	1.459659	0.826189	0.011768	1.424335	0.448968	44.50	0.77	1.741178	0.786	0.755039	0.755039	0.932423	56.84	56.78	0.99
	12C170_BA_PL65_Zr3	0.368400	0.003995	1.084306	1.198264	0.017562	1.465641	0.677257	0.009726	1.436038	0.579829	51.17	0.86	1.688042	0.759	0.724097	0.724097	0.923322	49.92	67.76	1.15
PL 67	12C171_BA_PL67_Zr1	2.009936	0.025204	1.253982	1.662460	0.024549	1.476691	1.018458	0.014511	1.424778	0.628479	197.03	3.59	1.821191	0.831	0.805736	0.805736	0.947003	72.89	237.39	4.34
	12C172_BA_PL67_Zr2	1.543420	0.019338	1.252959	1.483334	0.021736	1.465346	0.395449	0.005632	1.424122	0.273495	183.03	3.44	1.878640	0.745	0.708073	0.708073	0.918546	46.91	245.47	4.64
	12C173_BA_PL67_Zr3	0.837114	0.010680	1.275761	0.782401	0.011319	1.446745	0.202896	0.002915	1.436610	0.266038	188.43	3.55	1.884059	0.734	0.69578	0.69578	0.914853	44.82	256.41	4.87
PL 70	12C174_BA_PL70_Zr1	0.337395	0.002299	0.681386	1.191983	0.017233	1.445743	0.702910	0.010126	1.440558	0.604963	46.88	0.67	1.439761	0.714	0.673521	0.673521	0.908101	41.42	66.10	0.96
	12C175_BA_PL70_Zr2	0.647746	0.010660	1.645643	2.544518	0.037031	1.455320	1.183851	0.016894	1.426995	0.477299	43.32	0.91	2.104397	0.766	0.732728	0.732728	0.925876	51.69	56.74	1.20
	12C176_BA_PL70_Zr3	0.122764	0.002055	1.673957	0.694681	0.010110	1.455322	0.467254	0.006690	1.431773	0.690029	28.80	0.60	2.094940	0.726	0.687449	0.687449	0.912336	43.49	39.95	0.84

Table 4.5 – ZHe analytical data. A) measured data; B) calculated dat

B)

sample	replicate	corr date (Ma)	1s ± date (Ma)	1s ± date %	eU (ppm)	U (ppm)	dU (ppm)	Th (ppm)	dTh (ppm)	4He/g (nmol)	d 4He/g (nmol)	morph comments		
	12C147_BA_PL50_Zr1	**326.48**	**6.20**	1.90	227.61	211.02	3.05	70.61	1.02	294.45	3.78	inclusions	**160.39**	**143.89**
PL 50	12C148_BA_PL50_Zr2	**73.28**	**1.11**	1.51	414.46	398.01	5.76	69.98	1.02	115.84	0.69	inclusions		
	12C149_BA_PL50_Zr3	**81.42**	**1.24**	1.52	277.22	262.75	3.82	61.57	0.88	92.93	0.60	inclusions, slightly rounded		
	12C150_BA_PL52_Zr1	**46.38**	**0.71**	1.52	279.57	255.39	3.77	102.91	1.47	52.77	0.37	inclusions	**50.45**	**27.04**
PL 52	12C151_BA_PL52_Zr2	**79.29**	**1.13**	1.43	233.56	215.70	3.12	76.00	1.08	80.45	0.40	inclusions		
	12C152_BA_PL52_Zr3	**25.67**	**0.32**	1.26	291.38	241.90	3.51	210.59	2.99	28.76	0.09	inclusions		
	12C153_BA_PL55_Zr1	**116.97**	**1.70**	1.45	761.77	747.31	10.92	61.52	0.89	353.20	0.80	inclusions	**252.14**	**156.42**
PL 55	12C154_BA_PL55_Zr2	**423.47**	**6.38**	1.51	309.45	282.96	4.09	112.73	1.60	529.46	3.32	inclusions		
	12C155_BA_PL55_Zr3	**215.97**	**3.26**	1.51	417.59	388.31	5.62	124.60	1.79	347.17	2.23	many inclusions		
	12C156_BA_PL59_Zr1	**42.40**	**0.64**	1.51	273.50	260.82	3.78	53.97	0.77	45.40	0.28	slightly abraded, inclusions	**41.11**	**9.41**
PL 59	12C157_BA_PL59_Zr2	**31.13**	**0.42**	1.36	465.66	409.53	6.01	238.82	3.40	58.52	0.25	slightly abraded, inclusions		
	12C158_BA_PL59_Zr3	**49.81**	**0.73**	1.46	220.97	212.11	3.09	37.68	0.55	43.72	0.20	slightly abraded, inclusions		
	12C159_BA_PL60_Zr1	**109.58**	**1.62**	1.48	307.75	299.70	4.36	34.29	0.50	137.16	0.58	inclusions	**111.58**	**14.62**
PL 60	12C160_BA_PL60_Zr2	**127.10**	**1.87**	1.47	404.30	395.52	5.76	37.35	0.54	196.75	0.69	inclusions		
	12C161_BA_PL60_Zr3	**98.05**	**1.30**	1.33	448.05	398.77	5.75	209.68	2.99	160.72	0.47	many big inclusions		
	12C162_BA_PL62_Zr1	**206.38**	**3.65**	1.77	345.82	326.52	4.73	82.13	1.17	301.47	3.28	slightly abraded, coated, inclusio	**177.37**	**37.72**
PL 62	12C163_BA_PL62_Zr2	**191.00**	**3.30**	1.73	307.04	272.73	4.03	146.01	2.10	232.68	2.54	inclusions. Very slightly rounded		
	12C164_BA_PL62_Zr3	**134.73**	**2.39**	1.78	277.93	267.13	3.88	45.98	0.68	146.96	1.60	inclusions		
	12C165_BA_PL63_Zr1	**112.96**	**2.04**	1.80	426.38	411.53	5.96	63.19	0.91	186.43	2.10	slightly abraded, slightly coated,	**94.81**	**27.97**
PL 63	12C166_BA_PL63_Zr2	**62.61**	**1.18**	1.88	65.24	59.84	0.88	22.96	0.33	15.06	0.19	inclusions, slightly rounded		
	12C167_BA_PL63_Zr3	**108.88**	**1.89**	1.73	402.31	371.53	5.41	130.98	1.87	178.17	1.93	very abraded, inclusions		
	12C168_BA_PL65_Zr1	**100.97**	**1.69**	1.68	722.95	640.41	9.28	351.22	5.00	294.09	3.12	slightly abraded, many inclusions	**75.17**	**23.01**
PL 65	12C169_BA_PL65_Zr2	**56.78**	**0.99**	1.75	388.35	352.14	5.14	154.11	2.20	91.54	1.04	slightly abraded, inclusions		
	12C170_BA_PL65_Zr3	**67.76**	**1.15**	1.70	322.52	284.71	4.17	160.92	2.31	87.53	0.95	abraded, coated, inclusions		
	12C171_BA_PL67_Zr1	**237.39**	**4.34**	1.83	157.06	137.29	2.03	84.11	1.20	165.99	2.08	slightly abraded, inclusions, sligh	**246.42**	**9.55**
PL 67	12C172_BA_PL67_Zr2	**245.47**	**4.64**	1.89	385.22	362.51	5.31	96.64	1.38	377.20	4.73	inclusions		
	12C173_BA_PL67_Zr3	**256.41**	**4.87**	1.90	292.38	275.58	3.99	71.47	1.03	294.86	3.76	abraded, inclusions, slightly rounded		
	12C174_BA_PL70_Zr1	**66.10**	**0.96**	1.45	449.47	394.76	5.71	232.79	3.35	111.74	0.76	inclusions	**54.26**	**13.25**
PL 70	12C175_BA_PL70_Zr2	**56.74**	**1.20**	2.11	614.67	554.09	8.06	257.79	3.68	141.05	2.32	slightly abraded, inclusions		
	12C176_BA_PL70_Zr3	**39.95**	**0.84**	2.10	308.50	266.40	3.88	179.18	2.57	47.08	0.79	little abraded, coated, inclusions		

4.3.8. Analysis of AHe data

The correlation between single grain corrected ages and measured parameters (grain radius, [U], [Th], [Sm], Th/U) was tested in order to better understand the origin of grain dispersion.

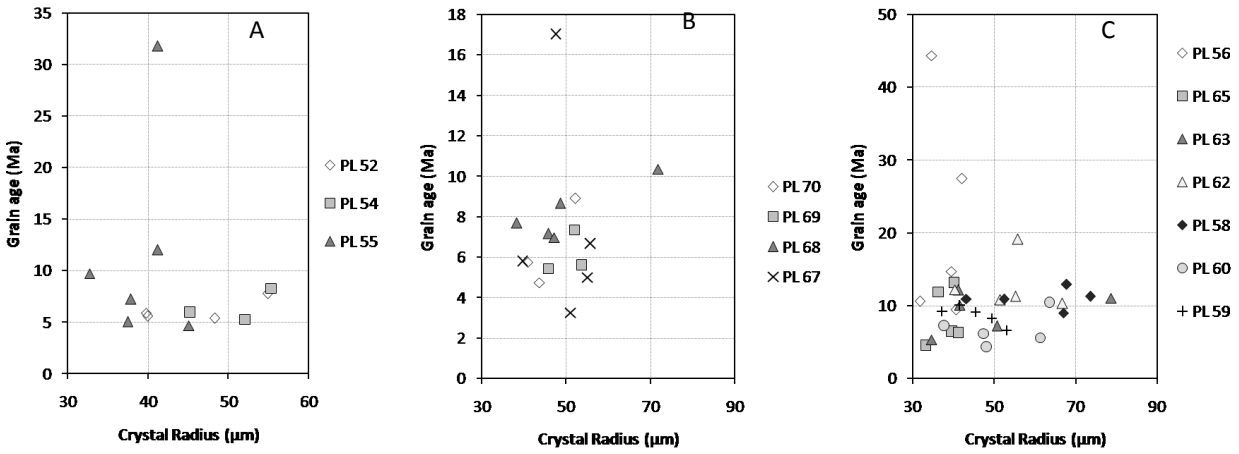

Figure 4.14 – Grain ages plotted against crystal radius. Plots are grouped by transect (A, B, C, Fig. 4.3)

Figure 4.16 – Single grain ages plotted against grain radius, eU, Th/U, [U], [Th],[Sm].

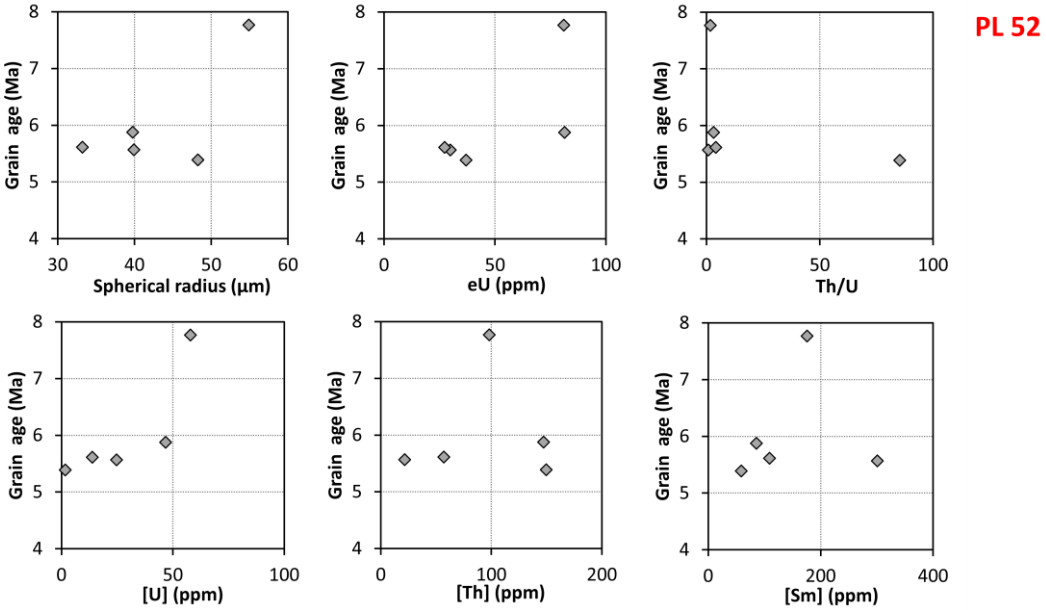

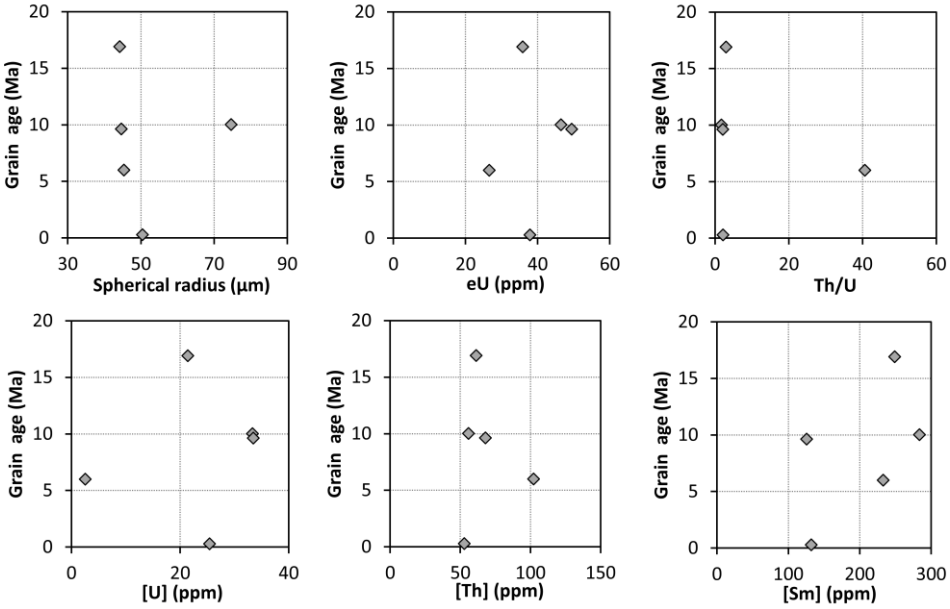
Grain age (Ma)
Spherical radius (µm)
eU (ppm)
Th/U
[U] (ppm)
[Th] (ppm)
[Sm] (ppm)

PL 53

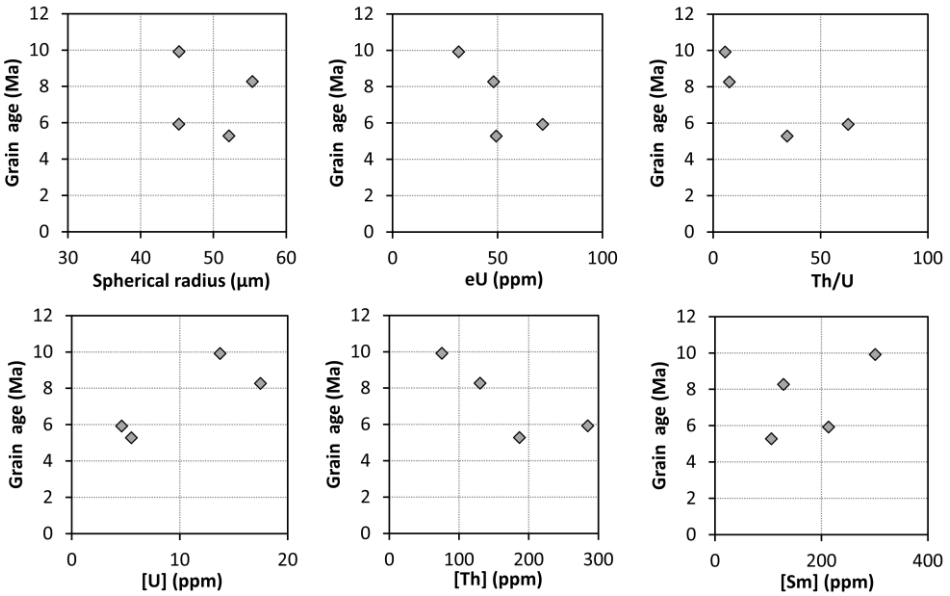
Grain age (Ma)
Spherical radius (µm)
eU (ppm)
Th/U
[U] (ppm)
[Th] (ppm)
[Sm] (ppm)

PL 54

PL 55

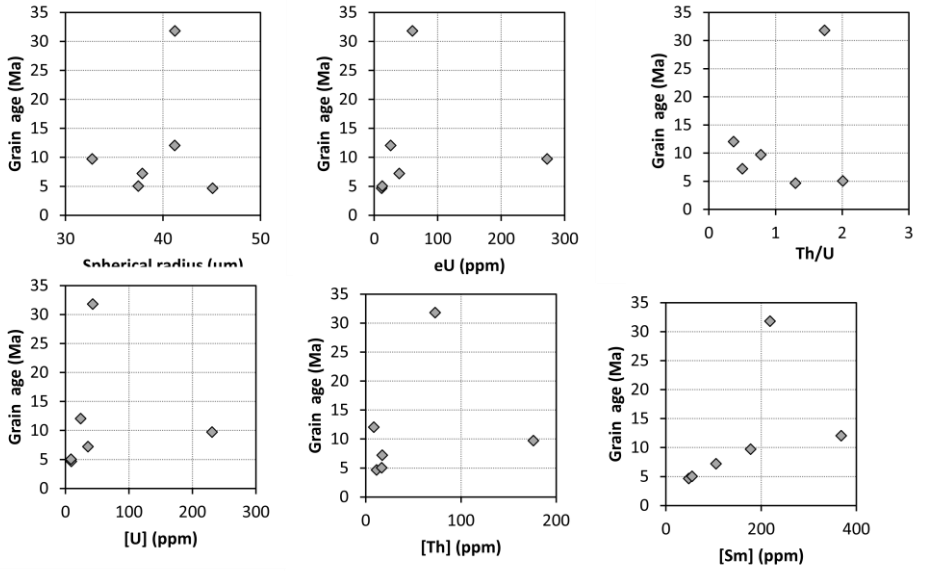
Grain age (Ma)
Spherical radius (µm)
eU (ppm)
Th/U
[U] (ppm)
[Th] (ppm)
[Sm] (ppm)

PL 56

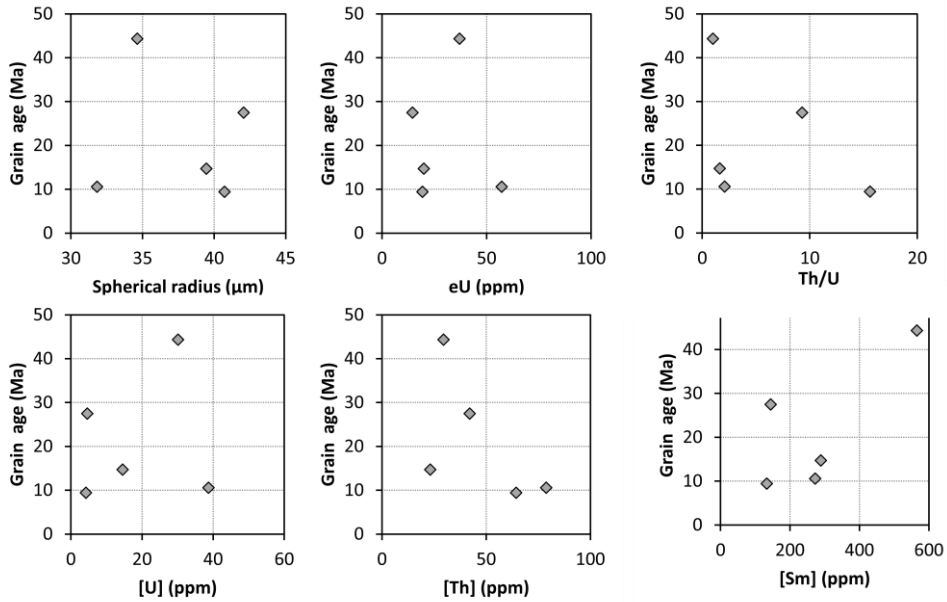
Grain age (Ma)
Spherical radius (µm)
eU (ppm)
Th/U
[U] (ppm)
[Th] (ppm)
[Sm] (ppm)

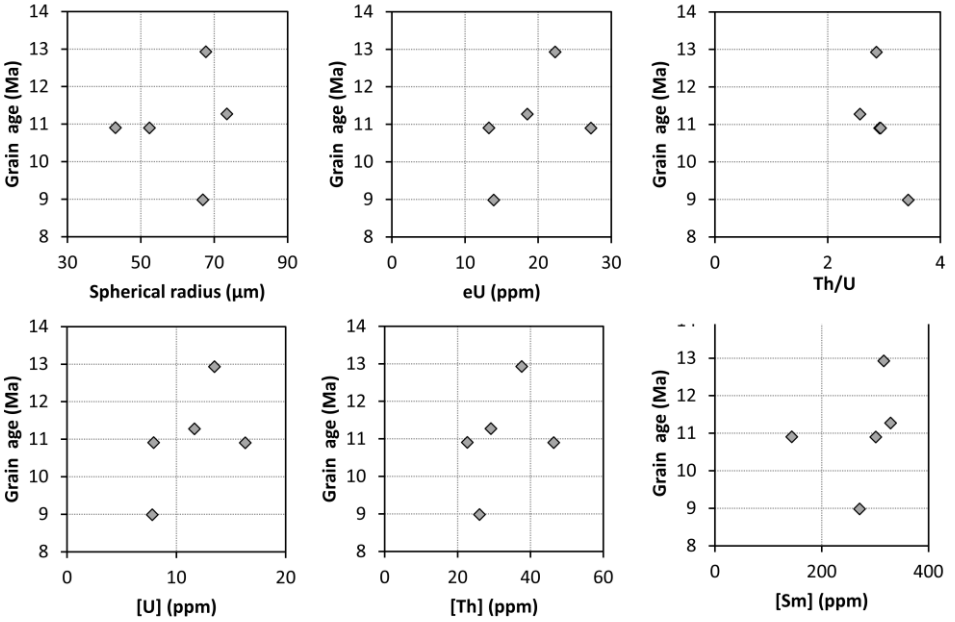
Grain age (Ma)
Spherical radius (µm)
eU (ppm)
Th/U
[U] (ppm)
[Th] (ppm)
[Sm] (ppm)

PL 58

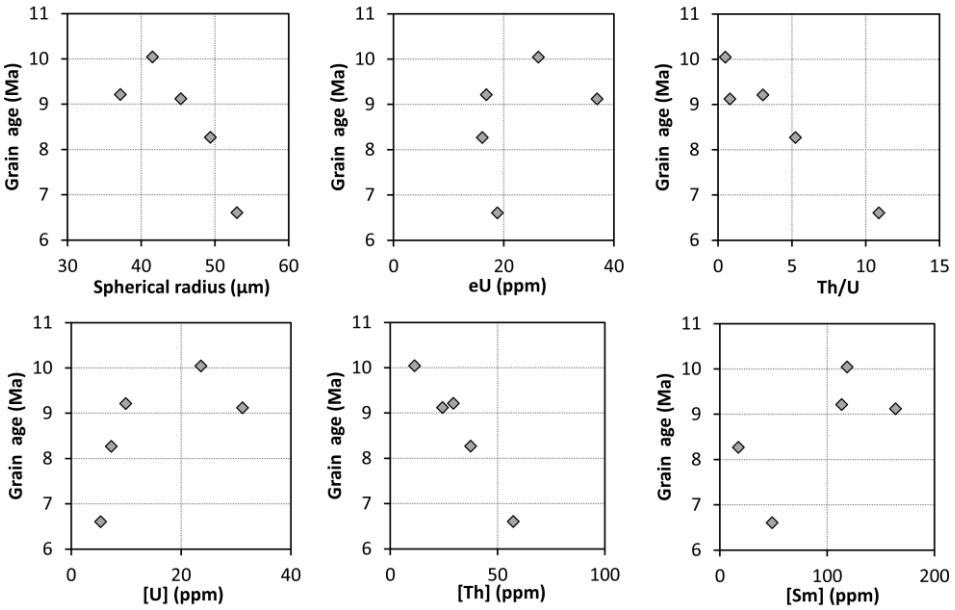
Grain age (Ma)
Spherical radius (µm)
eU (ppm)
Th/U
[U] (ppm)
[Th] (ppm)
[Sm] (ppm)

PL 59

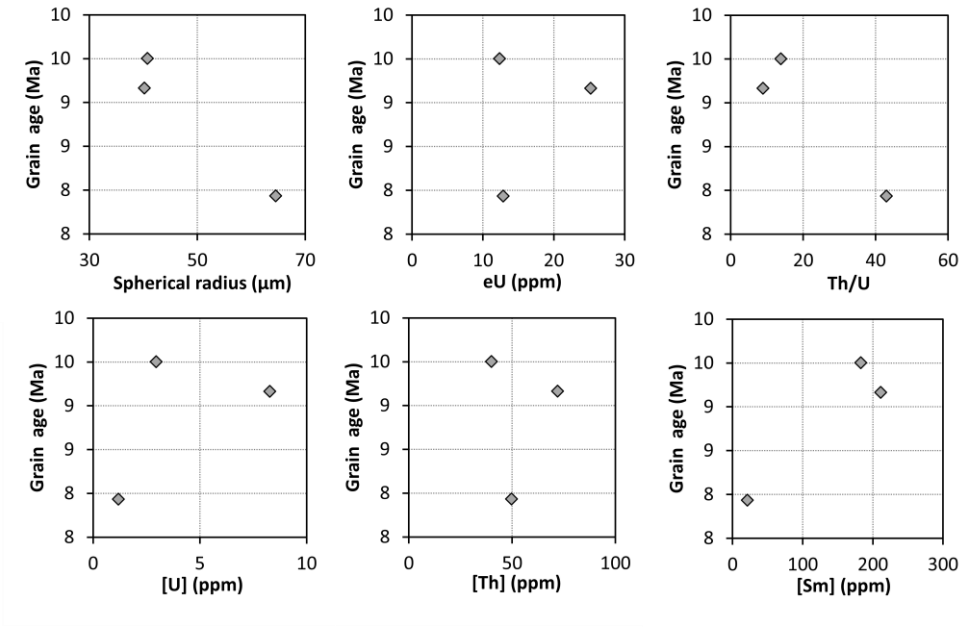
Grain age (Ma)
Spherical radius (µm)
eU (ppm)
Th/U
[U] (ppm)
[Th] (ppm)
[Sm] (ppm)

PL 61

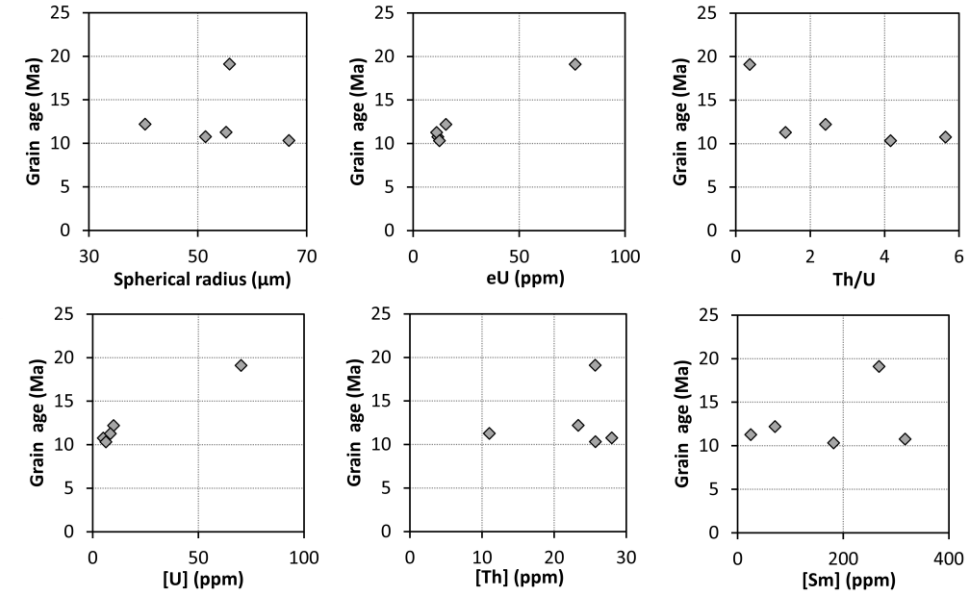
Grain age (Ma)
Spherical radius (µm)
eU (ppm)
Th/U
[U] (ppm)
[Th] (ppm)
[Sm] (ppm)

PL 62

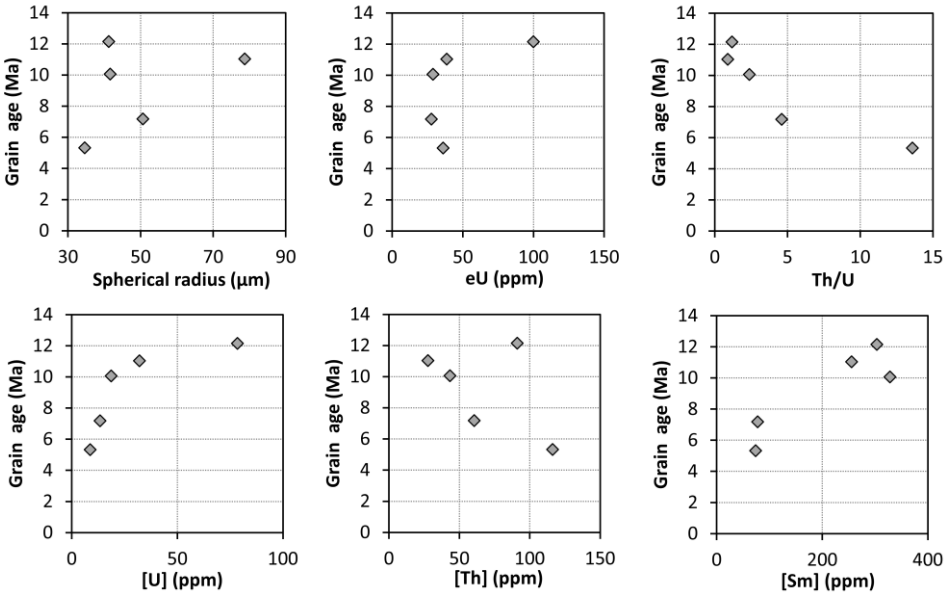
Grain age (Ma)
Spherical radius (µm)
eU (ppm)
Th/U
[U] (ppm)
[Th] (ppm)
[Sm] (ppm)

PL 63

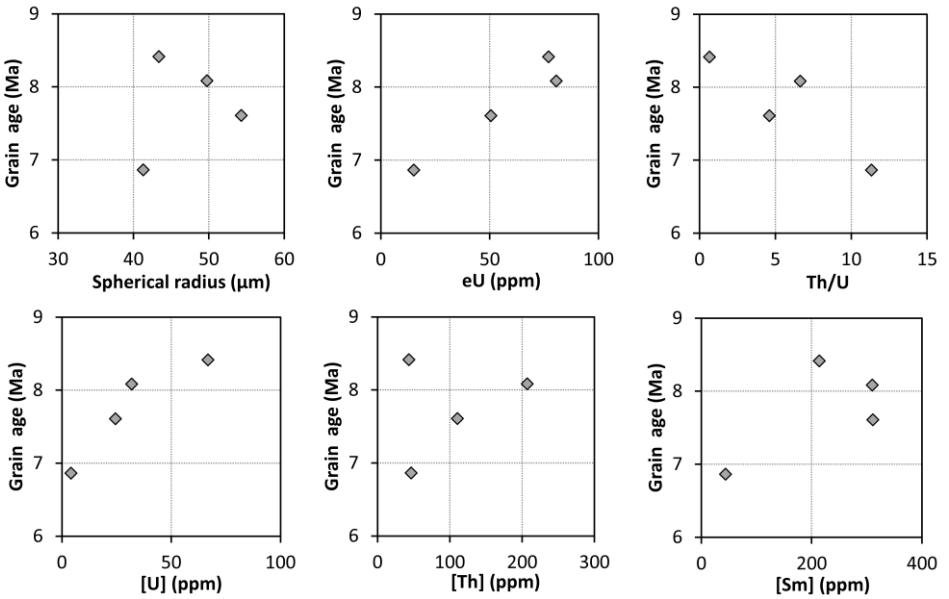
Grain age (Ma)
Spherical radius (µm)
eU (ppm)
Th/U
[U] (ppm)
[Th] (ppm)
[Sm] (ppm)

PL 64

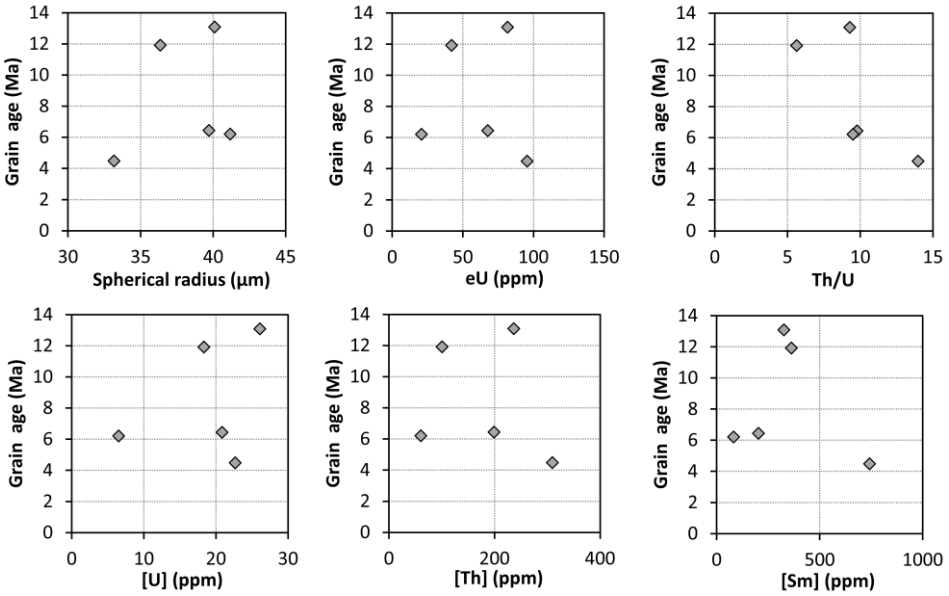
Grain age (Ma)
Spherical radius (µm)
eU (ppm)
Th/U
[U] (ppm)
[Th] (ppm)
[Sm] (ppm)

PL 65

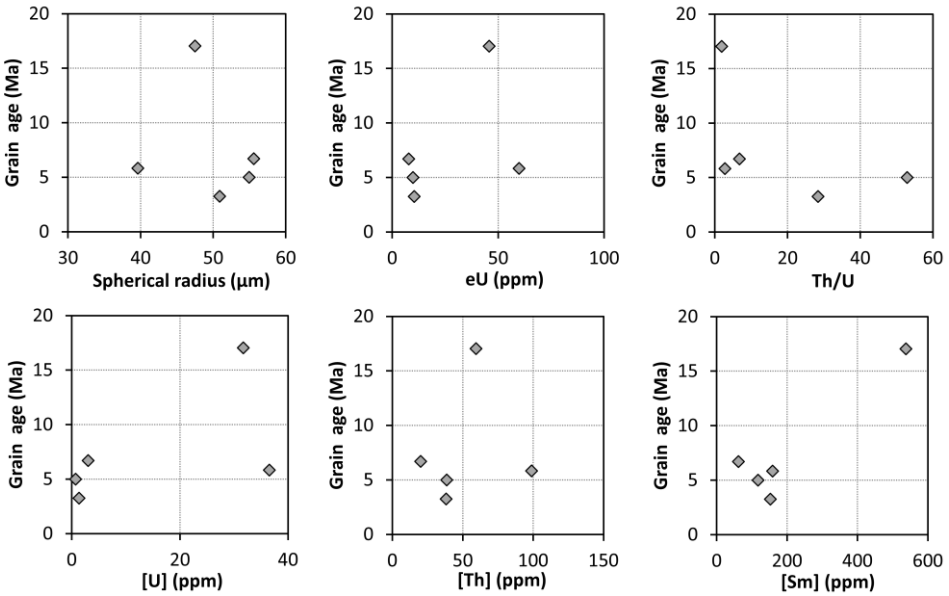
Grain age (Ma)
Spherical radius (µm)
eU (ppm)
Th/U
[U] (ppm)
[Th] (ppm)
[Sm] (ppm)

PL 67

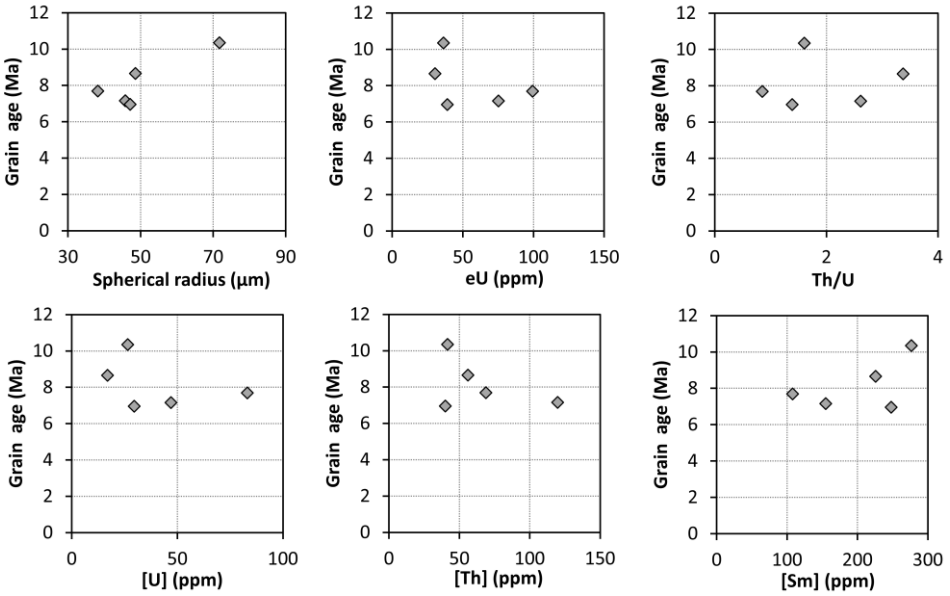
Grain age (Ma)
Spherical radius (µm)
eU (ppm)
Th/U
[U] (ppm)
[Th] (ppm)
[Sm] (ppm)

PL 68

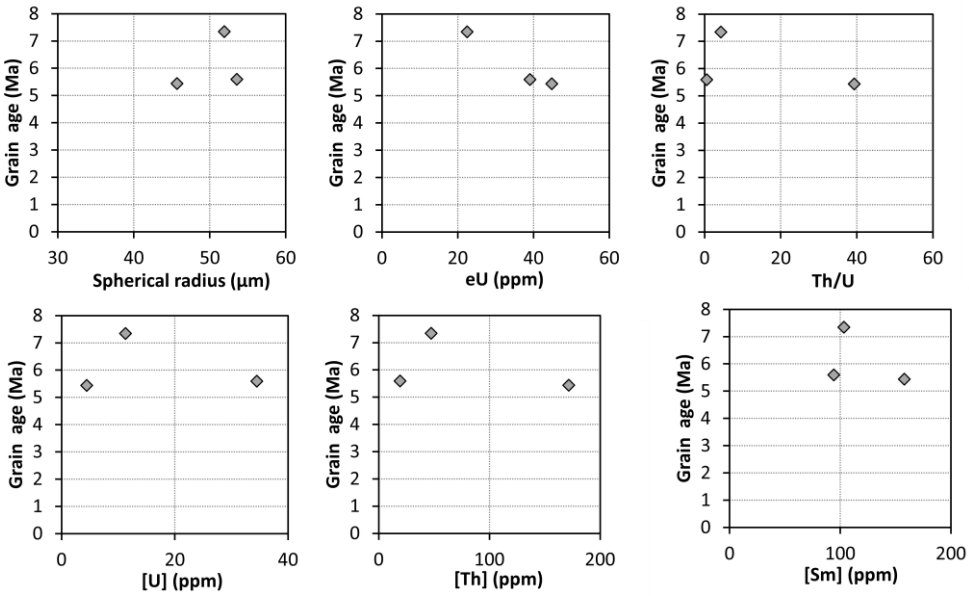
Grain age (Ma)
Spherical radius (µm)
eU (ppm)
Th/U
[U] (ppm)
[Th] (ppm)
[Sm] (ppm)

PL 69

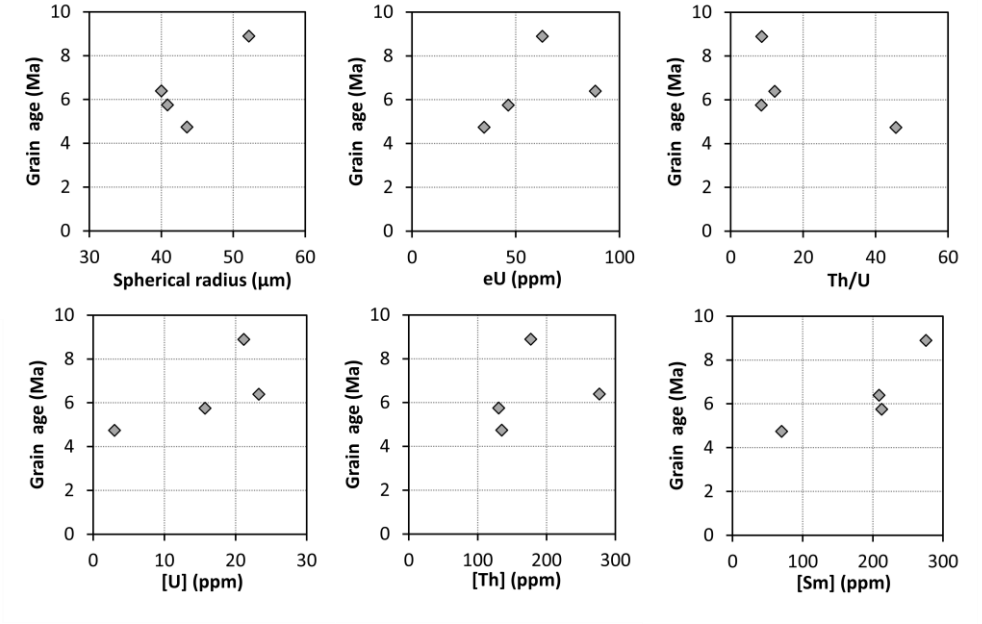

PL 70

CHAPTER V.

Geodynamics of the Carpathian-Pannonian region:

Insights from low temperature thermochronology

5.1. Overview

The geodynamic evolution of the Carpathian-Pannonian region has been in recent times the object of an heated scientific debate. Thermochronometry gives important constrains to the depths of burial and to timing and rates of exhumation. Each geodynamic scenario proposed for the Carpathian-Pannonian region would imply a different spatial distribution of burial and a different timing of exhumation. In this chapter we use a compilation of several low-temperature thermochronometric datasets, referred to the Polish and Ukrainian Carpathians, to evaluate their compatibility with the different geodynamic models proposed so far. A subdivision of the Polish and Ukrainian Carpathians in three different areas is proposed, based on geophysical and structural parameters. Each single area is characterized also by different burial-exhumation history and requires a specific explanation in terms of driving processes. The non homogeneous burial depths of the western and central sector of the study region are interpreted as an indication of the lack of slab subduction and subsequent break-off. The hypothesis that Miocene extension of the Carpathian-Pannonian region was triggered by gravitational instability and subsequent downwelling of the lithosphere appears better supported by the dataset presented in this work.

5.2. Features of the Carpathian-Pannonian region

The Carpathian-Pannonian region formed between the Late Jurassic and the Neogene by collision between the Adriatic Plate and the European Platform, and assumed its present day configuration mainly during the Miocene, when the extensional Pannonian Basin (PB) formed in retro-wedge position (Csontos et al., 1992), with estimated extension of ca. 180 to 290 Km (Ustaszewski et al., 2008).

At present the region appears as a wide depression (i.e. the PB) enclosed by the Carpathian mountain belt (Fig. 5.1) . Several extension-related volcanic complexes, which ages are younging SE-ward, are located along the borders of the basin (Fig. 5.2, e.g. Seghedi et al., 2004). The Carpathians are commonly subdivided in Inner Carpathians (IC), which constitute the proper collisional orogen, and Outer Carpathians (OC) that formed in the Tertiary as an accretionary wedge (Fig. 5.2; e.g. Tasarova et al., 2009 and reference therein).

As can be observed in Fig.5.3 and Fig. 4.1, the PB is characterized by high heat flow and by thinned crust and lithosphere (e.g. Lenkey et al., 1999; Bielik et al., 2004), as opposed to the surrounding Carpathian belt that has a more complex thermal structure, but with a generally lower heat flow and higher crustal ad lithospheric thickness. The highest lithosphere thickness is reached in an area that stretches along the Carpathian front at the boundary between Ukraine

and Romania (Fig.4.1 Dererova et al., 2006, Lenkey, 1999; Zeyen et al., 2002; Babuška et al., 1988; Horváth et al., 1993).

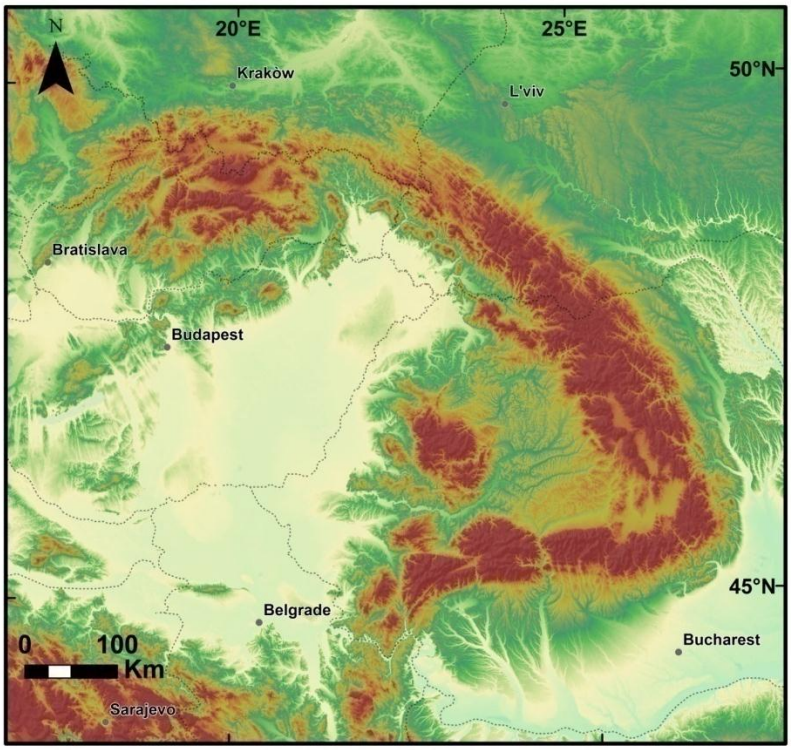

Figure 5.1 – DEM of the Carpathian-Pannonian region

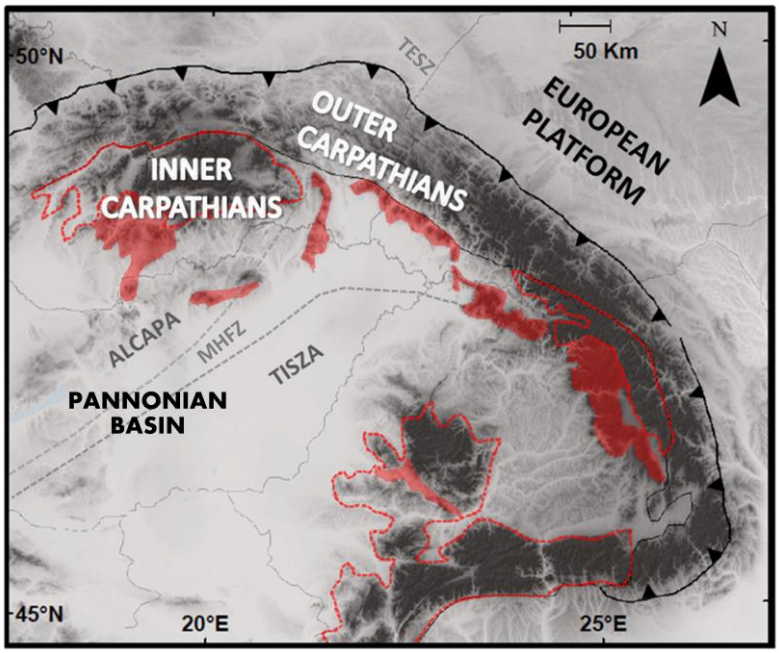

Figure 5.2- Tectonic sketch of the Carpathian-Pannonian region. Red dashed line bounds the Inner Carpathian outcrops; red fields indicate the Neogene volcanic complexes.

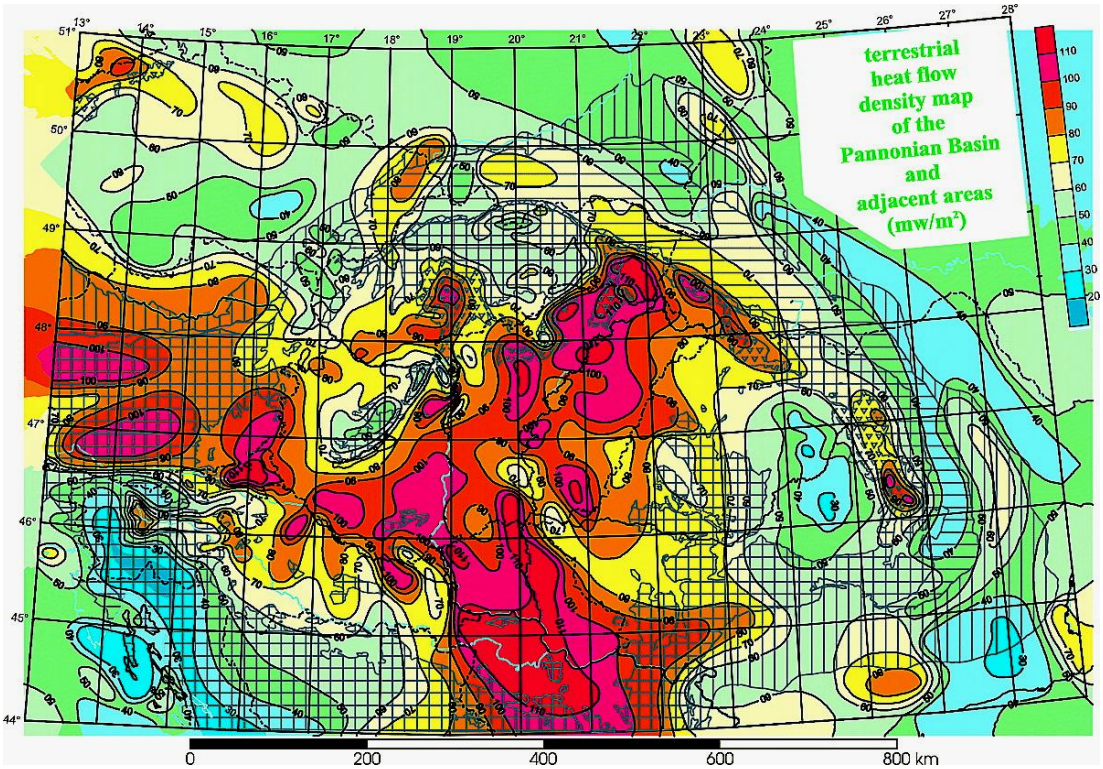

Figure 5.3 – Heat flow map of the Carpathian-Pannonian region (From Pospisil et al., 2006).

5.3. Alpine Evolution

The main evolutional stages of this region can be summarized as: (i) collision between the Alcapa and Tisza-Dacia microplates and the European platform, occurred between the late Cretaceous and the Early Miocene (ii) extension in the PB (Syn-rift stage), associated to volcanism along its margins and ongoing compression in the OC, between ca. 19 and 11.5 Ma (iii) minor extension and major subsidence in the Pannonian Basin, compression in the southern Carpathians at 11.5-0 Ma. During the Neogene a progressive shift of the tectonic activity from N to S along the present day strike of the Carpathians occurred, as testified by the ages of volcanic rocks along the PB margin (e.g. Harangi et al., 2002) and by E to S-directed migration of depocenters (Meulenkamp et al., 1996) and thrusting activity (Nemcok et al., 2006). We also stress that the Ukrainian and Romanian Carpathians, during their late stage evolution, collided with the Trans-European Suture Zone (TESZ), that is the boundary between the thick and rigid East-European craton and the thinner West-European Platform (Fig.5. 2, e.g. Pharaoh, 1999; Cloething et al., 2010).

This study focuses on the portion of the Carpathian-Pannonian Region originated by collision between the Alcapa microplate and the European Platform (Fig 5.2). Collision occurred in this area starting by the Late Cretaceous, whereas in the Early Miocene extension and counter clockwise rotation are envisaged as the main responsible for N to NE-ward extrusion toward the European foreland and concurrent separation from the Eastern Alps (e.g. Fodor, 2006) . The

juxtaposition to the Tisza-Dacia microplate, along the Mid-Hungarian Fault Zone (MHFZ, Fig.5.2), occurred between the Early and Middle Miocene, and, from that time on, the two microplates behaved like a unique crustal block (Fodor, 2006).

5.4. Synthesis of the principal geodynamic models for the Carpathian-Pannonian region

The most common and widely accepted interpretation for the formation of this region is based on a classical back-arc extension model and subsequent astenospheric upwelling (e.g. Horváth 1993; Huismans et al., 2001; Horváth et al., 2006). The presence of an high P-wave velocity anomaly in the mantle transition zone beneath the whole PB (Wortel and Spakman, 2000; Piromallo and Morelli, 2003) , the thickened lithosphere beneath the Eastern Carpathians (Bielik et al., 2004), the presence of an sub-vertical high velocity body at depths 60-400 Km beneath the Southern Carpathians (Fig. 5.4.A, McKenzie, 1970; Fuchs et al., 1979; Wortel and Spakman, 2000; Sperner et al., 2001, Nemcok et al, 1998) and the time and space progression of volcanism (Seghedi et al, 2004) have been envisaged as proofs for subduction and E to S-ward progressive slab break-off occurred along the Carpathians. Nonetheless several authors proposed other possible explanations for such features. Knapp et al. (2005) and Fillerup et al. (2010) suggest that the high velocity anomaly beneath the Vrancea region can be explained also as the consequence of lithospheric delamination, the presence of an oceanic slab being not independently demonstrated (Fig. 5.4.B).

Kovács and Szabó (2008) pointed out that in fact oceanic subduction is not essential to explain the Neogene evolution of volcanism along the Western Carpathians, that was rather related to lithospheric extension. They also suggested that extension was triggered by mantle flow, associated with the eastward extrusion of the Carpathians (Kovács et al., 2012). Based on numerical simulations and tomographic data, Gemmer and Houseman (2007), Houseman and Gemmer (2007), Lorinczi and Houseman (2009) and Ren et al. (2012) express in favour of gravitational instability of the lithosphere as the trigger for extension and astenosphere upwelling in the PB and coeval compression in the Carpathians (Fig. 5.4.C. Such scenario does not exclude the possible occurrence of subduction along part of the Carpathian margin.

In this chapter a compilation of thermochronometrical studies referred to the Alcapa-derived portion of the Carpathians is presented, with the aim to extrapolate constraints on the geodynamic processes that governed the evolution of the Carpathian-Pannonian region. In order to achieve this goal we examine the spatial distribution of burial depths and of ages and rates of exhumation and we put them in relation with the spatial trend of relief, heat flow (Pspisil et al., 2006; Pollack et al., 1993), crustal and lithospheric thickness (e.g. Dererova et al., 2006) and with structural settings. From the combined observations on burial-exhumation histories, physical and structural settings we obtain constraints that allow to rule out or accept the geodynamic processes proposed for the evolution of the Carpathian-Pannonian region.

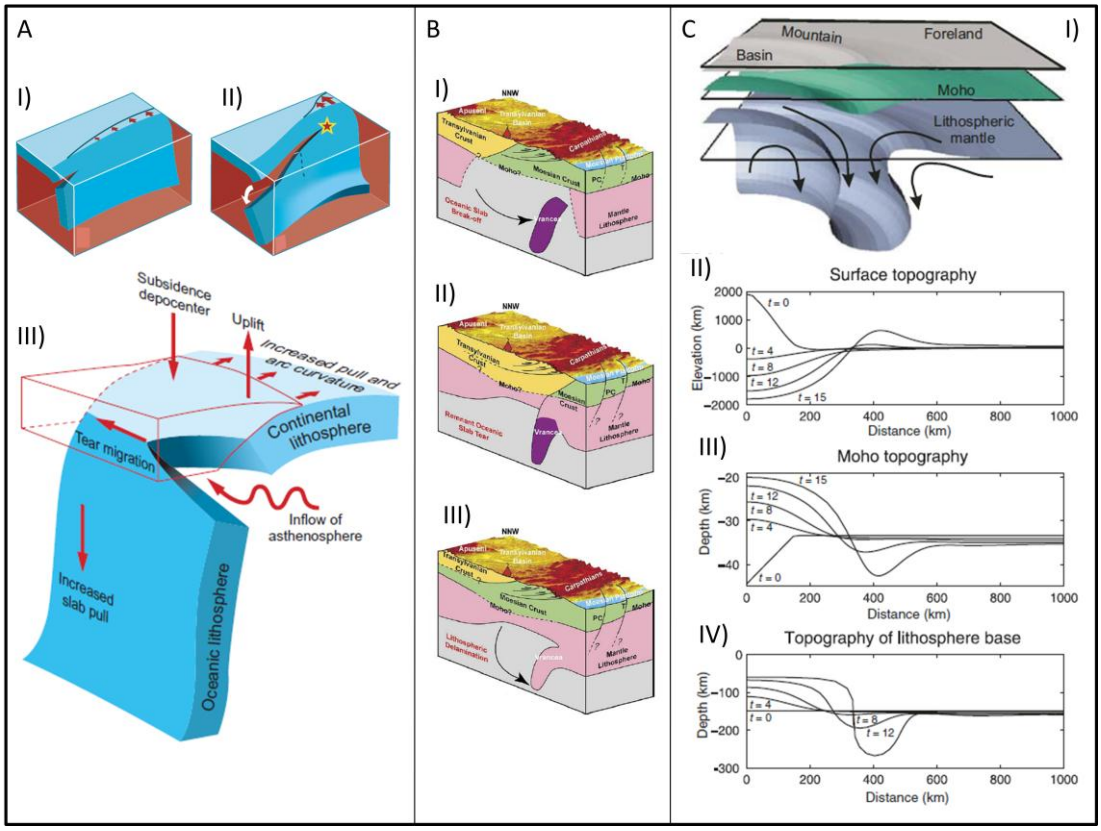

Figure 5.4 - Schematic representations of the main processes proposed to play a role in the Neogene evolution of the Carpathian-Pannonian region. A- Slab roll back and break-off (by Wortel and Spakman, 2000); B- Lithosphere delamination (III) is proposed as an alternative to the classical theories involving an oceanic slab (I, II) and suggested to be active at present day beneath the Vrancea region. C- Gravitational collapse of the lithosphere, proposed by Houseman and Gemmer, 2007: I) schematic representation of the process (surface, base of crust, base of mantle lithosphere; II) modeled variation in time of the surface topography; moho topography (III) and lithosphere base topography (IV).

5.5. Morphostructural subdivision of the Alcapa-Derived portion of the Carpathians

Based on structural setting (Fig. 5.2), topography (Fig. 5.1), heat flow (Fig. 5.3) and crustal and lithospheric thickness (Fig. 4.1) a subdivision of the study region (Fig. 5.5), already introduced in Chapter 1, is proposed. This subdivision is interpreted to reflect different scenarios of burial and exhumation.

In the **westernmost sector** of the study area (between 19° and ca. 21 ° E) the occurrence of normal faults reactivating and cutting thrusts (Jankowski et al., 2004; Mazzoli et al., 2010) and intramontane basins (e.g Orava basin) give to the Carpathians a complex structure and a topography characterized by heights and lows. The average relief of the Carpathians progressively increases southward and reaches its maximum in correspondence to the IC. In this sector the typical features of the PB, i.e. low relief, high heat flow, lithospheric and crustal thinning can be observed from the Neogene volcanics to the South.

Also in the **central sector** of the study area (between ca. 21° and 22.5° E), as described by Mazzoli et al. (2010), the Carpathians are characterized by the occurrence of normal faults, mainly NE-SW directed, dissecting or reactivating thrusts. The OC belt and its present day foredeep reach in this area their maximum width (Fig. 5.2), whereas, the relief is the lowermost of the whole mountain belt (Fig. 5.1). The lithosphere is thicker here than in the western sector, and thickness increases toward the SE (Fig. .4.1), whereas the crust appears relatively thin (30-35 Km). The heat flow increase occurs in correspondence to the first PB sediments south to the OC, where the relief also progressively decreases to the PB average values (Fig 5.1 and Fig. 5.3). The features of this region suggest that this area was either characterized by a lesser efficient shortening or affected by an high post-thrusting stretching.

The **easternmost sector** of the study area (comprised between ca. 22.5° and 25° E) is characterized by the progressive SE-ward transition from a very low to an higher and higher relief (Fig.5.1) and by a progressive narrowing of the OC band (Fig.5.2). The relief in this region reaches its maximum in the central portion of the OC, as opposed to the Western sector, where the maximum relief is reached in the IC. It can also be observed that a forearc basin likely to the Central Carpathian Basin is located in the southernmost portion of the study area.
Both lithosphere and crust are highly thickened in the Carpathians and thinned in the PB, and the transition between the two thickness ranges occur in a narrow band corresponding to the innermost Carpathian units (Fig. 4.1).Heat flow follows the same trend of crustal and lithospheric thickness, passing from high values in the Pannonian Basin, to low values in the outermost OC units, the passage between the two heat flow ranges occurring relatively sharply in correspondence of the innermost Carpathian units (Fig. 5.3).

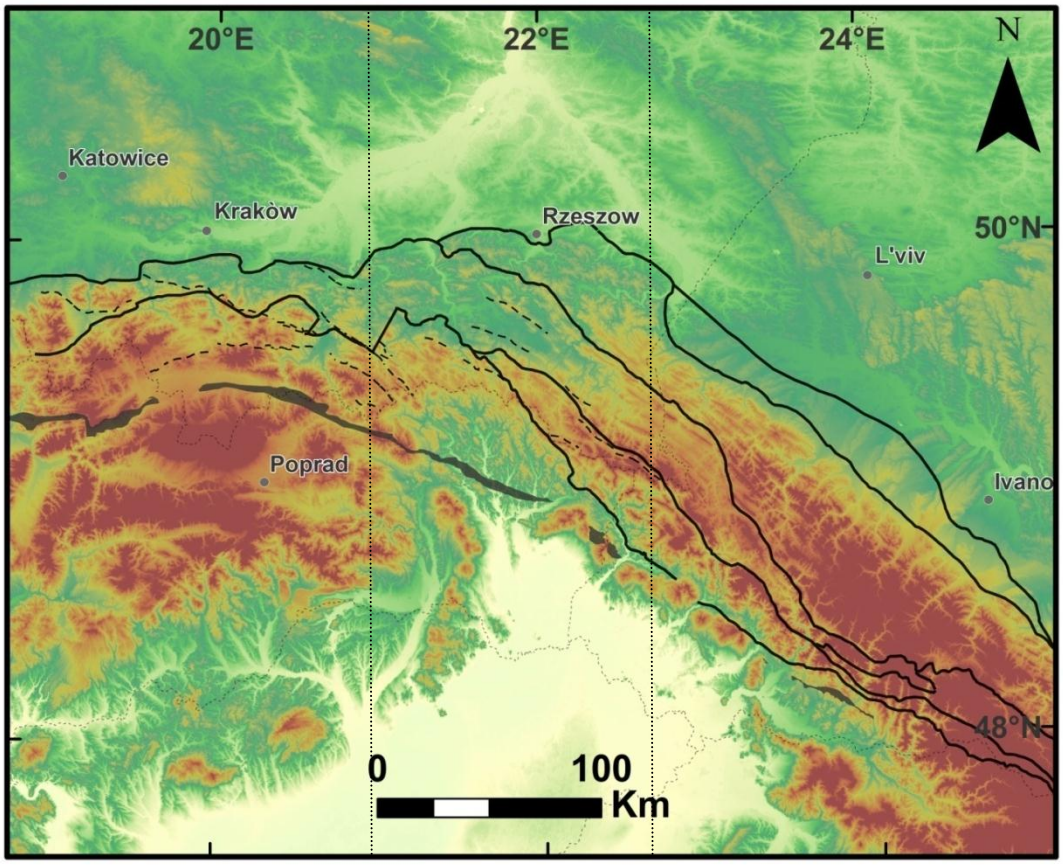

Figure 5.5 – Subdivision of the study region in three sectors

5.6. Thermochronology

The datasets comprised in this review are presented in Zattin et al. (2011), Syrek et al. (2009), Swiercszewska (2005), Danisik et al (years) and in the present work (Chapter 3 and Chapter 4).

The compilation of datasets comprises apatite fission track (AFT), apatite and zircon helium (AHe and ZHe) and vitrinite data. The fission track and helium systems are low-temperature thermochronometers, that, at a first approximation, indicate cooling ages through their closure temperatures (AFT Tc~120°C; AHe Tc~60°C; ZHe Tc~165°C; Reiners and Brandon, 2006). Furthermore, application of thermochronometry to sedimentary rocks (e.g. the rocks of the OC accretionary prism) or to rocks that underwent a second burial stage, allows to reconstruct their burial depths prior to exhumation, based on the reset degree reached by the thermochronometric systems. Vitrinite reflectance analysis is a paleo-thermal methodology that provide the maximum paleo-temperature underwent by the analyzed sample. For thorough descriptions of the thermochronometric and paleo-temperature analytical methods and for details on the data used in this work we address the reader to the papers listed above, in which the data are presented and discussed and to references quoted therein (e.g. Elhers and Farley. 2003; Donelik et al., 2005; Reiners and Brandon, 2006)

In Fig. 5.6 and 5.7 the heating and burial conditions reached by the OC during thrusting are reported. It can be observed a general increase of burial toward the Easternmost sector and a general decrease of burial toward the foredeep, along all the study area. Observing to an higher

detail the single region a major difference appears to distinguish the western and central from the eastern sector. In the first two sectors burial is laterally very inhomogeneous, even at a local scale, except in the outermost portions, characterized by a uniform very low burial. This suggests that the extent of burial and exhumation was mainly related to the single structures and geometries of the wedge. On the other hand, in the eastern sector the burial degree appears laterally uniform, and characterized by a progressive decrease toward both the innermost and the outermost units. This indicates in turn that burial and exhumation extent, in this portion of the Carpathians were related to the opening of the PB and to the small scale processes acting in the whole Carpathian-Pannonian region.

In Fig. 5.8 the ages of exhumation are indicated and ages of the last trusting stage along the OC are also reported. Exhumation occurred within ca. 23 and 5 Ma. In the western sector exhumation ages of the OC span the wide range of ca. 23-12 Ma and their distribution is highly variable, even at local scale, and appears related to the single structures of the wedge. We also point out that in this sector of the OC exhumation mainly occurred while thrusting was still active, even though younger exhumation also occurred. In the IC exhumation ages are in the range of 26-10 Ma, but the occurrence of young ages (13-10 Ma) is widely diffused, suggesting that exhumation of the IC occurred mainly in a post-thrusting stage.

In the central sector exhumation ages of the OC are comprised between ca. 25 and 6 Ma, but most of the samples exhumed between ca. 10 and 6 Ma with only few exceptions. In this sector the main stage of exhumation occurred then after the end of thrusting.

Exhumation occurred in the eastern sector between ca. 12 and 5 Ma, in the immediate post-thrusting stage. Although ages are generally homogeneous, a trend of slight NW-ward younging exhumation ages can be observed.

Spatial pattern of exhumation ages in the western OC suggest that the main exhumational stage occurred during thrusting, being driven by erosion of the accretionary prism. The velocity of the erosional exhumation process was likely enhanced by the thrusting process itself. In this same region post-thrusting exhumation also occurred, being likely related to erosion enhanced by normal reactivation of thrust faults.

In the central sector the post-thrusting ages of 10-6 Ma would suggest that exhumation was driven by post-thrusting isostatic uplift. Nonetheless the non-uniform burial and the occurrence of ages coeval to thrusting appears incompatible with uplift-related exhumation. Chapter 3 shows the connection between burial and exhumation and normal faulting in this region. Erosion and tectonic denudation processes, occurred during a post-thrusting extensional phase well explain both young ages and non-uniform burial.

In the eastern sector the uniform post-thrusting exhumation ages point to a major role of post-thrusting uplift as driving mechanism of exhumation in this region. This is supported also by the burial pattern, which appears related to crustal and lithospheric thickness and heat flow, indicating a connection between burial and exhumation of the wedge and the deep processes that shaped the whole Carpathian-Pannonian region.

To conclude this section we stress that in the western and central sectors of the study area burial and exhumation occurred as a response to crustal processes and no straightforward

connection with the opening of the PB can be found. In the eastern sector a clear relationship of the burial-exhumation history with the deep structure of the Carpathian-Pannonian region is observed.

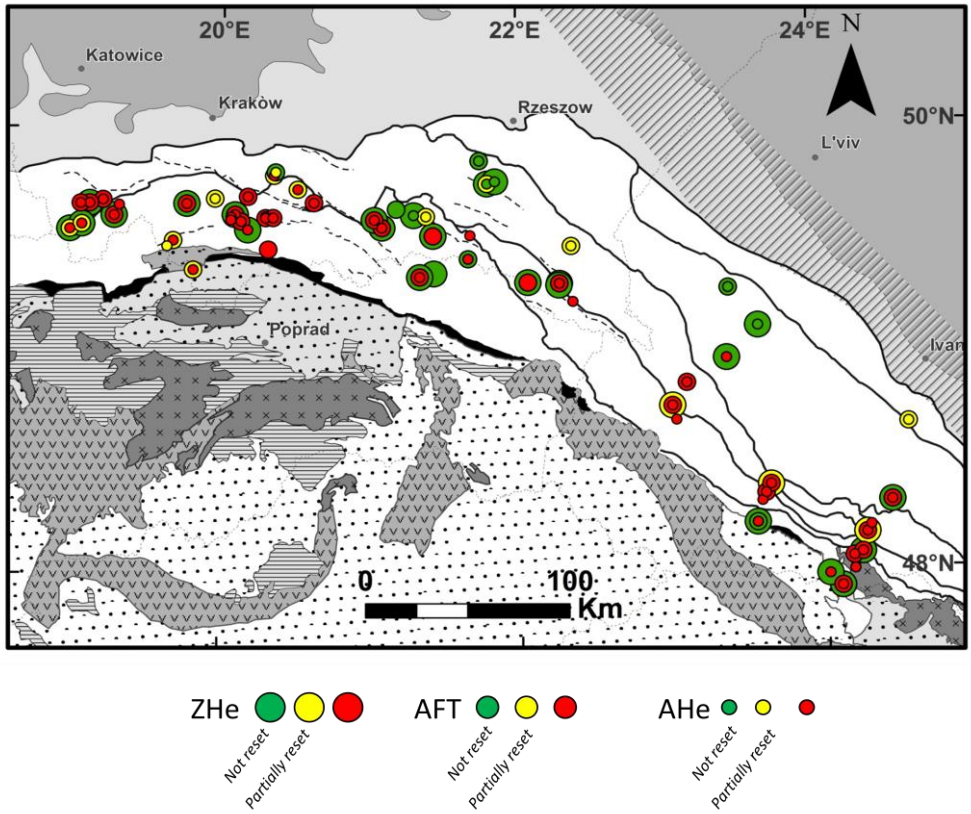

Figure 5.6 – ZHe, AFT and AHe degree of reset

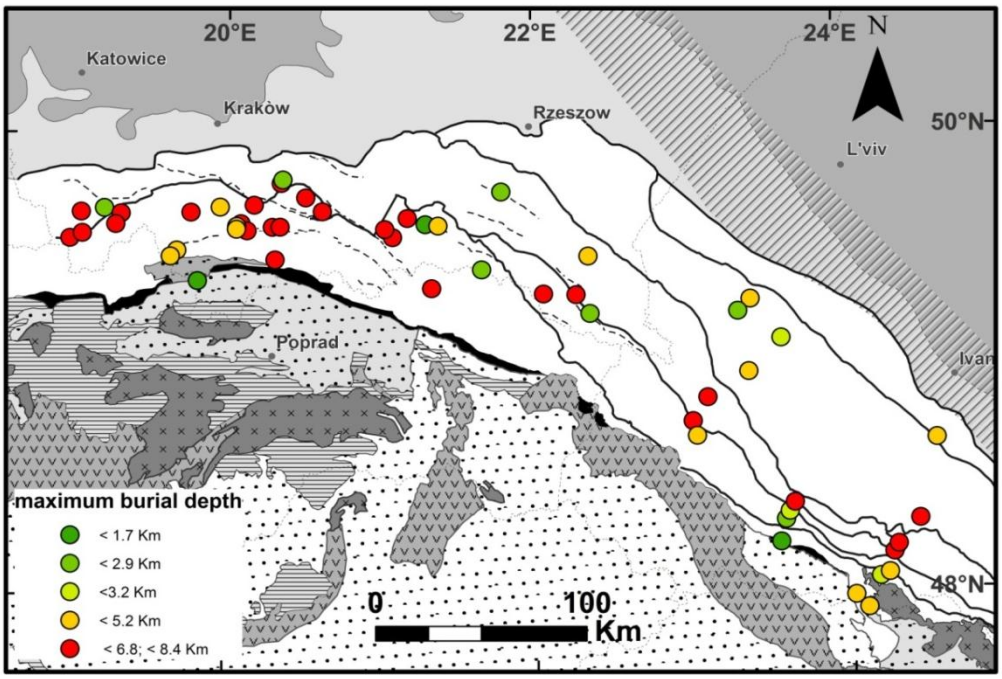

Figure 5.7 – Maximum burial depth estimated for the Polish and Ukrainian Carpathians.

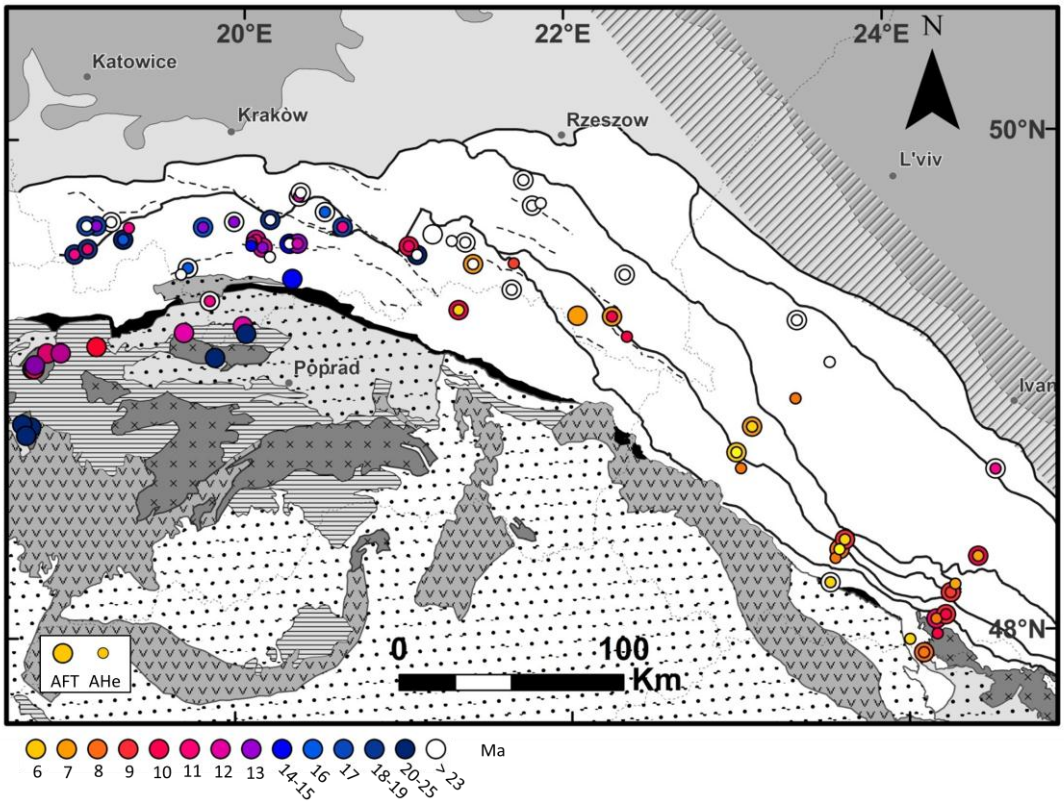

Figure 5.8- AFT central ages and AHe weighted mean ages of reset samples (unreset samples are indicated in white)

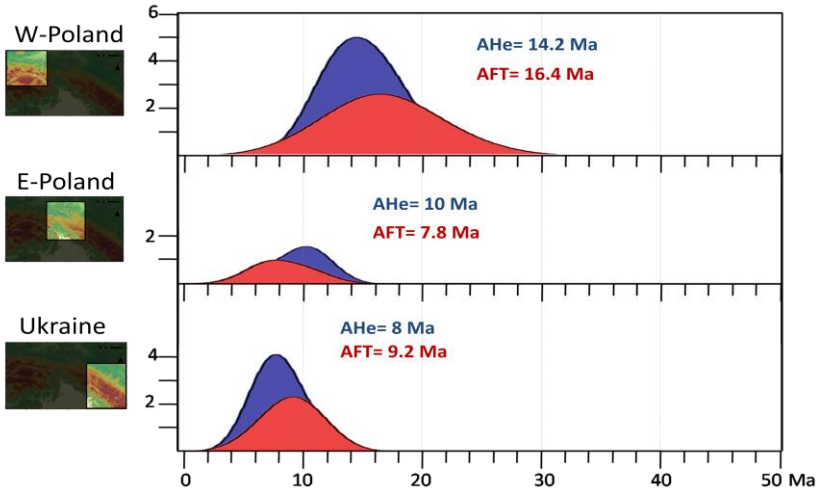

Figure 5.9 – Kernel density distribution of AHe and AFT ages in the three sectors

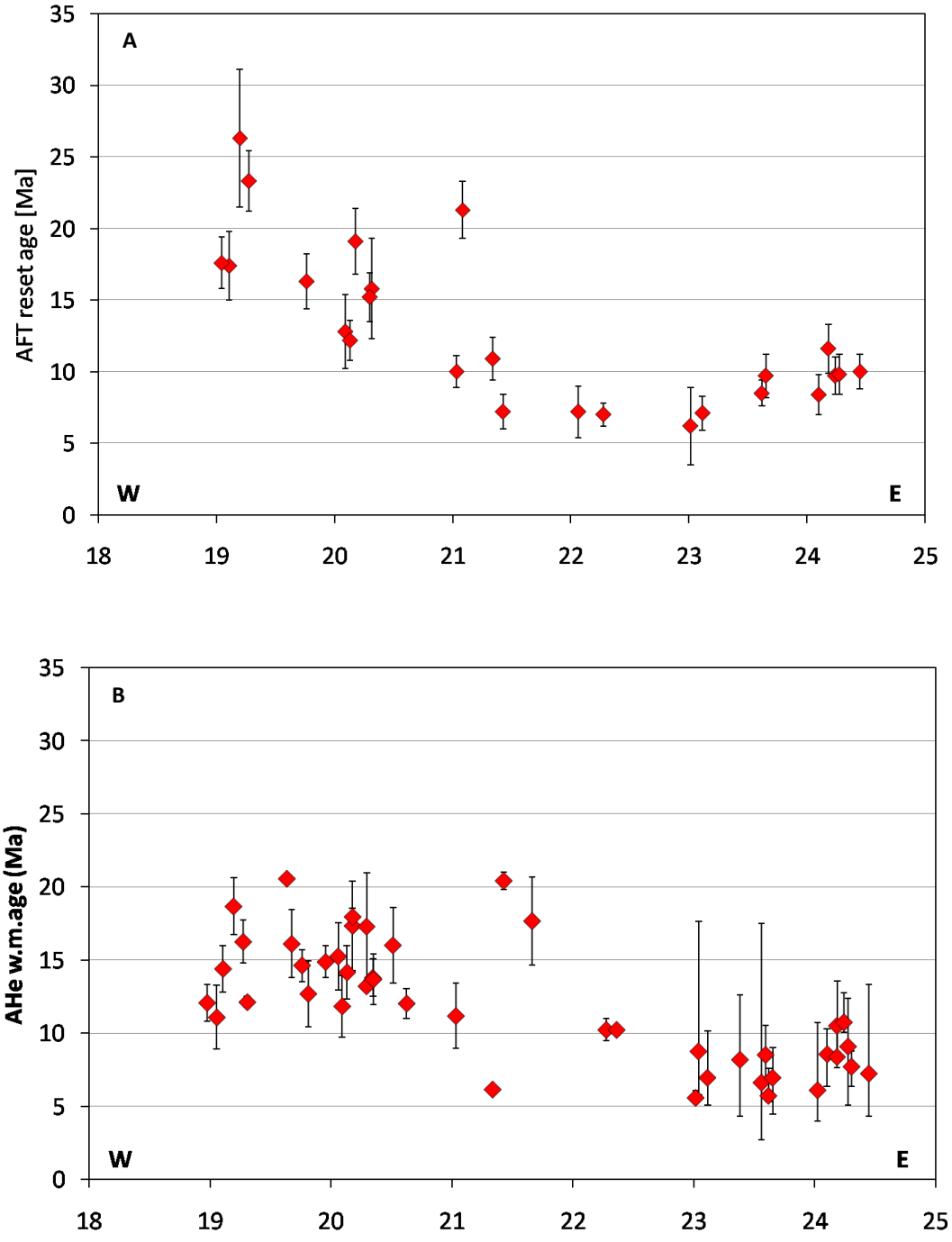

Figure 5.10 – AFT (A) and AHe eastward trend of reset ages

5.7. Interpretation

In order to constrain the geodynamic evolution of the Carpathian-Pannonian region from thermochronology of the Polish and Ukrainian Carpathians we summarized in Fig.5.11 the main tectonic events occurred in the Miocene in the single area of the study region and in the Pannonian Basin, as well as the exhumation events described in this thesis. The tectonic events that are supposed to have occurred according to the theory of slab roll-back and break off (e.g. Sperner et al., 2002) are also indicated.

Slab subduction and roll-back would have created a tear below the Carpathians, inducing deepening of the foredeep basin, outward migration of compression and thrusting and eventually extension in the innermost units of the wedge. Subsequent slab break-off, proposed by Sperner et al. (2002) to have shifted progressively from west to east, would have led to isostatic rebound of the overlying lithosphere and to cessation of thrusting.

In terms of burial and exhumation history of rocks this would have induced an homogeneous burial degree in the wedge and exhumation subsequent to the end of thrusting. In previous section we pointed out that burial degree in the western and, to a minor extent, in the central sector, is not homogeneous, with samples that were exhumed from very different depths (Fig 5.7.) located very close to each other. Furthermore thermal modelling confirms that several samples started to exhume during thrusting. Exhumation coeval to thrusting cannot therefore be related to slab break-off. On the other hand, post-thrusting exhumation, in the western and central sectors, appears related to extension rather than uplift. Thus, the burial and exhumation history of the Polish Carpathians appears unrelated to slab dynamics.

As already pointed out in previous chapters, several authors argued that the slab roll-back and break-off model is not the only possible explanation for the Neogene evolution of the Carpathian-Pannonian region and that the presence of detached slab beneath the Carpathians is inadequately supported by geophysical data (e.g. Ren et al., 2012). The data presented in this thesis, joint with these observations, suggest then that the Carpathian-Pannonian region was actually shaped by dynamics unrelated to slab subduction, roll-back and break-off.

On the other hand, it appears that the hypothesis of gravitational spreading of the lithosphere as deep driving process of the Neogene evolution of the Carpathians, is able to explain the burial and exhumation histories of the samples presented in this thesis, as well as the geophysical data referred to the Carpathian-Pannonian lithosphere (Fig. 4.1 and Fig. 5.3; e.g. Dererova et al., 2009; Pospisil et al., 2006). In particular lateral flow of the lithospheric mantle from beneath the Pannonian Basin toward the Carpathians can explain both crustal extension and thinning that characterized the Polish Carpathians and crustal and lithospheric thickening beneath the Ukrainian Carpathians.

An interpretation of the Miocene evolution of the study region is here presented, based on the data presented in this thesis and on the gravitational collapse model by Gemmer and Houseman (2007) and Houseman and Gemmer (2007). Nonetheless it has to be stressed that such interpretation is highly speculative and has the main objective to outline a picture of the

possible evolution of the Carpathian-Pannonian region that is able to give reason of the thermal and burial exhumation histories inferred in this study.

The location of the region of major lithospheric and crustal thickening (Fig. 4.1) suggests that lateral lithospheric flow, concurrent to the major astenospheric upwelling that occurred in the Middle Miocene (14-11.5 Ma, Fodor, 2010), was directed N to NE-ward, and that outward migration stopped and major thickening and downwelling started along the TESZ, where a thicker and more competent lithosphere impeded the compression to migrate further to the NE. As described by Gemmer and Houseman (2007) lithosphere flow induces crustal stretching, whereas, only in regions where a prolonged lithosphere downwelling occurs, also crustal thickening takes place. This is consistent with an initially N to NE-ward directed lithospheric flow, followed by major lithospheric downwelling beneath the present-day Ukrainian Carpathians, that would have induced major lithospheric and crustal thickening in the Ukrainian region, and minor lithospheric thickening and crustal thinning in the Polish-region. After ca. 12-11 Ma major compression shifted toward the Romanian Carpathians, uplift of the Ukrainian Carpathians started and major extensional stage in the PB terminated, giving way to major subsidence. This is interpreted to be due to S-ward shift of lithospheric downwelling. In particular, as introduced in Chapter 4, extension in the PB appears related to lithosphere downwelling beneath the Ukrainian Carpathians, and subsequent downwelling beneath the Romanian Carpathians likely had the role to preserve the thinned lithosphere in the PB, inducing only minor extension (Huismans et al., 2001). Post-thrusting uplift in the Eastern sector of the study region is interpreted to have occurred as a consequence of S-ward migration of active lithosphere downwelling and consequent cessation of tear beneath this region. A detachment of the lithospheric downwelling lithosphere seems to be not supported by tomographic data, whereas a partial re-absorption of the downwelled lithosphere may have occurred (e.g. Gemmer and Houseman, 2007).

Late Miocene (10-6 Ma) extension in the central, and to a minor extent, western sectors is the most controversial element to be interpreted. Extension occurred after the cessation of lithospheric downwelling beneath the Ukrainian Carpathians, therefore we exclude that it was driven by lithospheric flow. On the other hand the thinned crust and the thick lithosphere that characterize this region do not support the hypothesis of gravitational collapse of a thickened crust. Nonetheless it has to be pointed out that extensional faults are mainly strike-parallel to the chain in this region, with direction of the horizontal stress NE-SW (Mazzoli et al., 2010). Extension normal to the strike of the chain would be consistent with gravitational collapse. Janik et al. (2011) show that the central region is characterized by relatively thick OC sediments and European Platform cover with respect to the total crustal thickness, suggesting that gravitational instability may have developed within the crust as a consequence of sedimentary thickness and thrust imbrication in the OC. Therefore Late Miocene extension can be interpreted as induced by gravitational collapse occurred within the crust.

To summarize Miocene evolution of the Carpathian-Pannonian region is interpreted to have developed in several steps. In the Aquitanian compression was active all along the Carpathians and the PB was characterized by thickened crust and lithosphere. In the Burdigalian extensional

collapse of the crust in the PB occurred, while compression was active in the Carpathians. During compression and thrusting exhumation occurred in the western sector of the study region. Collapse of the thickened PB crust triggered thinning and lateral flow of lithosphere, that is suggested to have had, at the beginning, a N-NE direction and progressively migrated clockwise, as indicated by progressive migration of the tectonic activity. Lithosphere thinning intensified in the Serravallian, when compression progressively terminated along the Polish Carpathians. The thinned crust of the Polish Carpathians is considered as an indication that they experienced in this time crustal stretching induced by lithospheric flow. At ca. 12-11 Ma the lithosphere downwelling migrated further SE-ward along the TESZ. As a consequence thrusting terminated in the Ukrainian Carpathians as well as major extension in the PB. It can be argued that, in fact, downwelling in the Romanian Carpathians was sufficient to preserve the thinned lithosphere in the PB but not to induce further extension. After 12-11 Ma, while in the PB major subsidence and minor extension were active, the eastern sector of the study region underwent major uplift and exhumation (12-6 Ma) and the central sector (and to a minor extent the western sector) underwent exhumation induced by extension, that we interpret as due to gravitational collapse within the crust. This would imply that, at least in the Late Miocene the crust and mantle lithosphere beneath the Polish Carpathians were mechanically decoupled, whereas the lithosphere of the Ukrainian Carpathians behaved as a unique layer from the mechanical point of view.

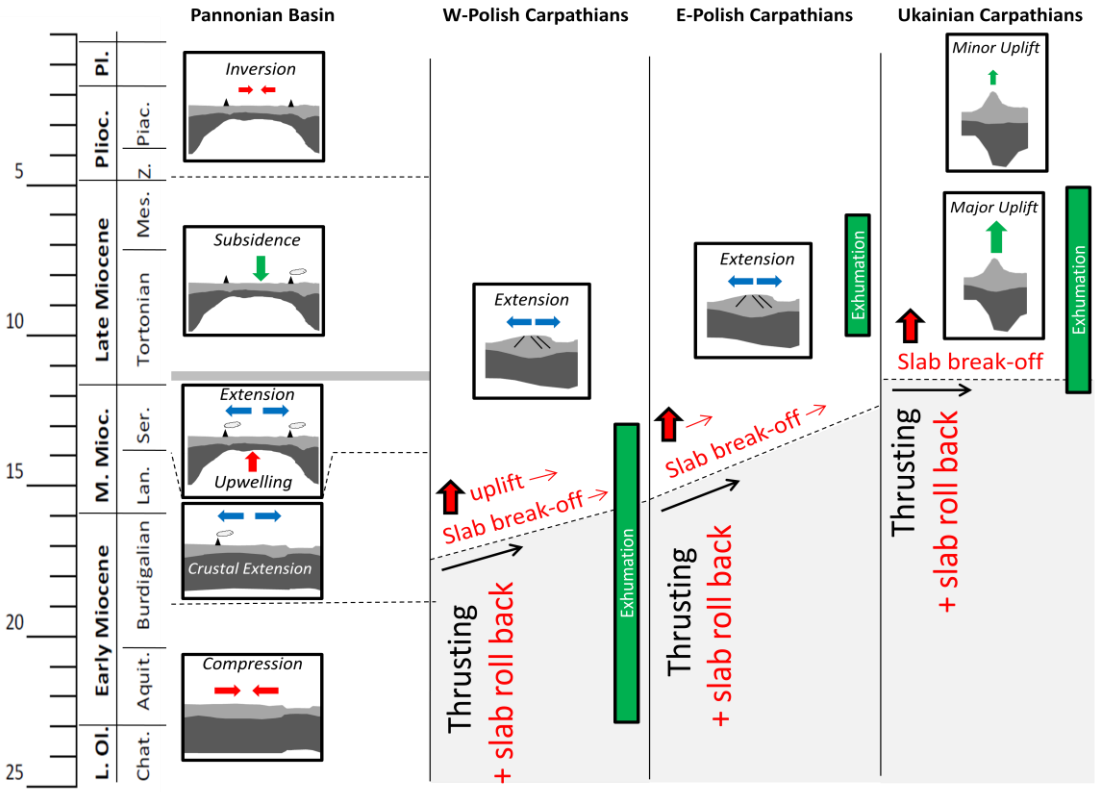

Figure 5.11 – synthesis of the main tectonic events occurred in the Neogene in the Pannonian Basin (From Huismans et al., 2001 and Fodor, 2011), and in the Carpathians. The events related to the slab roll back and break-off model are represented by the red text; the grey areas represent the stage of thrusting (Nemcok et al., 2006).

5.8. Synthesis

The data presented in this thesis constitute constrains to the geodynamic evolution of the entire Carpathian-Pannonian region, as each single model would have generated a different effect in burial-exhumation of the Carpathian thrust and fold belt. The consistency of the data presented in this thesis with the principal models proposed so far for the evolution of the Carpathian-Pannonian region was evaluated, and integrating the results with previously published geophysical data referred to the Carpathian-Pannonian region allowed to formulate an interpretation for the Miocene evolution of this region.

The main conclusions can be summarized as follows:

Three sectors characterized by different features can be identified in the study region: in the western sector exhumation occurred by erosion of the wedge and it started during thrusting (23-12 Ma), in the central sector it was driven by extension of the wedge occurred after the end of thrusting (10-6 Ma), and in the eastern sector it occurred by erosion during post-thrusting uplift (12-5);

It is argued that the not-homogeneous burial depths of samples belonging to the western and central sector, joint with the evidence for exhumation coeval to thrusting and the geophysical data that suggest the absence of a detached slab at depth, may indicate the lack of slab subduction, roll back and break-off beneath the Polish Carpathians.

Indications for the lack of slab-related processes point to the hypothesis of lithosphere flow induced by gravitational instability as the possible driving process for the Miocene evolution of the Carpathian-Pannonian region.

Based on this model thrusting would have been explained by downwelling of the lithosphere and the thinned crust of the central sector would have to be ascribed to NE-ward directed flow of the lithosphere, that is proposed to have stopped only in correspondence of the thick and competent lithosphere of the East European Platform along the TESZ. In the same way the thickened lithosphere and crust of the Ukrainian Carpathians would have been related to lithosphere thickening and downwelling at the contact with the TESZ.

The Miocene evolution of the Carpathian-Pannonian region proposed in this chapter can be summarized in the following steps: (i) in the early Miocene the thick Pannonian crust collapses while N-ward compression is active, in the western sector rocks start to exhume by erosion of the wedge during thrusting; (ii) in the Middle Miocene major lithosphere thinning takes place in the PB, and major lithosphere downwelling progressively shifts from the eastern Polish Carpathians toward the Ukrainian Carpathians. Exhumation continues in the western sector; (iii) at 12-11 Ma the lithosphere downwelling rapidly shifts SE-ward, toward the Romanian Carpathians and after that major uplift occurs in the Ukrainian Carpathians and major subsidence takes place in the PB.

Late Miocene extension in the central and (with a minor extent) western sector of the study region appears unrelated to regional scale dynamics, being likely induced by gravitational collapse occurred within the crust. Thus, mechanical decoupling of the crust and mantle

lithosphere is inferred for the central and western sector, whereas in the eastern sector the upper crustal processes reflect the whole-lithosphere dynamics.

CHAPTER VI.

CONCLUSIONS

In this work thermal and burial-exhumation history of the Polish and Ukrainian Carpathians were reconstructed as constrains to the Neogene evolution of the Carpathian-Pannonian region.

Thermal history was influenced by the positive thermal anomaly developed in the Pannonian Basin in the Middle Miocene only to a minor extent and only in the innermost units of the Ukrainian Carpathians. As a consequence thermal history entirely depended on the burial-exhumation history of samples.

Burial is generally higher in the innermost units of the wedge and lower in the more external units, indicating a general dependence on the wedge geometry. Nonetheless in the Polish region burial is not homogeneous even in the same structural position in the wedge, rather indicating a dependence on the single structure. In the innermost units in Poland burial varies between ca. 3.6 and 7.2 Km, whereas in Ukraine it varies Between ca. 2.6 and 6 Km. In the outermost units burial was generally lower than ca. 3.6-2.6 Km.

Based on the spatial trend of burial and exhumation and on structural and physical features the study region was subdivided in three sectors.

Exhumation of the western sector occurred by erosion of the wedge during thrusting (ca. 23-13 Ma) and during post-thrusting extension (13-12 Ma). In the central sector exhumation occurred by erosion and tectonic denudation during a post-thrusting extensional phase (10-6 Ma). Finally the eastern sector exhumed by erosion during post thrusting isostatic uplift (12-5 Ma).

The data regarding burial and exhumation were put in relation with (i) the spatial trend of the relief, (ii) heat flow, (iii) crustal and lithospheric thickness, and (iv) structural setting in order to interpret them in the framework of the Neogene evolution of the Carpathian-Pannonian region.

The non homogeneous burial in the western and central sector suggests the lack of slab subduction and subsequent break-off in these areas. Furthermore, the distribution of exhumation ages along the chain is not compatible with a clockwise (E to SE ward) progressive slab break-off, the youngest exhumation having occurred in the central area, at the Polish-Ukraine boundary.

The data presented in this thesis are therefore more consistent with models for the evolution of the Carpathian-Pannonian region that do not comprise slab-related dynamics, such as that based on gravitational collapse of a previously thickened lithosphere. Finally it could be observed that burial-exhumation history of the Ukrainian Carpathians are related to whole lithosphere dynamics, whereas that of the Polish Carpathians mainly depends on crustal processes. This indicates that, at least in the Middle Miocene, crust and mantle lithosphere were mechanically coupled in the Ukrainian Carpathians, and mechanically decoupled in the Polish Carpathians.

Besides the main subjects of the present thesis it has been possible to investigate two additional issues:

- The ZHe unreset ages of samples belonging to the accretionary wedge were used to determine timing of exhumation of source rocks of the sediments through the ZHe PRZ. The

source rocks cooled and exhumed part in response to the Variscan (Late Devonian to Triassic) and part to the Alpine (Late Jurassic to Early Paleocene) orogenesis, suggesting sedimentary provenance both from the southern margin and basement heights within the Outer Carpathian basin.

- AHe analysis performed on “bad” apatite grains provided the opportunity to verify that in case of fast cooling, well reproducible data can be obtained even from grains with significant defects. In several cases, in the present dataset, age dispersion correlates with Th concentration and Th/U content, suggesting a relevance of rich in Th oxide-oxhydroxide coating.

APPENDIX

I) Evaluation of reliability of AHe dates from "bad" grains

As illustrated in previous chapters the apatite grains available for AHe analysis were generally of bad quality, with respect to the standard apatite grain required for obtaining reliable results. In particular most of the grains were characterized by inclusions, oxide-oxhydroxide coating, abrasion, rounding (Fig. 4.4). In Fig. I.I the percentage of occurrence of each bad crystal feature with respect to the total of the analyzed grains is indicated. In Chapter 2. a brief summary of how the bad crystal features can affect ages is reported. In order to understand the significance of the AHe dataset it was necessary to evaluate the impact of bad crystal features on precision and accuracy of dates.

As described by Ehlers and Farley (2003), a first way to detect the effect of suspicious crystal features is to consider the age reproducibility. Most of the features that may adulterate the result are specific of each single grain, therefore samples with reproducible ages generally indicate no significant effect of bad crystal features. Nonetheless it has to be stressed that oxide-oxhydroxide coating or abrasion and rounding pervading the whole rock sample would be able to induce the same alteration in most of the grains of the sample, therefore affecting age accuracy rather than reproducibility.

Several analytical values are commonly used as proxies for impact of crystal features on age: in Tab. I the meaning of correlation of AHe ages and age-dispersion with proxies is reported.

An evaluation of the impact of bad crystal features on AHe dates was then performed testing the correlation with potential proxies for biased results of AHe single grain ages and AHe age dispersion for the whole population as well as for the single sample.

In Fig III the results of the regression tests for correlation with dates and date-dispersion for the whole dataset are reported. It can be observed that significant correlations are found for AHe ages with eU, Th, and Th/U. This can be interpreted as an effect of Th-rich coating.

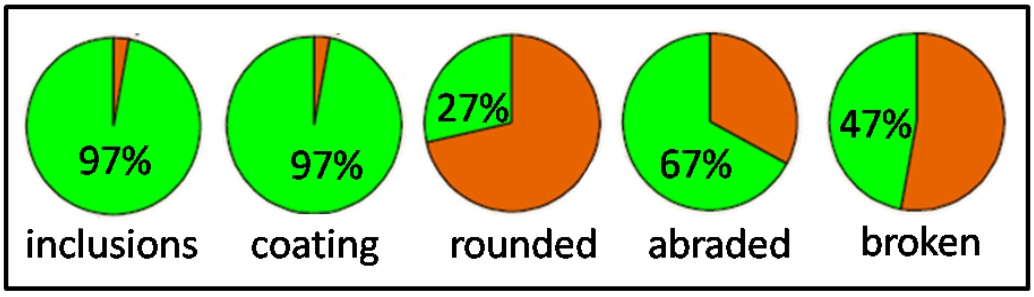

Figure I.I – percentages of occurrence of bad crystal features in the analyzed grains

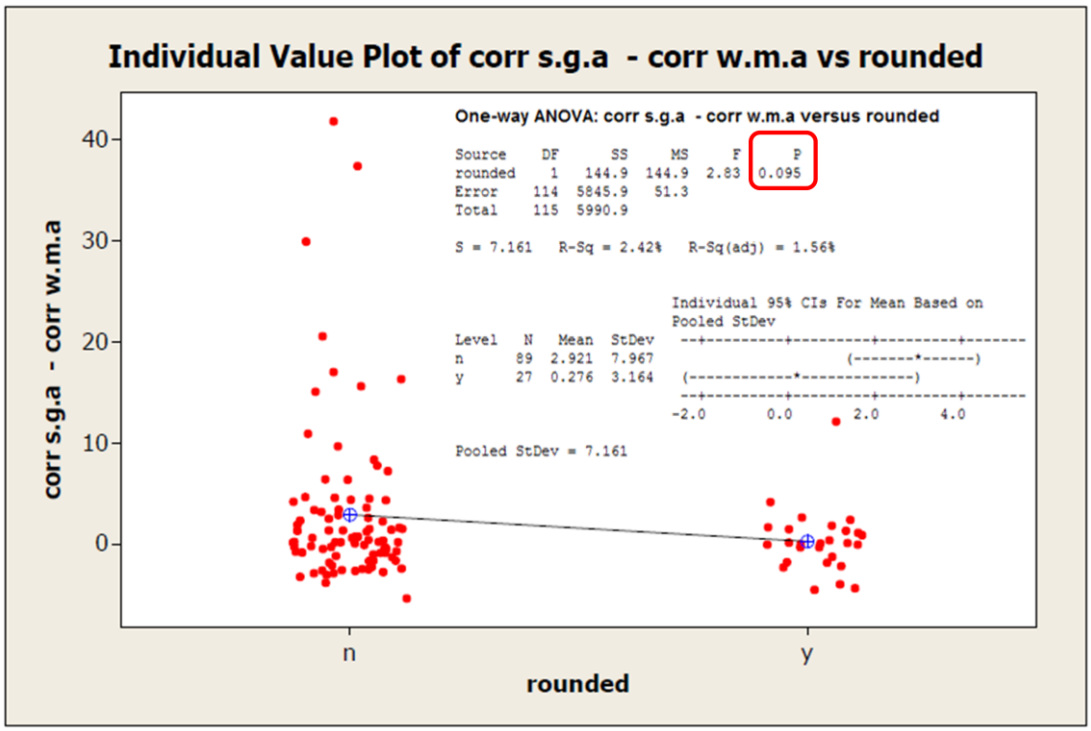

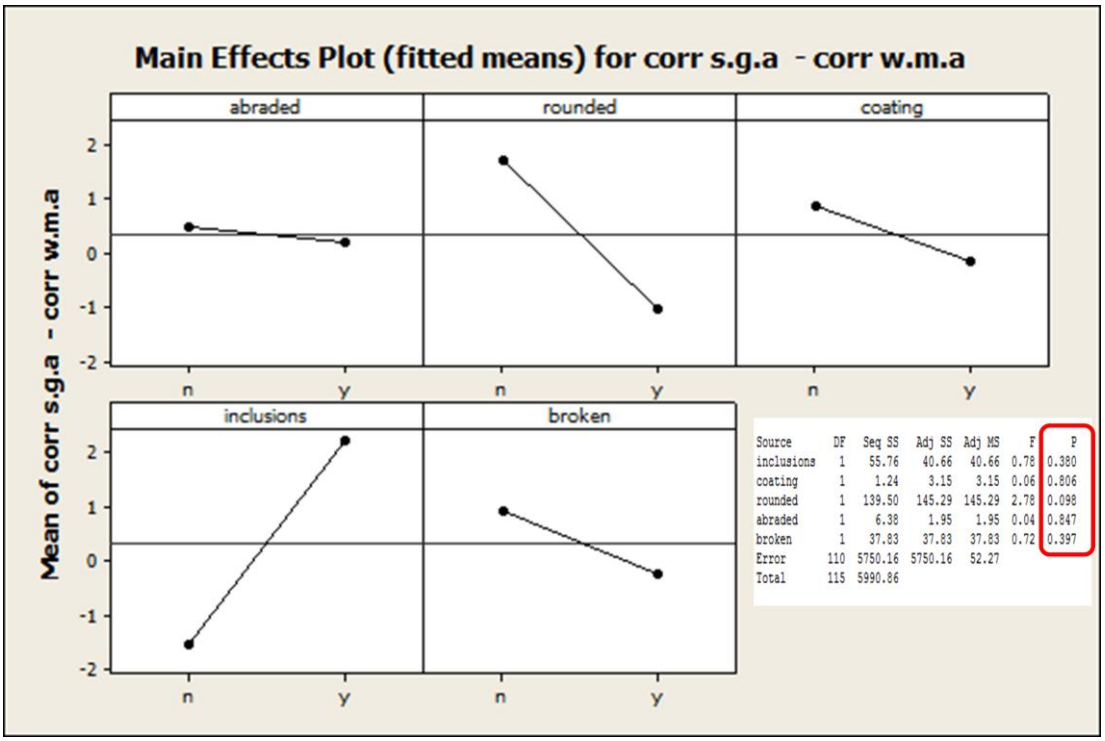

Figure I.II – results of the Anova One way test used to verify the significance of the correlation between age dispersion and bad crystal features. The test was performed using the Minitab software.

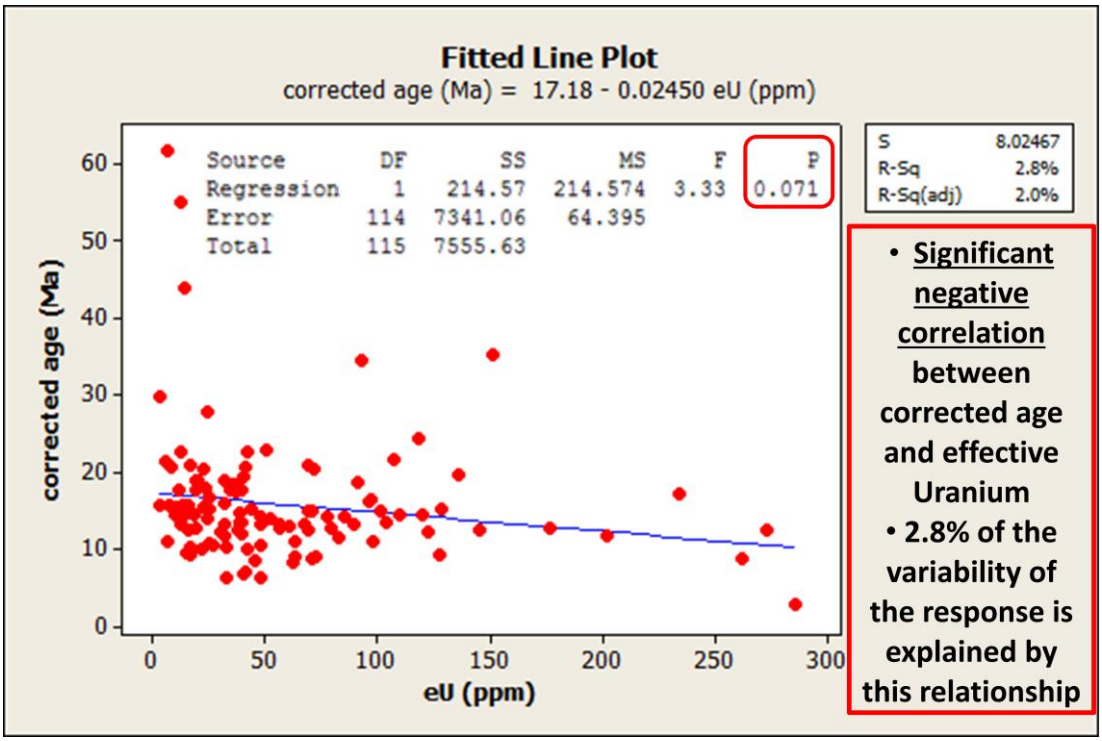
Fitted Line Plot
corrected age (Ma) = 17.18 - 0.02450 eU (ppm)
Source DF SS MS F P
Regression 1 214.57 214.574 3.33 0.071
Error 114 7341.06 64.395
Total 115 7555.63
S 8.02467
R-Sq 2.8%
R-Sq(adj) 2.0%
corrected age (Ma)
eU (ppm)
• Significant negative correlation between corrected age and effective Uranium
• 2.8% of the variability of the response is explained by this relationship

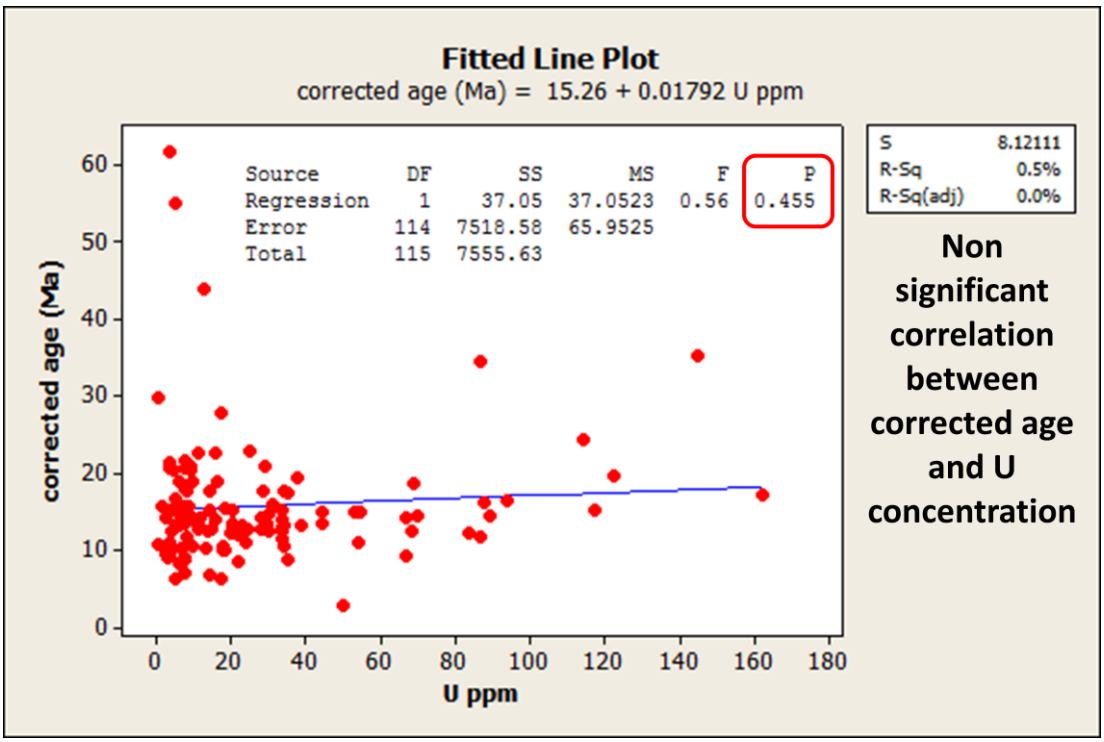
Fitted Line Plot
corrected age (Ma) = 15.26 + 0.01792 U ppm
Source DF SS MS F P
Regression 1 37.05 37.0523 0.56 0.455
Error 114 7518.58 65.9525
Total 115 7555.63
S 8.12111
R-Sq 0.5%
R-Sq(adj) 0.0%
corrected age (Ma)
U ppm
Non significant correlation between corrected age and U concentration

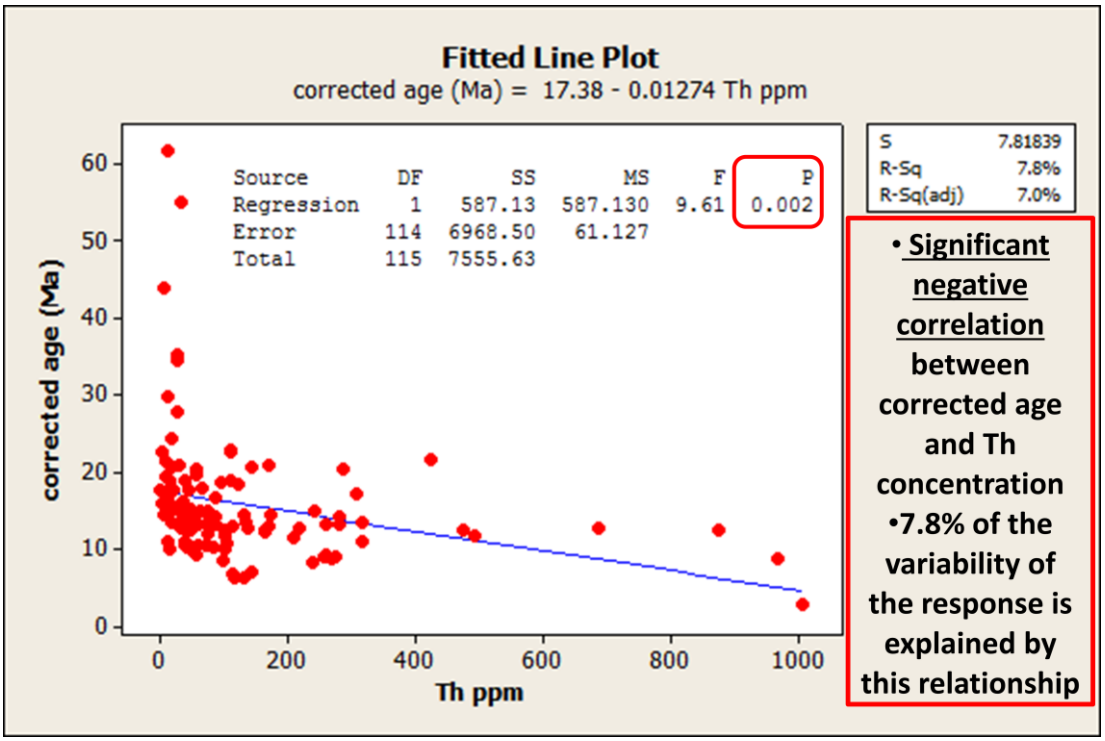
Fitted Line Plot
corrected age (Ma) = 17.38 - 0.01274 Th ppm
Source DF SS MS F P
Regression 1 587.13 587.130 9.61 0.002
Error 114 6968.50 61.127
Total 115 7555.63
S 7.81839
R-Sq 7.8%
R-Sq(adj) 7.0%
corrected age (Ma)
Th ppm
• Significant negative correlation between corrected age and Th concentration
•7.8% of the variability of the response is explained by this relationship

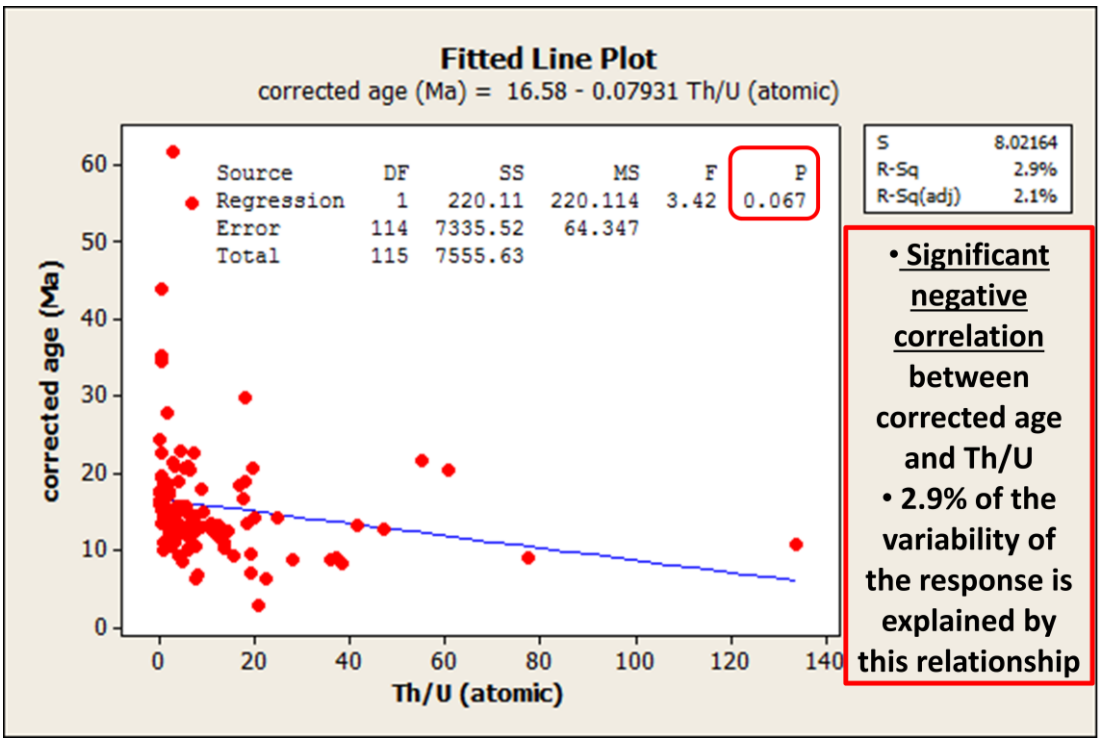
Fitted Line Plot
corrected age (Ma) = 16.58 - 0.07931 Th/U (atomic)
Source DF SS MS F P
Regression 1 220.11 220.114 3.42 0.067
Error 114 7335.52 64.347
Total 115 7555.63
S 8.02164
R-Sq 2.9%
R-Sq(adj) 2.1%
corrected age (Ma)
Th/U (atomic)
• Significant negative correlation between corrected age and Th/U
• 2.9% of the variability of the response is explained by this relationship

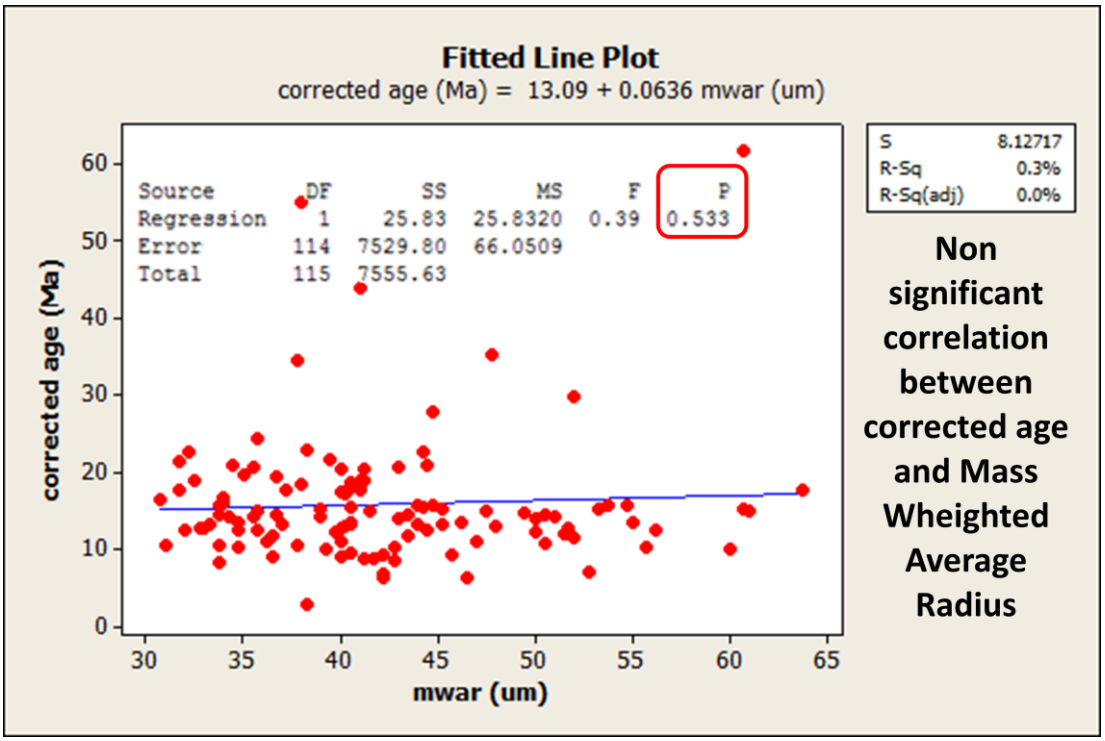

Figure I.III – Results of the regression analysis used to test the correlation between Corrected single grain age and measured parameters. The analysis was performed using the Minitab software.

II) Sample preparation procedures

The apatite and zircon separation from the rock samples was performed at the laboratory of sedimentary petrography of the Geosciences department of the University of Bologna, following the procedures described in Donelick et al. (2005). Rock disaggregation was performed using a disk-mill and a jaw crusher. After disaggregation the crushed material was sieved using 250 µm sieve-cloth and the >250 µm fraction was processed again in order to obtain material all of sand size. The material was then washed using a washing table with riffles, in order to discard the fine grained fraction. The sand-sized material was then processed with a Frantz Isodynamic magnetic separator, in order to discard the magnetic fraction. Afterwards heavy liquid separation was performed in two steps. The fraction with density higher than ρ=2.97 g/cm^3, obtained from the first separation with Tetrabromoethane, contains both apatite (ρ=3.1-3.35 g/cm^3) and zircon (ρ= 4-4.70 g/cm^3), that are split through the second separation with Diiodomethane (ρ=3.33 g/cm^3).

Manual picking of apatite and zircon grains for **He analysis** was performed part at the Geosciences department of the University of Arizona (Tucson), and part at the Geosciences department of the University of Padua. In both cases an optical stereoscope with an integrated camera was used in order to take pictures of the selected crystals and to measure them for α-ejection correction. Crystals were then packed in Nb tubes of 1mm heights that worked as a micro-furnace for crystal heating and He extraction during analysis.

Preparation of grain mounts for neutron irradiation was performed at the Geosciences department of the University of Padua. Apatite grains were first mounted in epoxy resin. Grain mounts were then polished to expose inner crystal surfaces and to smooth them to eliminate

defects that can obstruct track counting. After polishing the grain mounts are chemically etched with HNO_3 5M for 20 seconds, in order to highlight the spontaneous tracks. A mica sheet with low-U content was then placed over each grain mount to form a mount-mica couple fastened with adhesive tape. The mount-mica packages were then stacked in standard irradiation tubes; at the two ends of each stack of samples two packages constituted by standard CN5 glass, of known U content, and mica were placed in order to monitor neutron fluence during irradiation. Sample irradiation with thermal neutrons was performed in the reactor at the Radiation Center of Oregon State University with a nominal neutron fluence of 9×10^{15} n cm^{-2}. After irradiation each mount-mica package was opened and the mica sheets were chemically etched with HF 40% for 40 minutes in order to highlight the fission tracks induced by neutron irradiation. Apatite fission track analysis could then be performed on mount-mica couples mounted on microscope slides.

III) Analytical facilities and procedures

AHe and ZHe analysis

Helium analysis was performed at the Radiogenic Helium dating laboratory of the Geosciences department of the University of Arizona (Tucson, AZ). Details on the procedures and standards routinely used by the laboratory can be found in the laboratory's website (http://www.geo.arizona.edu/~reiners/arhdl/procs.htm). The packets containing the crystals to be analyzed, and the standard crystals are placed in a stainless steel planchet inside a laser cell (Fig.II.I.B)and heated with ND-YAG laser for 3 (apatites) to 15 minutes (zircons) at 1-5 W (Fig. II.I.C). Helium Blanks (0.1-0.05 fmol 4He) are determined by heating empty packets with the same procedure. The Gas was then spiked with 4pmol 3He, condensed in a cryogenic trap at 16K, then released at 37K into a small volume with an activated getter and the source of a Balzer quadrupole mass spectrometer with Channeltron electron multiplier. Masses of HD and H3+ are measured to correct the 3He/4He measured ratios. The obtained ratios are referenced to 4He standards measured in the same way. After 4He measurement samples are retrieved from the laser cell, each packet is put in a Teflon vial, spiked with calibrated 229Th, 233U, and 147Sm solution and dissolved by 30% NO3.

Natural-to-spike isotope ratios are then measured on a high-resolution (single-collector) Element2 ICP-MS (Fig. II.I.D with all-PFA Teflon sample introduction equipment and sample preparation/analytical equipment. Careful monitoring of procedural blanks and spike and normal concentrations (including evaporative effects) and isotopic compositions is essential for He dating.

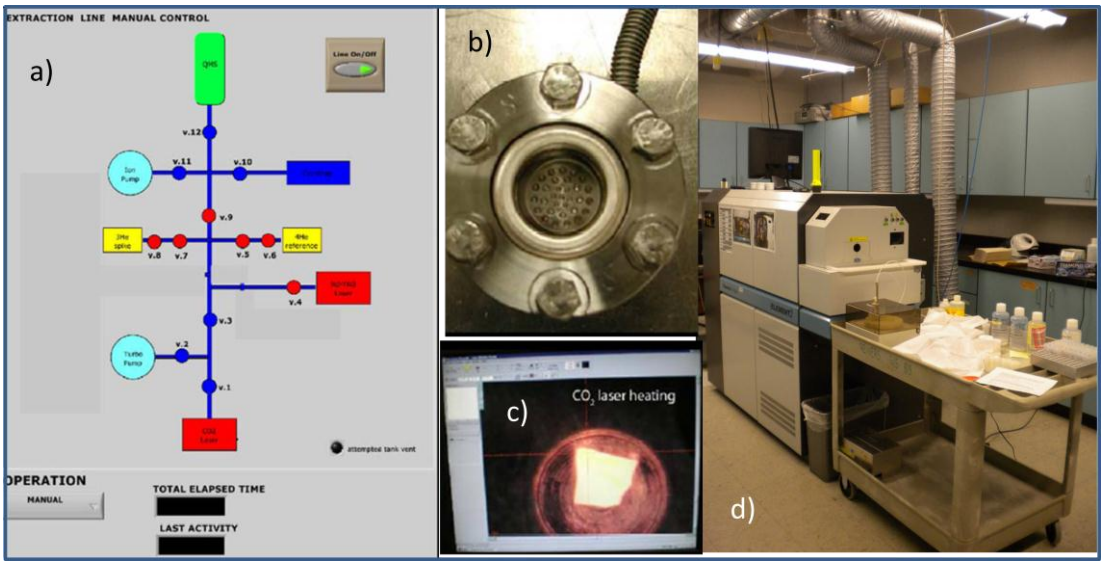

Fig. II.I – AHe and ZHe analytical procedures: a)scheme of the He quadruple mass spectrometer; b) stainless steel planchet for He analysis in the quadrupole mass spectrometer; c) sample being hit and heated by laser beam; d) Inductively coupled plasma MS for U, Th, Sm analysis.

AFT analysis

FT dates (up to 40 grains per sample) were calculated using the external-detector and the zeta-calibration methods (Hurford and Green 1983) with IUGS age standards (Durango, Fish Canyon and Mount Dromedary apatites; Hurford 1990) and a value of 0.5 for the $4\pi/2\pi$ geometry correction factor.

AFT analysis was performed at the Geosciences department of the University of Padua. The basic equipment used for analysis is a ZEISS Axioscope connected to a computer and to the high resolution drawing board CalComp™Drawing Board 2 with led pointer and 16-keys mouse. The sample slides are placed on a sliding table Kinetek™ driven through a joystick. The tracks are counted on the same area of each crystal on the crystal itself and on the corresponding image in the mica sheet. The software FT-Stage is used to calibrate the sliding table before track counting, using reference points in the grain mount and in the mica sheet, so that the coordinates of the selected crystals can be registered and the coordinates of the corresponding images in the mica can be automatically calculated.

REFERENCES

Anczkiewicz, A.A., Swierczewska, A., 2008. Thermal history and exhumation of the Polish Western Outer Carpathians: evidence from combined apatite fission track and illite-smectite data, in: Garver, J.I., Montario, M.J. (Eds.), Proceedings from the 11th International Conference on Thermochronometry Anchorage, Alaska, pp. 1–4.

"Babuˇska, V.,Plomerova´ , J., ˇSı´leny´ , J.,1987.Structuralmodelofthesubcrustal lithosphere inCentralEurope. GU Transactions, ed.FuchsandFroidevaux, Geodynamics Series,vol.16.pp.239–251."

Barbarand J, Carter A, Wood I, Hurford T. 2003. Compositional and structural control of fission-track annealing in apatite. Chem. Geol. 198:107–37

Barker, C.E., and Pawlewicz, M.J., 1994, Calculation of vitrinite reflectance from thermal histories and peak temperatures. A comparison of methods, in Mukhopadhyay, P.K., and Dow, W.G., eds., Vitrinite Reflectance as a Maturity Parameter: Applications and Limitations: American Chemical Society Symposium Series, v. 570, p. 216–229.

Bieda, F., S. Geroch, L. Koszarski, M. Ksiazkiewicz, and K. Zytko, 1963, Stratigraphie des Karpates externes polonaises:
Biuletyn Instytutu Geologicznego, v. 182, p. 5–174.

Bielik, M., and A. Adam, 2006, Structure of the lithospherein the C arpathian–Pannonian region, in J. Golonka and F. J. Picha, eds., The Carpathians and their foreland: Geology and hydrocarbon resources: AAPG Memoir 84, p. 699–706."

Bielik, M.,Sˇ efara, J., Kova´ c, M., Beza´ k, V. and Plasˇienka, D., 2004. The Western Carpathians-interaction of Hercynian and Alpine processes. Tectonophysics, 393, 63–86."

Birkenmajer, K., 2001. Pieniny Klippen Belt. Introduction, in: 12th meeting of the Association of European Geological Societies, 10–15 September, Krakow. Field Trip Guide, pp. 127–138.

Birkenmajer, K., Pécskay, Z., 2000. K-Ar Dating of the Miocene andesite intrusions, Pieniny Mts, West Carpathians, Poland: a supplement. St. Geol. Pol. 117, 7-25.

Brandon MT, Roden-Tice MK, Garver JI. 1998. Late Cenozoic exhumation of the Cascadia accretionary wedge in the Olympic Mountains, Northwest Washington State. Geol. Soc. Am. Bull. 110:985–1009.

Brandon MT. 1992. Decomposition of fission-track grain-age distributions. Am. J. Sci. 292:535–64"

Brandon MT. 2002. Decomposition of mixed grain-age distributions using BINOMFIT. On Track 24:13–18

Braun, J., van der Beek, P., and Batt, G., 2006, Quantitative Thermochronology: Numerical Methods for the Interpretation of Thermochronological Data: Cambridge, New York, Cambridge University Press, 258 p.

Broska, I., Uher, P., 2001. The whole rock chemistry and genetic typology of the West Carpathians Variscan granites. Geol. Carp. 52, 79-90.

Budzyń, B., Hetherington, C.J., Williams, M.L., Jercinovic, M.J., Dumond, G., Michalik, M., 2008. Application of electron probe microanalysis Th–U–total Pb geochronology to provenance studies of sedimentary rocks: An example from the Carpathian flysch. Chem. Geol. 254, 148–163.
Budzyn, B., Konecny, P., Michalik, M., Malata, T., Poprawa, P., 2006. U–Th–total Pb dating of primary and secondary monazite formation in gneiss and granulite clasts from the Silesian Unit (Western Outer Carpathians, Poland). Geol. Soc. Am. — Abstracts with Programs 38 (7), 562.

Burchart, J., 1972. Fission-track age determination of accessory apatite from the Tatra mountains, Poland. Earth Planet. Sci. Lett., 15, 418–422.

Bustin, R.M., Barnes, M.A. and Barnes, W.C., 1990. Determining levels of organic diagenesis in sediments and fossil fuels. In: Diagenesis. Geoscience Canada Reprint, 4th series (I.A. McIleareathand D.W. Morrow, eds), pp. 205–226. Geological Association of Canada.

Carlson WD, Donelick RA, Ketcham RA. 1999. Variability of apatite fission-track annealing kinetics. I. Experimental results. Am. Mineral. 84:1213–23.

Cloetingh et al., 2010. Lithosphere tectonics and thermo-mechanical properties: An integrated modelling approach for Enhanced Geothermal Systems exploration in Europe, Earth Science Reviews, doi:10.1016/j.earscirev.2010.05.003 http://www.sciencedirect.com/scidirimg/clear.gif

Crowley, K.D., Cameron, M., and Schaefer, R.L. (1991) Experimental studies of annealing etched fission tracks in fluorapatite. Geochimica et Cosmochimica Acta, 55, 1449–1465.

Csontos, L.,Nagymarosy,A.,Horva´ th, F.,Kova´ c, M.,1992.Tertiary evolution of the Intra-Carpathian Area:amodel.Tectonophysics208,221–241.

Dallmeyer, R. D., Németh, Z., Putiš, M., 2005. Regional tectonothermal events in Gemericum and adjacent units (Western Carpathians): Contribution by the 40Ar/39Ar dating. Slovak. Geol. Mag. 11, 2-3, 155-163.

Dallmeyer, R.D., Neubauer, F., Handler, R., Fritz, H., Müller, W., Pana, D., Putiš, M., 1996. Tectonothermal evolution of the internal Alps and Carpathians: evidence from 40Ar/39Ar mineral and whole-rock data. Eclogae Geol Helv. 89: 203–227.

Damon, P. E., and Kulp, J. L., 1957, Determination of radiogenic helium in zircon by stable isotope dilution technique: Am. Geophys. Union Trans., v. 38, p. 945-953

Danisˇı´k, M., Kohu´ t, M., Broska, I. and Frisch, W., 2010. Thermal evolution of the Mala´ Fatra Mountains (Central Western Carpathians): insights from zircon and apatite fission track thermochronology. Geol. Carpathica, 61, 19–27.

Danisˇı´k, M., Pa´ nek, T., Maty´ sek, D., Dunkl, I. and Frisch, W., 2008. Apatite fission track and (U-Th)/He dating of teschenite intrusions gives time constraints on accretionary processes and development of planation surfaces in the Outer Western Carpathians. Z. Geomorphol., 52／3, 273–289.

Danišìk, M., Kadlec, J., Glotzbach, C., Weisheit, A., Dunkl, I., Kohùt, M., Evans, N.J., Orvošová, M., McDonald, B.J.,2011. Metamorphism, exhumation and topographic evolution in orogenic belts by multiple thermochronology: a case study from the Nìzke Tatry Mts., Western Carpathians Swiss J Geosci. 104, 285–298.

"Dérerova J, Zeyen H, Bielik M and Salman K., 2006: Application of integrated geophysical modeling for determination of the continental lithospheric thermal structure in the eastern Carpathians. Tectonics 25: TC3009, doi:10.1029/2005TC001883."

Dixon, W.J., 1953, Processing data for outliers: Biometrics, 9(1), 74–89.

Donelick RA, Ketcham RA, CarlsonWD.1999.Variability of apatite fission-track annealing kinetics. II. Crystallographic orientation effects. Am. Mineral. 84:1224–34

Donelick, R.A., O'Sullivan, P.B., Ketcham, R.A., 2005. Apatite Fission-Track Analysis, in Reiners, P.W., Ehlers, T.A. (Eds.). Low Temperature Thermochronology: Techniques, Interpretations, and Applications: Rev. Min. Geochem. 58, 49-94.

Dumitru TA (2000) Fission-Track Geochronology. In: Quaternary Geochronology: Methods and Applications. Noller JS, Sowers JM, Lettis WR (eds) Am Geophys Union Ref Shelf 4, Washington, DC, American Geophysical Union, 131-155"
Dunkl, I., 2002. TRACKKEY: a Windows program for calculation and graphical presentation of fission track data. Comput. Geosc. 28/2, 3—12.

Ehlers, T., Farley, K., 2003. Apatite (U–Th)/He thermochronometry: methods and applications to problems in tectonic and surface processes. Earth Plan. Sci. Let. 206, 1-14.

Ehlers, T.A., Chaudhri, T., Kumar, S., Fuller, C.W., Willett, S.D., Ketcham, R.A., Brandon, M.T., Belton, D.X., Kohn, B.P., Gleadow, A.J.W., Dunai, T.J., Fu, F.Q., 2005. Computational tools for low-temperature thermochronometer interpretation. Rev.Min. Geoch. 58, 589–622.

"England P, Molnar P. 1990. Surface uplift, uplift of rocks, and exhumation of rocks. Geology 18:1173–77"

"Faccenna, C., Jolivet, L., Piromallo, C., Morelli, A., 2003. Subduction and the depth of convection in the Mediterranean mantle. Journal of Geophysical Research 108, 2099."

"Farley (2002Farley KA. 2002. (U-Th)/He dating: techniques, calibrations, and applications. In Noble Gases in Geochemistry and Cosmochemistry, Reviews in Mineralogy and Geochemistry, 47:819–44. Chantilly, VA: Mineral. Soc. Am., Geochem. Soc."

Farley, K. A., 2000. Helium diffusion from apatite: General behavior as illustrated by Durango fluorapatite. J. Geophys. Res., 105(B2), 2903–2914.

Farley, K.A., 2000, (U-Th)/He dating: Techniques, calibrations, and applications: Reviews in Mineralogy and Geochemistry, v. 47, p. 819–844.

Faryad, S.W., Henjes-Kunst, F., 1997. Petrological and K-Ar and 40Ar/39Ar age constraints for the tectonothermal evolution of the high-pressure Meliata unit, Western Carpathians (Slovakia). Tectonophys. 280, 141–156.

Fechtig, H. and Kalbitzer, S. (1966) The diffusion of argon in potassium-bearing solids. Potassium-Argon Dating (Schaeffer, O. A. and Zähringer, J., eds.), 68–106, Springer.

Fillerup, M.A.,Knapp,J.H.,Knapp,C.C.,Raileanu,V.,2010.Mantle earthquakes in the absence of subduction? Continental delamination in the Romanian Carpathians. Lithos2(5),333–340.

Finger, F., Broska, I., Haunschmid, B., Hrasko, L., Kohut, M., Krenn, E., Petrik, I., Riegler, G., Uher, P., 2003. Electron-microprobe dating of monazites from Western Carpathian basement granitoids: plutonic evidence for an important Permian rifting event subsequent to Variscan crustal anatexis. Internat. J. Earth Sci. 92, 86–98.

Fitzgerald, P. G., S. L. Baldwin, L. E. Webb, and P. B. O'Sullivan (2006), Interpretation of (U-Th)/He single grain ages from slowly cooled crustal terranes: A case study from the Transantarctic Mountains of southern Victoria Land, Chem. Geol., 225, 91–120, doi:10.1016/j.chemgeo.2005.09.001.

Fleischer RL, Price PB, Walker RM. 1965. Effects of temperature, pressure, and ionization of the formation and stability of fission tracks in minerals and glasses. J. Geophy. Res. 70:1497–502

Fleischer RL, Price PB, Walker RM. 1975. Nuclear Tracks in Solids. Berkely: Univ. Calif. Press. 605pp

Fleischer, R. L. and Price, P. B. (1964a). Techniques for geological dating of minerals by chemical etching of fission fragment tracks. Geochim. Cosmochim. Acta 28, 1705)14.

Flowers, R.M., Ketcham, R.A., Shuster, D.L., and Farley, K.A. (2009) Apatite (U-Th)/He thermochronometry using a radiation damage accumulation and annealing model. Geochimica et Cosmochimica Acta.

Fodor, L., Horváth, F., Ustaszewski, K., Dombrádi, E., 2011. Constraints for the extrusion tectonics and back-arc extension in the Pannonian basin: a state of the art. Geophysical Research Abstracts, EGU General Assembly 2011, Vienna. 13, EGU2011-8317-2.

Fowler, C. M. R. and Nisbet, E. G.: The thermal background to metamorphism II. Simple two-dimensional conductive models, Geosci. Canada, 9, 208–214, 1982.

Fuchs, K., et al., 1979, The Romanian earthquake of March 4, 1977: II. Aftershocks and migration of seismic activity:
Tectonophysics, v. 53, p. 225–247.

Gagała, L., Vergés, J., Saura, E., Malata, T., Ringenbach, J.C., Werner, P., Krzywiec, P., 2012. Architecture and orogenic evolution of the northeastern Outer Carpathians from cross-section balancing and forward modeling. Tectonophys. 532-535, 223-241.

Galbraith RF, Green PF. 1990. Estimating the component ages in a finite mixture. Nucl. Tracks Radiation Meas. 17:197–206.

Galbraith, R., 1981, On statistical models for fission track counts: Mathematical Geology, v. 13, p. 471–488.

Galbraith, R.F., Laslett, G.M, 1993. Statistical models for mixed fission track ages. Nucl. Tracks. 5, 3–14.

Gallagher K, Brown R, Johnson C (1998) Fission track analysis and its applications to geological problems. Ann Rev Earth Planet Sci 26:519-572.

Gemmer L; Houseman GA (2007) Convergence and extension driven by lithospheric gravitational instability: evolution of the Alpine-Carpathian-Pannonian system, GEOPHYS J INT, 168, pp.1276-1290. doi: 10.1111/j.1365-246X.2006.03327.x

Gleadow AJW, Belton DX, Kohn BP, Brown RW (2002) Fission track dating of phosphate minerals and the thermochronology of apatite. Rev Mineral Geochem 48:579-630.

Gleadow AJW, Duddy IR, Green PF, Lovering JF (1986) Confi ned fi ssion track lengths in apatite: a diagnostic tool for thermal history analysis. Contrib Mineral Petrol 94:405-415.

Golonka, J., Gahagan, L., Krobicki, M., Marko, F., Oszczypko, N.& Slaczka, A., 2006. Plate Tectonic Evolution and Paleogeography of the Circum-Carpathian Region. In: Golonka, J. & Picha, F. (eds.) The Carpathians and their foreland: Geology and hydrocarbon resources: American Association of Petroleum Geologists, Memoir. 84, 11-46.

Green PF, Duddy IR, Gleadow AJW, Tingate PR, Laslett GM (1986) Thermal annealing of fi ssion tracks in apatite: A qualitative description. Chem Geol 59:237-253.

Green PF, Duddy IR, Gleadow AJW, Tingate PR. 1985. Fission track annealing in apatite: track length measurements and the form of the Arrhenius plot. Nucl. Tracks Radiation Meas. 10:323–28.

Green PF, Duddy IR, Laslett GM, Hegarty KA, Gleadow AJW, Lovering JF. 1989. Thermal annealing of fission tracks in apatite, 4. Quantitative modeling techniques and extension to geological timescales. Chem. Geol. (Isotope Geosci. Sec.) 79:155–82.

Grubbs F. E., 1950, Sample Criteria for Testing Outlying Observations, Annals of Math. Statistics, vol. 21, pp. 27-58.

Grubbs F. E., 1969, Procedures for Detecting Outlying Observations in Samples, Technometrics, vol. 11, No. 1, pp. 13-14.

Harangi, S., Lenkey, L., 2007. Genesis of the Neogene to Quaternary volcanism in the Carpathian-Pannonian region: Role of subduction, extension, and mantle plume. Geol. Soc. of Am. Special Papers. 418, 67-92.

Harangi, Sz., Luka´cs, R., Czuppon, Gy., Szabo´ , Cs., 2002. Magma mixing in a compositionally layered magma chamber: a silicate melt inclusion study. Workshop on Volcanic Systems, Seiano, Italy, Proceedings, pp. 101– 106.

Horv´ath, F., D¨ov´enyi, P., and Lacz´o, I.: Geothermal effects of magmatism and its contribution to the maturation of organic matter in sedimentary basins, in: Lecture Notes in Earth Sciences, Vol. 5, Buntebarth, G. and Stegena, L. eds., Paleogeothermics: Springer-Verlag, Berlin/Heidelberg, 173–183, 1986.

Horva´ th, F.,Bada,G.,Szafia´ n, P.,Tari,G.,A´ da´m, A.,Cloetingh,S.,2006. Formation and deformation of the Pannonian Basin: constraints from observational data. In: Gee,D.,Stephensen,R.(Eds.),European Lithosphere Dynamics. Geological Society ofLondonMemoirs,vol.32.GeologicalSocietyofLondon,pp.191–206.

Horváth, F., 1993. Towards a mechanical model for the formation of the Pannonian basin, Tectonophys., 226, 333 – 357.

Horvath, F., and S. Cloetingh, 1996, Stress-induced late-stage subsidence anomalies in the Pannonian Basin: Tectonophysics, v. 266, p. 287–300.

Hourigan, J.K, Reiners, P.W, Brandon, M.T, 2005. U-Th zonation-dependent alpha-ejection in (U-Th)/He chronometry. Geoch. Cosm. Acta, 69, 3349–3365.

Houseman,G.A.,Gemmer,L.,2007.Intra-orogenic extension driven by gravitational instability: Carpathian–Pannonian orogeny.Geology35(12),1135–1138.

Hraško, L., Broska, I., Finger, F., 2002. Permian Granitic magmatism and disintegration of the Lower Paleozoic basement in the SW veporicum near Klenovec (Western Carpathians), in Michalik, J., Šimon, L., Vozár, J. (Eds), Proceedings of XVII. Congress of Carpathian-Balkan Geological Association Bratislava, September 1st - 4th. 53.

Huismans, R.S., Podladchikov, Y.Y., and Cloething, S., 2001. Dynamic modelling of the transition from passive to active rifting, application to the Pannonian Basin: Tectonics, v. 20, p. 1021–1039.

Hurai, V., Marko, F., Tokarski, A.K., Świerczewska, A., Kotulová, J., Biroň A., 2006. Fluid inclusion evidence for deep burial of the Tertiary accretionary wedge of the Carpathians. Terra Nova. 18, 440-446.

Hurford AJ, Green PF (1983) The zeta age calibration of fi ssion-track dating. Isotope Geoscience 1:285-317

Janák, M., Plašienka, D., Frey, M., Cosca, M., Schmidt, S., Lupták, B., Méres. Š., 2001. Cretaceous evolution of a metamorphic core complex, the Veporic unit, Western Carpathians (Slovakia) P-T conditions and in situ 40Ar/39Ar UV laser probe dating of metapelites. J. Metamorph. Geol. 19, 197–216.

Janik, T., Grad, M., Guterch, A., Vozár, J., Bielik, M., Vozárova, A., Hegedüs, E., Kovác, C.A., Kovác, I., Keller, G.R. and
CELEBRATION 2000 Working Group, 2011. Crustal structure of the Western Carpathians and Pannonian Basin: Seismic models from CELEBRATION 2000 data and geological implications. Journal of Geodynamics, v. 52, p. 97-113.

Jankowski, L. (2007). Chaotic complexes in Gorlice region (Polish outer Carpathians), Biuletyn Państwowego Instytutu Geologicznego,Vol. 426: 27-52.

Jankowski, L., Kopciowski, R., Rylko, W., 2004. Geological map of the Outer Carpathians: borderlands of Poland, Ukraine and Slovakia, 1:200.000. Pol. Geol. Inst., Warszawa.

Jiricek, R., 1979. Tectonic development of the Carpathian arc in the Oligocene and Neogene, in Machel, M. (Ed.), Tectonic Profiles through the Western Carpathians: Bratislava, Geological Institute of Dionýz Stúr, pp. 205–214.

Ketcham R. A., Carter A. C., Donelick R. A., Barbarand J., Hurford A. J.,2007. Improved modeling of fission-track annealing in apatite. Am. Mineral. 92, 799–810.

Ketcham RA, Donelick RA, Carlson WD. 1999. Variability of apatite fission-track annealing kinetics. III. Extrapolation to geological time scales. Am. Mineral. 84:1235–55

Ketcham, R. A., 2005, Forward and inverse modelling of low-temperature thermochronology data. Rev. Mineral. Geochem., 58, 275–314.

Knapp, J.H.,Knapp,C.C.,Raileanu,V.,Matenco, L.,Mocanu,V.,Dinu,C.,2005. Crustal constraints on the origin of mantle seismicity in the Vrancea Zone, Romania: the case for active continental lithospheric delamination. Tectono- physics 410,311–323.

Kohút, M., 2002. The Hercynian Granitic Rocks of the Western Carpathians in the Frame of European Hercynides, in Michalik, J., Šimon, L., Vozár, J. (Eds), Proceedings of XVII. Congress of Carpathian-Balkan Geological Association Bratislava, September 1st - 4th. 53.

Konečny, V., Kováč, M., Lexa, J., Šefara, J., 2002. Neogene evolution of the Carpatho-Pannonian region: an interplay of subduction and back-arc diapiric uprise in the mantle. EGU Stephan Mueller Spec. Pub. Series. 1, 105–123.

Koszarski L., and A. Slaczka, 1976, The Outer (Flysch) Carpathians: The Cretaceous, in S. Cieslinski, ed., Geology of Poland, v. I, Stratigraphy part 2: Instytut Geologiczny, Warszawa, p. 495–498, 657–679, 740–748.

Kotarba, M. J. & Koltun, Y. V., 2006. The origin and habitat of hydrocarbons of the Polish and Ukrainian Parts of the Carpathian Province. In: Golonka, J. & Picha, F. J. (eds), The Carpathians and their fore land: geology and hydrocarbon resources. American Association of Petroleum Geologists, Memoir, 84: 395–442.

Kova´ cs, I., Falus, G., Stuart, G., Hidas, K., Szabo´ , C., Flower, M.F.J., Heged¨ us, E., Posgay, K., Zilahi-Sebess,L.,2012.Seismic anisotropy and deformation patterns in upper mantle xenoliths from the central Carpathian–Pannonian region: asthenospheric flow as a driving force for Cenozoic extension and extrusion? Tectonophysics514–517,168–179.

Kova´cs, I., Szabo´, C.,2008.Middle Miocene volcanism in the vicinity of the Middle Hungarian Zone: evidence for an inherited enriched mantle source. J.Geody- nam. 45,1–17.

Kovac, M., Marko, F., Nemcok, M., 1990. Neogene history of intramontane basins in the western part of the Carpathians. Riv. It. Paleont. Strat. 96, 381–404.

Ksiazkiewicz, M., 1977, Tectonics of the Carpathians, in W. Pozaryski, ed., Geology of Poland, Tectonics: Warsaw, Poland, Wydawnictwa Geologiczne, v. 4, p. 476–604.

Ksiazkiewicz, M., ed., 1962, Geological atlas of Poland: Stratigraphic and facial problems: Warsaw, Poland, Instytut Geologiczny, Wydawnictwa Geologiczne, 24 p.

Kusiak, M.A., Paszkowski, M., Dziubinska, B., 2004. The First Precambrian Detrital Monazites from the Polish Eastern Carpathian, Appl. Min. 1, 141-144.

LaslettGM,Green PF, Duddy IR, Gleadow AJW. 1987. Thermal annealing of fission tracks in apatite 2. A quantitative analysis. Chem. Geol. (Isotope Geosci. Sect.) 65:1– 13

Lenkey, L., Dovenyi, P., Horva´th, F., Cloetingh, S.A.P.L., 2002. Geothermics of the Pannonian basin and its bearing on the neotectonics. EGU Stephen Mueller Special PublicationSeries3,pp.29–41.

Lenkey, L.: Geothermics of the Pannonian basin and its bearing on the tectonics of basin evolution, PhD thesis, Vrije Universiteit, Amsterdam, 215pp, 1999.

Linzer, H.G., 1996. Kinematics of retreating subduction along the Carpathian arc, Romania. Geol. 24,167 I70.

Lorinczi, P.,Houseman,G.A.,2009.Lithospheric gravitational instability beneath the Southeast Carpathians. Tectonophysics474,322–336.

Mahel, M., et al., 1968, Regional geology of Czechoslovakie: Part II. The West Carpathians: Praha, Geological Survey
of Czechoslovakia, p. 1–723.

Maluski, P., Rajlich, P., Matte, P., 1993. 40Ar=39Ar dating of the Inner Carpathian Variscan basement and Alpine mylonitic overprinting. Tectonophys. 223, 313–337.

Matenco, L., Bertotti, G., 2000.Tertiary tectonic evolution of the external East Carpathians (Romania).Tectonophys. 316, 255–286.

Mazzoli, S., Jankowski, L., Szaniawski, R. and Zattin, M., 2010. Low-T thermochronometric evidence for post-thrusting (<11 Ma) exhumation in the Western Outer Carpathians, Poland. Compte Rendue Geosci. 342, 162-169.

McKenzie, D.P.,1970.Plate tectonics of the Mediterranean region.Nature226, 239–243.

Meulenkamp, J. E., M. Kovac, and I. Cicha, 1996, On late Oligocene to Pliocene depocenter migrations and the evolution of Carpathian–Pannonian system: Tectonophysics, v. 266, p. 301–317.

Michalik, M., Budzyń, B., Gehrels, G., 2006. Cadomian granitoid clasts derived from the Silesian Ridge (results of the study of gneiss pebbles from Gródek at the Jezioro Rożnowskie Lake). Min. Pol. — Special Papers. 29, 168–171.

Murray, K. E.; Orme, D. A.; Reiners, P. W., 2011. Apatite (U-Th)/He Date Dispersion Due to Secondary Grain Boundary Phases: An Example from the Henry Mountains, Utah. American Geophysical Union, Fall Meeting 2011, abstract #V23A-2556

Naeser CW (1967) The use of apatite and sphene for fi ssion track age determinations. Bull Geol Soc Am 78: 1523-1526

Naeser ND, McCulloh TH (eds) (1989) Thermal History of Sedimentary Basins: Methods and Case Histories, Springer-Verlag, Berlin

Nemčok, M., Pospìšil, L., Hrušecky, I., Zsìros, T., 2006. Subduction in the remnant Carpathian Flysch Basin, in Golonka, J., Picha F. J. (Eds.), The Carpathians and their foreland: Geology and hydrocarbon resources. AAPG Memoir, pp. 767 – 785.

Nemčok, M., Pospíšil, L., Lexa, J., Donelick, R.A., 1998. Tertiary subduction and slab break-off model of the Carpathian–Pannonian region. Tectonophys. 295, 307-340.

Németh Z., Grecula P., Gazdačko Ľ., Kobulský, J., Hraško, Ľ.,2011. Gemericum (Inner W. Carpathians): Variscan and Alpine tectonic overprint expressed in a new geological map of the Spiš-Gemer Ore Mts. at a scale 1 : 50 000. Acta of the Otevřený kongres, Bratislav, 21-25 September 2011.

Németh, Z., Putiš, M., 2002. Some topics of Geodynamics evolution of Inner Western Carpathian. Proceedings of XVII Congress of Carpathian-Balkan Geological Association Bratislava, September 1st - 4th 2002. 53

Ondrejka, M., Uher, P.,2001. Composition and Origin of Triassic Potassium-Rich. Rhyolites of the Silicicum Superunit, Western Carpathians, Central Slovakia. GeoLines.13 98-99.

Orme D.A., Reiners P. W., 2010; Effects of External Parent Nuclides on Apatite Helium Dates: Sources and Solutions. Proceedings og the Thermo 2010 congress. Glasgow

Oszczypko, N., Krzywiec, P., Lemberger, M., Stefaniuk, M., Pietsch, K. and Trygar, H., 1998. Integrated geological-geophysical interpretation of the Rzeszow-Smilno profile (Western Carpathians). Carpathian–Balkan Geological Association XVI Congress, Vienna, Abstracts. 446.

Oszczypko, N., Krzywiec, P., Lemberger, M., Stefaniuk, M., Pietsch, K. and Trygar, H., 1998. Integrated geological geophysical interpretation of the Rzeszow-Smilno profile (Western Carpathians). Carpathian–Balkan Geological Association XVI Congress, 30 August - 2 September, Vienna, Abstracts, 446.

Pécskay, Z., Lexa, J., Szakács, A., Seghedi, I., Balogh, K., Konečny, V., Zelenka, T., Kovacs, M., Poka, T., Fulop, A.,Márton, E., Panaiotu, C. Cvetkovic, V., 2006. Geochronology of Neogene magmatism in the Carpathian arc and intra-Carpathian area. Geol. Carpathica, 57, 511–530.

Pharaoh, T.C., 1999. Paleozoic terranes and their lithospheric boundaries within theTrans-European Suture Zone (TESZ): a review, Tectonophysics, 314, 17–41.

Piromallo, C.,Morelli,A.,2003.P wave tomography of the mantle under the Alpine-Mediterranean area.J.Geophys.Res.108(B2),2065,http://dx.doi.org/ 10.1029/2002JB001757.

Plašienka, D., Broska, I., Kissová, D., Dunkl, I., 2007. Zircon fission-track dating of granites from the Vepor–Gemer Belt (Western Carpathians): constraints for the Early Alpine exhumation History. J. Geosci. 52, 113–123.

Plašienka, D., Grecula, P., Putiš, M., Kováč, M., Hovorka, D., 1997. Evolution and structure of the Western Carpathians: an overview. in: Grecula, P., Hovorka, D., Putiš, M. (Eds), Geological evolution of the Western Carpathians. Mineralnia Slov., pp1-24.

Pollack, H. N., Hurter, S. J., and Johnson, J. R.: Heat loss from the Earth's interior: analysis of the global data set, Reviews of Geophysics, 31, 267–280, 1993.

Poller, U., Janák, M., Kohút, M., Todt,W., 2000. Early Variscan magmatism in theWestern Carpathians: U–Pb zircon data from granitoids and orthogneisses of the Tatra Mountains (Slovakia). International Journal of Earth Sciences 89, 336–349.

Poprawa, P., Kusiak, M.A.,Malata, T., Paszkowski, M., Pecskay, Z., Skulich, J., 2005. Th-U-Pb chemical dating of monazite and K/Ar dating of mica combined: preliminary study of “exotic” crystalline clasts from the Western Outer Carpathian flysch (Poland). Min. Soc. Pol., Special Papers. 25 345-351.

Poprawa, P., Malata, T., Pécskay, Z., Banas, M., Skulich, J., Paszkowski, M., Kusiak, M.A., 2004. Geochronology of crystalline basement of the Western Outer Carpathians’ sediment source areas – preliminary data. Min. Soc. Pol. – Special Papers, 24: 329-332.

Poprawa, P., Malata, T., Pécskay, Z., Kusiak, M.A., Banaś, M., Paszkowski, M., 2006. Geochronology of the crystalline basement of the Western Outer Carpathians' source areas — constraints from the K/Ar dating of mica and Th–U–Pb chemical dating of monazite from the crystalline ‘exotic’ pebbles. Geolines 20, 110–112.

Poprawa, P.,Malata, T.,Oszczypko, N., 2002. Tectonic evolution of the Polish part of Outer Carpathian’s sedimentary basins – constraints from subsidence analysis. Prz. Geol. 50, 1092-1108.

Pospišil, L., Adám A., Bimka, J., Bodlak, P., Bodoky, T., Dövényi, P., Granser, H., Hegedüs, E., Joò, I., Kendzera, A., Lenkey, L., Nemčok, M., Posgay, k., Pylypyshyn, B., Sedlák, J., Stanley, W.D., Starodub, G., Szalaiová, V., Šály, B., Šutora, A., Várga, G., Zsìros, D., 2006. Crustal and lithospheric structure of the Carpathian –Pannonian region — A geophysical perspective: Regional geophysical data on the Carpathian – Pannonian lithosphere, in Golonka, J., Picha F.J. (Eds), The Carpathians and their foreland: Geology and hydrocarbon resources: AAPG Memoir 84, pp. 651 – 697.

Putiš, M., Sergeev, S., Ondrejka, M., Larionov, A., Siman, P., Spišiak, J., Uher, P., Paderin, I., 2008. Cambrian–Ordovician metaigneous rocks associated with Cadomian fragments in the West-Carpathian basement dated by SHRIMP on zircons: a record from the Gondwana active margin setting. Geol. Carp. 59, 1.

Reiners PW, Campbell IH, Nicolescu S, Allen CM, Hourigan JK, et al. 2005a. (U-Th)/(He-Pb) double dating of detrital zircons. Am. J. Sci. 305:259–311

Reiners PW, Ehlers TA, eds. 2005. Low-Temperature Thermochronology: Techniques, Interpretations, Applications. Reviews in Mineralogy and Geochemistry, Vol. 58. Chantilly, VA: Mineral. Soc. Am., Geochem. Soc. 622pp.

Reiners, P.W., and Farley, K.A., 2001, Influence of crystal size on apatite (U-Th)/He thermochronology: An example from the Bighorn Mountains, Wyoming, Earth and Planetary Science Letters, v. 188, p. 413-420.

Reiners, P.W., Brandon, M.T., 2006, Using Thermochronology to Understand Orogenic Erosion, Ann. Rev. Earth Plan. Sci., v. 34, p. 419-466.

Reiners, P.W., Spell, T.L., Nicolescu, S., Zanetti, K.A., 2004. Zircon (U-Th)/He thermochronometry: He diffusion and comparisons with 40Ar/39Ar dating. Geochim. Cosmochim. Acta. 68:1857–87

Reiners, P.W., Thomson, S.N., McPhillips, D., Donelick, R.A., and Roering, J.J., 2007, Wildfire thermochronology and the fate and transport of apatite in hillslope and fluvial environments, Journal of Geophysical Research-Earth Surface, v. 112, F04001, doi:10.1029/2007JF000759.

Ren Y; Stuart GW; Houseman GA; Dando B; Ionescu C; Hegedus E; Radovanovic S; Shen Y (2012) Upper mantle structures beneath the Carpathian-Pannonian region: Implications for the geodynamics of continental collision, Earth and Planetary Science Letters, 349-350, pp.139-152. doi: 10.1016/j.epsl.2012.06.037

Royden, L. H., F. Horvath, and B. C. Burchfiel, 1982, Transform faulting, extension and subduction in the Carpathian–
Pannonian region: Geological Society of America Bulletin, v. 93, p. 717–725.

Schiattarella M., Di Leo P., Beneduce P., Giano S.I. & Martino C. 2006: Tectonically driven exhumation of a young orogen: an example from southern Apennines, Italy. In: Willett S.D., Hovius N., Brandon M.T. & Fisher D. (Eds.): Tectonics, climate, and landscape evolution. Geol. Soc. Amer., Spec. Pap. 398, Penrose Conference Series, 371—385.

Seghedi, I., Downesb, H., Szakacsa, D., Masonc, P.R.D., Thirlwalld, M.F., Rosue, E.,Pecskayf, Z., Marton, E., Panaiotuh, C., 2004. Neogene–Quaternary magmatism and geodynamics in the Carpathian–Pannonian region: a synthesis. Lithos. 72, 117–146.

Shuster D.L. and Farley, K.A., (2009) The influence of artificial radiation damage and thermal annealing on helium diffusion kinetics in apatite, Geochimica Et Cosmochimica Acta 73(1),6183-196

Shuster, D.L., Flowers, R.M., and Farley, K.A., 2006, The influence of natural radiation damage on helium diffusion kinetics in apatite: Earth and Planetary Science Letters, v. 249, p. 148–161, doi: 10.1016/j.epsl.2006.07.028.

Slaczka, A., S. Kruglow, J. Golonka, N. Oszczypko, and I. Popadyuk, 2006, Geology and hydrocarbon resources of the Outer Carpathians, Poland, Slovakia, and Ukraine: The general geology of the Outer Carpathians, Poland, Slovakia, and Ukraine, in J. Golonka and F. J. Picha, eds., The Carpathians and their foreland: Geology and hydrocarbon resources: AAPG Memoir 84, p. 221–258.

Sperner, B., Ratschbacher, L., Nemčok, M., 2002. Interplay between subduction retreat and lateral extrusion: tectonics of the Western Carpathians. Tectonics, 21, 1051.

Sperner, B., Lorentz, F., Bonjer, K.P., Hettel, S., Muller, B., Wenzel, F., 2001. Slab break-off—abrupt cut or gradual detachment? New insights from the Vrancea region (SE-Carpathians, Romania).TerraNova13,172–179.

Steiger RH, Jäger E (1977) Subcommission on geochronology: Convention on the use of decay constants in geo- and cosmochronology. Earth Planet Sci Lett 36:359-362

Suranyi, G., Konya, B., and Lenkey, L.: Concentrations of natural radioactive isotopes in Neogene volcanic rocks from the Pannonian basin, EGS 2002, XXVII General Assembly, Nice, France, 21–26 April 2002, SE2.10-1FR5P-022, 2002.
Swierczewska, A., 2005. The interplay of the thermal and structural histories of the Magura Nappe (Outer Carpathians) in Poland and Slovakia. Min. Pol. 36, 91-144.
Syrek, M., 2009. Stopień uwęglenia rozproszonego materiału organicznego w jednostce magurskiej i strefie okiennej (Karpaty Zewnętrzne). Materiały Krakowskiej Konferencji Młodych Uczonych 2009, Kraków, 17–19 września 2009, Akademia Górniczo-Hutnicza im. Stanisława Staszica w Krakowie, 195–202.

Tagami T, O'Sullivan PB (2005) Fundamentals of fi ssion-track thermochronology. Rev Mineral Geochem 58:

19-47

Tasarova, A., Afonso, J.C., Bielik, M., Gotze, H.J., Hok, J., 2009. The lithospheric structure of the Western Carpathian–Pannonian Basin region based on the CELEBRATION 2000 seismic experiment and gravity modeling. Tectonophysics. 475, 454–469

Tesauro, M.; Kaban, M. K.; Cloetingh, S. (2009): A new thermal and rheological model of the European lithosphere. Tectonophysics, 476, 3-4, 478-495.

Thomson, S.N., Brandon, M.T., Reiners, P.W., Zattin, M., Isaacson, P.J. & Balestrieri, M.L. (2010). Thermochronologic evidence for orogen-parallel variability in wedge kinematics during extending convergent orogenesis of the northern Apennines, Italy, Geological Society of America, Bulletin, 122, p. 1160-1179, doi: 10.1130/B26573.1

Tokarski A., Swierczewska, A., Zuchiewicz, W., Márton, E., Hurai, V., Anczkiewicz, A., Michalik, M., Szeliga, W., Rauch-Wlodarska, M., 2006.Conference Excursion 1: Structural Development of the Magura Nappe (Outer Carpathians): From Subduction to Collapse. GeoLines. 20, 145-164

Uher, P., Broska, I., Ondrejka, M., 2002. Permian to Triassic granitic and Rhyolitic magmatism in the Western Carpathians: composition, evolution and origin, in Michalik, J., Šimon, L., Vozár, J. (Eds), Proceedings of XVII. Congress of Carpathian-Balkan Geological Association Bratislava, September 1st - 4th. 53.

Ustaszewski, K., Schmid, S., Fugenschuh, B., Tischler, M., Kissling, E., Spakman, W., 2008. A map-view restoration of the Alpine–Carpathian–Dinaridic system for the Early MioceneSwiss.J.Geocsci.101,273–294.

Van den haute, P., De Corte, F., Jonckheere, R., Bellemans, F. (1998). The parameters that govern the accuracy of fission-track age determinations: a re-appraisal. In: Van den haute, P., De Corte, F. (Eds) Advances in Fission-Track Geochronology. Kluwer Academic Publishers, Dordrecht, 33-46.

Vermeesch, P (2012) On the visualisation of detrital age distributions. Chemical Geology , 312–313 10.1016/j.chemgeo.2012.04.021.

Vermeesch, P., 2008. Three new ways to calculate average (U-Th)/He ages. Chemical Geology 249, 339–347.

Vermeesch, P., Seward, D., Latkoczy, C., Wipf, M., Guenther, D., Baur, H.,2007. Alpha-emitting mineral inclusions in apatite, their effect on (U–Th)/He ages, and how to reduce it. Geoch. Cosm. Acta. 71, 1737–1746.

Vityk M. O., Bodnar R. J. and Dudok I. V. (1996) — Fluid inclusions in “Marmarosh Diamonds”: evidence for tectonic history of the folded Carpathian Mts, Ukraine. Tectonophysics, 255: 163–174.
Wagner GA (1968) Fission track dating of apatites. Earth Planet Sci Lett 4:411-415

Wagner GA (1969) Spuren der spontanen Kernspaltung des 238Urans als Mittel zur Datierung von Apatiten und ein Beitrag zur Geochronologie des Odenwaldes. N Jahrb Mineral Abh 110:252-286

Wagner GA, van den Haute P. 1992. Fission-Track Dating. Dordrecht: Kluwer Acad. Publ. 285pp.

Wolf, R.A., Farley, K.A., Kass, D.M. Modeling of the temperature sensitivity of the apatite _ U–Th/ rHe thermochronometer DiÍision of Geological and Planetary Sciences, California Institute of Technology, MS 170-25, Pasadena, CA 91125, USA Received 13 August 1997; accepted 30 January 1998

Wortel, M.,Spakman,W.,2000.Subduction and slab detachment in the Mediterranean Carpathian region. Science290,1910–1917.

Zattin, M., Andreucci, B., Jankowski L., Mazzoli S., Szaniawski, R.,2011. Neogene exhumation in the Outer Western Carpathians. Terra Nova. 23, 283–291.

Zeyen, H., J. Dererova´, and M. Bielik (2002), Determination of the continental lithosphere thermal structure in the western Carpathians: Integrated modelling of surface heat flow, gravity anomalies and topography, Phys. Earth Planet. Inter., 134, 89 – 104.